OXIDATIVELY TRIGGERED CARBON-CARBON COUPLING IN FIRST ROW TRANSITION METAL ENE-AMIDE COMPLEXES AND PROGRESS TOWARDS DEVELOPMENT OF IRON(IV) ALKYLIDENES

A Dissertation

Presented to the Faculty of the Graduate School

of Cornell University

In Partial Fulfillment of the Requirements for the Degree of

Doctor of Philosophy

by

Brian Patrick Jacobs

August 2017

OXIDATIVELY TRIGGERED CARBON-CARBON COUPLING IN FIRST ROW TRANSITION METAL ENE-AMIDE COMPLEXES AND PROGRESS TOWARDS DEVELOPMENT OF IRON(IV) ALKYLIDENES

Brian Patrick Jacobs, Ph. D.

Cornell University 2017

A series of transition metal ene-amide complexes {(2,6-$^{i}Pr_2$-C_6H_3)(1-^{c}Hexenyl)N}$_2$M (M = Cr, **1**-Cr; $FePMe_3$, **2**-Fe; $Copy_2$, **3**-Co) were prepared, and oxidation studies were conducted to assess intramolecular CC coupling. Addition of $CrCl_3$ to **1**-Cr, and $FeCl_3$ to **2**-Fe afforded the organic product *rac*-2,2'-di(2,6-$^{i}Pr_2C_6H_3N=)_2$-dicyclohexane (**EA$_2$**) via an oxidatively triggered CC bond formation. Various lithium ene-amides were coupled, yet attempts to hydrolyze the diimine products produced pyrroles, rather than the target 1,4-diketone species. Some ferrous compounds (e.g., **2**-Fe, $FeCl_2$) catalyzed C-arylation of {(2,6-^{i}Pr-C_6H_3)(1-^{c}Hexenyl)N}Li upon exposure to phenyl bromide, yet the catalysis was modest (4-9 TO) and featured extended reaction times (3-4 d).

A series of octahedral Fe(II) vinyl chelates complexes *mer*,*trans*-{κ^3-N,N,C-2-py-CH=NCH_2-CH=CH}Fe$(PMe_3)_2CH_3$ (**12**), *mer*,*trans*-{κ^3-N,N,C-2-py-CH=NCH_2-CH=CH}Fe$(PMe_3)_2$I (**15**) and *mer*,*trans*-{κ^3-N,N,C-(2-py)CH=NC(Me_2)CH=CPh}Fe$(PMe_3)_2CH_3$ (**18**) were prepared as potential precursors for the synthesis of Fe(IV) alkylidenes. While protonation of these complexes resulted in degradation, exposure of **15** to KO^{t}Bu yielded *mer*-{κ^3-N,N,C-2-py-CH=NCH_2-

CH=CH}Fe(PMe_3)$_3$ (**17**). Structural characterization of complexes **15** and **17** revealed the latter to be consistent with an Fe(II) center coordinated by a conjugated vinyl ligand with delocalization in its π-system. Electronic structures of the prior Fe(IV) alkylidenes [*mer*-{κ^3-C,N,C-(2-C_6H_4)CH=N(1,2-C_6H_4)C(^{i}Pr)=}Fe(PMe_3)$_3$] [BAr^F_4] (**6**) and *mer*,*trans*-{κ^3-C,N,C-(2-C_6H_4)CH(Bn)N(1,2-C_6H_4)C(^{i}Pr)=}Fe(PMe_3)$_2N_2$ (**9**) were calculated, and portray the "alkylidene" of **6** as carbenium-like and **9** as a vinyl carbon.

A series of Fe chelate complexes [Fe(*o*-$CH_2C_6H_4NMe_2$)]$_2$(κ-μ-CH_2,N-*o*-$CH_2C_6H_4NMe_2$)$_2$ (**1**), [*fac*-Fe(κ-C,P-*o*-$CH_2C_6H_4PPh_2$)$_3$][Li(TMEDA)$_2$] (**2**), (Me_2IPr)Fe($CH_2C_6H_4NMe_2$)$_2$ (**3**-C,N), (PMe_3)$_2$Fe(κ-C,P-CH_2PMe_2)$_2$ (**5**) and *trans*,*cis*-(PMe_3)$_2$Fe(κ-C,P-$CH_2C_6H_4$-*o*-PMe_2)$_2$ (**6**) were prepared through either salt metathesis or C-H bond activation. The viability of these compounds as Fe alkylidene precursors was probed, and oxidations of each chelate complex yielded organic degradation products.

Several low-valent Fe(II) neopentyl (**1**-L_n) and norbornyl (**4**-L_n) complexes were prepared bearing ancillary ligands (e.g., TMEDA, PMe_3). Efforts to yield Fe alkylidenes via oxidation yielded CC coupled degradation, yet exposure to adamtanyl azide afforded the Fe(IV) imido complexes (Me_2IPr)Fe(=N(1-Ad))($CH_2C(CH_3)_3$)$_2$ (**2**-Im) and (Me_2IPr)Fe(=N(1-Ad))(1-nor)$_2$ (**6**-Im). Both Fe imido species exhibit migratory insertion to yield Fe(II) amides. Kinetics indicated the ^{neo}Pe system was more favorable with $\Delta\Delta G^{\ddagger}$ (298 K) = 3.6 kcal mol^{-1}.

BIOGRAPHICAL SKETCH

Brian Patrick Jacobs was born in Tampa Bay, FL to David Jacobs, a surgical technician in the Air Force, and Judy Jacobs, a worker in the food service industry. Brian grew up in Colorado Springs, CO as the youngest of three brothers. Despite lukewarm success in high school chemistry courses, Brian decided to follow his father's footsteps and pursued a pre-medical profession at the University of Colorado Colorado Springs in 2007. The pre-medical profession proved to be a passing interest, as Brian withdrew himself from that direction and pursued a major in chemistry after 2 years of study. During his 4^{th} year of study, Brian finally discovered his interest in the field of inorganic chemistry thanks to the strict teachings of Dr. Ronald Ruminski, more commonly referred to as the "Gatekeeper." After graduating in 2011 with a B. Sc. in chemistry, Brian chose to apply for graduate studies to pursue an interest in chemical education. A fleeting interest in developing a career in various chemical processing industries within Colorado yielded no results. Brian applied and was accepted to the chemistry department at Cornell University in 2012, where he joined the laboratory of Peter T. Wolczanski to pursue studies in organometallic synthesis. Despite initial problems encountered while getting used to working in a research laboratory, Brian successfully acquired his M. Sc. in 2014. Three additional years of intensive research culminated in Brian completing his doctoral studies in June 2017.

To my parents and friends,
Who have always supported me.

ACKNOWLEDGMENTS

First I want to thank my advisor and mentor Pete Wolczanski, who has been instrumental in my development at Cornell University. His numerous suggestions on new synthetic methods have enhanced my appreciation for the diversity of approaches one can take to solve a single problem, and he has constantly challenged me to better myself both scientifically and personally.

I would like to give my sincere thanks to my additional committee members, Geoff Coates and Kyle Lancaster. Geoff has been considerably helpful in framing my research within a synthetic organic perspective, one which I admittedly often forget to consider. Kyle has been a valuable friend since I began my graduate studies, and I greatly appreciate both him and his group for providing assistance in acquiring UV/Vis and Raman spectroscopy. Additional thanks go to Dave Collum, who never failed to greet me in the morning, and has provided valuable advice on chemical preparation methods and future career prospects. Tom Cundari (University of North Texas) is also thanked for his computational support, which appears in Chapters 2 and 4. I would also like to acknowledge Bill Brennessel (University of Rochester) for his help in obtaining elemental analysis data for our group. Karsten Meyer (Friedrich Alexander University Erlangen-Nürnberg) and his group are thanked for acquiring Mössbauer spectra for several iron complexes presented in Chapter 2. Ivan Keresvtes and Tony Condo are thanked for their assistance in the NMR and mass spectrometry facilities, and have always been willing to help interpret puzzling NMR spectra. A great many thanks go to Emil Lobkovsky for crystal structure determinations

presented in Chapters 1 and 2. Sam MacMillan has been tremendously helpful for crystal structure determinations given in Chapters 2, 3 and 4, and I express sincere gratitude for her help figuring out the structural quirks of my more complicated molecules.

I would like to give thanks to Pat Hine and Cynthia Kinsland for numerous interactions I've had with them, including helpful discussions on the business side of being a graduate student. Thanks go to Josh Wakeman who made trips to the chemistry stockroom enjoyable, and occasionally stops by after disposing of chemical waste containers for our group. Dave Neish and Larry Stull have been helpful in keeping the lab running, and are always willing to strike up engaging conversation. I would also like to thank Dave Wise for happily tending to our glassware issues.

I would like to give thanks to past Wolczanski group members Erika Bartholomew, Wes Morris, Valerie Williams and Brian Lindley for acting as mentors in learning chemical synthesis. Their assistance in teaching me how to be a synthetic chemist has been invaluable, and I can't thank them enough. Special thanks go to Brian Lindley, who has never failed to entertain discussions, scientific or not. I would also like to thank Ala'aeddeen Swidan and Rishi Agarwal for their assistance in developing the groundwork for iron alkylidene synthesis with Brian Lindley, and their work is presented in Chapter 2.

Special thanks go to current group members Spencer Heins, Matt Piedmonte and undergrad Devika Pokhriyal. Spencer has been very helpful for all things relating to upkeep of the labs to helpful discussions for the last 4 years I have known him.

While I have not known Devika for long, her enthusiasm for research and quick grasp of chemical concepts will serve her well for her tenure in our group.

Lastly, I would like to thank my family and old friends back in Colorado Springs. It's difficult to express how important my parents' support has been, and I genuinely believe I wouldn't have made it this far without them. My father and friends in particular have always challenged me to express why my research matters, and this difference in perspective always led me to understand the value in seeing the broader impact of my studies.

TABLE OF CONTENTS

LIST OF FIGURES

LIST OF SCHEMES

LIST OF TABLES

Chapter 1

Synthesis of 1st row Transition Metal Ene-amide Complexes and Subsequent CC Bond Forming Reactions Triggered via Oxidation

Introduction

Industrial applications of transition metal catalysts with respect to organic synthesis have led to a burgeoning interest in developing first row transition metal complexes that can supplant traditional second and third row congeners.[1-10] The low toxicity and higher abundance of base metals such as Fe can allow for synthetic methodologies that are more cost effective.[3-10] Metal-mediated organic transformations usually invoke two-electron processes. This can prove problematic for first row metal complexes, as they tend to engage in one-electron transformations that can result in undesirable alternative reactivity that detracts from the target method. One approach to cause such complexes to engage in two-electron transformations more befitting of their higher congener analogues employs redox non-innocent (RNI) ligands, i.e. ligands that can accommodate multiple redox states (for brief reviews of RNI ligands, see references 11 and 12).[11-47] RNI ligands can undergo ligand-centered redox processes by virtue of the closely matched energies of the RNI ligand orbitals and the metal d-orbitals, which results in delocalization of the electron density. Such ligands may act as two-electron reservoirs, allowing the ligand to effect two-electron processes by modulating electron density at the metal center. An issue that can arise with RNI ligands, due to their redox properties, is the potential formation of ligand-localized radicals.

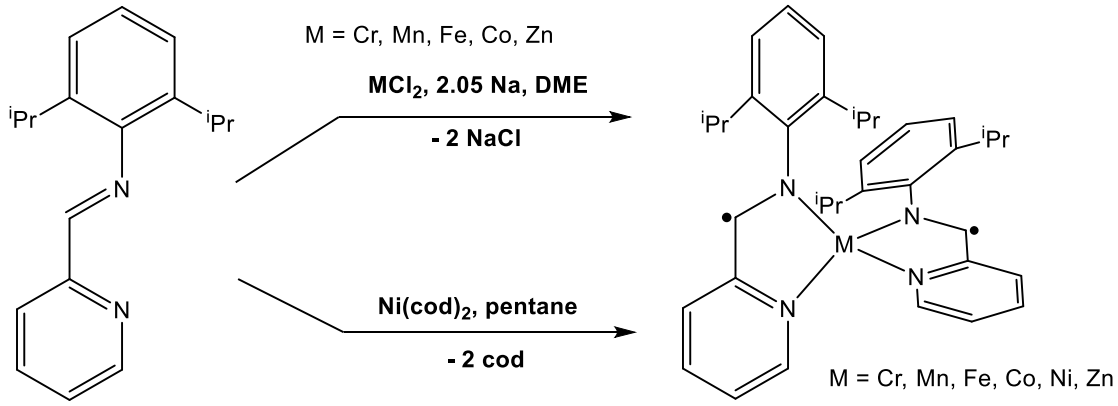

Scheme 1.1. Preparation of (α-iminopyridine)$_2$M^0 complexes

Pyridine-imine (PI) ligands chelated to metal centers are readily reduced, and metal complex structural parameters are indicative of one- or two-electron reduced ligand states.[48-57] Wieghardt *et al*. reported the preparation and characterization of pseudo-tetrahedral (α-iminopyridine)$_2$M$^{0/+1}$ (M = Cr, Mn, Fe, Co, Ni, Zn).[48] As Scheme 1.1 indicates, metalation of an α-iminopyridine with MCl_2, followed by reduction with Na^o, yields the neutral four-coordinate species. Treatment of Ni(cod)$_2$ with 2 equiv. of the iminopyridine was suitable for preparation of the Ni variant. Structural analysis confirms the oxidation state of the ligands to be consistent with radical anions. Temperature-dependent plots of the effective magnetic moments for each metal complex confirm divalent metal centers, and Mössbauer parameters of the Fe species are consistent with a high-spin Fe(II) center (δ = 0.75 mm s^{-1}; ΔE_Q = 1.29 mm s^{-1}).

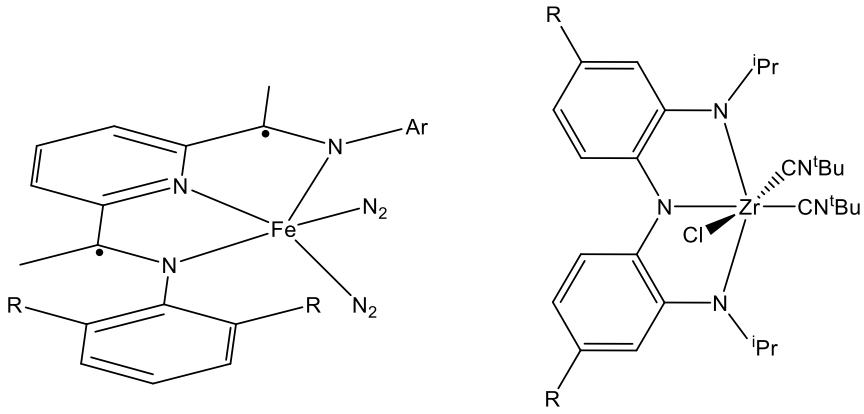

Figure 1.1. Transition metal complexes incorporating RNI ligands developed by Chirik *et al*. (left) and Heyduk *et al*. (right)

Additional RNI ligand scaffolds have been employed by Chirik and Heyduk to generate new metal complexes that are effective precatalysts for a range of organic transformations, such as hydrogenations,[20,22,24-26] olefin polymerizations[31-33] and group transfer reactions[41-47] (Figure 1.1). The redox non-innocence of the ligands has been implicated in the reaction mechanisms for most of these reactions.

Pyridine-imine ligand frameworks have been a focus for RNI behavior within this research group.[58-65] Lindley *et. al.* reported on transition-metal mediated cyclization of bis-ene-amide complexes to form indolamides.[66] Complexes of the formulation {κ-*N*,*N*-N-(2,6-$^{i}Pr_2C_6H_3$)C(=CH_2)-2-pyridyl)M (M = Cr, Mn, Fe, Co(py)) were observed to cyclize upon heating to 140 ^{o}C, a process that was also found to be operative for precursor Li-ene-amides at similar temperatures (Scheme 1.2). Computational and kinetics experiments confirm the CC bond forming step to be rate-determining ($\Delta H^{\ddagger}$ = 26.9(2) kcal mol^{-1}), yet the actual barrier to CC coupling is quite

small. The intermediate HAT product is at such a high energy its ΔH^{o} constitutes the primary component of the activation enthalpy. Prior art in metal-templated indolamide formation employing (pyridine-diimine)Rh(I) azide and (nacnac)Fe(III) imido complexes, was interpreted as a HAT process.[67,68] While a similar hydrogen transfer process may be present in the M-ene-amide cyclizations, it occurs within a preequilibrium, and CC bond formation is the rate-determining step.

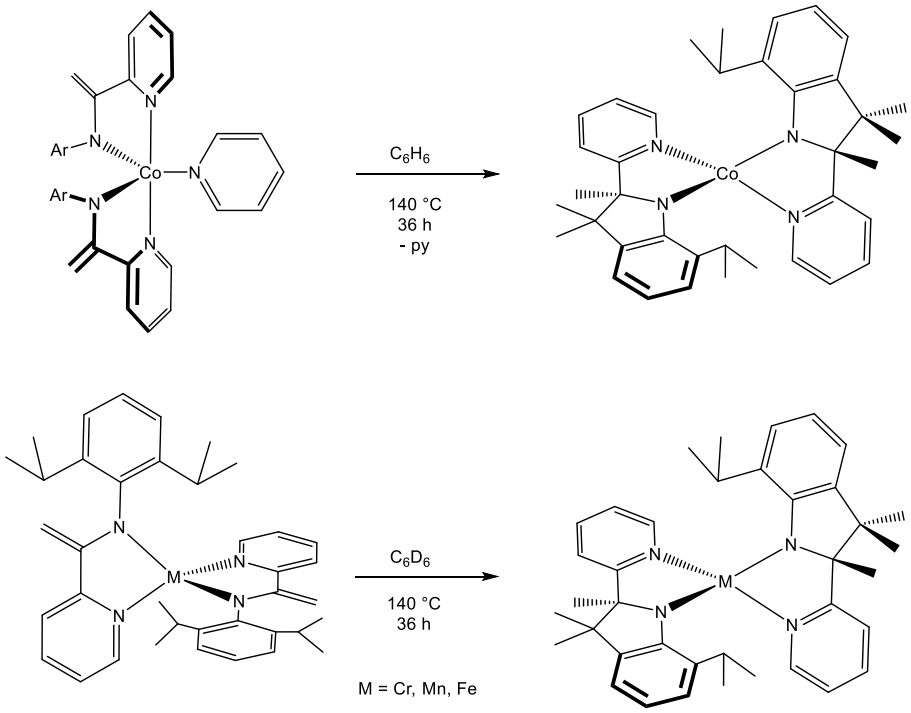

Scheme. 1.2. Metal-mediated indolamide cyclizations of bis-ene-amide complexes

The formation of a new quaternary CC bond in the aforementioned ene-amide cyclizations prompted studies into triggering CC bond formations involving ene-amide $C{=}CH_2$ functionalities. Intramolecular coupling of the alkene for the prior bis-ene-amide complexes was not realized, likely due to the conflicting orientation of the alkenes. Bulky, monodentate ene-amides were envisaged to be more competent

towards CC coupling by positioning the alkene groups in closer proximity due to sterics of the ligand.

The preparation of low-coordinate amide complexes have been reported with regular frequency.[69-72] In addition, base metal-mediated CC coupling featuring Fe, for example, has received considerable attention with respect to stoichiometric and catalytic applications in organic synthesis.[7-10] We report the preparation of the ene-amide complexes $\{(2,6\text{-}^{i}Pr_2\text{-}C_6H_3)(1\text{-}^{c}Hexenyl)N\}_2M$ (M = Cr, **1**-Cr; $FePMe_3$, **2**-Fe; $Copy_2$, **3**-Co). Both **1**-Cr and **2**-Fe were found to exhibit CC coupling of the ene-amide group to furnish 1,4-diimines or pyrroles in relatively good yields upon treatment with MCl_3 as suitable oxidants. **2**-Fe exhibited a unique β-arylation of the ene-amide at the carbon center exclusively, and corresponding catalysis of this process employing the Li-ene-amide was observed to proceed with relatively modest turnovers.

Results and Discussion

1.1 Synthesis of Ligands and Transition Metal Ene-amides

A series of aryl imines were synthesized through standard condensation protocols, either (a) employing TsOH as an acid catalyst with a Dean-Stark trap or (b) through treatment of the reaction mixture with 4 Å molecular sieves as drying agents (Scheme 1.3). Cyclic ketones and alkyl phenyl ketones were condensed with aniline or 2,6-disubstituted anilines. Aniline based condensations were capable of being driven merely by drying the solution with molecular sieves, while the 2,6-disubstituted aniline condensations required acid-catalysis to effect imine formation. The imine products were either distilled or recrystallized to afford pure compounds in relatively

good yields (34-87%). Deprotonation of the imines could be done using either ^{n}BuLi or LDA. The former base was observed to attack the C=N unit of PhN=C(CH_2)$_5$, so LDA was chosen for unsubstituted aryl imines, while ^{n}BuLi was suitable for deprotonation of disubstituted aryl imines.

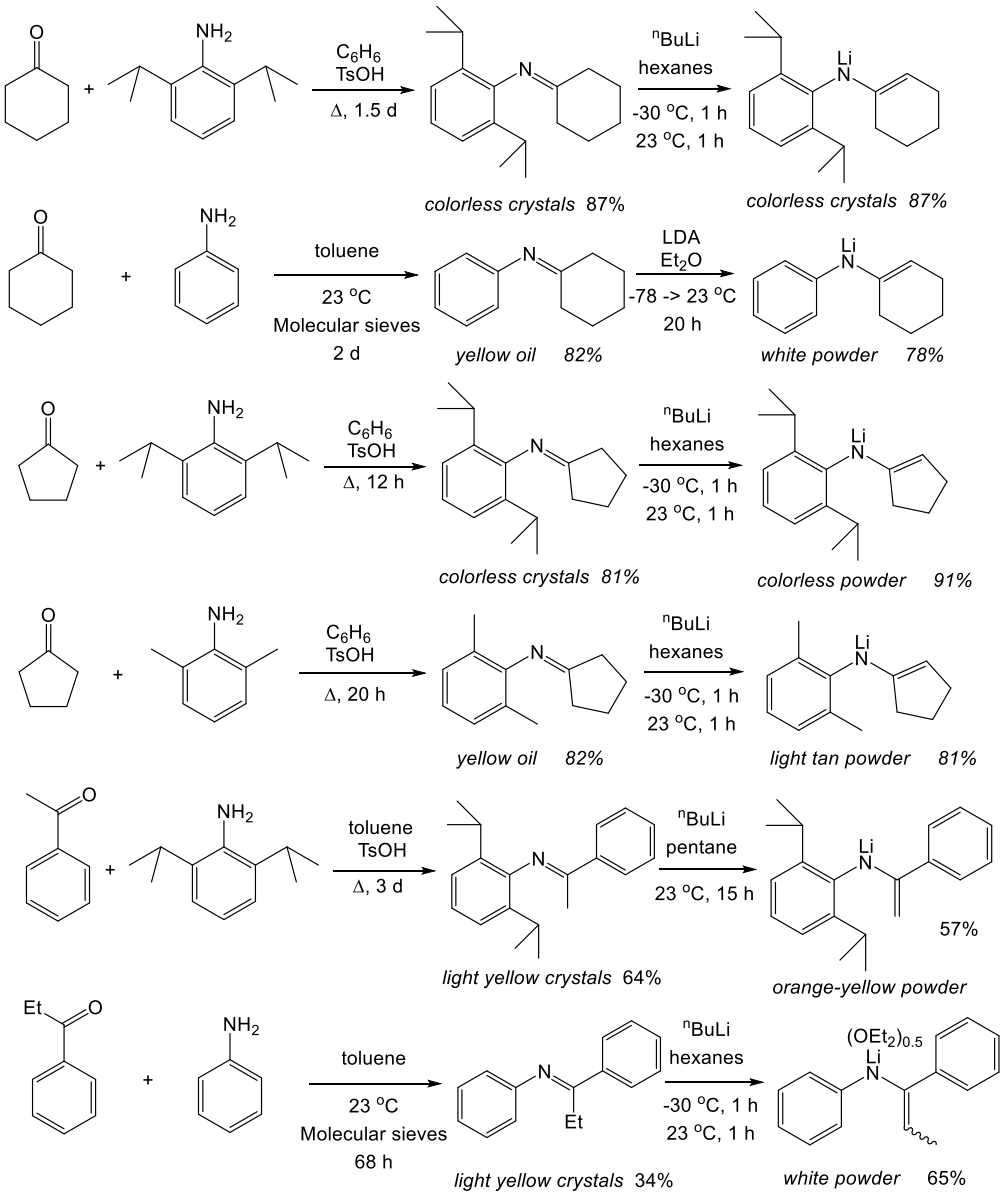

Scheme 1.3. Synthesis of imines and corresponding Li-ene-amides

Initial attempts to synthesize ene-amide complexes of first row transition metals focused on Cr, Mn, Fe, Co and Ni. It was found that treating 2 equiv. of {(2,6-^{i}Pr-C_6H_3)(1-^{c}Hexenyl)N}Li with $FeCl_2$, $CoCl_2$ or $CoCl_2(PMe_3)_2$ yielded intractable mixtures of broad, diamagnetic products, with no observable paramagnetic species present. Additionally, treatment of {(2,6-^{i}Pr-C_6H_3)(1-^{c}Hexenyl)N}Li with $MnCl_2$ lead to a faint yellow solid that was composed of several organic products and several broad paramagnetically shifted resonances. Attempts to grow crystals of the unknown product were unsuccessful, and the pursuit of a Mn complex was subsequently abandoned. Lastly, treatment of {(2,6-^{i}Pr-C_6H_3)(1-^{c}Hexenyl)N}Li with $NiCl_2$(DME) or $NiCl_2$ generated red-orange residues, with ^{1}H NMR spectra showing a complex mixture of diamagnetic products had been produced for each Ni starting material. Difficulties in isolating a clean product led to investigating alternative transition metal starting materials.

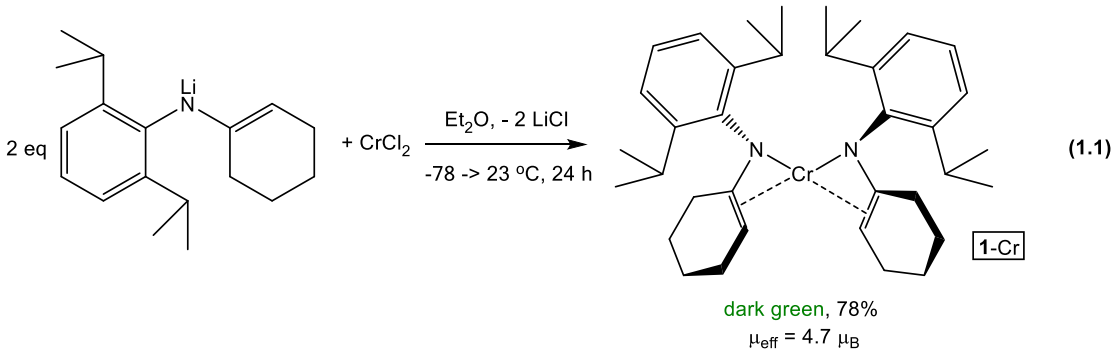

(1.1)

Treatment of 2 equiv. of {(2,6-^{i}Pr-C_6H_3)(1-^{c}Hexenyl)N}Li with $CrCl_2$ in diethyl ether at -78 °C led to the formation of {(2,6-^{i}Pr$_2$-C_6H_3)(1-^{c}Hexenyl)N}$_2$Cr (**1**-Cr) as dark green crystals in 78% yield (Eq. 1.1). Magnetic measurements of **1**-Cr were carried out using by Evans' method,[73] which provided a μ_{eff} of 4.7 μ_B. This value

is consistent with a high spin S = 2 Cr(II) center, with slight attenuation of the spin-only value due to spin-orbit coupling of the d^4 Cr center.

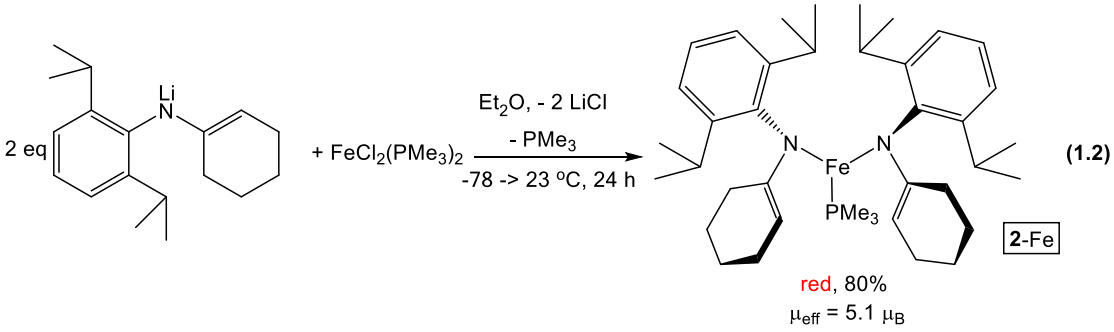

(1.2)

In surveying Fe starting materials, it was found that {(2,6-^{i}Pr-C_6H_3)(1-^{c}Hexenyl)N}Li successfully metalated with $FeCl_2(PMe_3)_2$ in C_6H_6 at 23 °C to yield {(2,6-^{i}Pr$_2$-C_6H_3)(1-^{c}Hexenyl)N}$_2$FePMe$_3$ (**2**-Fe) as red crystals in 80% yield (Eq. 1.2). Evans' method measurements[73] of **2**-Fe afforded a μ_{eff} of 5.1 μ_B, a value that is slightly greater than the spin-only value predicted for an S = 2 Fe(II) center. This observation is consistent with modest spin-orbit coupling of the d^6 Fe center.

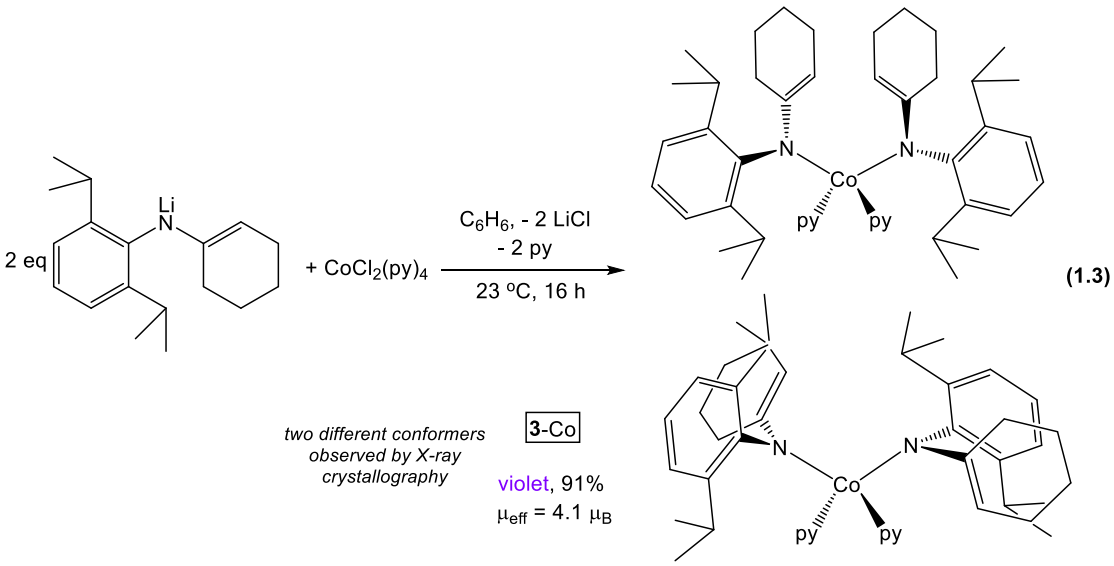

(1.3)

Use of $CoCl_2py_4$ allowed for productive metalation with {(2,6-^{i}Pr-C_6H_3)(1-^{c}Hexenyl)N}Li, furnishing {(2,6-^{i}Pr$_2$-C_6H_3)(1-^{c}Hexenyl)N}$_2$Copy$_2$ (**3**-Co) as dark violet crystals in 91% yield (Eq. 1.3). Magnetism studies of **3**-Co done by Evans' method[73] yielded a μ_{eff} of 4.1 μ_B. This is consistent with an S = 3/2 spin center that features considerable spin-orbit coupling.

1.2 X-Ray Crystal Structures of 1-Cr

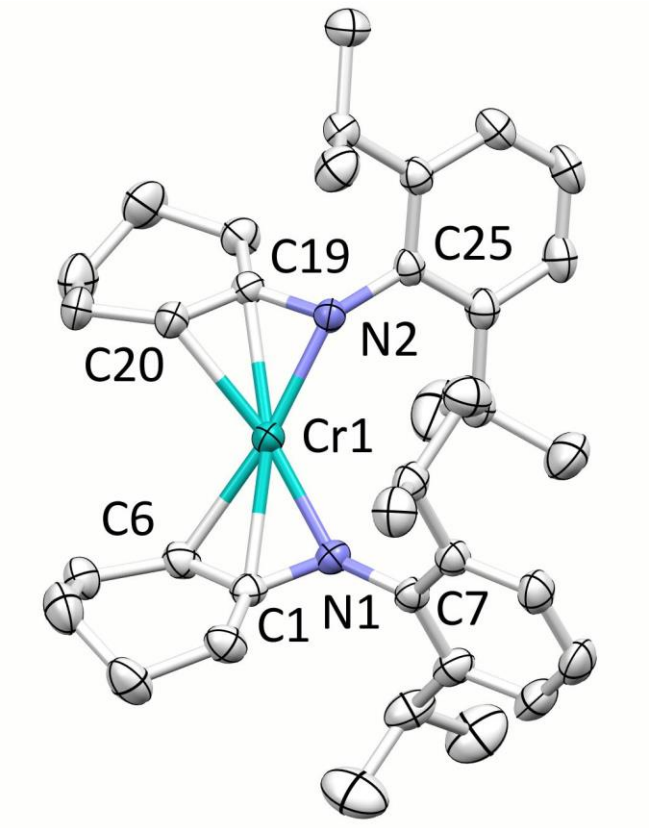

Figure 1.2. Molecular view of {(2,6-^{i}Pr$_2$-C_6H_3)(1-^{c}Hexenyl)N}$_2$Cr (**1**-Cr) and selected interatomic distances (Å) and angles (^{o}): Cr-N1, 2.0131(11); Cr-N2, 2.0217(11); Cr-C1, 2.3040(13); Cr-C6, 2.2622(14); Cr-C19, 2.2859(13); Cr-C20, 2.2619(14); N1-C1, 1.3527(17); C1-C6, 1.3884(19); N2-C19, 1.3637(16); C19-C20, 1.3766(19); N1-C7, 1.4238(16); N2-C25, 1.4156(16); N1-Cr-N2, 124.75(4); N1-C1-C6, 116.17(12); N1-Cr-C19, 158.52(5); N1-Cr-C20, 165.62(5); N2-C19-C20, 117.23(12); N2-Cr-C1, 158.14(5); N2-Cr-C6, 165.68(5); C1-Cr-C19, 165.10(5); C1-Cr-C20, 131.46(5); C6-Cr-C19, 131.11(5); C6-Cr-C20, 105.91(5).

Crystals of {(2,6-^{i}Pr$_2$-C$_6$H$_3$)(1-^{c}Hexenyl)N}$_2$Cr (**1**-Cr) suitable for X-ray diffraction studies were obtained by slow evaporation of a concentrated pentane solution. The structure of **1**-Cr is shown in Figure 1.2, with pertinent metrics in the caption, while additional crystallographic information is included in Table 1.1. **1**-Cr features a C_2 η_3-di-1-azaallyl structure that is comparable to Hanusa's Cr^{II}(allyl)$_2$ species.[74,75] The N–C bond lengths corroborate the observed conjugation of the ene-amide in that the ene-amide N–C(sp^2) bond (av. 1.358(8) Å) is shorter than the corresponding N–C(aryl, sp^2) bond (av. 1.420(6)). The olefin bond distance (av. 1.383(8)) is only slightly longer than has been reported for alkenes,[76] making it difficult to ascribe any lengthening to π-backbonding. The widened N1–Cr–N2 angle (124.75(4)^o) relative to C6–Cr–C20 (105.91(5)^o) is likely due to the difference in the Cr–N (av. 2.017(6) Å) and Cr–C (av. 2.262(2) and 2.296(13) Å) bond distances. The widened N1–Cr–N2 angle has been observed for prior examples of two-coordinate Cr amides such as Power's Cr{N(H)(C$_6$H$_5$-2,6(C$_6$H$_2$-2,4,6-Me$_3$)$_2$)}$_2$,[77] which exhibits a bent N–Cr–N angle of 120.9(5)^o. In addition, Power's complex features Cr---C (2.2337(4) and 2.485(5) Å) interactions to the *ipso* carbons of the mesityls of the terphenyl group (Figure 1.3).

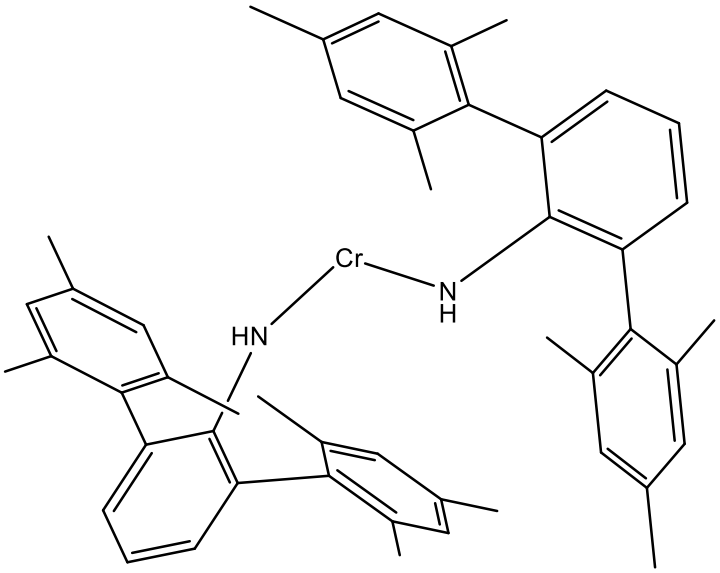

Figure 1.3. Molecular structure of Power's Cr{N(H)Ar^{Me6}}$_2$ complex[77]

1.3 X-Ray Crystal Structures of 2-Fe

Crystals of {(2,6-^{i}Pr$_2$-C$_6$H$_3$)(1-^{c}Hexenyl)N}$_2$FePMe$_3$ (**2**-Fe) suitable for X-ray diffraction studies were obtained by slow evaporation of a concentrated pentane solution at -30 ^{o}C, and the structure is shown in Figure 1.4. The molecule exhibits C_{2v} symmetry, with core angles as follows: N3–Fe–N4 = 136.52(10)^{o}, N4–Fe–P2 = 112.84(7)^{o} and N3–Fe–P2 = 110.60(8)^{o}. The difference in the observed N-Fe-P angles is modest, and likely contributes little angular distortion. In comparison, the amides are twisted by 39.4^{o} from one another, a significant distortion from C_{2v} symmetry. The ene-amide C=C bond lengths average 1.331(4) Å, shortened from the analogous bond in **1**-Cr, and more akin to that of a double bond.[76] In addition, the C–N distances of the ene-amides have elongated to 1.402(4) and 1.401(4) Å relative to **1**-Cr. Taken together, these metrics support an η_1-di-ene-amide, which is further supported by the long Fe-olefin distances (>2.95 Å).

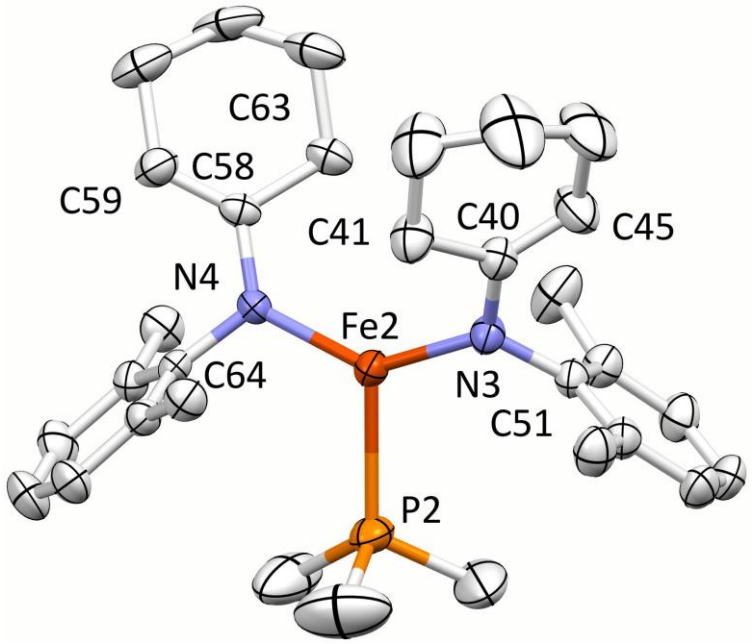

Figure 1.4. Molecular view of one of two inequivalent {(2,6-$^{i}Pr_2$-C_6H_3)(1-^{c}Hexenyl)N}$_2$FePMe$_3$ (**2**-Fe) molecules and selected interatomic distances (Å) and angles (^{o}): Fe2-N3, 1.920(2); Fe2-N4, 1.927(2); Fe2-P2, 2.4490(9); N3-C40, 1.402(4); N3-C51, 1.427(3); C40-C41, 1.502(4); C40-C45, 1.329(4); C58-C63, 1.508(4); N3-Fe2-N3, 136.53(10); N3-Fe2-P2, 110.59(7); N4-Fe2-P2, 112.84(7); Fe2-N3-C40, 124.23(18); Fe2-N3-C51, 118.06(18); C40-N3-C51, 116.9(2); Fe2-N4-C58, 127.19(18); Fe2-N4-C64, 115.26(16); C58-N4-C64, 117.5(2).

1.4 X-Ray Crystal Structures of 3-Co

Crystals of {(2,6-$^{i}Pr_2$-C_6H_3)(1-^{c}Hexenyl)N}$_2$Copy$_2$ (**3**-Co) suitable for X-ray diffraction studies were obtained by slow evaporation of a concentrated ether solution, with Figure 1.5 showing the structure and pertinent metrics. The asymmetric unit contains two molecules, each in a particular conformation. The conformer that contains Co1 features rough eclipsing of the CNC fragment of the ene-amides, while the Co2 conformer features the same CNC fragment in a staggered orientation. Despite the different conformers present, both molecules exhibit C_2 symmetry. For both configurations, d(Co–N_{am}) and d(Co–N_{py}) average 1.952(9) and 2.117(22) Å

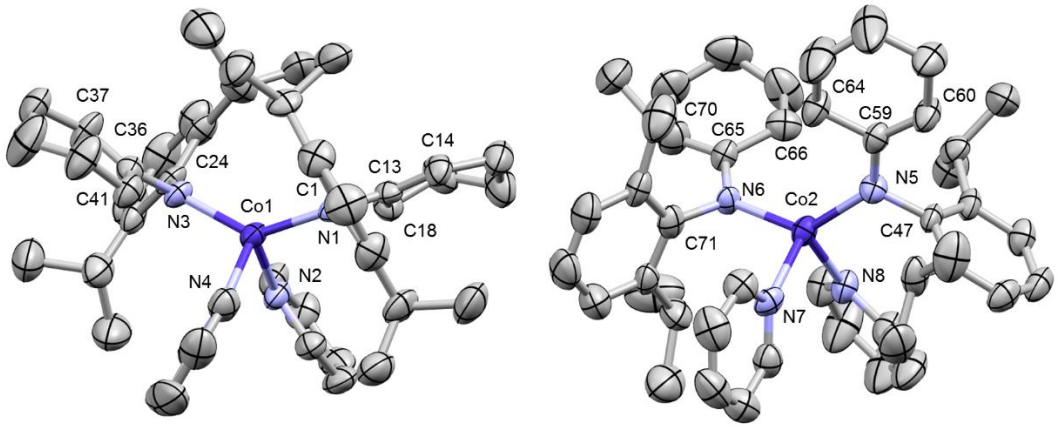

Figure 1.5. Molecular view of two inequivalent {(2,6-$^{i}Pr_2$-C_6H_3)(1-^{c}Hexenyl)N}$_2$Copy$_2$ (**3**-Co) molecules and selected interatomic distances (Å) and angles (^{o}): Co1-N1, 1.954(5); Co1-N2, 2.145(5); Co1-N3, 1.941(5); Co1-N4, 2.108(6); N1-C1, 1.427(7); N3-C24, 1.421(8); N1-C13, 1.429(7); N3-C36, 1.422(7); C13-C14, 1.332(8); C13-C18, 1.486(8); C36-C37, 1.346(8); C36-C41, 1.495(8); N1-Co1-N2, 102.3(3); N1-Co1-N3, 135.2(2); N1-Co1-N4, 107.2(2); N2-Co1-N3, 106.6(2); N2-Co1-N4, 95.5(2); N3-Co1-N4, 103.3(2); Co2-N5, 1.963(5); Co2-N6, 1.949(4); Co2-N7, 2.093(5); Co2-N8, 2.122(5); N5-C59, 1.391(7); N5-C47, 1.436(7); C59-C60, 1.340(8); C59-C64, 1.491(8); N6-C65, 1.397(7); N6-C71, 1.422(7); C65-C66, 1.494(8); C65-C70, 1.338(8); N5-Co2-N6, 131.5(2); N5-Co2-N7, 113.1(2); N5-Co2-N8, 104.4(2); N6-Co2-N7, 99.03(19); N6-Co2-N8, 106.4(2); N7-Co2-N8, 97.6(2).

respectively. Conversely, the eclipsed conformer opens up N1–Co1–N3 to 135.2(2)^{o} relative to staggered conformer N5–Co2–N6 angle of 131.5(2)^{o}. This leads to a compression of N2–Co1–N4 angle relative to N7–Co2–N8 (95.5(2)^{o} vs 97.6(20)^{o}, respectively). The ene-amide C=C bond lengths average 1.339(6) Å, comparable to **2**-Fe and shorter than **1**-Cr, signifying no conjugation of the ene-amide.

Table 1.1. Select crystallographic and refinement data for {(2,6-$^{i}Pr_2$-C_6H_3)(1-^{c}Hexenyl)N}$_2$Cr (**1**-Cr), {(2,6-$^{i}Pr_2$-C_6H_3)(1-^{c}Hexenyl)N}$_2$FePMe$_3$ (**2**-Fe) and {(2,6-$^{i}Pr_2$-C_6H_3)(1-^{c}Hexenyl)N}$_2$Copy$_2$ (**3**-Co) and **EA$_2$**.

	1-Cr	**2**-Fe	**3**-Co	**EA$_2$**
formula	$C_{36}H_{52}CrN_2$	$C_{39}H_{61}FeN_2P$	$C_{46}H_{62}CoN_4$	$C_{36}H_{52}N_2$
formula wt	564.80	644.72	729.93	512.80
space group	$P\bar{1}$	$P\bar{1}$	$P2_1/n$	$C2/c$
Z	2	4	4	4
a, Å	11.320(2)	10.3180(5)	10.6653(10)	15.550(6)
b, Å	11.5351(19)	18.3944(10)	36.834(4)	9.151(5)
c, Å	13.336(3)	22.0796(11)	21.080(2)	24.380(11)
α, deg	87.146(8)	68.324(3)	90	90
β, deg	82.848(9)	78.952(3)	97.136(4)	107.24(3)
γ, deg	70.228(7)	86.630(3)	90	90
V, Å^3	1626.5(5)	3821.7(3)	8217.1(13)	3313(3)
ρ_{calc}, g cm^{-3}	1.153	1.121	1.180	1.028
μ, mm^{-1}	0.377	0.463	0.453	0.059
temp, K	233(2)	223(2)	223(2)	296(2)
λ (Å)	0.71073	0.71073	0.71073	0.71073
R indices	R1 = 0.0388	R1 = 0.0443	R1 = 0.0575	R1 = 0.0413
$[I > 2\sigma(I)]^{a,b}$	wR2 = 0.0904	wR2 = 0.095	wR2 = 0.1234	wR2 = 0.1019
R indices^{b}	R1 = 0.0569	R1 = 0.0863	R1 = 0.1316	R1 = 0.0688
(all data)^{a}	wR2 = 0.0998	wR2 = 0.1169	wR2 = 0.1622	wR2 = 0.1181
GOF^{c}	1.034	1.009	1.068	1.002

$^{a}R_1 = \Sigma F_o| - |F_c|| / \Sigma |F_o|$. $^{b}wR_2 = [\Sigma w(|F_o| - |F_c|)^2 / \Sigma w F_o^2]^{1/2}$. ^{c}GOF (all data) $= [\Sigma w(|F_o| - |F_c|)^2/(n - p)]^{1/2}$, n = number of independent reflections, p = number of parameters.

1.5 Oxidative Coupling Reactivity of 1-Cr

Initial efforts towards triggering CC coupling of the ene-amides focused on treatment of {(2,6-$^{i}Pr_2$-C_6H_3)(1-^{c}Hexenyl)N}$_2$Cr (**1**-Cr) with oxidants. In Eq. 1.4, treatment of **1**-Cr with $CrCl_3$ effected coupling of the ene-amides to produce *rac*-2,2'-di(2,6-$^{i}Pr_2C_6H_3N=)_2$-dicyclohexane (**EA$_2$**). No observable paramagnetic species were produced, and only one organic product was produced. UV-vis spectra of the product

confirmed the presence of $CrCl_2(THF)_2$ as the byproduct of the coupling reaction, when compared to a sample of $CrCl_2$ dissolved in THF (λ_{max} = 811 nm).

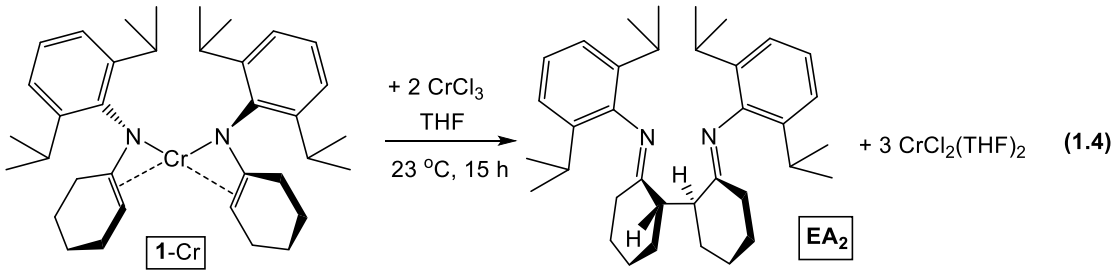

(1.4)

Synthesis of a Cr tris-ene-amide was initially pursued through treatment of $CrCl_3$ with {(2,6-^{i}Pr-C_6H_3)(1-^{c}Hexenyl)N}Li (Eq. 1.5). NMR spectroscopy confirmed the formation of **EA2**, but broad paramagnetic resonances mandated structural analysis for assignment of the Cr complex. Green-yellow dichroic crystals suitable for X-ray diffraction were grown via slow evaporation of a concentrated pentane solution. Structural analysis of the crystals confirmed it as **1**-Cr, albeit as a monoclinic polymorph. A potential pathway to make the observed products may involve initial formation of {(2,6-^{i}Pr$_2$-C_6H_3)(1-^{c}Hexenyl)N}$_2$CrCl, followed by disproportionation to make **1**-Cr and {(2,6-^{i}Pr$_2$-C_6H_3)(1-^{c}Hexenyl)N}$_2$$CrCl_2$, which could then oxidatively couple the ene-amides to make **EA2**. To corroborate suspicions as to the stability of any Cr(III) ene-amide complexes, treatment of $CrCl_3$ with 2 equiv.

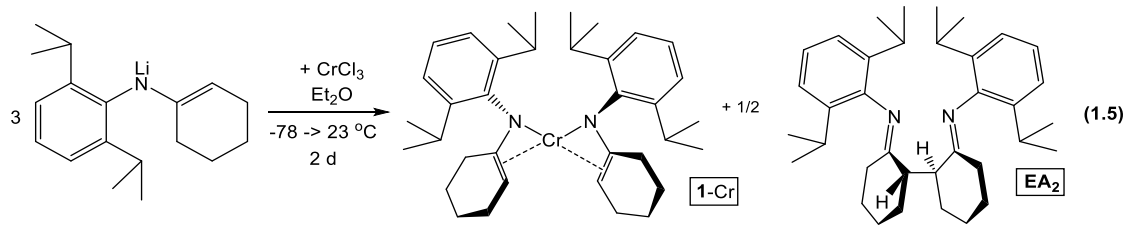

(1.5)

of {(2,6-^{i}Pr-C_6H_3)(1-^{c}Hexenyl)N}Li led to formation of **EA2** (Eq. 1.6). Given the reasonable yield of the CC coupling of the Li-ene-amide, in conjunction with the inexpensive cost of $CrCl_3$, subsequent Cr-mediated CC coupling studies were pursued using $CrCl_3$ as the oxidant.

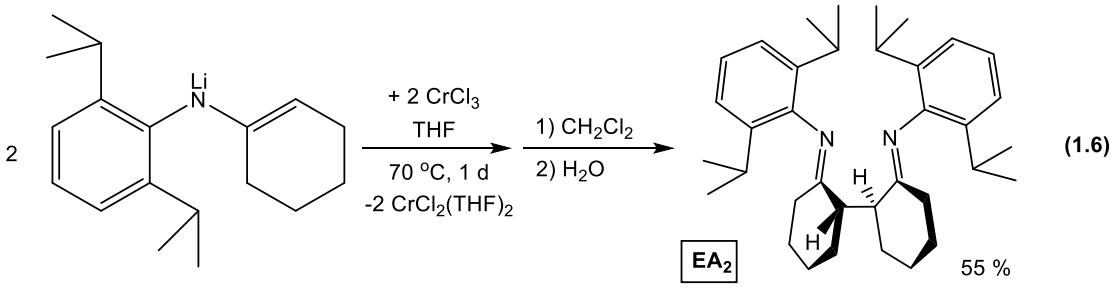

(1.6)

The stereochemistry of **EA2** could not be determined through NMR spectroscopy, given that the spectrum was consistent with either the *rac*- or the *meso*-isomers. Hydrolysis of **EA2** employing TsOH as the acid of choice, in an attempt to correlate the product to the known corresponding diketone, resulted in formation of dicyclohexyl 2,6-diisopropylphenyl pyrrole via Paal-Knorr pyrrole cyclization (Eq. 1.7). Paal-Knorr pyrrole syntheses employ protic conditions to form hemiaminals from 1,4-diketones and primary amines, which subsequently undergo dehydration to yield

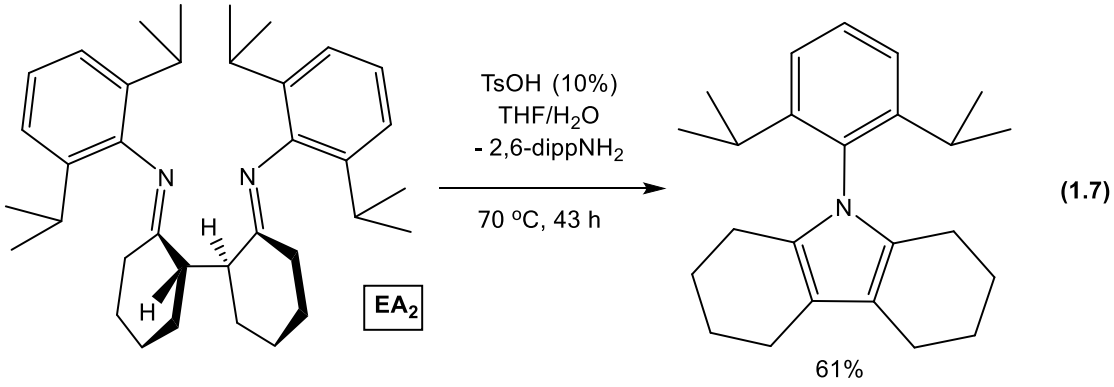

(1.7)

the heterocycles.[78-80] Since the stereochemical site of **EA2** was lost in the course of hydrolysis, the C_2-stereochemistry was proven via X-ray diffraction, with the structure of **EA2** shown in Figure 1.6. The metrics of **EA2** were consistent with expected values for organic molecules, with no significant deviations observed.[76]

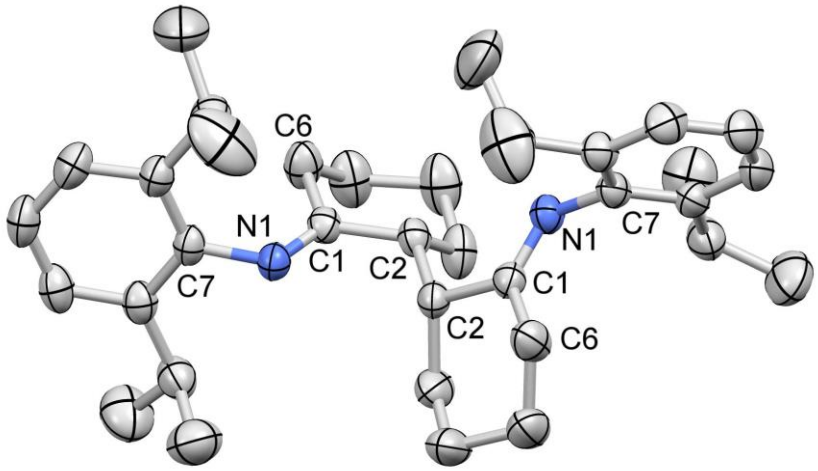

Figure 1.6. Molecular view of **EA2** with selected interatomic distances (Å) and angles(°): N1-C1, 1.273(2); N1-C7, 1.4254(19); C1-C2, 1.515(2); C1-C6, 1.522(2); C2-C2A, 1.539(3); C1-N1-C7, 120.86(13); N1-C1-C6, 125.33(14); N1-C1-C2, 119.38(14); C1-C2-C2A, 113.78(16).

Additional couplings were evaluated to determine the scope of the CC coupling process (Scheme 1.4). After the specified amount of time, the reaction mixtures were subjected to an aqueous workup, and extracted with CH_2Cl_2 to remove LiCl and Cr byproducts. The organic solution was then evaporated to yield the organic products in good yields and high purity, making for a simple approach towards the synthesis of 1,4-diimines and pyrroles. $CrCl_3$ oxidation of cyclic {(2,6-$^{i}Pr_2$-C_6H_3)(1-^{c}Pentenyl)N}Li produces the coupled product in 68% yield, comparable to that observed for **EA2**. Acyclic {(2,6-$^{i}Pr_2$-C_6H_3)(C=CH_2(Ph))N}Li successfully couples to

a modest extent (23% yield) with extended reaction time, showing that the coupling methodology is not limited to cyclics. In examining Li-ene-amides that feature reduced sterics on the aryl-amide group, the aqueous workup resulted in hydrolysis to form pyrroles.[78-80] Cyclic {Ph(1-^{c}Hexenyl)N}Li and acyclic

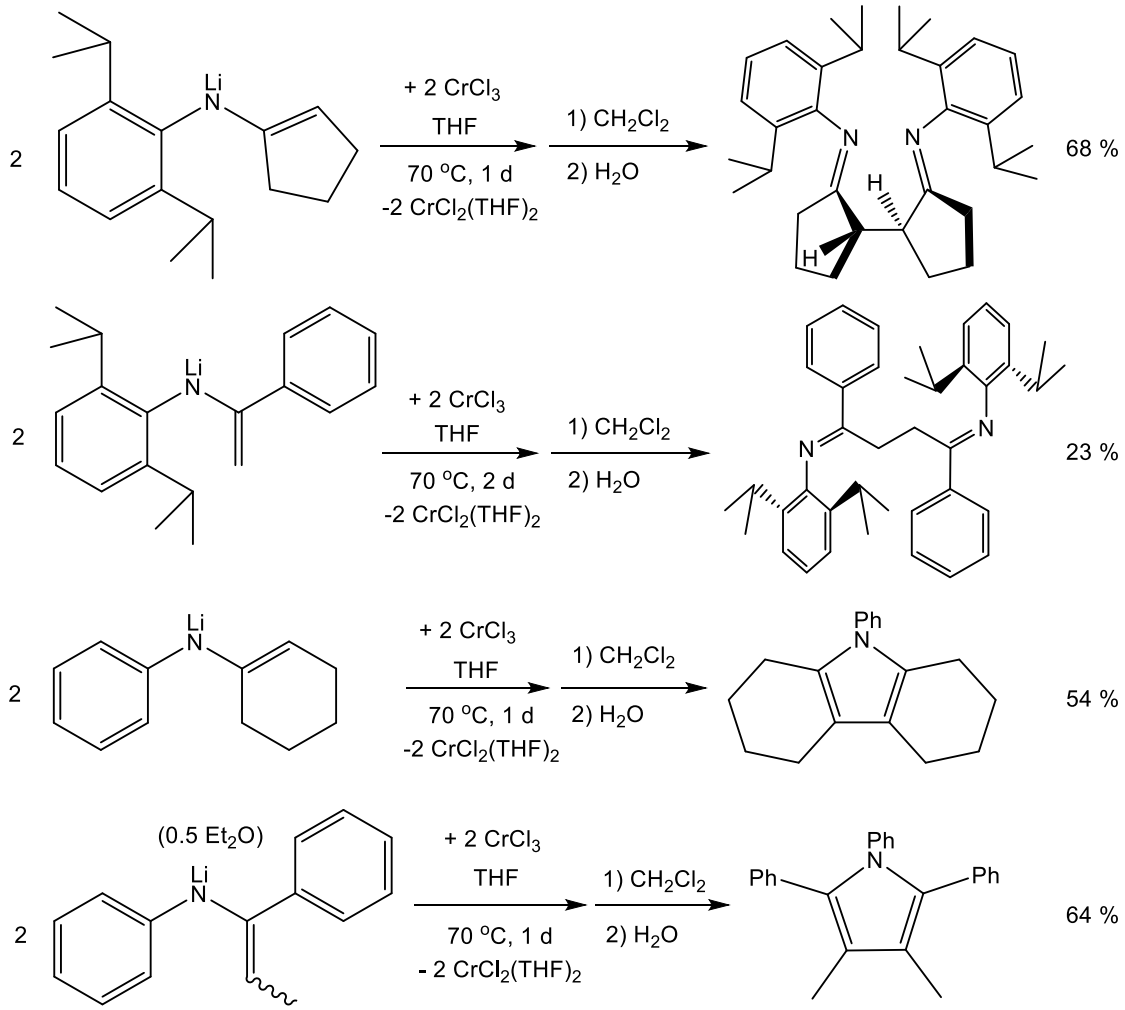

Scheme 1.4. Generality of CC coupling protocol

{(C_6H_5)(C=CHCH$_3$(Ph))N}Li·(Et_2O)$_{0.5}$ were shown to yield their corresponding products dicyclohexyl-N-phenyl pyrrole (54%) and 3,4-dimethyl-1,5-diphenyl-N-phenyl pyrrole (64%) upon aqueous workup, both in good yields. Preparation of 1,4-diketones via hydrolysis of 1,4-diimines was not feasible due to alternate pyrrole cyclizations that are difficult to circumvent with this developed method.

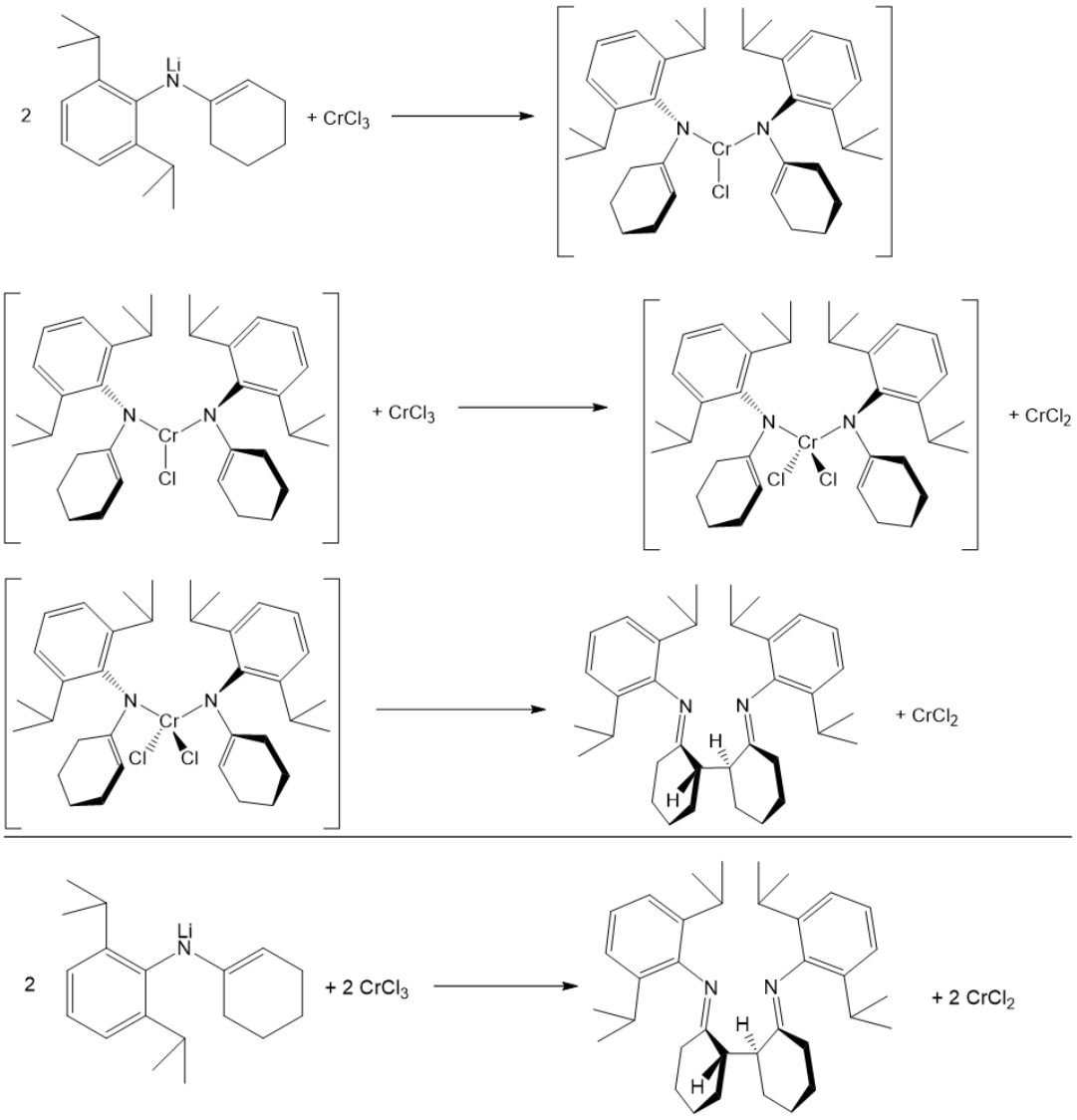

Scheme 1.5. Mechanism for Cr(II)/Cr(IV) ene-amide coupling

Scheme 1.5 illustrates the postulated mechanism for the Cr ene-amide coupling pathway. Due to the broad, paramagnetic resonances for **1**-Cr, definitive assignments of intermediates by NMR spectroscopy are limited, and as such, mechanistic studies are predicated on stoichiometric probes. It was envisaged that initial formation of $\{(2,6\text{-}^{i}Pr_2\text{-}C_6H_3)(1\text{-}^{c}Hexenyl)N\}_2CrCl$ may undergo chlorine atom transfer from $CrCl_3$ via a $\{(2,6\text{-}^{i}Pr_2\text{-}C_6H_3)(1\text{-}^{c}Hexenyl)N\}_2CrC(\mu\text{-}Cl)_2CrCl_2$ binuclear species, producing $CrCl_2$ and a transient $\{(2,6\text{-}^{i}Pr_2\text{-}C_6H_3)(1\text{-}^{c}Hexenyl)N\}_2CrCl_2$. Oxidative coupling of the Cr(IV) species would generate **EA2** and $CrCl_2$. Potential disproportionation of $\{(2,6\text{-}^{i}Pr_2\text{-}C_6H_3)(1\text{-}^{c}Hexenyl)N\}_2CrCl$ may yield **1**-Cr and the transient Cr(IV) species, yet no observation of **1**-Cr was noted. If **1**-Cr is produced via disproportionation, its oxidation to the transient Cr(III) species must be rapid.

1.6 CC Coupling Reactivity of 2-Fe Compared to 1-Cr

CC coupling protocols developed for generating *rac*-2,2'-di$(2,6\text{-}^{i}Pr_2C_6H_3N=)_2$-dicyclohexane (**EA2**) from $\{(2,6\text{-}^{i}Pr_2\text{-}C_6H_3)(1\text{-}^{c}Hexenyl)N\}_2Cr$ (**1**-Cr) were applied to CC coupling reactions of $\{(2,6\text{-}^{i}Pr_2\text{-}C_6H_3)(1\text{-}^{c}Hexenyl)N\}_2FePMe_3$ (**2**-Fe). Eq. 1.8 indicates that treatment of **2**-Fe with $FeCl_3$ successfully coupled the ene-amides to yield **EA2** in only 2 h at ambient temperature in 65% yield. To assess the competence

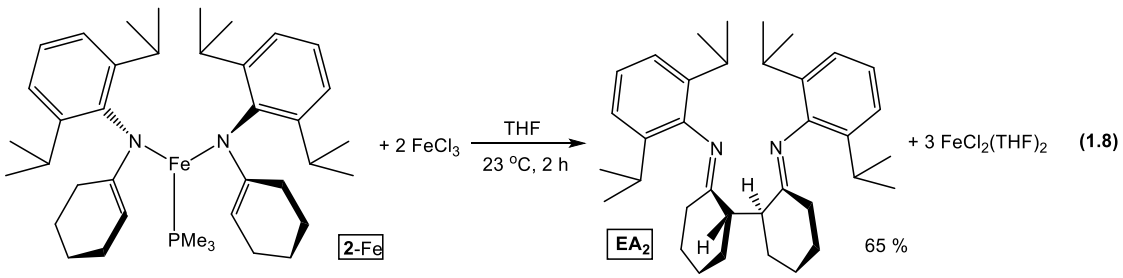

(1.8)

for stoichiometric coupling of Li-ene-amides for Fe in comparison to Cr, {(2,6-^{i}Pr-C_6H_3)(1-^{c}Hexenyl)N}Li was treated with $FeCl_3$ (Eq. 1.9). While formation of **EA$_2$** was confirmed, extended reaction time (2 days) and a lower yield (42%) limited coupling studies employing Fe to {(2,6-^{i}Pr-C_6H_3)(1-^{c}Hexenyl)N}Li, since the Cr coupling technology was more efficient. If an Fe(III) intermediate of the formulation "{(2,6-

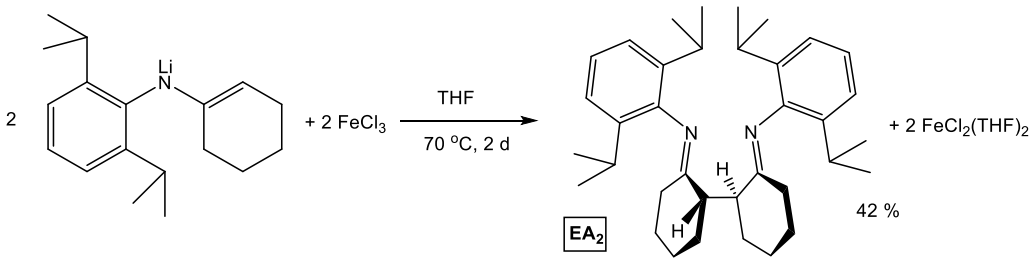

(1.9)

^{i}Pr$_2$-C_6H_3)(1-^{c}Hexenyl)N}$_2$FeCl" is formed, solubility of the species may affect the efficiency of the coupling process. Addition of 5 mol % **2**-Fe to the standard Fe coupling protocol resulted in definitive improvement to the method, with a shortened reaction time (1 day) and modestly greater yield (57%), as shown in Eq. 1.10. This improvement seems to agree with the prior solubility argument, as the greater availability of soluble Fe species should improve the efficiency of the method.

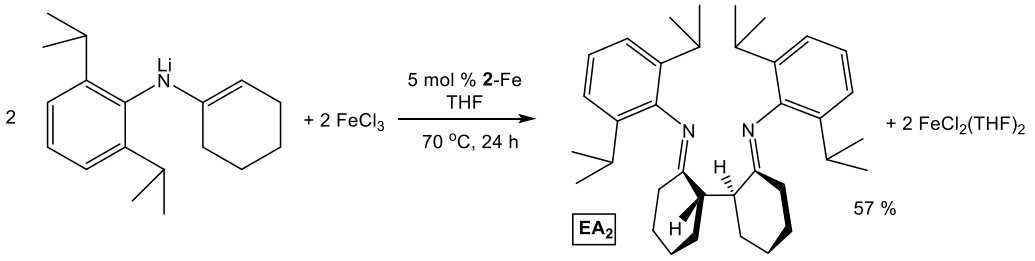

(1.10)

While $FeCl_3$ was found to promote CC ene-amide coupling with modest efficiency, coupling was also observed when **2**-Fe was exposed to $[Cp_2Fe]PF_6$, an outer sphere oxidant, as shown in Eq. 1.11. Despite the modest yield of **EA$_2$** (38%),

the result points towards an intermediate Fe(III) species that couples the ene-amides to make **EA$_2$** and an Fe(I) intermediate, which subsequently disproportionates.

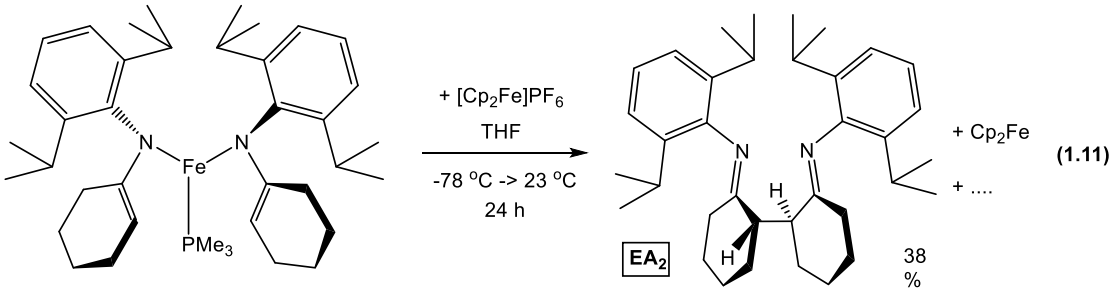

(1.11)

Given the prior CC coupling studies effected through treatment of **2**-Fe with $FeCl_3$ or $[Cp_2Fe]PF_6$, a single electron oxidant, a plausible mechanism for Fe-mediated ene-amide coupling likely utilizes an Fe(I)/Fe(III) pathway (Scheme 1.6).

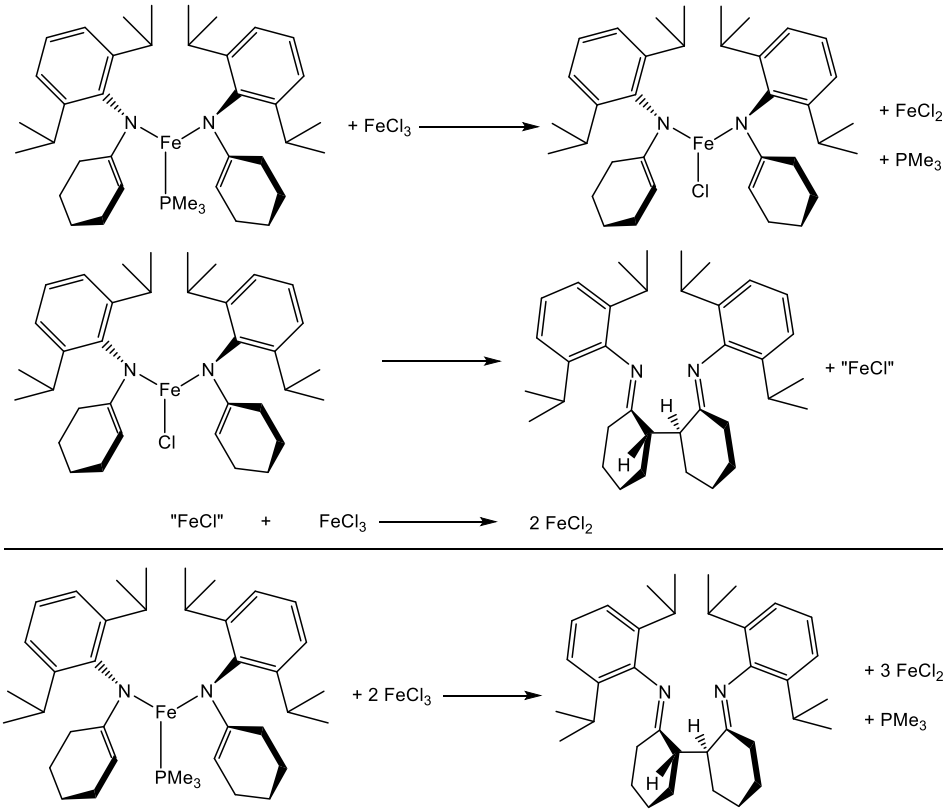

Scheme 1.6. Mechanism for Fe(I)/Fe(III) ene-amide coupling

Initial oxidation of **2**-Fe by $FeCl_3$ to yield $\{(2,6\text{-}^{i}Pr_2\text{-}C_6H_3)(1\text{-}^{c}Hexenyl)N\}_2FeCl$ can subsequently lead to ene-amide coupling to generate **EA2** and FeCl. The transient Fe(I) species can then undergo comproportionation with $FeCl_3$ to generate the $FeCl_2$ byproduct. Given the lack of **2**-Fe in the product mixture, continued oxidation to generate an Fe(IV) intermediate seems unlikely, hence the postulated Cr(II)/Cr(IV) pathway was deemed unlikely to be accessible for the Fe-mediated coupling. In contrast, while the Fe(I)/Fe(III) pathway could rationalize the observed Cr ene-amide coupling, the dearth of established Cr(I) species and precedent for Cr(IV) complexes argues against this conclusion.[81-85]

1.7 Ene-amide *β*-Arylation Mediated by 2-Fe

In surveying oxidants for triggering ene-amide coupling of **2**-Fe, an unusual *β*-arylation was observed upon exposure of $\{(2,6\text{-}^{i}Pr_2\text{-}C_6H_3)(1\text{-}^{c}Hexenyl)N\}_2FePMe_3$ (**2**-Fe) to PhBr (Eq. 1.12). As shown in Eq. 1.13, hydrolysis of the crude reaction mixture

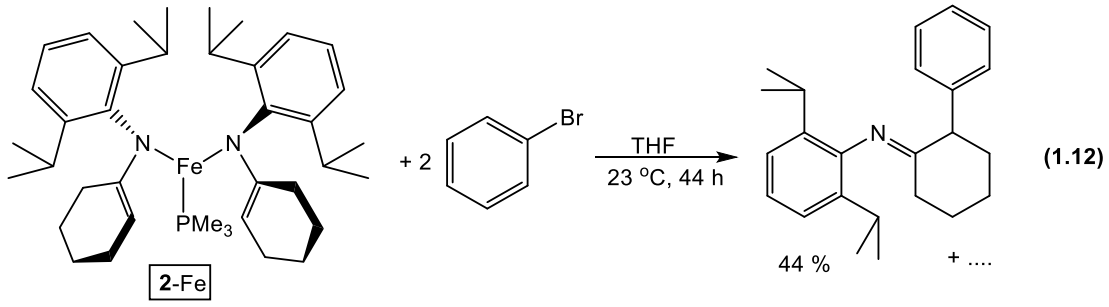

(1.12)

yielded impure 2-phenylcyclohexanone, which was correlated by NMR spectroscopy to the known ketone. In addition, its molecular ion peak was consistent with the stated ketone according to mass spectrometry. The correlation confirmed the arylation did not occur at the nitrogen atom.

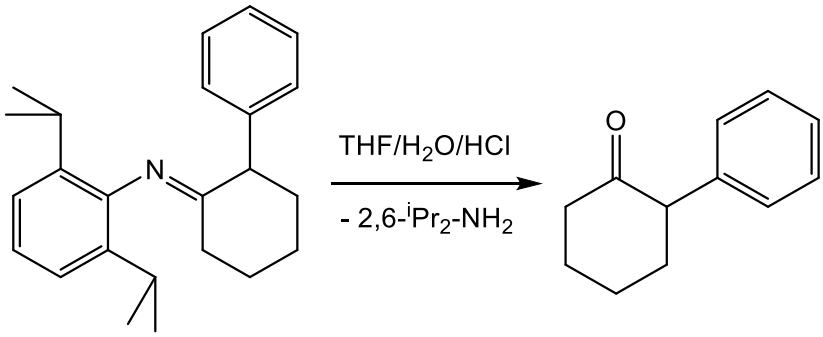

(1.13)

Table 1.2. Fe catalyst screening for β-arylation of {(2,6-^{i}Pr-C_6H_3)(1-^{c}Hexenyl)N}Li

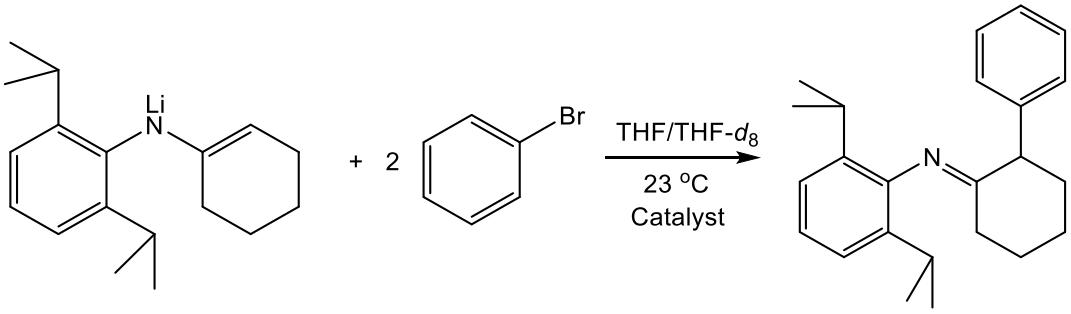

Entry	Catalyst	Mol %	Time (h)	Yield	T/O
1	**2**-Fe	10	96	44	4
2	$FeCl_2$	10	96	54	5
3	$FeCl_2(PMe_3)_2$	10	70	53	5
4	$FeCl_2(PMe_3)_2$	5	70	47	9
5	——	——	96	0	0

Fe reduction likely occurs in concert with the arylation step, and since PhBr may be a potential oxidant to generate "FeBr", catalytic arylation of Li-ene-amides was pursued. Table 1.2 summarizes the various catalysts used for successful arylation of {(2,6-^{i}Pr-C_6H_3)(1-^{c}Hexenyl)N}Li with PhBr. Entry 1 confirmed that **2**-Fe served as a suitable catalyst, with 44% (~4 TO) conversion to product observed. Despite the intractable mixture observed when attempting to metalate {(2,6-^{i}Pr-C_6H_3)(1-

^{c}Hexenyl)N}Li with $FeCl_2$, $FeCl_2$ proved to be compatible with the arylation method, generating the product in 54% (entry 2, ~5 TO) yield. Entries 3 and 4 show that the precursor to **2**-Fe, $FeCl_2(PMe_3)_2$,[86] was competent for arylation, with 53% (~5 TO) and 47% (~9 TO) yields observed, respectively. Catalyst loading could be reduced to 5 mol % with little change observed in product yields, and the reaction time was reduced to 70 h. Extending the reaction time further did not improve product yields, and leaving out the Fe catalyst led to no observable product formation, confirming the Fe-mediated nature of the reaction (entry 5).

Further investigations into additional Fe catalysts proved unsuccessful. Employing $FeBr_2(PMe_3)_2$[86] or $FeBr_3$ resulted in no product conversion, while attempted catalysis using "$Fe(PMe_3)_4$"[87] generated the parent imine exclusively. It was proposed that trace water present in the PhBr may have initiated the process, but a test reaction with {(2,6-^{i}Pr-C_6H_3)(1-^{c}Hexenyl)N}Li and PhBr in the presence of 10 mol % $FeCl_2(OH_2)_4$ resulted in production of the parent imine, with no coupled product. Repeating entry 1 of Table 1.2 with PhI only resulted in formation of 22% yield of the coupled product, nearly half that of the bromide variant. Given the lack of improvement in the β-arylation efficiency through varying the catalyst, and with modest yields observed, no further investigations were pursued.

A possible mechanism for β-arylation may involve disproportionation of **2**-Fe and $FeCl_2$ to yield an Fe(I)-amide product. Subsequent oxidative addition of the Fe(I) species with PhBr should yield an Fe(III) complex, and reductive elimination would generate the arylated product and FeBr.

An alternative radical chain mechanism is provided in Scheme 1.7. FeX (formed via disproportionation of FeX_2) could oxidatively add PhBr to generate an Fe(III) species. If phenyl radical is lost, it may oxidize **2**-Fe to form the bis-ene-amide Fe(III)-phenyl complex. The arylated product could be formed through elimination, yielding Fe(I)-amide as the byproduct. Subsequent addition of PhBr and loss of phenyl radical would then continue propagating the radical chain process for generation of the organic product.

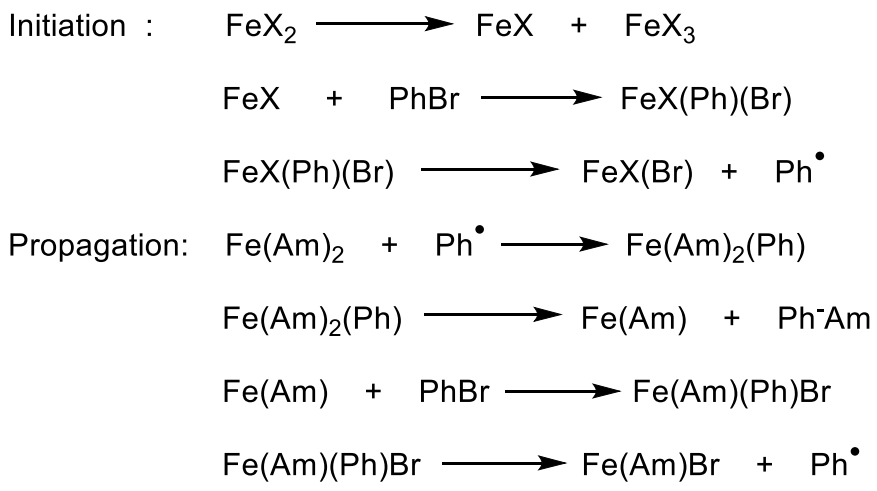

Scheme 1.7. Chain radical mechanism for arylation of **2**-Fe

The latter mechanistic scenario relates closely to radical pathways initially suggested by Kochi.[88-90] A considerable number of investigations into Fe cross-coupling reactions also invoke radical pathways.[91-96] Due to the modest nature of the catalysis in this report, mechanistic studies were not pursued, so discussions were deemed to be speculative.

1.8 Oxidation Studies of 3-Co

Attempts to induce CC coupling from {(2,6-^{i}Pr$_2$-C$_6$H$_3$)(1-^{c}Hexenyl)N}$_2$Copy$_2$ (**3**-Co) were based mostly on the use of organic oxidants, given the lack of accessible, inexpensive Co(III) oxidants. Treatment of **3**-Co with tert-butyl chloride or iodide resulted in formation of the parent imine and Co(II) halide byproducts (Eq. 1.14). Dehydrohalogenation of *tert*-butyl chloride to isobutylene could generate $CoCl_2$ and the parent imine, although it was not feasible to observe isobutylene since the reactions were conducted on small pot scale. Quantitative formation of the parent imine and $CoCl_2$ was observed upon treating **3**-Co with $SnCl_4(THF)_2$. Exposure of **3**-Co to PhBr resulted in no observed *β*-arylation product, and only slight decomposition to the parent imine. None of the above reactions showed evidence of CC coupling products.

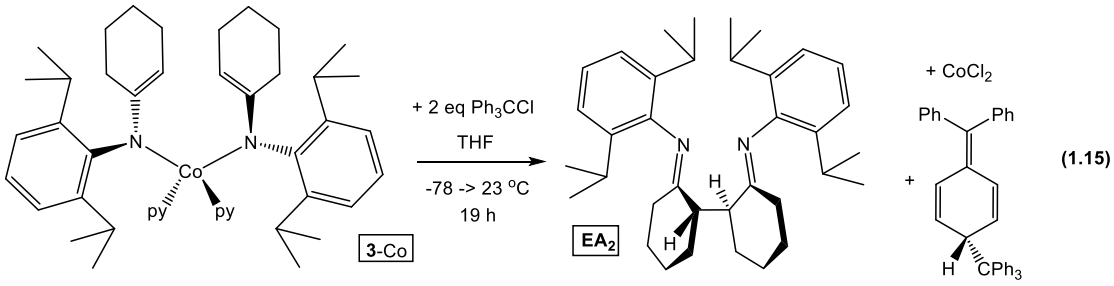

(1.15)

It was found that treatment of **3**-Co with trityl chloride (Ph_3CCl) successfully produced *rac*-2,2'-di(2,6-^{i}Pr$_2$C$_6$H$_3$N=)$_2$-dicyclohexane (**EA$_2$**), $CoCl_2$ and Gomberg's dimer (Eq. 1.15).[97] However, the same oxidant was found to chlorinate {(2,6-^{i}Pr-C$_6$H$_3$)(1-^{c}Hexenyl)N}Li to give (2,6-^{i}Pr-C$_6$H$_3$)(1-^{c}Hexenyl)NCl (observed via mass

spectrometry), precluding its incorporation into any Co-mediated Li-ene-amide coupling method.

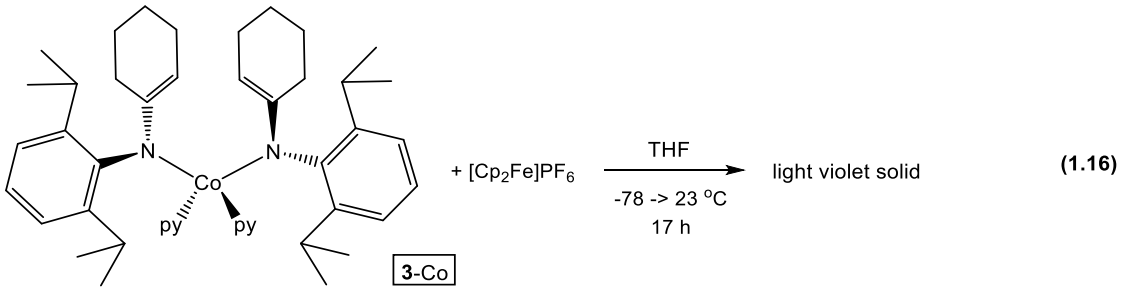

While **2**-Fe could undergo CC coupling upon exposure to $[Cp_2Fe]PF_6$, **3**-Co did not undergo the same coupling process (Eq. 1.16). A light violet solid was isolated, with the quench of the material showing the absence of **EA2** by mass spectrometry. Poor solubility of the "Co(III)" product complicated assessing its magnetism through Evans' method,[73] and attempts to grow crystals for X-ray diffraction studies failed. Given the lack of promising results towards **EA2** formation in the absence of alternative reactivity, oxidation studies of **3**-Co were concluded.

1.9 Reversibility of the Newly Formed 1,4-Diimine CC Bond

With the CC coupling studies concluded for the ene-amide complexes {(2,6-$^{i}Pr_2$-C_6H_3)(1-^{c}Hexenyl)N}$_2$M (M = Cr, **1**-Cr; $FePMe_3$, **2**-Fe; $Copy_2$, **3**-Co), our attention turned towards investigating the possibility of decoupling the newly formed CC bond of *rac*-2,2'-di(2,6-$^{i}Pr_2C_6H_3N=)_2$-dicyclohexane (**EA2**). Scheme 1.8 illustrates a potential redox cycle of forming/breaking the CC bond of **EA2** as part of an organometallic complex. For example, initial coupling of (ene-amide)$_2$M(L_n) (**B**), via addition of X_2, should generate **EA2**-MX_2 (**A**), which might be capable of transferring

X_2 to an incoming substrate. Loss of X_2 would be seen as a formal reductive elimination from the metal center, yet ligation of **EA₂** may allow for a ligand-centered reduction to occur instead. Reducing **EA₂** by two-electrons may break the CC single bond, regenerating species **B** and closing the redox cycle. If such a process could be developed, then **EA₂** would function as an RNI ligand, where the CC bond functions as both storage and release of two-electrons.

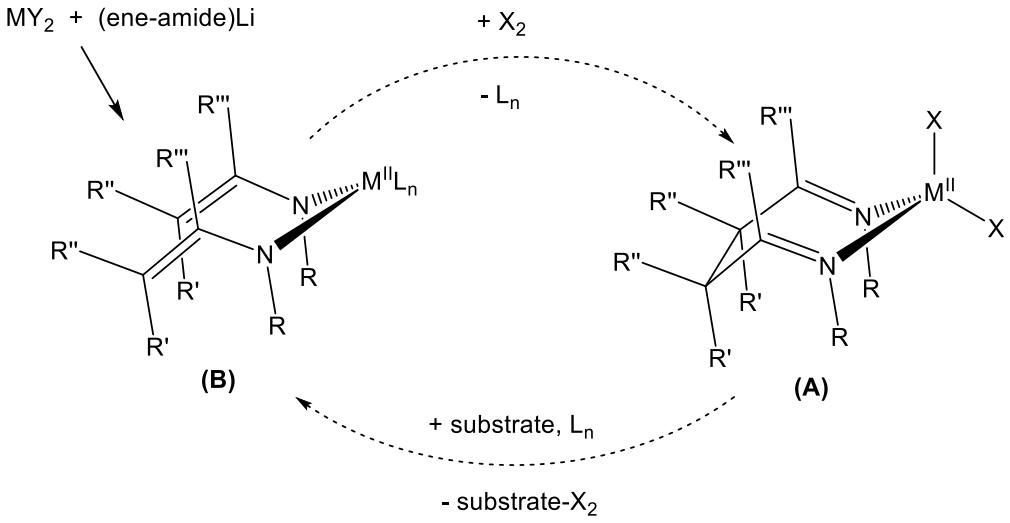

Scheme 1.8. Proposed redox cycle for employing **EA₂** as an RNI ligand

Since **EA₂** forms readily under oxidative conditions, studies were undertaken to determine if exposing the coupled product to reducing conditions may break the newly formed CC bond. Initial treatment of the coupled cyclopentyl-analogue *rac*-bis(2,6-$^{i}Pr_2$-C_6H_3)-[1,1'-bi(cyclopentane)]-2,2'-diimine (**EA₂'**) with 2 equiv. KC_8 resulted in the isolation of a yellow powder (47% yield) whose NMR spectra was similar to the precursor Li-ene-amide spectra (Eq. 1.17). Mass spectrometry confirmed the presence of the parent imine (2,6-$^{i}Pr_2$-C_6H_3)N=C$(CH_2)_4$ and the absence of **EA₂'**,

solidifying the identity of the new product as {(2,6-$^{i}Pr_2$-C_6H_3)(1-^{c}Pentenyl)N}K. Since this experiment confirmed the reductively triggered CC decoupling of **EA$_2$′** was feasible, no other reducing agents were tested.

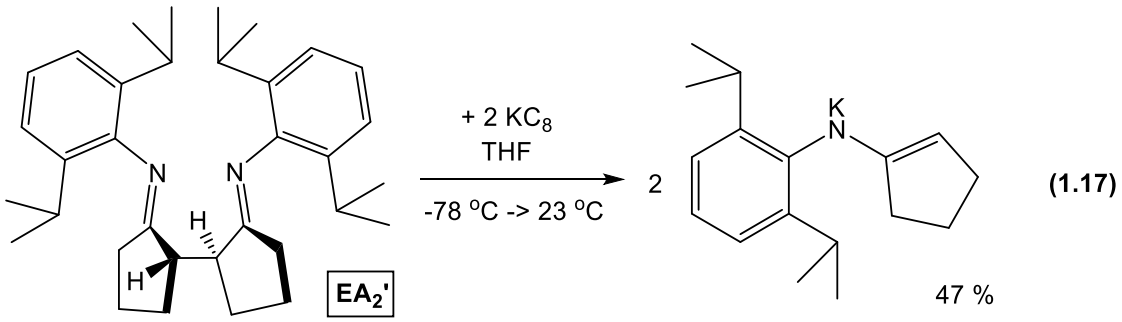

(1.17)

Given the success of oxidatively coupling ene-amides and reductively decoupling the dimer product, studies were undertaken to see if **EA$_2$′** could be ligated to a transition metal. Treatment of **EA$_2$′** with MCl_2 (M = Cr, Fe, Co) resulted in only the observation of free ligand by NMR spectroscopy, with no new product formation seen, as shown in Eq. 1.18. Imines tend to be poor σ-donors, and given the large ring size formed upon chelation, the lack of chelation for these metal starting materials seems reasonable. While it was postulated that either $TiCl_2(TMEDA)_2$ or $Fe(PMe_3)_4$ might be amenable to chelation of **EA$_2$′**, studies were discontinued due to changing research interests.

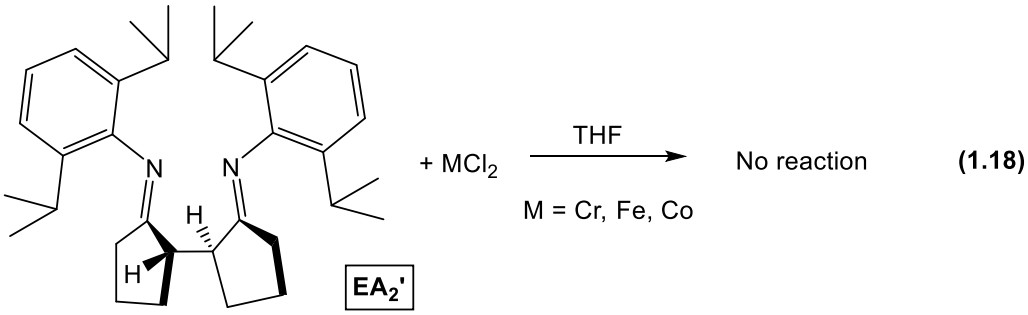

(1.18)

1.10 Alternate Metal-Mediated Imine Coupling Systems

Recent reports on reversible CC imine coupling employing transition metals illustrate the scarcity of such chemical processes. Rauchfuss *et. al.* reported on the conversion of an Fe(0) phosphino-imine (**1**) to an Fe(II) phosphino-1,2-diamide (**2**) (Scheme 1.9).[98] Initial loss of CO and "complexation the phosphine" renders the chelated imine nucleophilic. Nucleophilic attack on the additional imine generates the 1,2-diamide moiety. It was found that oxidation of **2** resulted in breaking of the CC bond to generate the Fe(II) bis(phosphino-imine) (**3**). This process illustrates an example of an oxidatively triggered decoupling of an ethylenediammine fragment to form **3**, all while preserving the oxidation state of the metal.

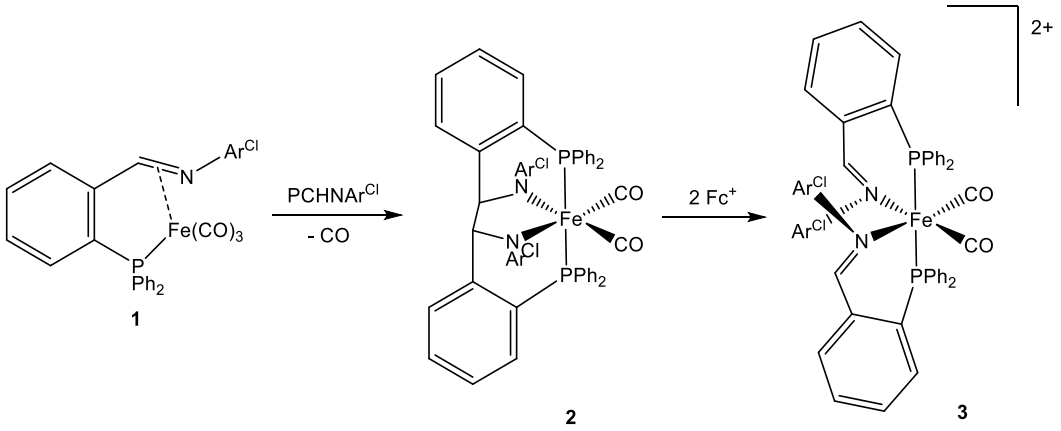

Scheme 1.9. Fe-mediated CC coupling/decoupling of a phosphino-imine ligand

In comparison, an oxidatively triggered CC bond forming reaction from a tungsten 1-azavinylidene system has been recently reported by Templeton and coworkers.[99] Treatment of **1** with I_2 triggers CC coupling at the imine carbon to form the bimetallic dimer **2** (Eq. 1.19) as the major product as a single diastereomer. Dimer

formation was hypothesized to occur via initial carbon-based radical formation upon oxidation, followed by subsequent radical coupling. The dimer forms only if one metal center encounters its enantiomer, but if it reacts with another metal center of the same stereochemistry (50% chance), then H-atom abstraction may occur, yielding the noted byproducts in yields consistent with expectations. Studies detailing reversibility in the newly formed bond were not reported however.

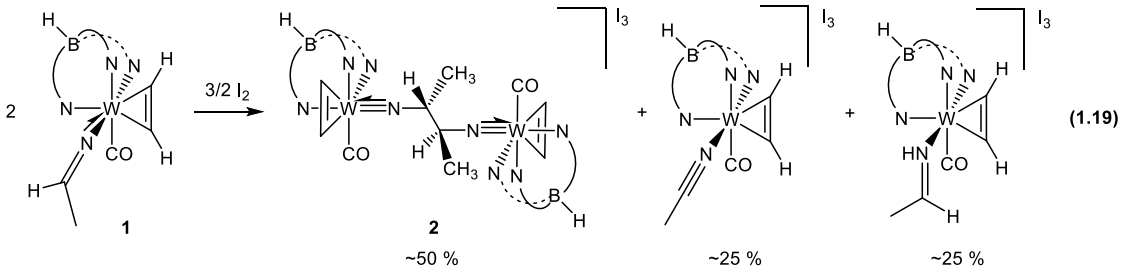

1.11 Comparison of Ene-Amide β-Arylation to Alternative Methods

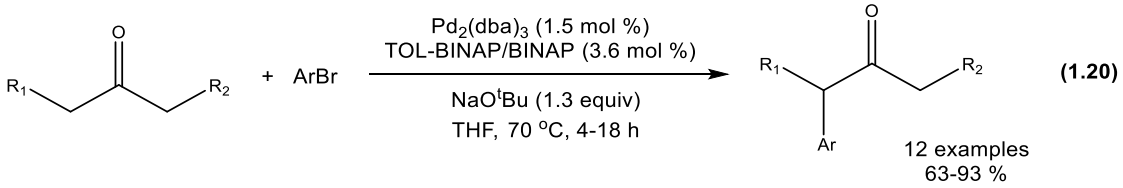

There is ample precedent for Pd-catalyzed β-arylation of ketones,[100-102] one example shown in Eq. 1.20. An early report from Buchwald *et. al.* detailed the coupling of ketones and aryl bromides via *in situ* deprotonation of the ketone with NaO^{t}Bu as the base of choice.[100] Oxidative addition of ArBr to Pd(0), salt metathesis of the Pd(II) intermediate with the sodium enolate, and reductive elimination to form the β-aryl ketone product closes the catalytic cycle. The method delivers good yields

of the CC coupled products (63-93%), featuring several functional groups including nitriles, chlorides and amines.

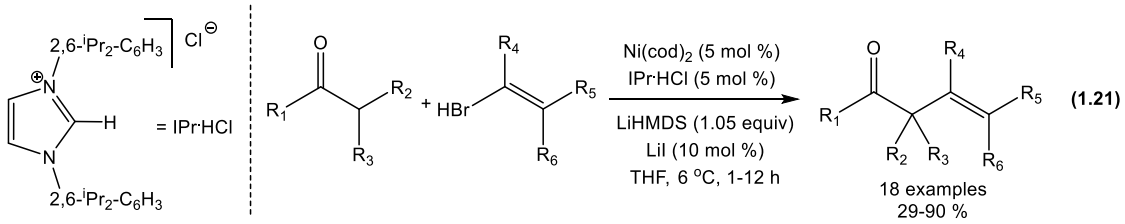

(1.21)

Recent investigations into Ni-catalyzed cross-coupling reactions have resulted in catalytic β-vinylation of ketones.[103] Helquist *et. al.* reported developing a mild, rapid coupling of ketones with vinyl bromides, employing a sterically bulky N-heterocyclic carbene (NHC) as the ancillary ligand for the catalyst, and using LiHMDS as the base for *in situ* deprotonation of the ketone (Eq. 1.21). Reactions were completed within 1-12 h at 6 °C, with variable yields (29-90%), and were tolerant of amines, esters and CF_3 groups. Cyclic and acyclic ketones are amenable to the coupling protocol with similar efficiencies.

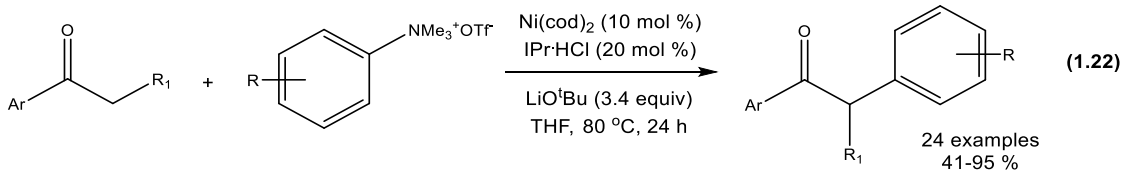

(1.22)

In further developing Ni-catalysts as surrogates for Pd in ketone cross-coupling, Wang *et. al.* reported on the Ni-catalyzed β-arylation of ketones, employing aryltrimethylammonium triflates as the aryl group source (Eq. 1.22).[104] The method requires initial preparation of the ammonium triflate electrophile, but still employs

LiO^{t}Bu as the base for formation of the Li-enolate. While reaction conditions were slightly harsher (80 ^{o}C, 24 h), reasonable yields were attained (41-95%).

Limited studies into the Fe-mediated β-arylation of Li-ene-amides in this report make for difficult comparisons. Catalyst loadings for Fe salts are comparable to the aforementioned Ni-catalyzed cross-couplings. While modest yields were observed for the Fe-cross coupling (~4-9 TO), evaluation of only one substrate does not give a reasonable sense of the efficiency of the catalysis. In addition, significantly extended reaction times (3-4 days) reduces the appeal of the current method. It is conceivable that a change in substrate to ketones or Li-enolates may have led to an improvement in the overall catalysis, but this approach was not evaluated.

Conclusion

Several low-coordinate bis-ene-amide complexes {(2,6-^{i}Pr$_2$-C$_6$H$_3$)(1-^{c}Hexenyl)N}$_2$M (M = Cr, **1**-Cr; FePMe$_3$, **2**-Fe; Copy$_2$, **3**-Co) were prepared through metathetical methods employing {(2,6-^{i}Pr-C$_6$H$_3$)(1-^{c}Hexenyl)N}Li and suitable metal halides. **1**-Cr features an η_3-ene-amide motif, yet this feature is absent for both **2**-Fe and **3**-Co. Despite the disparate hapticity, both **1**-Cr and **2**-Fe diastereoselectively couple the ene-amide fragments to produce *rac*-2,2'-di-(2,6-^{i}Pr$_2$-C$_6$H$_3$N=)$_2$-dicyclohexane (**EA$_2$**) upon oxidation with $CrCl_3$ or $FeCl_3$, respectively. Similar CC coupling behavior with **3**-Co was not observed upon treatment with oxidants. A survey of oxidants that trigger **EA$_2$** formation from **2**-Fe revealed a peculiar C-arylation event when PhBr was employed, a result unique to **2**-Fe. Stoichiometric and catalytic arylation of **2**-Fe and {(2,6-^{i}Pr-C$_6$H$_3$)(1-^{c}Hexenyl)N}Li were productive, yet the yields were fairly modest (~4-9 TO). Extended reaction times and low turnovers, in comparison to competing technologies, concluded the study. Reductive decoupling of the CC bond in **EA$_2$'** was observed upon treatment with KC_8 to yield {(2,6-^{i}Pr-C$_6$H$_3$)(1-^{c}Pentenyl)N}K. Metallations of **EA$_2$'** with MCl_2 (M = Cr, Fe, Co) were unsuccessful, preventing any studies into possible redox non-innocent behavior of **EA$_2$** complexes.

Experimental

General considerations. All manipulations were performed using either glovebox or high vacuum line techniques, unless stated otherwise. All glassware was oven dried at 180 °C. THF and ether were distilled under nitrogen from purple sodium benzophenone ketyl and vacuum transferred from the same prior to use. Hydrocarbon solvents were treated in the same manner with the addition of 1-2 mL/L tetraglyme. Benzene-d_6 was dried over sodium, vacuum transferred, and stored over sodium. THF-d_8 was dried over sodium, and vacuum transferred from sodium benzophenone ketyl prior to use. Chloroform-d_1 (Cambridge Isotope Laboratories) was used as received. $FeCl_2(PMe_3)_2$[86] was prepared by stirring $FeCl_2$ with 2 equiv of PMe_3 in THF and heating to reflux for 1.5 hours under argon, followed by filtration to yield a faint blue/colorless powder. $FeBr_2(PMe_3)_2$[86] was prepared in the same manner, and isolated as light fuchsia crystals. $CoCl_2(py)_4$[105] was prepared by stirring $CoCl_2$ in an excess of pyridine at room temperature overnight, followed by filtration to yield pink microcrystals. LDA was prepared by treating diisopropylamine with n-butyllithium, followed by recrystallization in hexanes and filtration to yield a white powder. Ferrocene was employed as a standard in noted ^{1}H NMR studies (C_6D_6: δ 4.00 ppm; THF-d_8: δ 4.11 ppm). 2,6-diisopropylaniline, 2,6-dimethylaniline and aniline were distilled *in vacuo* prior to use. All other chemicals obtained commercially (Aldrich) were used as received.

NMR spectra were obtained using Mercury 300 MHz, INOVA 400 MHz, and 500 MHz spectrometers. Chemical shifts are reported relative to benzene-d_6 (^{1}H δ

7.16; $^{13}C\{1H\}$ δ 128.39), THF-d_8 (^1H δ 3.58; $^{13}C\{1H\}$ δ 67.57), and chloroform-d_1 (^1H δ 7.26; $^{13}C\{1H\}$ δ 77.16). Multidimensional techniques were conducted using INOVA software affiliated with the spectrometers. Accurate mass data were acquired on an Exactive Orbitrap mass spectrometer (Thermo Scientific) using a DART (IonSense Inc., Saugus, MA) ion source in positive ion mode using helium for DART ionization, while software affiliated with the spectrometer was used to calculate the molecular weight. UV-vis spectra were recorded on an Agilent Cary 60 UV-Vis spectrophotometer. Solution magnetic measurements were conducted via Evans' method in benzene-d_6 and THF-d_8.[73] Elemental analyses were performed by Complete Analysis Laboratories, Inc. (E & R Microanalytical Division), Parsippany, New Jersey, and Robertson Microlit Laboratories, Madison, New Jersey.

Procedures.

1. (2,6-^{i}Pr$_2$-C$_6$H$_3$)N=C(CH$_2$)$_5$. A 250 mL flask adapted with a Dean-Stark trap was charged with 2,6-diisopropylaniline (15.00 g, 84.6 mmol), cyclohexanone (9.14 g, 93.1 mmol), a catalytic amount of TsOH·H_2O (402 mg, 2.12 mmol) and 45 mL of benzene. The yellow solution was heated at reflux for 1.5 d as water was collected. Volatiles were removed *in vacuo* to give a yellow oil, which gradually crystallized. 50 mL CH2Cl2 and 5 mL sat. $NaHCO_3$ (aq) were added, and the layers were separated. The aqueous layer was extracted with CH_2Cl_2 (2x20 mL), and the combined organic extracts were dried over $MgSO_4$, filtered, and the solvent was removed. The solid was recrystallized from hexanes at -78 ^oC, and filtered to afford colorless crystals (18.882 g, 87%). ^1H NMR (C_6D_6): δ 1.19 (6H, d, 7 Hz, ^{i}Pr CH_3), 1.22 (6H, d, 7 Hz, ^{i}Pr CH_3),

1.29 (4H, m, CH_2), 1.56 (2H, m, CH_2), 1.80 (2H, m, CH_2), 2.42 (2H, t, 6 Hz, CH_2), 3.00 (2H, sept, 7 Hz, ^{i}Pr C-H), 7.11 (1H, m, *p*-Ph C-H), 7.18 (2H, m, *m*-Ph C-H). ^{13}C NMR (C_6D_6): δ 23.28, 23.67, 25.97, 26.85, 27.84, 28.31, 31.87, 38.97, 67.12, 123.27, 123.57, 136.70, 146.50, 172.47. HRMS (DART-MS) m/z: [M + H]+ Calcd for 258.2177; Found 258.2212.

2. (2,6-^{i}Pr$_2$-C$_6$H$_3$)N=C(CH$_2$)$_4$. A 250-mL flask adapted with a Dean-Stark trap was charged with 2,6-diisopropylaniline (10.00 g, 56.40 mmol), cyclopentanone (7.117 g, 84.61 mmol), TsOH·H_2O (266 mg, 1.40 mmol), and 45 mL of benzene. The yellow solution was refluxed for 12 h as water was collected via the trap. Volatiles were removed *in vacuo* to leave a yellow oil. 40 mL CH_2Cl_2 and 5 mL sat. $NaHCO_3$ (aq) were added, and the layers were separated. The aqueous layer was extracted with CH_2Cl_2 (2x15 mL), and the combined organic extracts were dried over $MgSO_4$, filtered, and the solvent was removed. The solid was recrystallized from hexanes at -78 ^{o}C, and filtered to afford colorless crystals (11.1 g, 81%). ^{1}H NMR (C_6D_6): δ 1.19 (6H, d, 7 Hz, ^{i}Pr CH_3), 1.22 (6H, d, 7 Hz, ^{i}Pr CH_3), 1.32 (2H, quint, 7 Hz, CH_2), 1.41 (2H, quint, 7 Hz, CH_2), 1.71 (2H, t, 7Hz, CH_2), 2.37 (2H, t, 7 Hz, CH_2), 2.99 (2H, sept, 7 Hz, ^{i}Pr C-H), 7.10 (1H, m, *p*-Ph C-H), 7.15-7.18 (2H, m, *m*-Ph C-H). ^{13}C NMR (C_6D_6): δ 23.13, 23.82, 24.46, 24.95, 28.55, 31.78, 35.42, 67.12, 123.52, 123.78, 136.07, 148.59, 180.53. HRMS (DART-MS) m/z: [M + H]+ Calcd for 244.2021; Found 244.2057.

3. (2,6-^{i}Pr$_2$-C$_6$H$_3$)N=CMePh. A 250-mL flask adapted with a Dean-Stark trap was charged with 2,6-diisopropylaniline (4.427 g, 22.21 mmol), acetophenone (3.000 g,

24.97 mmol), $TsOH{\cdot}H_2O$ (119 mg, 0.625 mmol), and 15 mL of toluene. The yellow solution was refluxed for 3 d as water was collected via the trap. Volatiles were removed *in vacuo* to give a yellow oil. CH_2Cl_2 and sat. $NaHCO_3$ (aq) were added. The layers were separated and the aqueous layer was extracted with CH_2Cl_2 (2x10 mL). The combined organic extracts were dried over $MgSO_4$, filtered, and the solvent was removed. The solid was crystallized from pentane at -78 ^oC, filtered, and washed with cold pentane to afford faint yellow crystals (4.499 g, 64%). ^1H NMR ($CDCl_3$): δ 1.21 (12H, t, 7 Hz, ^iPr CH_3), 2.16 (3H, s, N=C-CH_3), 2.82 (2H, sept, 7 Hz, ^iPr CH), 7.14 (1H, t, 8 Hz, *p*-Ph C-H), 7.20 (2H, d, 8 Hz, *m*-Ph C-H), 7.52-7.55 (3H, m, Ph C-H), 8.09-8.12 (2H, m, Ph C-H). ^{13}C NMR ($CDCl_3$): δ 18.22, 23.09, 23.37, 28.35, 123.07, 123.43, 127.25, 128.54, 130.51, 136.20, 139.25, 146.88, 164.86. HRMS (DART-MS) m/z: [M + H]+ Calcd for 280.2021; Found 280.2056.

4. $PhN=C(CH_2)_5$. To a 100-mL flask containing aniline (5.000 g, 53.69 mmol) and cyclohexanone (6.323 g, 64.42 mmol) was added 27 mL toluene. Oven dried 4 Å sieves (15 g) were added to the yellow solution, and the flask was covered with a rubber stopper and stirred for 2 d. The solution was filtered through celite, and the volatiles were removed. The product was distilled at 65 ^oC (10^{-3}-10^{-4} Torr) as a yellow oil (7.59 g, 82%). ^1H NMR ($CDCl_3$): δ 1.61-1.70 (4H, m, CH_2), 1.86 (2H, quint, 6 Hz, CH_2), 2.18 (2H, t, 6 Hz, CH_2), 2.47 (2H, t, 6 Hz, CH_2), 6.71-6.73 (2H, m, Ph C-H), 7.04 (1H, t, 8 Hz, *p*-Ph C-H), 7.29 (2H, t, 8 Hz, Ph C-H). ^{13}C NMR ($CDCl_3$): δ 25.87, 27.72, 27.94, 31.37, 39.50, 119.93, 123.02, 128.85, 150.88, 175.08). HRMS (DART-MS) m/z: [M + H]+ Calcd for 174.1238; Found 174.1271.

5. PhN=CEtPh. To a 100-mL flask containing aniline (4.000 g, 42.51 mmol) and PhCOEt (4.802 g, 35.79 mmol) was added 22 mL toluene. Oven dried 4 Å sieves (14 g) were added to the yellow solution, and the flask was covered with a rubber stopper and stirred for 68 h. The solution was filtered through celite, and the volatiles were evaporated. The product was crystallized in pentane at -78 ºC and filtered. The crystals were washed with ice cold pentane, affording light yellow crystals (2.51 g, 34%). ^{1}H NMR ($CDCl_3$): δ 1.11 (3H, t, 8 Hz, N=C-CH_2-CH_3), 2.68 (2H, q, 8 Hz, N=C-CH_2), 6.81 (2H, d, 8 Hz, Ph CH), 7.10 (1H, t, 8 Hz, Ph C-H), 7.37 (2H, t, 8 Hz, Ph C-H), 7.45-7.49 (3H, m, Ph C-H), 7.94-7.97 (2H, m, Ph C-H). ^{13}C NMR ($CDCl_3$): δ 13.00, 23.57, 119.18, 120.98, 123.07, 127.70, 128.58, 129.05, 130.42, 138.14, 151.72, 170.80. HRMS (DART-MS) m/z: [M + H]+ Calcd for 210.1238; Found 210.1276.

6. (2,6-Me_2-C_6H_3)N=C(CH_2)$_4$. A 100-mL flask adapted with a Dean-Stark trap was charged with 2,6- dimethylaniline (5.000 g, 41.26 mmol), cyclopentanone (5.206 g, 61.89 mmol), TsOH·H_2O (195 mg, 1.03 mmol), and 20 mL of benzene. The yellow solution was refluxed for 20 h as water was collected via the trap. Volatiles were removed *in vacuo* to give a yellow oil. 20 mL CH_2Cl_2 and 5 mL sat. $NaHCO_3$ (aq) were added, and the layers were separated. The aqueous layer was extracted with CH_2Cl_2 (2x10 mL), and the combined organic extracts were dried over $MgSO_4$, filtered, and the solvent was removed *in vacuo*. The product was purified by removing the residual aniline by distillation, yielding a yellow oil (6.33 g, 82% yield). ^{1}H NMR ($CDCl_3$): δ 1.77-1.89 (6H, m, CH_2), 2.04 (6H, s, CH_3), 2.58 (2H, t, 7 Hz, CH_2), 6.87 (1H, t, 8 Hz, *p*-Ph C-H), 6.99 (2H, d, 8 Hz, *m*-Ph C-H). ^{13}C NMR ($CDCl_3$): δ 17.95,

24.63, 24.96, 31.69, 35.57, 122.75, 125.71, 128.01, 150.08, 182.18. HRMS (DART-MS) m/z: [M + H]+ Calcd for 188.1395; Found 188.1437.

7. {(2,6-^{i}Pr-C$_6$H$_3$)(1-^{c}Hexenyl)N}Li. To a 500-mL flask charged with (2,6-^{i}Pr$_2$-C$_6$H$_3$)N=C(CH$_2$)$_5$ (18.80 g, 73.09 mmol) was added 150 mL hexanes via vacuum transfer at -78 ^{o}C. The solution was warmed to -30 ^{o}C, and 45.6 mL of ^{n}BuLi in hexanes (1.6 M, 73.1 mmol) was added. The solution stirred for 1 h and allowed to warm to 23 °C for another hour, as a white precipitate formed. The solution was filtered and the colorless solid was collected via filtration and washed with hexanes, yielding 16.75 g (87%, ~98% pure by ^{1}H NMR spectroscopic analysis) upon drying. ^{1}H NMR (THF-d$_8$): δ 1.04 (6H, d, 7 Hz, ^{i}Pr CH$_3$), 1.11 (6H, d, 7 Hz, ^{i}Pr CH$_3$), 1.51 (2H, quint, 6 Hz, CH$_2$), 1.64 (2H, quint, 6 Hz, CH$_2$), 2.03 (2H, m, CH$_2$), 2.17 (2H, t, 6 Hz, CH$_2$), 2.80 (1H, t, 3 Hz, N-C=CH), 3.57 (2H, sept, 7 Hz, ^{i}Pr C-H), 6.63 (1H, t, 8 Hz, *p*-Ph C-H), 6.81 (2H, d, 8 Hz, *m*-Ph C-H). ^{13}C NMR (THF-d$_8$): δ 25.05, 26.12, 26.51, 26.59, 27.41, 27.99, 33.79, 80.45, 119.51, 122.68, 145.83, 153.15, 156.50.

8. {(2,6-^{i}Pr$_2$-C$_6$H$_3$)(1-^{c}Pentenyl)N}Li. To a 100-mL flask was charged with (2,6-^{i}Pr$_2$-C$_6$H$_3$)N=C(CH$_2$)$_4$ (3.001 g, 12.34 mmol) was added 25 mL hexanes via vacuum transfer at -78 ^{o}C. The solution was warmed to -30 ^{o}C, and 7.7 mL of ^{n}BuLi in hexanes (1.6 M, 12.32 mmol) was added. The solution stirred for 1 h, and allowed to warm to 23 °C for another hour, as a white precipitate formed. The solution was filtered and the colorless solid was collected via filtration, and washed with hexanes, yielding 2.805 g (91%, ~96% pure by ^{1}H NMR spectroscopic analysis) upon drying. ^{1}H NMR (THF-d$_8$): δ 1.07 (12H, m, ^{i}Pr CH$_2$), 1.71 (2H, quint, 7 Hz, CH$_2$), 2.23 (4H,

m, CH_2), 2.78 (1H, m, N-C=CH), 3.60 (2H, sept, 7 Hz, ^{i}Pr CH), 6.64 (1H, t, 8 Hz, *p*-Ph C-H), 6.82 (2H, d, 8 Hz, *m*-Ph C-H). ^{13}C NMR (THF-d_8): δ 25.44, 28.06, 32.44, 36.98, 78.65, 119.83, 122.69, 145.25, 157.33, 161.10.

9. {(2,6-^{i}Pr$_2$-C$_6$H$_3$)(C=CH$_2$(Ph))N}Li. To a 250 mL flask charged with (2,6-^{i}Pr$_2$-C_6H_3)N=CMePh (300 mg, 1.07 mmol) was added 12 mL hexanes via vacuum transfer at -78 ^{o}C. The solution was warmed to -30 ^{o}C, and 0.67 mL of ^{n}BuLi in hexanes (1.6 M, 1.1 mmol) was added. The solution was warmed slowly to 23 °C with stirring for 15 h, upon which an orange-yellow precipitate formed. The mixture was filtered, and the precipitate was collected via filtration and washed with hexanes, yielding 173 mg (57%, ~92% purity by ^{1}H NMR spectroscopic analysis) of an orange-yellow powder upon drying. ^{1}H NMR (THF-d_8): δ 1.12 (6H, d, 7 Hz, ^{i}Pr CH_3), 1.24 (6H, d, 7 Hz, ^{i}Pr CH_3), 2.36 (1H, d, 2 Hz, N-C=CH), 2.92 (1H, d, 2 Hz, N-C=CH), 3.70 (2H, sept, 7 Hz, ^{i}Pr C-H), 6.78 (1H, t, 8 Hz, *p*-dipp C-H), 6.95 (2H, d, 8 Hz, *m*-dipp CH), 7.10 (1H, t, 7 Hz, *p*-Ph C-H), 7.20 (2H, t, 8 Hz, *m*-Ph C-H), 7.71 (2H, d, 8 Hz, *o*-Ph C-H). ^{13}C NMR (THF-d_8): δ 25.11, 26.25, 28.25, 70.63, 120.90, 123.20, 126.04, 127.95, 128.10, 145.62, 151.27, 155.49, 162.86.

10. {Ph(1-^{c}Hexenyl)N}Li. To a 50-mL flask was charged with PhN=C$(CH_2)_5$ (704 mg, 4.06 mmol) and LDA (435 mg, 4.06 mmol) was added 25 mL Et_2O via vacuum transfer at -78 ^{o}C. The solution was slowly warmed to 23 °C with stirring for 20 h. The volatiles were removed, and the residue washed with pentane (3x25 mL). A white precipitate was collected upon filtration, and washed with pentane, yielding 568 mg (78%, ~96% purity by ^{1}H NMR spectroscopic analysis) upon drying. ^{1}H NMR (THF-

d_8): δ 1.59- 1.68 (4H, m, CH_2), 2.10 (4H, m, CH_2), 4.76 (1H, br t, N-C=CH), 5.84 (1H, t, 7 Hz, *p*-Ph C-H), 6.14 (2H, d, 8 Hz, *o*-Ph C-H), 6.67 (2H, t, 7 Hz, *m*-Ph C-H). ^{13}C NMR (THF-d_8): δ 24.89, 25.54, 26.80, 29.30, 105.78, 108.36, 115.81, 129.09, 152.22, 160.29.

11. {(C_6H_5)(C=CHCH$_3$(Ph))N}Li·(Et_2O)$_{0.5}$. To a 50-mL flask charged with PhN=CEtPh (1.000 g, 4.782 mmol) and LDA (0.511 g, 4.78 mmol) was added 25 mL Et_2O via vacuum transfer at -78 °C. The solution was slowly warmed to 23 °C with stirring for 20 h. The volatiles were removed, and the residue washed with pentane (3x25 mL), affording a white precipitate. The precipitate was collected upon filtration, and washed with pentane, yielding 786 mg (65%, ~95% purity by ^{1}H NMR spectroscopic analysis) upon drying. ^{1}H NMR (THF-d_8): δ 1.11 (2.6H, t, 7 Hz, Et_2O CH_3), 1.71 (3H, d, 7 Hz, N-C=CHCH_3), 3.37 (1.7H, q, 7 Hz, Et_2O CH_2), 4.87 (1H, q, 7 Hz, N-C=CH), 5.72 (1H, t, 7 Hz, p-Ph C-H), 6.10 (2H, d, 8 Hz, *o*-Ph C-H), 6.51 (2H, t, 7 Hz, *m*-Ph C-H), 6.97 (1H, t, 7 Hz, *p*-Ph C-H), 7.10 (2H, t, 7 Hz, *m*-Ph CH), 7.42 (2H, d, 8 Hz, *o*-Ph C-H). ^{13}C NMR (THF-d_8): δ 15.43, 15.85, 66.47, 103.17, 108.13, 116.52, 125.88, 127.60, 128.55, 130.82, 145.08, 154.69, 160.98.

12. {(2,6-Me_2-C_6H_3)(1-^{c}Pentenyl)N}Li. To a 250-mL flask charged with (2,6-Me_2-C_6H_3)N=C(CH_2)$_4$ (5.000 g, 26.72 mmol) was added 50 mL hexanes via vacuum transfer at -78 °C. The solution was warmed to -30 °C, and 16.7 mL of ^{n}BuLi in hexanes (1.6 M, 26.7 mmol) was added. The solution was stirred for 1 h, and allowed to warm to 23 °C for an additional h, as a white precipitate formed. The solution was filtered, and the white solid was collected via filtration and washed with hexanes. A

second crop was similarly collected upon concentration of the filtrate, and the amount of white product totaled 4.172 g (81%, ~98% purity by ^{1}H NMR spectroscopic analysis) upon drying. ^{1}H NMR (C_6D_6): δ 1.71 (2H, quint, 7 Hz, CH_2), 1.89 (2H, t, 7 Hz, CH_2), 2.00 (6H, s, CH_3), 2.32 (2H, t, 7 Hz, CH_2), 4.25 (1H, s, NC=CH), 6.87 (1H, t, 7 Hz, *p*-Ph C-H), 6.96 (2H, d, 7 Hz, *m*-Ph C-H). ^{13}C NMR (C_6D_6): δ 18.90, 24.01, 30.34, 33.20, 84.25, 122.77, 128.98, 133.23, 152.26, 160.57.

13. {(2,6-^{i}Pr$_2$-C$_6$H$_3$)(1-^{c}Hexenyl)N}$_2$Cr (1-Cr). To a 100 mL flask charged with {(2,6-^{i}Pr$_2$-C$_6$H$_3$)(1-^{c}Hexenyl)N}Li (2.000 g, 7.594 mmol) and $CrCl_2$ (0.466 g, 3.79 mmol) was added 50 mL diethyl ether via vacuum transfer at -78 °C. The solution was allowed to warm to 23 °C and was stirred for 1 d. The solution was filtered, and the volatiles were removed and replaced with 40 mL pentane via vacuum transfer. The solution was cooled to -78 °C for 15 minutes, affording dark green crystals that were collected by filtration (1.664 g, 78%). Crystals suitable for X-ray diffraction were obtained via slow evaporation of a concentrated pentane solution. ^{1}H NMR (C_6D_6): δ -3.57 ($\nu_{1/2}$ = 224 Hz), 16.99 ($\nu_{1/2}$ = 323 Hz). μ_{eff} (Evans) = 4.7 μ_B. Anal. for $C_{36}H_{52}CrN_2$ (calc.) C 76.55, H 9.28, N 4.96; (found) C 76.39, H 9.29, N 5.18.

14. {(2,6-^{i}Pr$_2$-C$_6$H$_3$)(1-^{c}Hexenyl)N}$_2$FePMe$_3$ (2-Fe). To a 50 mL flask was charged with {(2,6-^{i}Pr$_2$-C$_6$H$_3$)(1-^{c}Hexenyl)N}Li (1.000 g, 3.800 mmol) and $FeCl_2(PMe_3)_2$ (0.529 g, 1.90 mmol) was added 25 mL benzene via vacuum transfer at -78 °C. The mixture was allowed to thaw and was stirred at 23 °C for 1 day. The volatiles were removed, and the resulting red solid was taken up in pentane and filtered. The solution was concentrated and cooled to -78 °C, affording red crystals (0.984 g, 80%) that were

collected upon filtration. Crystals suitable for X-ray diffraction were obtained via slow evaporation of a concentrated pentane solution at -30 °C. ^{1}H NMR (C_6D_6): δ 12.66 ($\nu_{1/2}$ = 135 Hz), 26.77 ($\nu_{1/2}$ = 2103 Hz), 44.69 ($\nu_{1/2}$ = 694 Hz), 62.87 ($\nu_{1/2}$ = 341 Hz). μ_{eff} (Evans) = 5.1 μ_B. Anal. for $C_{39}H_{61}FeN_2P$ (calc.) C 72.65, H 9.54, N 4.34; (found) C 71.67, H 9.82, N 4.46.

15. {(2,6-^{i}Pr$_2$-C$_6$H$_3$)(1-^{c}Hexenyl)N}$_2$Copy$_2$ (3-Co). To a 100 mL flask charged with {(2,6-^{i}Pr-C_6H_3)(1-^{c}Hexenyl)N}Li (1.000 g, 3.800 mmol) and $CoCl_2(py)_4$ (0.856 g, 1.92 mmol) was added 50 mL benzene via vacuum transfer at -78 °C. The mixture was allowed to thaw, and was stirred at 23 °C for 16 h. The solution was filtered, and the volatiles were removed. The solid was dissolved in pentane and cooled to -78 °C, affording purple crystals (1.255 g, 91%) that were collected by filtration. Crystals suitable for X-ray diffraction were obtained via slow evaporation of a concentrated diethyl ether solution. ^{1}H NMR (C_6D_6): δ -22.34 ($\nu_{1/2}$ = 72 Hz), -1.16 ($\nu_{1/2}$ = 240 Hz), 8.46 ($\nu_{1/2}$ = 92 Hz), 17.73 ($\nu_{1/2}$ = 49 Hz), 22.43 ($\nu_{1/2}$ = 1343 Hz), 39.55 ($\nu_{1/2}$ = 226 Hz). μ_{eff} (Evans) = 4.1 μ_B. Anal. for $C_{46}H_{62}CoN_4$ (calc.) C 75.69, H 8.56, N 7.68; (found; two samples, two EA apiece) C 72.49(11), H 9.30(17), N 4.89(13); C 72.63(18), H 8.44(17), N 6.85(18).

16. EA$_2$ formation from 1-Cr and CrCl$_3$. To a 25-mL flask charged with 1-Cr (100 mg, 0.177 mmol) and $CrCl_3$ (57 mg, 0.35 mmol) was added 12 mL THF via vacuum transfer at -78 °C. The solution was warmed to 23 °C and stirred for 15 h. The green solution gradually changed to blue with an off-white precipitate. The volatiles were removed, and the light blue solid was washed with hexanes (3x10 mL). ^{1}H NMR of

the solid residue in C_6D_6 showed quantitative production of EA_2. UV-Vis spectra of the crude product mixture was obtained in THF, and compared to spectra of pure $CrCl_2$ in THF (0.081 mM), which verified the production of $CrCl_2(THF)_2$ (λ_{max} = 811 nm).

17. 1-Cr and EA_2 from $CrCl_3$ and {(2,6-^{i}Pr$_2$-C_6H_3)(1-^{c}Hexenyl)N}Li. To a 25 mL flask charged with {(2,6-^{i}Pr$_2$-C_6H_3)(1-^{c}Hexenyl)N}Li (500 mg, 1.90 mmol) and $CrCl_3$ (95 mg, 0.60 mmol) was added 12 mL Et_2O via vacuum transfer at -78 ^{o}C. The solution was allowed to warm to 23 °C, and stirred for 2 d, turning green over the duration. The volatiles were removed, and the residue was taken up in hexanes and filtered. The LiCl was washed with hexanes, and the hexanes solution was concentrated, cooled to -78 ^{o}C, and filtered to afford pale green solid (102 mg). A ^{1}H NMR spectrum of the solid in C_6D_6 showed production of EA_2 and 1-Cr (peak at 6.37 ppm is C6D6 in a separate capillary within the NMR sample). Crystals suitable for X-ray diffraction were obtained by slow evaporation of a concentrated pentane solution. The crystals were shown to be consistent with 1-Cr.

18. *rac*-2,2'-di-(2,6-^{i}Pr$_2$-C_6H_3N=)$_2$-dicyclohexane (EA_2). To a 25 mL flask charged with {(2,6-^{i}Pr$_2$-C_6H_3)(1-^{c}Hexenyl)N}Li (500 mg, 1.90 mmol) and $CrCl_3$ (301 mg, 1.90 mmol) was added 12 mL THF via vacuum transfer at -78 °C. The mixture was warmed to 23 °C, and refluxed for 1 d. The solution was cooled to 23 °C, and the solvent was removed. The residue was taken up in 10 mL CH_2Cl_2 and washed with 10 mL H_2O. The layers were separated, and the aqueous layer was extracted with CH_2Cl_2 (2x10 mL). The combined organic layers were dried over $MgSO_4$, filtered and the

solvent removed. The tan residue was taken up in 3 mL pentane and filtered, affording the product as a light tan powder (270 mg, 55% yield). Crystals suitable for X-ray diffraction were obtained via slow evaporation of a concentrated CH_2Cl_2 solution at 0 ^oC. ^1H NMR (C_6D_6): δ 1.19 (6H, d, 7 Hz, ^iPr CH_3), 1.21 (6H, d, 7 Hz, ^iPr CH_3), 1.23 (6H, d, 7 Hz, ^iPr CH_3), 1.26 (6H, d, 7 Hz, ^iPr CH_3), 1.46-1.63 (9H, m, CH_2), 1.70-1.74 (2H, m, CH_2), 2.28-2.32 (2H, m, CH_2), 2.42-2.46 (2H, m, CH_2), 2.83 (2H, sept, 7 Hz, ^iPr C-H), 3.05 (2H, sept, 7 Hz, ^iPr C-H), 3.89-3.93 (2H, dd, 5 Hz and 12 Hz, N=C-CH-CH_2), 7.09-7.14 (2H, m, *p*-Ph C-H), 7.16-7.21 (4H, m, *m*-Ph C-H). ^{13}C NMR (C_6D_6): δ 22.94, 23.02, 23.37, 23.78, 26.19, 27.26, 28.26, 28.98, 29.57, 32.55, 45.07, 123.20, 123.38, 123.42, 136.22, 136.37, 147.02, 173.75.

19. rac-bis(2,6-$^iPr_2$-C_6H_3)-[1,1'-bi(cyclopentane)]-2,2'-diimine (EA_2'). To a 25 mL flask charged with {(2,6-$^iPr_2$-C_6H_3)(1-^{c}Pentenyl)N}Li (300 mg, 1.20 mmol) and $CrCl_3$ (191 mg, 1.21 mmol) was added 12 mL THF via vacuum transfer at -78 °C. The mixture was warmed to 23 °C, and refluxed for 1 d. The solution was cooled to 23 °C, and the solvent was removed. The residue was taken up in 10 mL CH_2Cl_2 and washed with 10 mL H_2O. The layers were separated, and the aqueous layer was extracted with CH_2Cl_2 (2x10 mL). The combined organic layers were dried over $MgSO_4$, filtered and the solvent was removed. The residue was taken up in 3 mL pentane and filtered, affording the product as a light tan powder (200 mg, 68% yield). ^1H NMR (C_6D_6): δ 1.13 (6H, d, 7 Hz, ^iPr CH_3), 1.14 (6H, d, 7 Hz, ^iPr CH_3), 1.24 (6H, d, 7 Hz, ^iPr CH_3), 1.27 (6H, d, 7 Hz, ^iPr CH_3), 1.37-1.45 (4H, m, CH_2), 1.47-1.54 (2H, m, CH_2), 1.61-1.70 (2H, m, CH_2), 1.94-2.00 (2H, m, CH_2), 2.11 (2H, m, CH_2), 2.94 (2H, sept, 7 Hz,

^{i}Pr C-H), 3.00 (2H sept, 7 Hz, ^{i}Pr C-H), 3.80 (2H, t, 8 Hz, N=C-CH-CH_2), 7.09-7.15 (2H, m, *p*-Ph C-H), 7.16-7.20 (4H, m, *m*-Ph C-H). ^{13}C NMR (C_6D_6): δ 22.90, 23.11, 23.16, 23.69, 23.90, 25.91, 28.45, 28.50, 32.30, 47.22, 123.20, 123.76, 123.88, 135.93, 136.39, 148.45, 181.85. HRMS (DART-MS) m/z: [M + H]+ Calcd for 485.3851; Found 485.3875.

20. bis-(2,6-^{i}Pr$_2$-C$_6$H$_3$)-1,4-diphenylbutane-1,4-diimine. To a 25 mL flask charged with {(2,6-^{i}Pr$_2$-C_6H_3)(C=CH_2(Ph))N}Li (300 mg, 1.05 mmol) and $CrCl_3$ (167 mg, 1.05 mmol) was added 12 mL THF via vacuum transfer at -78 °C. The mixture was warmed to 23 °C and refluxed for 2 d. The solution was cooled to 23 °C, and the solvent was removed. The residue was taken up in 10 mL CH_2Cl_2 and washed with 10 mL H_2O. The layers were separated, and the aqueous layer was extracted with CH_2Cl_2 (2x10 mL). The combined organic layers were dried over $MgSO_4$, filtered and the solvent was removed. The green residue was taken up in 3 mL pentane and filtered, affording the product as 66 mg of a light tan powder (23%, ~96% purity by ^{1}H NMR spectroscopic analysis) upon drying. ^{1}H NMR ($CDCl_3$): δ 1.12 (12H, d, 7 Hz, ^{i}Pr CH_3), 1.16 (12H, d, 7 Hz, ^{i}Pr CH_3), 2.54 (4H, s, CH_2), 2.67 (4H, sept, 7 Hz, ^{i}Pr C-H), 7.20-7.23 (2H, m, Ph C-H), 7.24 (3H, s, Ph C-H), 7.25 (1H, s, Ph C-H), 7.27 (1H, s, Ph C-H), 7.29 (2H, s, Ph C-H), 7.31 (1H, s, Ph C-H), 7.40 (6H, m, Ph C-H). ^{13}C NMR ($CDCl_3$): δ 21.74, 23.79, 27.64, 28.61, 123.26, 123.76, 127.39, 128.63, 130.42, 135.62, 137.25, 146.63, 166.08. HRMS (DART-MS) m/z: [M + H]+ Calcd for 557.3851; Found 557.3891.

21. {(-C=C-)(-$CH_2CH_2CH_2CH_2$-)}$_2$NPh pyrrole. To a 25 mL flask charged with {Ph(1-^{c}Hexenyl)N}Li (500 mg, 2.79 mmol) and $CrCl_3$ (442 mg, 2.79 mmol) was added 12 mL THF via vacuum transfer at -78 °C. The mixture was warmed to 23 °C, and heated to reflux for 1 day. The solution was cooled to 23 °C, and the solvent was removed. The residue was taken up in 10 mL CH_2Cl_2 and washed with 10 mL H_2O. The layers were separated, and the aqueous layer was extracted with CH_2Cl_2 (2x10 mL). The combined organic layers were dried over $MgSO_4$, filtered and the solvent removed, affording a yellow oil. The product was purified via column chromatography using silica gel with hexanes/ethyl acetate (50:50), yielding the product as 190 mg of a dark yellow oil (54%, 97% purity by ^{1}H NMR spectroscopic analysis). ^{1}H NMR ($CDCl_3$): δ 1.81 (8H, m, CH_2), 2.45 (4H, t, 5 Hz, CH_2), 2.52 (4H, t, 5 Hz, CH_2), 7.25 (1H, m, Ph C-H), 7.27 (1H, m, Ph C-H), 7.34 (1H, tt, 2 Hz and 7 Hz, Ph C-H), 7.44 (2H, t, 8 Hz, Ph C-H). ^{13}C NMR ($CDCl_3$): δ 21.48, 23.00, 23.66, 23.79, 115.93, 126.68, 127.16, 127.23, 128.96, 138.58. HRMS (DART-MS) m/z: [M + H]+ Calcd for 252.1708; Found 252.1740.

22. 3,4-dimethyl-1,2,5-triphenyl-pyrrole. To a 25 mL flask charged with {(C_6H_5)(C=CHCH_3(Ph))N}Li·(Et_2O)$_{0.5}$ (500 mg, 1.98 mmol) and $CrCl_3$ (314 mg, 1.98 mmol) was added 12 mL THF via vacuum transfer at -78 °C. The mixture was warmed to 23 °C, and heated to reflux for 1 day. The solution was cooled to 23 °C, and the solvent was removed. The residue was taken up in 10 mL CH_2Cl_2 and washed with 10 mL H_2O. The layers were separated, and the aqueous layer was extracted with CH_2Cl_2 (2x10 mL). The combined organic layers were dried over $MgSO_4$, filtered and the solvent removed, affording an off-white residue. The product was purified via

column chromatography using hexanes/ethyl acetate (50:50), yielding a white powder (205 mg, 64% yield). ^{1}H NMR ($CDCl_3$): δ 2.17 (6H, s, CH_3), 6.86 (2H, m, Ph C-H), 7.08 (7H, m, Ph C-H), 7.14-7.23 (6H, m, Ph C-H). ^{13}C NMR ($CDCl_3$): δ 10.41, 117.69, 126.26, 127.76, 128.33, 128.91, 130.75, 131.13, 133.03, 139.33. HRMS (DART-MS) m/z: [M + H]+ Calcd for 324.1708; Found 324.1740.

23. {(-C=C-)(-$CH_2CH_2CH_2CH_2$-)}$_2$N-(2,6-$^{i}Pr_2$-C_6H_3) pyrrole. To a 25 mL flask charged with EA_2 (472 mg, 0.920 mmol) and $TsOH{\cdot}H_2O$ (18 mg, 0.092 mmol) was added 5 mL THF and 5 mL H_2O. The mixture was warmed to 23 °C, and refluxed for 43 h. The solution was removed, affording an offwhite solid. The solid was taken up in 10 mL CH_2Cl_2 and 2 mL sat. $NaHCO_3$ (aq), and the layers were separated. The aqueous layer extracted with CH_2Cl_2 (2x10 mL), and the organic layers were combined and dried over $MgSO_4$ and filtered. The solvent was removed and the product was purified via column chromatography using silica gel and CH_2Cl_2, yielding a white solid (188 mg, 61% yield). ^{1}H NMR ($CDCl_3$): δ 1.11 (12H, d, 7 Hz, ^{i}Pr CH_3), 1.73-1.78 (8H, m, CH_2), 2.15 (4H, t, 5 Hz, CH_2), 2.46 (2H, sept, 7 Hz, ^{i}Pr C-H), 2.51 (4H, t, 5 Hz, CH_2), 7.21 (2H, d, 8 Hz, *m*-Ph C-H), 7.37 (1H, t, 8 Hz, *p*-Ph C-H). ^{13}C NMR ($CDCl_3$): δ 21.65, 22.70, 23.80, 24.04, 24.33, 27.83, 114.52, 123.66, 127.71, 128.66, 133.94, 148.01. HRMS (DART-MS) m/z: [M + H]+ Calcd for 336.2647; Found 336.2676.

24. EA_2 from 2-Fe and $FeCl_3$. To a 25-mL flask charged with 2-Fe (100 mg, 0.155 mmol) and $FeCl_3$ (51 mg, 0.31 mmol) was added 12 mL THF via vacuum transfer at -78 °C. The solution was warmed to 23 °C, and changed color from a red to a yellow

solution within 30 min. The mixture was stirred for 2 h, and the volatiles were removed, followed by washing the tan solid with hexanes (3x10 mL). A ^{1}H NMR spectrum of the solid residue in C_6D_6 showed production of EA_2; the sample was quenched with H_2O, and the resulting ^{1}H NMR spectrum showed a 65% conversion of 2-Fe to EA_2.

25. EA_2 from {(2,6-^{i}Pr$_2$-C$_6$H$_3$)(1-^{c}Hexenyl)N}Li and $FeCl_3$. To a 25 mL flask charged with {(2,6-^{i}Pr$_2$-C$_6$H$_3$)(1-^{c}Hexenyl)N}Li (300 mg, 1.14 mmol) and $FeCl_3$ (185 mg, 1.14 mmol) was added 12 mL THF via vacuum transfer at -78 °C. The solution was warmed to 23 °C, and refluxed for 2 d. The volatiles were removed, and the tan solid washed with hexanes (3 x 10 mL). A ^{1}H NMR spectrum of the solid in C_6D_6 showed the production of EA_2. The sample was quenched with H_2O, and the ^{1}H NMR spectrum showed 42% conversion of {(2,6-^{i}Pr$_2$-C$_6$H$_3$)(1-^{c}Hexenyl)N}Li to EA_2. No additional conversion of the crude reaction mixture was observed upon heating to reflux in THF for an additional 16 h. The addition of 5 mol% $FeCl_2$ (8 mg, 0.06 mmol) and heating to reflux in THF for another day only improved the conversion to 44%.

26. EA_2 from {(2,6-^{i}Pr$_2$-C$_6$H$_3$)(1-^{c}Hexenyl)N}Li and $FeCl_3$ with 5 mol% 2-Fe. To a 25 mL flask charged with {(2,6-^{i}Pr$_2$-C$_6$H$_3$)(1-^{c}Hexenyl)N}Li (200 mg, 0.759 mmol), $FeCl_3$ (124 mg, 0.765 mmol), and 2-Fe (24 mg, 0.038 mmol) was added 12 mL THF via vacuum transfer at -78 °C. The mixture was warmed to 23 °C, and refluxed for 1 d. The volatiles were removed, and the tan solid washed with hexanes (3x10 mL). A ^{1}H NMR spectrum of the solid in C_6D_6 showed the production of EA_2. The sample was

quenched with H_2O, and the ^1H NMR spectrum showed 57% conversion of {(2,6-^{i}Pr$_2$-C_6H_3)(1-^{c}Hexenyl)N}Li to EA_2.

27. 2-Fe and [Cp$_2$Fe]PF$_6$. To a 25-mL flask charged with 2-Fe (100 mg, 0.155 mmol) and [Cp_2Fe]PF_6 (52 mg, 0.16 mmol) was added 12 mL Et_2O via vacuum transfer at -78 ^{o}C. The mixture was allowed to warm to 23 °C, and stirred for 1 d. The volatiles were removed, and the residue was washed with hexanes (3x10 mL). A ^1H NMR spectrum of the crude solid in C_6D_6 revealed the production of EA_2 and Cp_2Fe, and quenching the sample with H_2O showed that the imine precursor (2,6-^{i}Pr$_2$-C_6H_3)N=^{c}Hex:EA_2 ratio to be 1.6:1 respectively, indicating a 38% conversion of the starting Fe complex to product.

28. 2-Fe and PhBr arylation. Into a 25-mL flask charged with 2-Fe (100 mg, 0.155 mmol) and 12 mL THF, was syringed PhBr (33 µL, 0.31 mmol) at 23°C. The solution was stirred for 44 h, the volatiles were removed, and the residue washed with hexanes (3x10 mL). A ^1H NMR spectrum of the residue in C_6D_6 revealed a new product, and quenching the sample with H_2O showed a 44% conversion to the arylation product, (2,6-^{i}Pr$_2$-C_6H_3)N=(2-Ph-^{c}Hex) (API), with the remainder assigned as (2,6-^{i}Pr^2-C_6H_3)N=^{c}Hex (PI). HRMS (DART-MS) m/z: [M + H]+ Calcd for 334.2490; Found 334.2529.

29. Hydrolysis of API and PI. A 10 mg mixture of (2,6-^{i}Pr$_2$-C_6H_3)N=(2-Ph-^{c}Hex) (API) and (2,6-^{i}Pr$_2$-C_6H_3)N=^{c}Hex (PI) was dissolved in 6 mL THF and 6 mL H_2O. HCl (2 mL, 12 M) was added, and the solution was heated to reflux for 19 h. A sample of the solution was analyzed by mass spectrometry, which showed a molecular ion

peak consistent with 2-phenylcyclohexanone. No ion peak was detected for API. HRMS (DART-MS) m/z: [M + H]+ Calcd for 175.1078; Found 175.1113.

30. Catalytic LiPI arylation with PhBr: 10 mol% 2-Fe (Eq. 15). A vial was charged with {(2,6-$^{i}Pr_2$-C_6H_3)(1-^{c}Hexenyl)N}Li (12 mg, 0.046 mmol), PhBr (15 mg, 0.091 mmol) and 493 mg THF-d_8, followed by addition of 2-Fe (3 mg, 0.005 mmol). ^{1}H NMR spectra were obtained over the course of four days at room temperature. Quenching the NMR sample with water showed production of API in 44% yield.

31. Catalytic LiPI arylation with PhI: 10 mol% 2-Fe. A vial was charged with {(2,6-$^{i}Pr_2$-C_6H_3)(1-^{c}Hexenyl)N}Li (12 mg, 0.046 mmol), PhI (19 mg, 0.091 mmol) and 490 mg THF-d_8, followed by addition of 2-Fe (3 mg, 0.005 mmol). ^{1}H NMR spectra were obtained over the course of 4 d at 23 °C. Quenching the NMR sample with water showed production of API in 22% yield, according to ^{1}H NMR spectroscopy.

32. Catalytic LiPI arylation with PhBr. a. 5 mol% $FeCl_2(PMe_3)_2$. To a 25 mL flask charged with {(2,6-$^{i}Pr_2$-C_6H_3)(1-^{c}Hexenyl)N}Li (300 mg, 1.14 mmol) and 12 mL THF was added PhBr (179 mg, 1.14 mmol), followed by $FeCl_2(PMe_3)_2$ (16 mg, 0.057 mmol). The solution turned red, then changed to yellow upon stirring, which was continued for 70 h. The volatiles were removed, and the residue washed with hexanes (3x10 mL). The residue was dissolved in 10 mL CH_2Cl_2 and washed with 10 mL H_2O. The layers were separated, and the aqueous layer was extracted with CH_2Cl_2 (2 x 7 mL). The combined organic layers were dried over $MgSO_4$, filtered, and the solvent evaporated to leave a yellow oil. ^{1}H NMR spectral analysis revealed API formed in

47% conversion (~9 TON), with the residual identified as the parent imine (PI). **b. 10 mol% $FeCl_2(PMe_3)_2$.** A vial was charged with {(2,6-$^{i}Pr_2$-C_6H_3)(1-^{c}Hexenyl)N}Li (19 mg, 0.072 mmol), PhBr (23 mg, 0.14 mmol) and 508 mg THF-d_8, followed by addition of $FeCl_2(PMe_3)_2$ (2 mg, 0.007 mmol). ^{1}H NMR spectra were obtained over the course of four d at 23°C, and quenching of the sample with water showed production of API in 53% yield.

33. Attempted Arylation Catalysis: $FeBr_2(PMe_3)_2$. A vial was charged with {(2,6-$^{i}Pr_2$-C_6H_3)(1-^{c}Hexenyl)N}Li (19 mg, 0.072 mmol), PhBr (15 µL, 0.14 mmol) and 500 mg C_6D_6 (ferrocene (2 mg, 0.01 mmol) standard). A ^{1}H NMR spectrum of the starting material solution was taken prior to addition of $FeBr_2(PMe_3)_2$. $FeBr_2(PMe_3)_2$ (1 mg, 0.003 mmol) was dissolved in C_6D_6, and added to the vial, causing the solution to go red-orange immediately. ^{1}H NMR spectra were obtained each h for 12 h, with no conversion indicated.

34. Attempted Arylation Catalysis: $FeBr_3$. A vial was charged with {(2,6-$^{i}Pr_2$-C_6H_3)(1-^{c}Hexenyl)N}Li (19 mg, 0.072 mmol), PhBr (15 µL, 0.14 mmol) and 414 mg THF-d_8 (ferrocene (2 mg, 0.01 mmol) standard). A ^{1}H NMR spectrum of the starting material solution was taken prior to addition of $FeBr_3$. $FeBr_3$ (1 mg, 0.004 mmol) was dissolved in THF-d_8 and added to the vial, and ^{1}H NMR spectra were obtained each h for 8 h. The spectra indicated no conversion.

35. Attempted Arylation Catalysis: "$Fe(PMe_3)_4$". A vial was charged with {(2,6-$^{i}Pr_2$-C_6H_3)(1-^{c}Hexenyl)N}Li (19 mg, 0.072 mmol), bromobenzene (15 µL, 0.14 mmol) and 530 mg THF-d_8 (ferrocene (2 mg, 0.01 mmol) standard). A ^{1}H NMR spectrum of

the starting material solution was taken prior to addition of $Fe(PMe_3)_4$. $Fe(PMe_3)_4$ (48 mg, 0.13 mmol) was dissolved in 0.521 mL THF-d_8, and 14 µL of the solution (0.256 M) was added to the vial. ^{1}H NMR spectra were obtained each h for 6 h. The spectra indicated that the parent imine (PI) was formed in quantitative yield, with no consumption of the PhBr.

36. Attempted Arylation without Fe. A vial was charged with {(2,6-^{i}Pr$_2$-C$_6$H$_3$)(1-^{c}Hexenyl)N}Li (19 mg, 0.072 mmol), PhBr (23 mg, 0.14 mmol) and 520 mg THF-d_8. A ^{1}H NMR spectrum taken after 4 d at 23 °C revealed a 78:22 ratio of starting lithium amide to parent imine (PI). No arylation product (API) was detected upon quenching the reaction mixture.

37. Attempted Arylation Catalysis: $FeCl_2(OH_2)_4$. A vial was charged with {(2,6-^{i}Pr$_2$-C$_6$H$_3$)(1-^{c}Hexenyl)N}Li (13 mg, 0.050 mmol), PhBr (16 mg, 0.10 mmol) and 353 mg THF-d_8, followed by addition of $FeCl_2(OH_2)_4$ (1 mg, 0.005 mmol). ^{1}H NMR spectra were obtained over the course of four d at 23 °C, and decomposition to PI was observed by ^{1}H NMR, with no production of API during the course of the reaction or upon an aqueous quench.

38. {(2,6-^{i}Pr$_2$-C$_6$H$_3$)(1-^{c}Pentenyl)N}K. To a 25-mL flask charged with **EA$_2$'** (100 mg, 0.206 mmol) and KC_8 (56 mg, 0.41 mmol) was added via vacuum transfer 10 mL THF at -78 ^{o}C. The mixture was allowed to warm slowly with stirring for 21 h, resulting in a yellow solution with dark solid. The THF solution was filtered, and the solvent evaporated. The residue was washed with pentane (3 x 10 mL), resulting in a yellow powder (54 mg, 47%) that was collected via filtration. ^{1}H NMR (C_6D_6): δ 1.21 (6H, d,

7 Hz, ^{i}Pr CH_3), 1.24 (6H, d, 7 Hz, ^{i}Pr CH_3), 1.41 (2H, t, 6 Hz, CH_2), 1.72 (2H, t, 7 Hz, CH_2), 2.38 (2H, t, 7 Hz, CH_2), 3.57 (1H, t, 6 Hz, N-C=CH), 7.14 (2H, m), 7.17 (1H, m).

Single crystal X-ray diffraction studies. Upon isolation, the crystals were covered in polyisobutenes and placed under a cold N_2 stream on the goniometer head of a Siemens P4 SMART CCD area detector (graphite-monochromated MoKα radiation, λ = 0.71073 Å). The structures were solved by direct methods (SHELXS). All non-hydrogen atoms were refined anisotropically unless stated, and hydrogen atoms were treated as idealized contributions (Riding model).

References

(1) Chirik, P. J.; Gunnoe, T. B. *ACS Catal.* **2015**, *5*, 5584.

(2) Morris, R. H. *Acc. Chem. Res.* **2015**, *48*, 1494.

(3) Gaillard, S.; Renaud, J.-L. *Chem. Sus. Chem* **2008**, *1*, 505.

(4) Thayer, A. M. *Chem. Eng. News* **2013**, *91*, 10.

(5) Gordon, R. B.; Bertram, M.; Graedel, T. E. *Proc. Natl. Acad. Sci.* **2006**, *103*, 1209.

(6) Cawthorn, R. G. *South African J. of Science* **1999**, *95*, 481-489.

(7) Bauer, I.; Knolker, H. J. *Chem. Rev.* **2015**, *115*, 3170.

(8) Sherry, B. D.; Fürstner, A. *Acc. Chem. Res.* **2008**, *41*, 1500.

(9) Bedford, R. B. *Acc. Chem. Res.* **2015**, *48*, 1485.

(10) Rana, S.; Modak, A.; Maity, S.; Patra, T.; Maiti, D. Iron Catalysis in Synthetic Chemistry. In *Progress in Inorganic Chemistry*; Karlin, K. D., Ed.; John Wiley & Sons, Inc.: Hoboken, NJ, 2014; Vol. 59, pp 1-188.

(11) Chirik, P. J.; Wieghardt, K. *Science* **2010**, *327*, 794.

(12) Chirik, P. J. *Inorg. Chem.* **2011**, *50*, 9737.

(13) Blanchard, S.; Derat, E.; Desage-El Murr, M.; Fensterbank, L.; Malacria, M.; Mouries-Mansuy, V. *Eur. J. Inorg. Chem.* **2012**, 376.

(14) Khusniyarov, M. M.; Weyhermüller, T.; Bill, E.; Wieghardt, K. *J. Am. Chem. Soc.* **2009**, *131*, 1208.

(15) Darmon, J. M.; Stieber, S. C.; Sylvester, K. L.; Fernández, I.; Lobkovsky, E. B.; Semproni, S. P.; Bill, E.; Wieghardt, K.; DeBeer, S.; Chirik, P. J. *J. Am. Chem. Soc.* **2012**, *134*, 17125.

(16) Bart, S. C.; Lobkovsky, E. B.; Bill, E.; Chirik, P. J. *J. Am. Chem. Soc.* **2006**, *128*, 5302.

(17) Sylvester, K. T.; Chirik, P. J. *J. Am. Chem. Soc.* **2009**, *131*, 8772.

(18) Bouwkamp, M. W.; Bowman, A. C.; Lobkovsky, E. B.; Chirik, P. J. *J. Am. Chem. Soc.* **2006**, *128*, 13340.

(19) Russel, S. K.; Lobkovsky, E. B.; Chirik, P. J. *J. Am. Chem. Soc.* **2011**, *133*, 8858.

(20) Russel, S. K.; Lobkovsky, E. B.; Chirik, P. J. *J. Am. Chem. Soc.* **2009**, *131*, 36.

(21) Monfette, S.; Turner, Z. R.; Semproni, S. P.; Chirik, P. J. *J. Am. Chem. Soc* **2012**, *134*, 4561.

(22) Russel, S. K.; Darmon, J. M.; Lobkovsky, E. B.; Chirik, P. J. *Inorg. Chem.* **2010**, *49*, 2782.

(23) Yu, R. P.; Darmon, J. M.; Hoyt, H. M.; Margulieux, G. W.; Turner, Z.; Chirik, P. J. *ACS Catal.* **2012**, *2*, 1760.

(24) Tondreau, A. M.; Darmon, J. D.; Wile, B. M.; Floyd, S. K.; Lobkovsky, E. B.; Chirik, P. J. *Organometallics* **2009**, *28*, 3928.

(25) Trovitch, R. J.; Lobkovsky, E. B.; Bill, E.; Chirik, P. J. *Organometallics* **2008**, *27*, 1470.

(26) Bart, S. C.; Lobkovsky, E. B.; Chirik, P. J. *J. Am. Chem. Soc.* **2004**, *126*, 13794.

(27) Archer, A. M.; Bouwkamp, M. W.; Cortez, M.-P.; Lobkovsky, E. B.; Chirik, P. J. *Organometallics* **2006**, *25*, 4269.

(28) Tondreau, A. M.; Atienza, C. C. H. A.; Weller, N. J.; Nye, S. A.; Lewis, K. M.; Delis, J. G. P.; Chirik, P. J. *Science* **2012**, *335*, 567.

(29) Tondreau, A. M.; Atienza, C. C. H. A.; Darmon, J. M.; Milsmann, C.; Hoyt, H. M.; Weller, K. J.; Nye, S. A.; Lewis, K. N.; Boyer, J. L.; Delis, J. G. P.; Lobkovsky, E. B.; Chirik, P. J. *Organometallics* **2012**, *31*, 4886.

(30) Atienza, C. C. H. A.; Tondreau, A. M.; Weller, K. J.; Lewis, K. M.; Cruse, R.; Nye, S. A.; Boyer, J. L.; Delis, J. P.; Chirik, P. J. *ACS Catal.* **2012**, *2*, 2169.

(31) Tondreau, A. M.; Lobkovsky, E. B.; Chirik, P. J. *Org. Lett.* **2008**, *10*, 2789.

(32) Atienza, C. C. H. A.; Milsmann, C.; Lobkovsky, E. B.; Chirik, P. J. *Angew. Chem. Int. Ed.* **2011**, *50*, 8143.

(33) Tondreau, A. M.; Milsmann, C.; Patrick, A. D.; Hoyt, H. M.; Lobkovsky, E. B.; Wieghardt, K.; Chirik, P. J. *J. Am. Chem. Soc.* **2010**, *132*, 15046.

(34) Bouwkamp, M. W.; Lobkovsky, E. B.; Chirik, P. J. *J. Am. Chem. Soc.* **2005**, *127*, 9660.

(35) Atienza, C. C. H. A.; Bowman, A. C.; Lobkovsky, E. B.; Chirik, P. J. *J. Am. Chem. Soc.* **2010**, *132*, 16343.

(36) Trovitch, R. J.; Lobkovsky, E. B.; Bouwkamp, M. W.; Chirik, P. J. *Organometallics* **2008**, *27*, 6264.

(37) Trovitch, R. J.; Lobkovsky, E. B.; Chirik, P. J. *J. Am. Chem. Soc.* **2008**, *130*, 11631.

(38) Bowman, A. C.; Bart, S. C.; Heinemann, F. W.; Meyer, K.; Chirik, P. J. *Inorg. Chem.* **2009**, *48*, 5587.

(39) Obligacion, J. V.; Chirik, P. J. *J. Am. Chem. Soc.* **2013**, *135*, 19107.

(40) Obligacion, J. V.; Chirik, P. J. *Org. Lett.* **2013**, *15*, 2680.

(41) Obligacion, J. V.; Semproni, S. P.; Chirik, P. J. *J. Am. Chem. Soc.* **2014**, *136*, 4133.

(42) Haneline, M. R.; Heyduk, A. F. *J. Am. Chem. Soc.* **2006**, *128*, 8410.

(43) Blackmore, K. J.; Ziller, J. W.; Heyduk, A. F. *Inorg. Chem.* **2005**, *44*, 5559.

(44) Zarkesh, R. A.; Ziller, J. W.; Heyduk, A. F. *Angew. Chem. Int. Ed.* **2008**, *47*, 4715.

(45) Blackmore, K. J.; Lal, N.; Ziller, J. W.; Heyduk, A. F. *J. Am. Chem. Soc.* **2008**, *130*, 2728.

(46) Nguyen, A. I.; Zarkesh, R. A.; Lacy, D. C.; Thorson, M. K.; Heyduk, A. F. *Chem. Sci.* **2011**, *2*, 166.

(47) Ketterer, N. A.; Fan, H.; Blackmore, K. J.; Yang, X.; Ziller, J. W.; Baik, M.-H.; Heyduk, A. F. *J. Am. Chem. Soc.* **2008**, *130*, 4364.

(48) Lu, C. C.; Bill, E.; Weyhermüller, T.; Bothe, E.; Wieghardt, K. *J. Am. Chem. Soc.* **2008**, *130*, 3181.

(49) Trifonov, A. A.; Fedorova, E. A.; Borovkov, I. A.; Fukin, G. K.; Baranov, E. V.; Larionova, J.; Druzhkov, N. O. *Organometallics* **2007**, *26*, 2488.

(50) Mondal, A.; Weyhermüller, T.; Wieghardt, K. *Chem. Commun.* **2009**, 6098.

(51) Zhu, D.; Budzelaar, P. H. M. *Organometallics* **2010**, *29*, 5759.

(52) Zhu, D.; Korobkov, I.; Budzelaar, P. H. M. *Organometallics* **2012**, *31*, 3958.

(53) Knijnenburg, Q.; Hetterscheid, D.; Kooistra, T. M.; Budzelaar, P. H. M. *Eur. J. Inorg. Chem.* **2004**, 1204.

(54) Zhu, D.; Thapa, I.; Korobkov, I.; Gambarotta, S.; Budzelaar, P. H. M. *Inorg. Chem.* **2011**, *50*, 9879.

(55) Knijnenburg, Q.; Gambarotta, S.; Budzelaar, P. H. M. *Dalton Trans.* **2006**, 5442.

(56) Budzelaar, P. H. M. *Eur. J. Inorg. Chem.* **2012**, 530.

(57) Heyduk, A. F.; Zarkesh, R. A.; Nguyen, A. I. *Inorg. Chem.* **2011**, *50*, 9849.

(58) Frazier, B. A.; Wolczanski, P. T.; Lobkovsky, E. B. *Inorg. Chem.* **2009**, *48*, 11576.

(59) Frazier, B. A.; Bartholomew, E. R.; Wolczanski, P. T.; DeBeer, S.; Santiago-Berrios, M.; Abruña, H. D.; Lobkovsky, E. B.; Bart, S. C.; Mossin, S.; Meyer, K.; Cundari, T. R. *Inorg. Chem.* **2011**, *50*, 12414.

(60) Frazier, B. A.; Wolczanski, P. T.; Keresztes, I.; DeBeer, S.; Lobkovsky, E. B.; Pierpont, A. W.; Cundari, P. T. *Inorg. Chem.* **2012**, *51*, 8177.

(61) Williams, V. A.; Wolczanski, P. T.; Sutter, J.; Meyer, K.; Lobkovsky, E. B.; Cundari, T. R. *Inorg. Chem.* **2014**, *53*, 4459.

(62) Hulley, E. B.; Wolczanski, P. T.; Lobkovsky, E. B. *J. Am. Chem. Soc.* **2011**, *133*, 18058.

(63) Frazier, B. A.; Wolczanski, P. T.; Lobkovsky, E. B.; Cundari, T. R. *J. Am. Chem. Soc.* **2009**, *131*, 3428.

(64) Frazier, B. A.; Williams, V. A.; Wolczanski, P. T.; Bart, S.; Meyer, K.; Cundari, T. R.; Lobkovsky, E. B. *Inorg. Chem.* **2013**, *52*, 3295.

(65) Morris, W. D.; Wolczanski, P. T.; Sutter, J.; Meyer, K.; Cundari, T. R.; Lobkovsky, E. B. *Inorg. Chem.* **2014**, *53*, 7467.

(66) Lindley, B. M.; Wolczanski, P. T.; Cundari, T. R.; Lobkovsky, E. B. *Organometallics* **2015**, *34*, 4656.

(67) Schöffel, J.; Šušnjar, N.; Nückel, S.; Sieh, D.; Burger, P. *Eur. J. Inorg. Chem.* **2010**, *2010* (31), 4911–4915.

(68) Eckert, N. A.; Vaddadi, S.; Stoian, S.; Lachicotte, R. J.; Cundari, T. R.; Holland, P. L. *Angew. Chem. Int. Ed.* **2006**, *45* (41), 6868–6871.

(69) Power, P. P. *Chem. Rev.* **2012**, *112*, 3482.

(70) Zadrozny,J. M.; Atanasov, A.; Bryan, A. M.; Lin, C.-Y.; Rekken, B. D.; Power, P. P.; Neese, F.; Long, J. R. *Chem. Sci.* **2013**, *4*, 125.

(71) Lipschutz, M. I.; Tilley, T. D. *Angew. Chem. Int. Ed.* **2014**, *53*, 7290.

(72) Lipschutz, M. I.; Yang, X. Z.; Chatterjee, R.; Tilley, T. D. *J. Am. Chem. Soc.* **2013**, *135*, 15298.

(73) (a) Evans, D. F. *J. Chem. Soc.* **1959**, 2003. (b) Schubert, E. M. *J. Chem. Ed.* **1992**, *69*, 62.

(74) Smith, J. D.; Hanusa, T. P.; Young, V. G. *J. Am. Chem. Soc.* **2001**, *123*, 6455.

(75) Rightmire, N. R.; Quisenberry, K. T.; Hanusa, T. P. *Organometallics* **2014**, *33*, 5678.

(76) Allen, F. H.; Kennard, O.; Watson, D. G.; Brammer, L.; Orpen, A. G.; Taylor, R. *J. Chem. Soc., Perkin Trans. II* **1987**, S1-S19.

(77) Boynton, J. N.; Merrill, W. A.; Fettinger, J. C.; Reiff, W. M.; Power, P. P. *Inorg. Chem.* **2012**, *51*, 3212.

(78) Maiti, S.; Biswas, S.; Jana, U. *J. Org. Chem.* **2010**, *75*, 1674.

(79) Srimani, D.; Ben-David, Y.; Milstein, D. *Angew. Chem. Int. Ed.* **2013**, *52*, 4012.

(80) Schley, N. D.; Dobereiner, G. E.; Crabtree, R. H. *Organometallics* **2011**, *30*, 4174.

(81) Kruse, W. *J. Organomet. Chem.* **1972**, 42, C39.

(82) Filippou, A. C.; Schneider, S. *Organometallics* **2003**, 22, 3010.

(83) McGowan, K. P.; Abboud, K. A.; Veige, A. S. *Organometallics* **2011**, 30, 4949.

(84) Schulzke, C.; Sugiyama, H.; LeBlanc, G.; Gambarotta, S.; Yap, G. P. A. *Organometallics* **2002**, 21, 3810.

(85) Ajjou, J. A. N.; Scott, S. L.; Paquet, V. *J. Am. Chem. Soc.* **1998**, 120, 415.

(86) H. H. Karsch, *Chem. Ber.* **1977**, *110*, 2222-2235.

(87) H. Guan, P. Bhattacharya, J. A. Krause, *Organometallics* **2011**, *30*, 4720.

(88) Tamura, M.; Kochi, J. K. *J. Am. Chem. Soc.* **1971**, *93*, 1487.

(89) Neumann, S. M.; Kochi, J. K. *J. Org. Chem.* **1975**, *40*, 599.

(90) Smith, R. S.; Kochi, J. K. *J. Org. Chem.* **1976**, *41*, 502.

(91) Fürstner, A.; Leitner, A.; Méndez, M.; Krause, H. *J. Am. Chem. Soc.* **2002**, *124*, 13856.

(92) Daifuku, S. L.; Kneebone, J. L.; Snyder, B. E. R.; Neidig, M. L. *J. Am. Chem. Soc.* **2015**, *137*, 11432.

(93) Bedford, R. B.; Brenner, P. B.; Carter, E.; Cogswell, P. M.; Haddow, M. F.; Harvey, J. N.; Murphy, D. M.; Nunn, J.; Woodall, C. H. *Angew. Chem. Int. Ed.* **2014**, *53*, 1804.

(94) Hatakeyama, T.; Hashimoto, T.; Kathriarachchi, K. K. A. D. S.; Zenmyo, T.; Seike, H.; Nakamura, M. *Angew. Chem. Int. Ed.* **2012**, *51*, 8834.

(95) Liu, Y.; Xiao, J.; Wang, L.; Song, Y.; Deng, L. *Organometallics* **2015**, *34*, 599.

(96) Steib, A. K.; Thaler, T.; Komeyama, K.; Mayer, P.; Knochel, P. *Angew. Chem. Int. Ed.* **2011**, *50*, 3303.

(97) Gomberg, M. *J. Am. Chem. Soc.* **1900**, *22*, 757.

(98) Chu, W.-Y.; Richers, C. P.; Kahle, E. R.; Rauchfuss, T. B. *Organometallics* **2016**, *35*, 2782.

(99) Beattie, R. J.; White, P. S.; Templeton, J. L. *J. Organomet. Chem.* **2017**, Ahead of Print.

(100) Palucki, M.; Buchwald, S. L. *J. Am. Chem. Soc.* **1997**, *119*, 11108.

(101) Culkin, D. A.; Hartwig, J. F. *Acc. Chem. Res.* **2003**, *36*, 234.

(102) Muratake, H.; Hayakawa, A.; Natsume, M. *Tetrahedron Lett.* **1997**, *38*, 7577.

(103) Grigalunas, M.; Norrby, P.-O.; Wiest, O.; Helquist, P. *Angew. Chem. Int. Ed.* **2015**, *54*, 11822.

(104) Li, J.; Wang, Z.-X. *Org. Biomol. Chem.* **2016**, *14*, 7579.

(105) Z. Di, F. F. B. J. Janssen, P. H. M. Budzelaar, *Organometallics* **2010**, *29*, 1897.

Chapter 2

Octahedral Fe(II) Vinyl Chelates as Potential Fe(IV) Alkylidene Precursors and Reevaluation of Prior Cationic and Neutral Fe(IV) Alkylidenes

Introduction

Olefin metathesis entails the purposeful rearrangement of alkene fragments via scission and regeneration of carbon-carbon double bonds to yield new olefin products. For example, the Shell Higher Olefin Process (SHOP) employs a heterogeneous Mo catalyst to metathesize non-saleable olefins into viable commercial alkenes (C_{10}-C_{14}) that are distributed to additional companies to generate further products, such as surfactants.[1,2] Olefin metathesis generates few byproducts, with the most hazardous species likely being the transition metal catalyst employed. Transition metal alkylidene catalysts usually incorporate 2nd row transition metals such as Mo or Ru (Figure 2.1).[3-5] While is a cornerstone of the SHOP method, and Ru catalysts feature reasonable functional group tolerance and air-tolerance, there are limitations to the

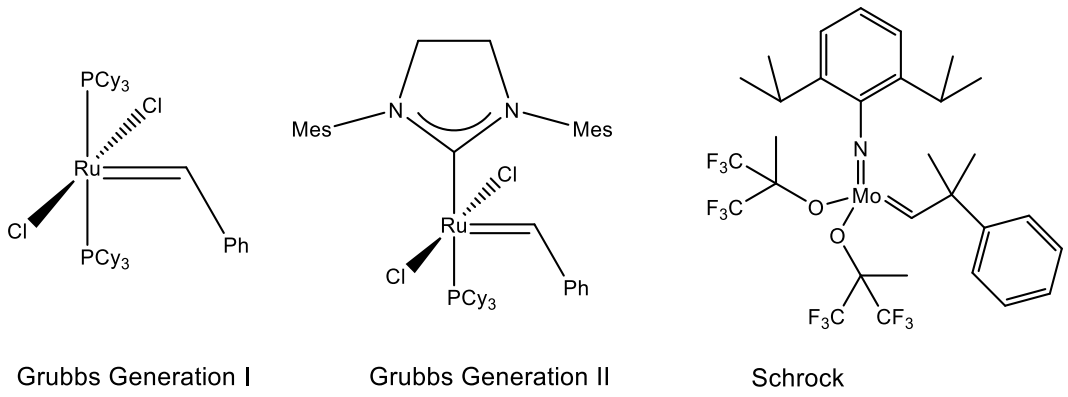

Figure 2.1. Examples of olefin metathesis catalysts

functional group tolerance (Mo) and issues with general abundance (Ru). Despite these shortcomings, the synthetic value of olefin metathesis was recognized with the 2005 Nobel Prize in Chemistry, which was awarded to Richard Schrock, Robert Grubbs and Yves Chauvin for their seminal work in the field.[6-8] In looking to solve the limitations of the current catalysts employed for olefin metathesis, development of 1st row transition metal catalysts present an attractive alternative due to their low cost.

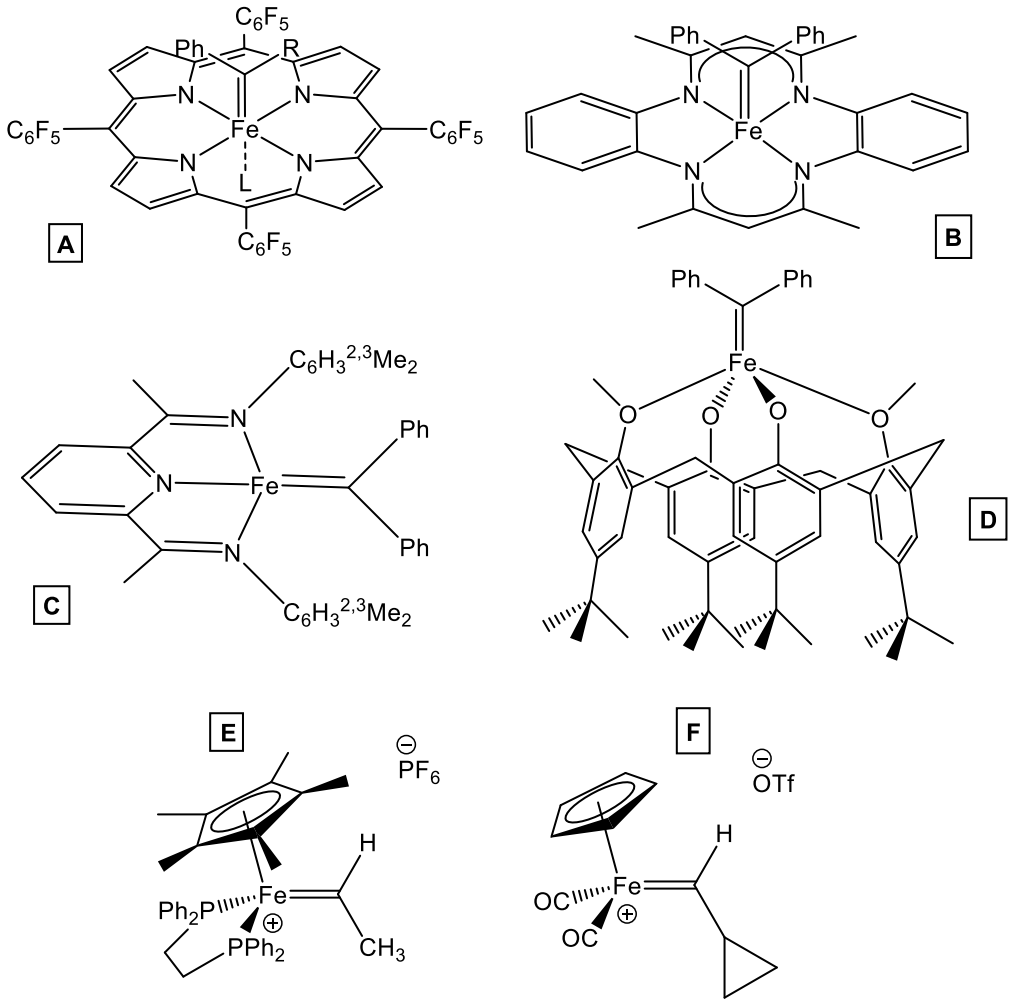

Figure 2.2. Select examples of Fe alkylidenes

Initial interest in developing 1st row transition metal alkylidenes to supplant traditional catalysts focused on Fe, being the 1st row congener of the well-studied Ru catalysts. One limitation towards designing metal alkylidene catalysts competent for olefin metathesis was reported by Hoffmann *et al*,[9] which suggests that the catalysts need to be d^n ($n \leq 4$). Given this argument, Fe(IV) alkylidenes are the target of choice for Fe-based catalysts, especially in light of the oxidation state for effective Ru-catalysts. Actual preparation of Fe alkylidene complexes remains a challenge, with several examples shown in Figure 2.2. Complexes **A**-**D** were prepared through addition of diazoalkanes.[10-13] While **E** was prepared through acid-mediated loss of methanol,[14] complex **F** forms through silyl-mediated methoxide abstraction.[15] However, for all of these examples, none of the Fe alkylidenes catalyze olefin metathesis. While several examples affect cyclopropanation of olefin substrates,[14,15] reactivity studies are noticeably absent for several Fe alkylidenes. Chirik's pyridyl-diimine (PDI) Fe alkylidene **C** participates in group transfer reactions towards CO and azides, however.[12]

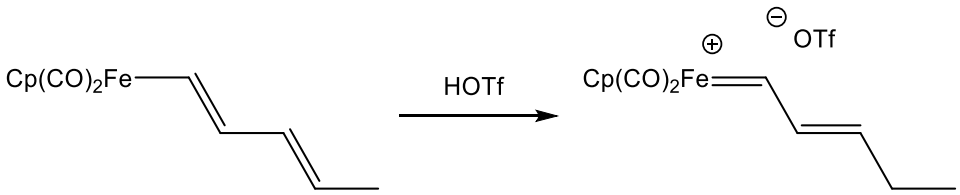

(2.1)

Eq 2.1 illustrates an alternative approach towards the synthesis of Fe(IV) alkylidenes via protonation of an Fe(II) vinyl complex, as reported by Helquist *et al.*,[16]

a transformation that has been modestly explored.[17-21] Our group's initial interest in pursuing Fe(IV) alkylidenes centered on further developing this protonation method.

Preliminary work by former colleagues Ala'aeddeen Swidan and Brian Lindley focused on the synthesis of tetra- and tridentate ligands as suitable precursors to Fe(II) vinyl chelates (Scheme 2.1). Karsch's *cis*-$Me_2Fe(PMe_3)_4$ complex[22] has been shown to affect C-H bond activations,[23-26] and was envisioned to provide access to Fe(II) vinyl

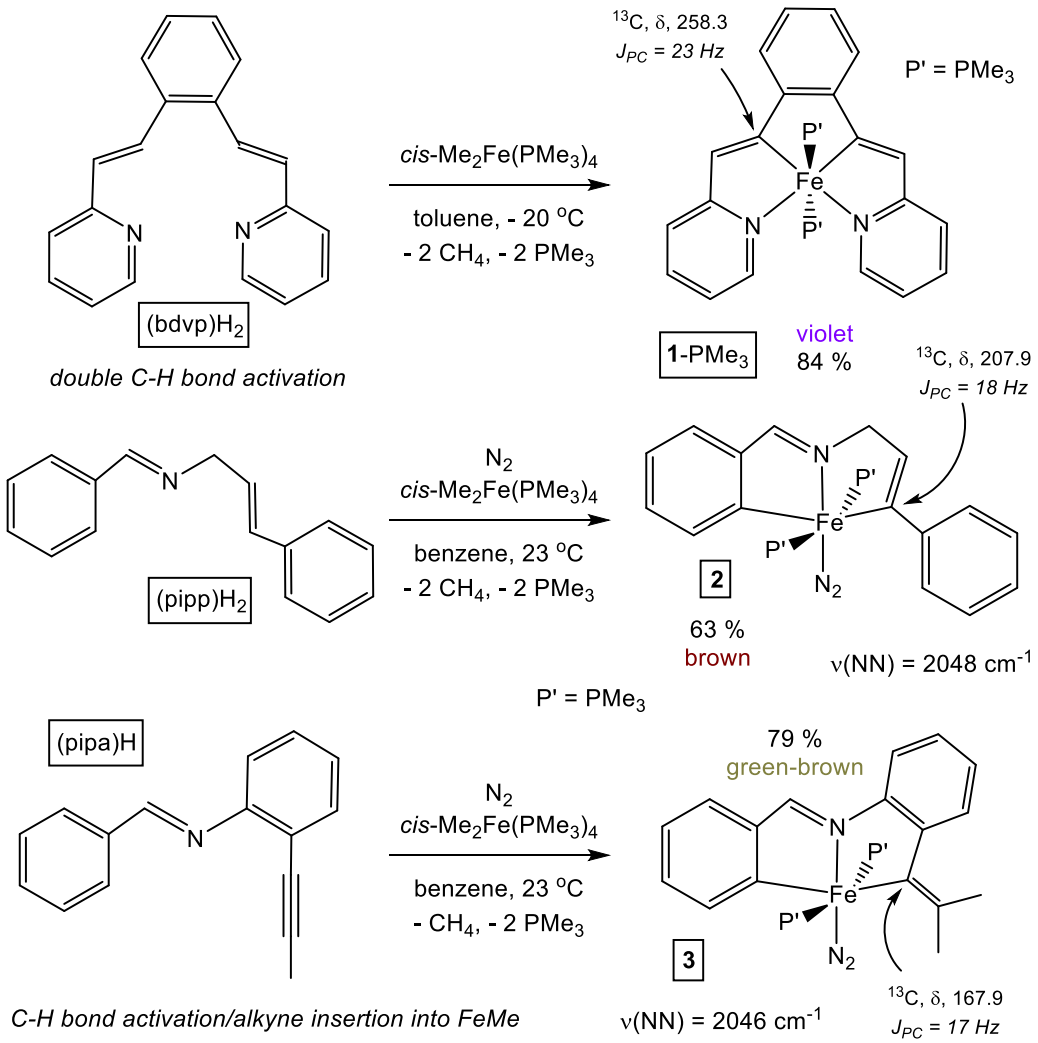

Scheme 2.1. Preparation of tetra- and tridentate Fe(II) vinyl chelates

complexes. Treatment of the prepared ligands with *cis*-$Me_2Fe(PMe_3)_4$ led to the formation of complexes (bdvp)$Fe(PMe_3)_2$ (**1**-PMe_3) and *trans*-(pipp)$Fe(PMe_3)_2N_2$ (**2**) via double C-H activation, while *trans*-(pipvd)$Fe(PMe_3)_2N_2$ (**3**) was formed through single C-H activation followed by alkyne insertion. The tridentate complexes were isolated as dinitrogen adducts, with the ligand discerned via IR spectroscopy, revealing ν(NN) at 2048 and 2046 cm^{-1} for **2** and **3**, respectively. **1**-PMe_3 was characterized through NMR spectroscopy and X-ray diffraction studies, with the bound vinyl carbon featuring a downfield ^{13}C chemical shift of δ 258.3, and short Fe-C bonds of 1.883(8) Å (ave).

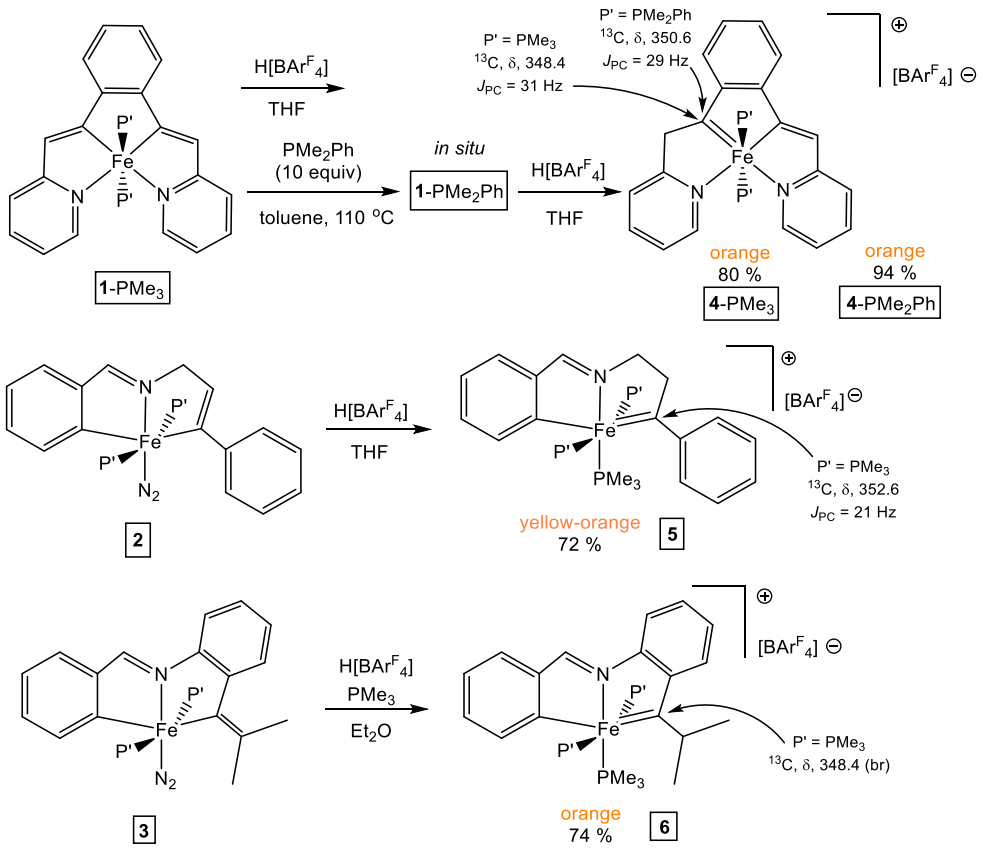

Scheme 2.2. Synthesis of Fe(IV) alkylidenes via protonation

With the Fe(II) vinyl precursors in hand, protonation studies were undertaken, as shown in Scheme 2.2. Treatment of the Fe(II) vinyl chelates with Brookhart's acid $[H(OEt_2)_2]BAr^F_4$ (Ar^F = 3,5-$(CF_3)_2C_6H_3$)[27] led to the formation of the cationic Fe(IV) alkylidene complexes $[(bavp)Fe(PMe_3)_2][BAr^F_4]$ (**4**-PMe_3), $[(piap)Fe(PMe_3)_3][BAr^F_4]$ (**5**) and $[(pipvd)Fe(PMe_3)_3][BAr^F_4]$ (**6**) in good yields. It was found that protonating complexes **2** and **3** led to decomposition, yet repeating the protonation in the presence of excess PMe_3 led to clean formation of **5** and **6**, respectively. In assessing the lability of **1**-PMe_3, exposing it to excess PMe_2Ph, evaporating volatile PMe_3 over several cycles, and protonating the crude **1**-PMe_2Ph with $H[BAr^F_4]$ led to formation of pure $[(bavp)Fe(PMe_3)_2][BAr^F_4]$ (**4**-PMe_2Ph). The noted ^{13}C NMR chemical shifts of the Fe(IV) alkylidene complexes revealed a significant downfield shift of the Fe-bound carbon. X-ray diffraction studies for **4**-PMe_3 and **5** revealed Fe=C distances of 1.809(4) and 1.867(7), respectively.

The crystal structure of $[(pipvd)Fe(PMe_3)_3][BAr^F_4]$ (**6**) is shown in Figure 2.3, with relevant metrics included in the caption. The Fe=C bond length of 1.899(3) Å is the longest observed for the series of Fe(IV) alkylidenes prepared. Table 2.1 shows a comparison to known Fe(IV) alkylidenes with reference to Fe=C and ^{13}C NMR chemical shifts. Of the diamagnetic complexes, **6** features the longest Fe=C bond. *Trans*-influence seems to be responsible for observed bond variances, as Floriani's dianionic tetradentate (tmtaa)Fe=CPh_2 (**B**) complex features a fairly short Fe=C bond, with no ligand *trans* to the diphenylcarbene.[11] The methylimidazole adduct of (TPFPP)Fe=CPh_2 (**A**)[10] features an elongation of the Fe=C bond by 0.55 Å, in agreement with *trans*-influence affecting the bond length.

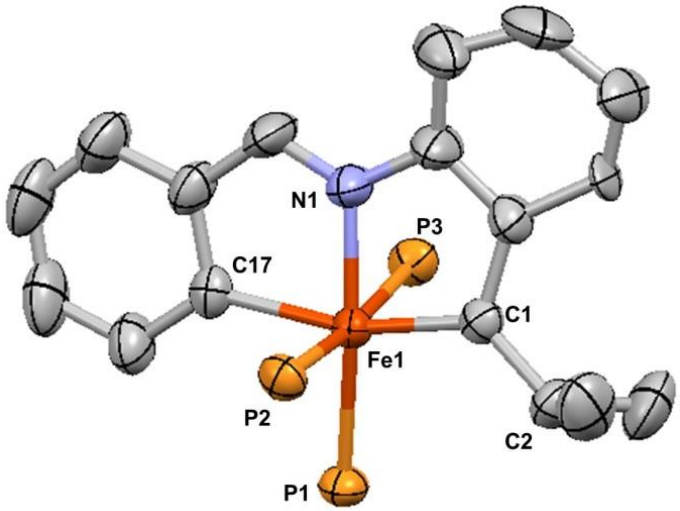

Figure 2.3. X-Ray Crystal Structure of [(pipvd)Fe(PMe_3)$_3$][BAr^F_4] (**6**). Hydrogens, BAr^F_4, and phosphine methyls omitted for clarity. Interatomic distances (Å) and angles (°): Fe-C1, 1.899(3); Fe-N1, 1.933(3); Fe-C17, 2.059(3); Fe-P1, 2.317(2); Fe-P2, 2.226(3); Fe-P3, 2.367(3); C1-C2, 1.525(5); N1-Fe-C17, 80.04(14); C1-Fe-C17, 163.36(15); C17-Fe-P1, 92.03(12); C17-Fe-P2, 88.28(13); C17-Fe-P3, 87.16(12); N1-Fe-C1, 83.34(14); N1-Fe-P1, 167.04(14); N1-Fe-P2, 96.52(16); N1-Fe-P3, 79.34(14); C1-Fe-P1, 104.46(12); C1-Fe-P2, 92.87(12); C1-Fe-P3, 90.53(13).

Table 2.1. Fe=C bond lengths and ^{13}C NMR chemical shifts of select Fe alkylidenes

Compound[a]	*d*(Fe=C) (Å)	δ (^{13}C=Fe)
(tmtaa)Fe=CPh_2 (**B**)[b]	1.794(3)	313.2
(TPFPP)Fe=CPh_2 (**A**)[c]	1.767(3)	359.0
(TPfPP)Fe=CPh_2(MeIm) (**A**)[c]	1.827(5)	385.4
[Cp^*(dppe)Fe=CH(Me)]PF_6 (**E**)[d]	1.787(8)	336.6
(^{Et}PDI)Fe=Ph_2 (**C**)[e]	1.9205(19)	*Para*
[*p*-^{t}Bu-calix[4]$(O)_2(OMe)_2$]Fe=CPh_2 (**D**)[f]	1.943(8)	*Para*
[(bavp)Fe(PMe_3)$_2$][BAr^F_4] (**4**-PMe_3)	1.809(4)	350.6
[(piap)Fe(PMe_3)$_3$][BAr^F_4] (**5**)	1.867(7)	352.6
[(pipvd)Fe(PMe_3)$_3$][BAr^F_4] (**6**)	1.899(3)	348.4

[a] See Fig. 2.2 for ligand structural types corresponding to **A**-**E**. [b] Ref. 11. [c] Ref. 10. [d] Ref. 14. [e] Ref. 12. [f] Ref. 13.

To test the metathesis activity of complexes [(bavp)Fe(PMe_3)$_2$][BAr^F_4] (**4**-PMe_3), [(bavp)Fe(PMe_3)$_2$][BAr^F_4] (**4**-PMe_2Ph), [(piap)Fe(PMe_3)$_3$][BAr^F_4] (**5**) and [(pipvd)Fe(PMe_3)$_3$][BAr^F_4] (**6**), each Fe(IV) alkylidene was exposed to olefin substrates such as *cis*-2-pentene, ethyl vinyl ether or norbornene. It was found that regardless of reaction conditions (23 ^oC, 80 ^oC, exposing to UV light), no metathesis products were observed, and decomposition of the metal complex occurred. Phosphines could competitively bind to the electrophilic metal center over alkenes, which may explain the lack of metathesis activity for complexes **4**-**6**.

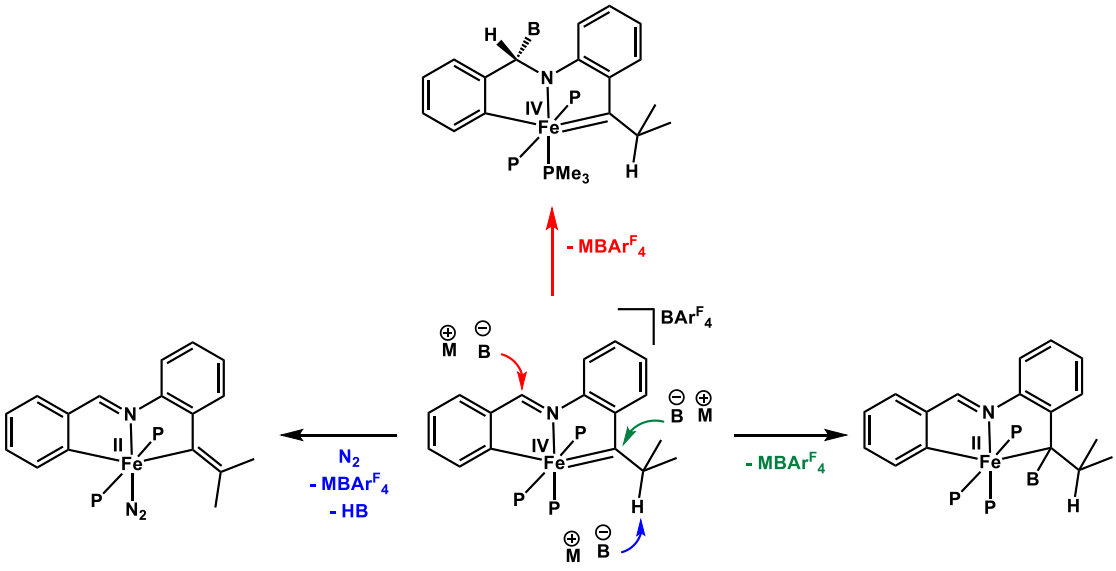

Scheme 2.3. Competing Reaction Pathways of **6** with anionic nucleophiles

Since phosphine dissociation seemed unlikely given the cationic nature of complexes **4**-**6**, generating a neutral Fe(IV) alkylidene should aid in phosphine dissociation. Converting one of the ligands' neutral donors into an anion would produce the desired neutral species. For example, it was thought that a nucleophile

may attack the imine carbon, yielding an amide in the process. Several alternative processes could occur however (Scheme 2.3), such as a) nucleophilic substitution of a phosphine, b) deprotonation to yield the precursor Fe(II) vinyl species, or c) nucleophilic attack at the alkylidene, resulting in an Fe(II) alkyl species.

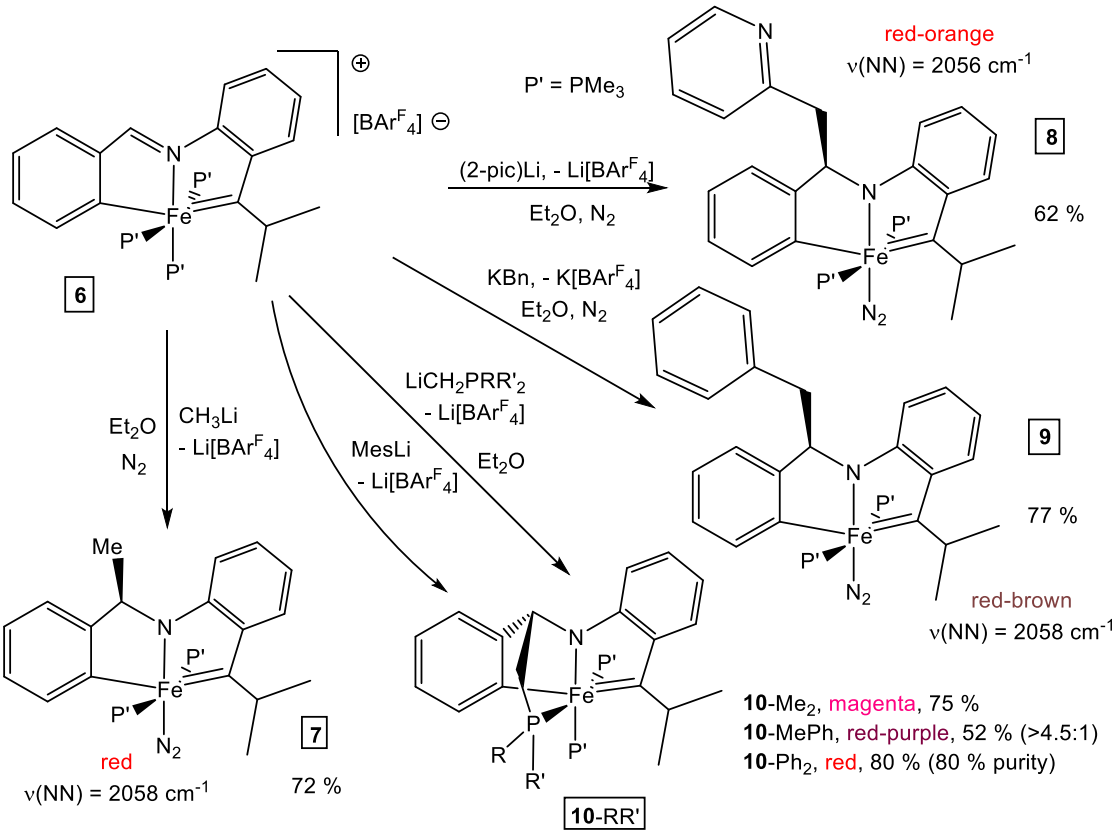

Scheme 2.4. Syntheses of neutral Fe(IV) alkylidenes via nucleophilic attack

Initial studies into treatment of cationic Fe(IV) alkylidenes with nucleophiles focused on the exposure of [(pipvd)Fe(PMe_3)$_3$][BAr^F_4] (**6**) to alkali metal alkyl reagents, as shown in Scheme 2.4. Treatment of **6** with MeLi, 2-picolyllithium[28] and benzyl potassium[29] resulted in selective alkylation at the imine carbon, furnishing the neutral Fe(IV) alkylidene complexes *mer*-{κ-C,N,C-(C_6H_4-yl)-2-CH(R)N(2-C_6H_4)-

C(^{i}Pr)=)}Fe{*trans*-PMe_3}$_2N_2$ (R = Me, **7**; R = 2-pic, **8**; R = Bn, **9**). Curiously, it was found that following the same protocol with MeMgCl led to PMe_3 substitution instead, generating a neutral methyl complex. For compounds **7**, **8** and **9**, displacement of PMe_3 and formation of an N_2 adduct was confirmed via IR spectroscopy, with ν(NN) = 2058, 2056 and 2058 cm^{-1}, respectively, values remarkably close to that possessed by the Fe(II) vinyl precursor *trans*-(pipvd)Fe(PMe_3)$_2N_2$ (**3**) (2046 cm^{-1}).

It was thought that 2-picolyl as a pendant group on the ligand may enable dissociation of PMe_3 and binding of pyridine, but ^{1}H NMR spectroscopy confirmed the presence of two PMe_3 groups. In accordance with this pendant chelation approach, complexes **6** (R = R' = Me,[30] Ph;[31] R = Me, R' = Ph[30]) were treated with nucleophiles LiCH_2PRR', which yielded {κ-C,N,C,P-(C_6H_4-yl)-2-CH(CH_2PRR')N(2-C_6H_4-C(^{i}Pr)=)}Fe(PMe_3)$_2$ (R = R' = Me, **10**-Me_2; R = Me, R' = Ph, **10**-MePh; R = R' = Ph, **10**-Ph_2). Only **10**-Me_2 was isolated as pure magenta crystals, and efforts to purify **10**-Ph_2 led to decomposition products. Since bulkier phosphines were expected to exhibit greater propensity to dissociate, this instability seemed promising. Treatment of **6** with mesityllithium[48] led to deprotonation of PMe_3, which subsequently attacked the imine, providing an alternate route to **10**-Me_2.

The X-ray crystal structure of *mer*-{κ-C,N,C-(C_6H_4-yl)-2-CH(Bn)N(2-C_6H_4)-C(^{i}Pr)=)}Fe{*trans*-PMe_3}$_2N_2$ (**9**) exhibits an Fe=C length of 1.9535(16) Å, comparatively longer than [(pipvd)Fe(PMe_3)$_3$][$BAr^F{}_4$] (**6**) (1.899(2) Å), an expected difference due to the change from cation to neutral. Additional features of the crystal

structure include N_{am}–C_{aryl} and C_{alk}–C_{aryl} distances of 1.326(2) and 1.420(2) Å, which are 0.01-0.02 Å and 0.05 Å shorter than expected.[32]

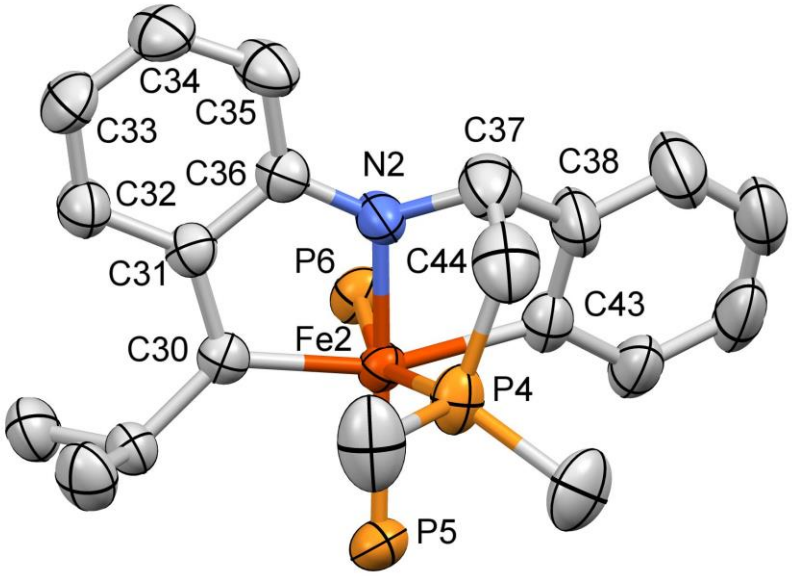

Figure 2.4. Molecular view of one of two independent enantiomers of {κ-C,N,C,P-(C_6H_4-yl)-2-CH(CH_2PMe_2)N(2-C_6H_4-C(^{i}Pr)=)}Fe(PMe_3)$_2$ (**10**-Me_2) with PMe_3 methyl groups removed for clarity. Interatomic distances (Å) and angles (^{o}): Fe2-C30, 1.947(3); Fe2-C43, 2.083(3); Fe2-N2, 1.916(2); Fe2-P4, 2.2142(9); Fe2-P5, 2.2008(9); Fe2-P6, 2.2254(9); N2-C36, 1.329(4); C35-C36, 1.409(4); C34-C35, 1.344(5); C33-C34, 1.390(5); C32-C33, 1.364(4); C31-C32, 1.421(4); C31-C36, 1.420(4); C30-C31, 1.421(4); N2-C37, 1.472(4); C37-C38, 1.493(5); C38-C43, 1.383(5); C37-C44, 1.583(6); P4-C44, 1.820(4); N2-Fe-P5, 174.84(8); C30-Fe2-C43, 161.30(12); P4-Fe2-P6, 159.69(4).

Crystals of {κ-C,N,C,P-(C_6H_4-yl)-2-CH(CH_2PMe_2)N(2-C_6H_4-C(^{i}Pr)=)}Fe(PMe_3)$_2$ (**10**-Me_2) were characterized via X-ray diffraction, and one of two independent enantiomers is depicted in Figure 2.4. Table 2.2 details select crystallographic and refinement data for complexes [(pipvd)Fe(PMe_3)$_3$][$BAr^F{}_4$] (**6**) and **10**-Me_2. The structure of **10**-Me_2 shows an unusual tetradentate ligand that chelates to all but *cis*-sites on an octahedron, and features a long Fe=C bond of

Table 2.2. Select crystallographic and refinement data for [(pipvd)Fe(PMe_3)$_3$][$BAr^F{}_4$] (**6**) and {κ-C,N,C,P-(C_6H_4-yl)-2-CH(CH_2PMe_2)N(2-C_6H_4-C(^{i}Pr)=)}Fe(PMe_3)$_2$ (**10**-Me_2).

	6	**10**-Me_2
formula	$C_{58}H_{55}BF_{24}FeNP_3$	$C_{26}H_{42}FeNP_3$
formula wt	1381.60	517.37
space group	$P2_1/c$	$P2_1/c$
Z	4	8
a, Å	18.4232(6)	17.283(3)
b, Å	13.0619(4)	19.422(3)
c, Å	25.9802(8)	15.933(3)
α, deg	90	90
β, deg	99.5300(10)	92.103(8)
γ, deg	90	90
V, Å^3	6165.6(3)	5344.5(16)
ρ_{calc}, g cm^{-3}	1.488	1.286
μ, mm^{-1}	0.434	0.758
temp, K	233(2)	223(2)
λ (Å)	0.71073	0.71073
R indices	R1 = 0.0476	R1 = 0.0468
[$I > 2\sigma(I)$][a,b]	wR2 = 0.1109	wR2 = 0.1196
R indices[b]	R1 = 0.0780	R1 = 0.0698
(all data)[a]	wR2 = 0.1273	wR2 = 0.1331
GOF[c]	1.050	1.040

[a] $R_1 = \Sigma|F_o| - |F_c||/\Sigma|F_o|$. [b] $wR_2 = [\Sigma w(|F_o| - |F_c|)^2/\Sigma wF_o^2]^{1/2}$. [c] *GOF* (all data) = $[\Sigma w(|F_o| - |F_c|)^2/(n - p)]^{1/2}$, n = number of independent reflections, p = number of parameters.

1.943(6) Å. **10**-Me_2 shares similar unexpected ligand metrics with **6**, such as a short N–C_{ar} distance of 1.329(4) and a long C_{alk}–C_{aryl} distance of 1.426(6) Å. In addition, arene distances suggest an alternative Fe(II) valence bond structure, depicted in Figure 2.5, in which dearomatization has occurred to afford an Fe(II) vinyl species.

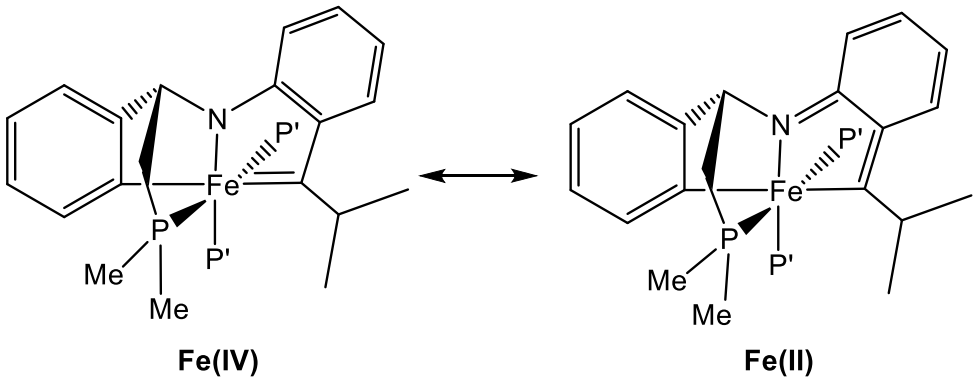

Figure 2.5. Fe(IV) and Fe(II) resonance structures for {κ-C,N,C,P-(C_6H_4-yl)-2-$CH(CH_2PMe_2)N(2\text{-}C_6H_4\text{-}C(^iPr)=)$}$Fe(PMe_3)_2$ (**10**-Me_2) and related complexes

With the successful preparation of a series of neutral Fe(IV) alkylidene complexes *mer*-{κ-C,N,C-(C_6H_4-yl)-2-CH(R)N(2-C_6H_4)-$C(^iPr)=)$}Fe{*trans*-PMe_3}$_2N_2$ (R = Me, **7**; R = 2-pic, **8**; R = Bn, **9**) and the tetradentate variants {κ-C,N,C,P-(C_6H_4-yl)-2-$CH(CH_2PRR')N(2\text{-}C_6H_4\text{-}C(^iPr)=)$}$Fe(PMe_3)_2$ (R = R' = Me, **10**-Me_2; R = Me, R' = Ph, **10**-MePh; R = R' = Ph, **10**-Ph_2), exposure of these compounds to olefins commenced with treatment of **7** with styrene or ethyl vinyl ether. No substantive reactivity was observed, and similar protocols employing complexes **8** and **9** gave the same result. Efforts to trap the unstable **10**-Ph_2 complex with styrene led to no observed product formation, only decomposition. Despite moving from cationic to neutral alkylidenes, no metathesis behavior was observed. Successful Ru-alkylidene catalysts employ Ru(IV)=CHR fragments,[3,4,33] and it seemed likely that the bulky ^{i}Pr group on the alkylidene for our examples may be deleterious to productive metathesis. As such, efforts to prepare Fe(IV)=CHR species with labile ligands were undertaken. In addition, calculations of the electronic ground states of complexes

[(pipvd)Fe(PMe_3)$_3$][BAr^F_4] (**6**) and **9** were obtained to address the metathesis-inactive nature of the cationic and neutral alkylidenes.

Results and Discussion

2.1 Synthesis and Metalation of 2-py-CH=NCH_2-CH=CH_2

Initial efforts in preparing Fe(II) vinyl chelates began with synthesizing a pyridine-imine ligand with a tethered olefin. A simple condensation protocol was efficient for the preparation of 2-py-CH=NCH_2-CH=CH_2 from 2-pyridine-carboxaldehyde and allylamine (Eq 2.2)[34].

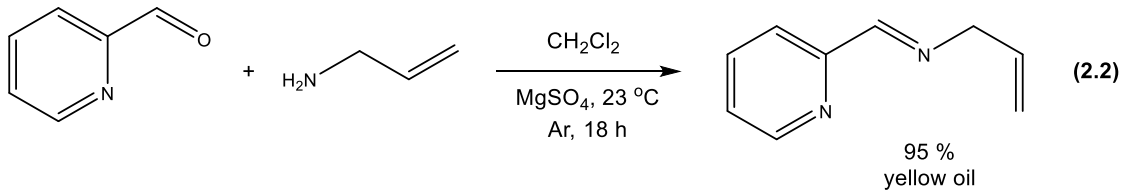

(2.2)

It was envisaged that activation of the olefin C-H bond via Karsch's complex should yield a tridentate Fe(II) vinyl complex. Treatment of 2-py-CH=NCH_2-CH=CH_2 with *cis*-$Me_2Fe(PMe_3)_4$ in benzene resulted in immediate formation of a dark violet solution (Scheme 2.5). ^{1}H NMR spectral analysis revealed one diamagnetic product consistent with the formulation *cis,trans,cis*-{κ^2-N,N-2-py-CH=NCH_2-CH=CH_2}$Fe(PMe_3)_2(CH_3)_2$ (**11**). The C_2-symmetric molecule exhibits one singlet in the $^{31}P\{^1H\}$ NMR spectrum at δ -1.69, confirming the *trans* positioning of the two PMe_3 ligands. Both methyl groups are triplets at δ -0.05 and 1.37 (J_{HP} = 13 Hz). Upon warming **11** in benzene to 30 °C for 2 days, brown diamagnetic *mer,trans*-{κ^3-N,N,C-2-py-CH=NCH_2-CH=CH}$Fe(PMe_3)_2CH_3$ (**12**) was produced in excellent yield (90%).

One triplet in the ^{1}H NMR spectum at δ 1.37 (J_{HP} = 13 Hz) corresponds to the $FeCH_3$, and a singlet in the $^{31}P\{^{1}H\}$ spectrum at δ 9.04 confirms the *mer*,*trans*-conformation.

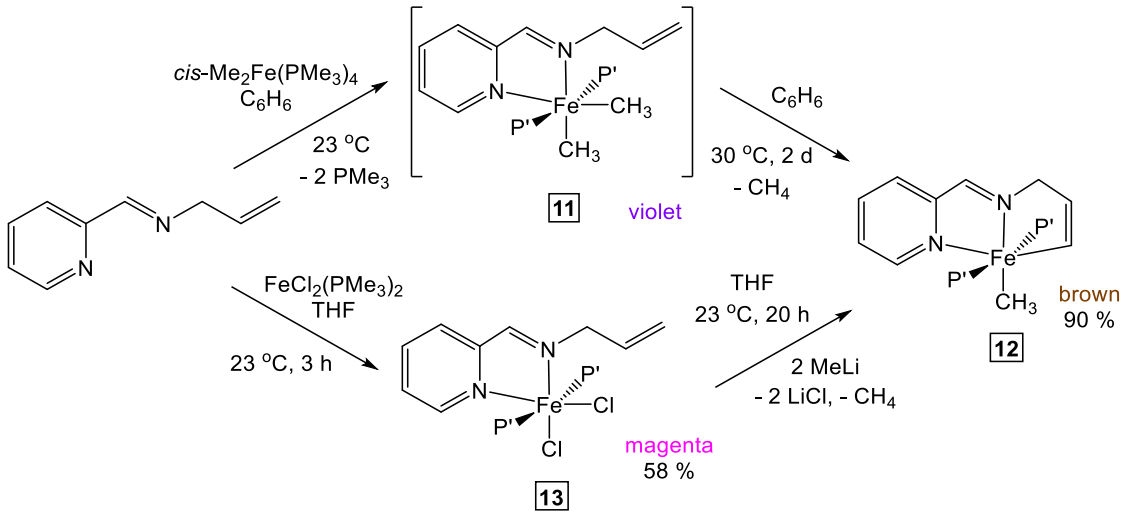

Scheme 2.5. C-H activation and dehydrochlorination approaches to **12**

Given the thermal instability of *cis*-$Me_2Fe(PMe_3)_4$ and the cost of its preparation, an alternative approach incorporating chelation of 2-py-CH=NCH_2-CH=CH_2 to $FeCl_2(PMe_3)_2$,[35] followed by treatment with base, seemed to be an attractive route to *mer*,*trans*-{κ^3-N,N,C-2-py-CH=NCH_2-CH=CH}$Fe(PMe_3)_2CH_3$ (**12**). Combining the ligand with $FeCl_2(PMe_3)_2$ resulted in isolation of *cis*,*trans*-(2-py-CH=$NCH_2CH=CH_2$)$FeCl_2(PMe_3)_2$ (**13**) as sparingly soluble magenta crystals (58% yield). Without purification, alkylation of **13** with 2 equiv MeLi led to formation of a dark brown solution. While the formation of **12** was observed in the crude material, impurities were noted, and the route was abandoned in favor of the initial method.

2.2 Protonation and Oxidation Studies of 12

Since the cationic Fe(IV) alkylidene complexes were prepared via protonation of the *β*-vinyl carbon, an identical approach was undertaken for the protonation of *mer*,*trans*-{κ^3-N,N,C-2-py-CH=NCH$_2$-CH=CH}Fe(PMe$_3$)$_2$CH$_3$ (**12**). Scheme 2.6 shows that exposure of **12** to H[BAr$^F_4$] led to the formation of a mixture of products including methane. Loss of methane would yield a 5-coordinate Fe species, which may further decompose. Additional proton sources such as [BH]Cl (B = lutidine, NEt$_3$) failed to elicit any reactivity with **12**.

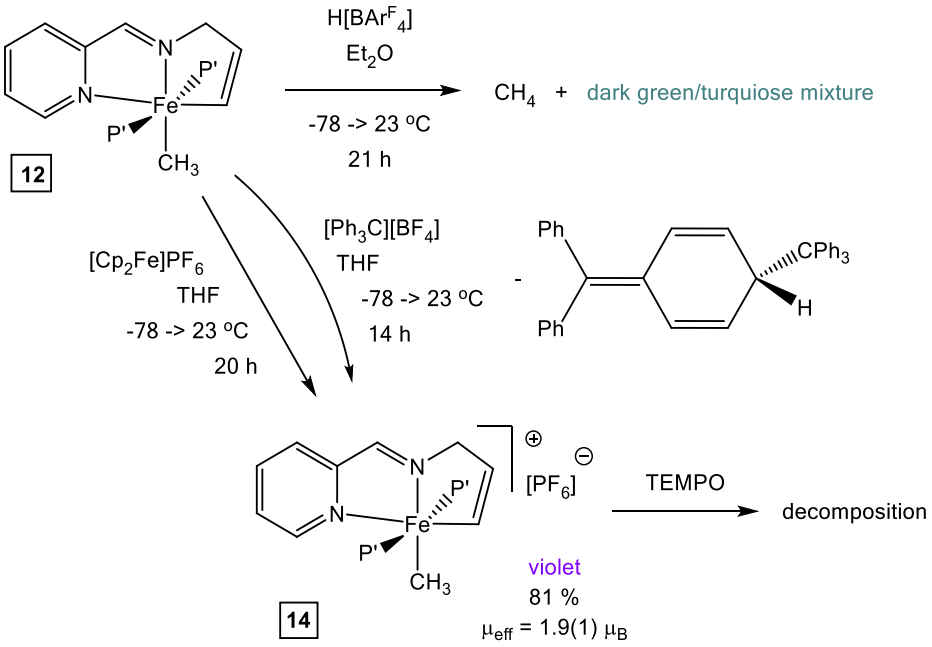

Scheme 2.6. Protonation/oxidation studies of *mer*,*trans*-{κ^3-N,N,C-2-py-CH=NCH$_2$-CH=CH}Fe(PMe$_3$)$_2$CH$_3$ (**12**)

Since protonation of *mer*,*trans*-{κ^3-N,N,C-2-py-CH=NCH$_2$-CH=CH}Fe(PMe$_3$)$_2$CH$_3$ (**12**) was unsuccessful, additional reactivity studies were

carried out to probe the prospect of **12** as a precursor to an Fe(IV) alkylidene. Hydride abstraction from the ligand methylene unit could prepare a totally conjugated Fe(IV) alkylidene, although abstraction from the methyl group was possible, but unlikely to yield a stable species. Treatment of **12** with $[Ph_3C]BF_4$ led to formation of a light violet paramagnetic species and Gomberg's dimer, $(Ph_3C)_2$,[36] consistent with oxidation of the Fe complex. An alternate oxidation of **12** with $[Cp_2Fe]PF_6$ led to clean formation of a similarly violet-colored paramagnetic solid formulated as [*mer,trans*-{κ^3-N,N,C-2-py-CH=NCH_2-CH=CH}Fe$(PMe_3)_2CH_3$][X^-] (**14**, X^- = BF_4^- or PF_6^-). An Evans' method measurement[37] of **14** yields a μ_{eff} of 1.9 μ_B, consistent with a low spin d^5 Fe(III) center with spin-orbit coupling. While hydride abstraction from **12** was unsuccessful, H-atom abstraction from **14** was envisaged to be a potential path to an Fe(IV) alkylidene. Unfortunately, treatment of **14** with TEMPO only led to decomposition of **13**, and further oxidation studies of **12** were abandoned.

2.3 Attempts at Methyl Substitution for Alternative X^- Groups

Given the basicity of the methyl group for complex *mer,trans*-{κ^3-N,N,C-2-py-CH=NCH_2-CH=CH}Fe$(PMe_3)_2CH_3$ (**12**), efforts focused on replacing it with alternate X^- ligands that may exhibit greater stability upon protonation. Attempts to protonate **12** with phenol or the bulky alcohol $PhCMe_2OH$ surprisingly resulted in no

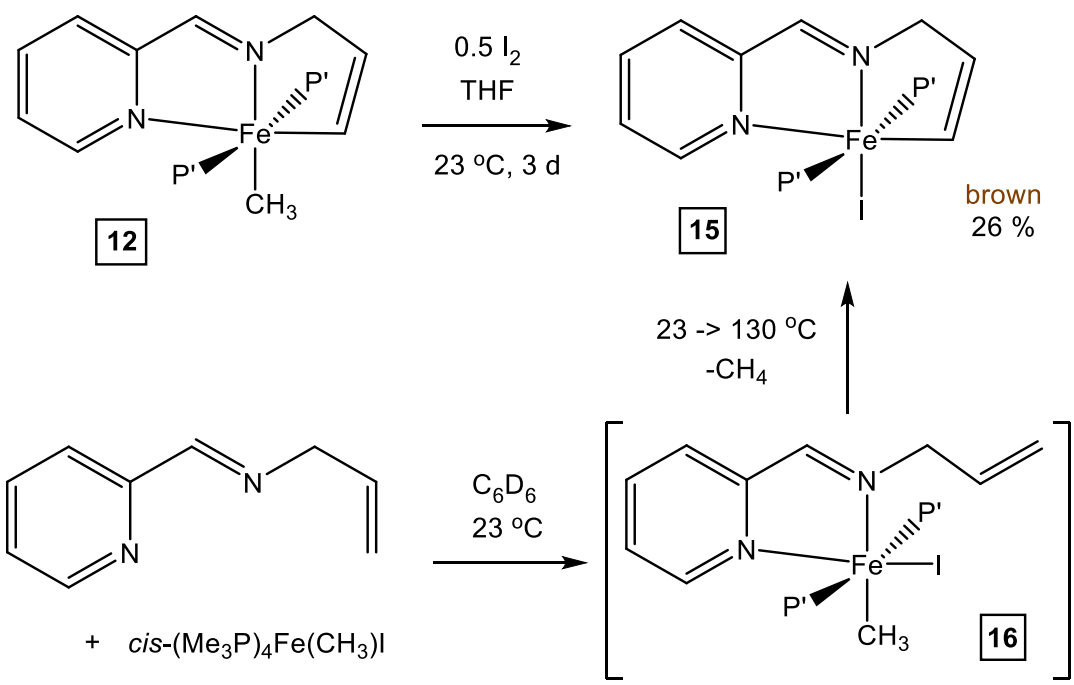

Scheme 2.7. Approaches to I substitution for complex **12**

reaction, with no observed Fe(II) alkoxide formation observed. Earlier treatments of *mer,trans*-{κ^3-N,N,C-2-py-CH=NCH$_2$-CH=CH}Fe(PMe$_3$)$_2$CH$_3$ (**12**) with HCl resulted in the formation of unidentified paramagnetic species, so attempts to install a halide group focused on employing X_2 as a source, with CH_3X as the byproduct. Exposure of **12** to 0.5 equiv I_2 afforded *mer,trans*-{κ^3-N,N,C-2-py-CH=NCH$_2$-CH=CH}Fe(PMe$_3$)$_2$I (**15**) as brown crystals in modest yield (26%), as shown in Scheme 2.7. ^{1}H NMR spectroscopy confirmed the *in situ* formation of ethane and methane as the sole byproducts (3.6:1), with no CH_3I observed. The modest yield and extended reaction time for the preparation of **15** prompted alternative synthetic approaches. Metalation of 2-py-CH=NCH$_2$-CH=CH$_2$ with the Karsch complex variant *cis*-(Me$_3$P)$_4$Fe(CH$_3$)I[22] afforded a dark green solution. A new species was tentatively

formulated as *trans*-{κ^2-N,N-2-py-CH=NCH$_2$-CH=CH$_2$}Fe(PMe$_3$)$_2$(CH$_3$)I (**16**) based on ^{1}H and ^{31}P{^{1}H} NMR spectra. Thermolysis of the mixture led to formation of **15** in 54%, but low purity of the product led to abandoning this route in favor of the earlier method.

The stability of *mer*,*trans*-{κ^3-N,N,C-2-py-CH=NCH$_2$-CH=CH}Fe(PMe$_3$)$_2$I (**15**) to protonation was probed through treatment of it with HBAr$^F_4$, which only resulted in decomposition. A minor product within the mixture possessed a *mer*-(PMe$_3$)$_3$ spectral signature (ABB') in the ^{31}P{^{1}H} NMR spectrum, which has been correlated with addition of an equivalent of PMe$_3$. This process is likely a consequence of protonation of the Fe-vinyl group.

2.4 Deprotonation of 15

Failed attempts to generate Fe(II) alkoxide species from complex *mer*,*trans*-{κ^3-N,N,C-2-py-CH=NCH$_2$-CH=CH}Fe(PMe$_3$)$_2$CH$_3$ (**12**) prompted an alternate metathesis approach starting from *mer*,*trans*-{κ^3-N,N,C-2-py-CH=NCH$_2$-CH=CH}Fe(PMe$_3$)$_2$I (**15**). Treatment of **15** with KO^{t}Bu led to a brown solution composed of several products, one of which featured an ABB' pattern in the ^{31}P{^{1}H} NMR spectrum (Eq 2.3). Since this product implicated decomposition,[38] treatment of **15** with KO^{t}Bu in the presence of PMe$_3$ led to clean formation of the formal Fe(II) alkylidene *mer*-{κ^3-N,N,C-2-py-CH=NCH$_2$-CH=CH}Fe(PMe$_3$)$_3$ (**17**) through a formal dehydroiodination pathway. Notable NMR features include the "alkylidene" proton observed at δ 6.93 ($^3J_{HP2}$ = 2, $^3J_{PH}$ = 3, $^3J_{HH}$) in the ^{1}H NMR and at δ 189.39 (J_{CP2} = 25, J_{CP} = 12) in the ^{13}C{^{1}H} spectrum. The "alkylidene" ^{13}C{^{1}H} chemical shift was

likely attributable to a Fe-vinyl group, rather than a formal alkylidene. For comparison, the analogous Fe-vinyl chemical shifts for complexes *trans*-(pipp)Fe(PMe_3)$_2N_2$ (**2**) and *trans*-(pipvd)Fe(PMe_3)$_2N_2$ (**3**) are δ 207.9 and 167.9, respectively.

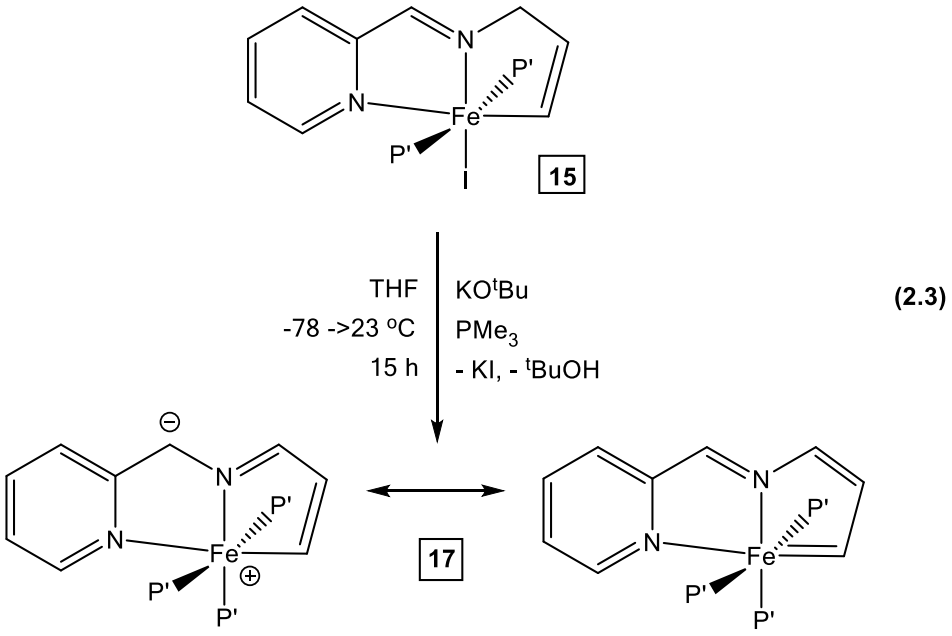

2.5 X-Ray Crystal Structures of 15 and 17

Since the NMR spectroscopic features of complex *mer*-{κ^3-N,N,C-2-py-CH=NCH_2-CH=CH}Fe(PMe_3)$_3$ (**17**) suggested it was an Fe-vinyl species, the geometric and electronic structure was examined. Prior to analysis of the Fe(II) "alkylidene", the structure of *mer,trans*-{κ^3-N,N,C-2-py-CH=NCH_2-CH=CH}Fe(PMe_3)$_2$I (**15**) was determined as a genuine Fe(II) vinyl species for comparison. Crystals of **15** were characterized via X-ray diffraction, with a view shown in Figure 2.6, and pertinent metrics given in the caption. Table 2.3 lists select crystallographic and refinement data for complexes **15** and **17**. The Fe-vinyl distance

of 1.961(2) Å is essentially the same as the "Fe=C" distances for the neutral alkylidene complexes *mer*-{κ-C,N,C-(C_6H_4-yl)-2-CH(Bn)N(2-C_6H_4)-C(^{i}Pr)=)}Fe{*trans*-PMe_3}$_2N_2$ (**9**) and {κ-C,N,C,P-(C_6H_4-yl)-2-CH(CH_2PMe_2)N(2-C_6H_4-C(^{i}Pr)=)}Fe(PMe_3)$_2$ (**10**-Me_2).[39] The remaining ligand metrics match the valence bond depiction, with both d(C1–C2) = 1.332(3) and d(N1–C4) = 1.307(3) Å distances consistent with double bonds, and single bond lengths observed for d(C2–C3) = 1.490(3) and d(N1–C3) = 1.470(3) Å.[32]

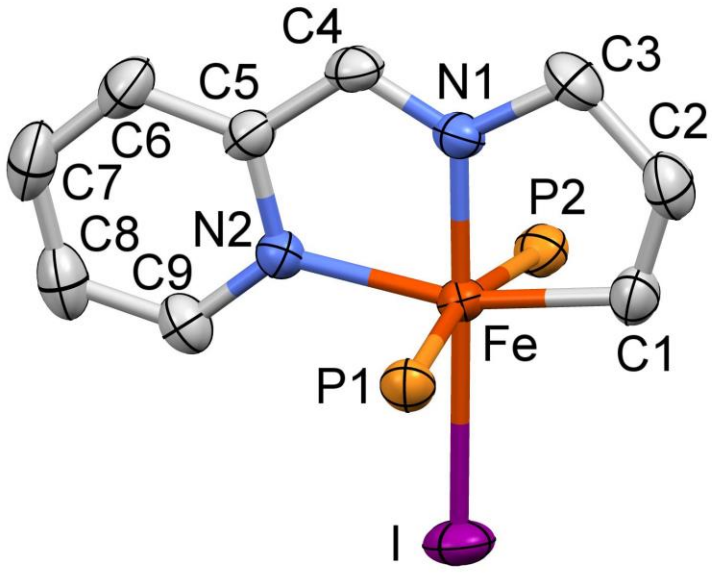

Figure 2.6. Molecular view of *mer*,*trans*-{κ^3-N,N,C-2-py-CH=NCH_2-CH=CH}Fe(PMe_3)$_2$I (**15**) with methyl groups of PMe_3 removed for clarity. Selected interatomic distances (Å) and angles (°): Fe-N1. 1.8514(16); Fe-N2, 2.0129(17); Fe-C1, 1.961(2); Fe-P1, 2.2472(7); Fe-P2, 2.2461(7); Fe-I, 2.7132(5); C1-C2, 1.332(3); C2-C3, 1.490(3); N1-C3, 1.470(3); N1-C4, 1.307(3); C4-C5, 1.428(3); N2-C5, 1.371(3); N2-C9, 1.347(3); C5-C6, 1.396(3); C6-C7, 1.369(3); C7-C8, 1.385(4); C8-C9, 1.373(3); N1-Fe-N2, 80.37(7); N1-Fe-C1, 82.34(9); N1-Fe-P1, 93.94(5); N1-Fe-P2, 95.33(5); N1-Fe-I, 178.78(5); N2-Fe-C1, 162.49(9); N2-Fe-P1, 93.94(5); N2-Fe-P2, 96.72(5); N2-Fe-I, 98.54(5); C1-Fe-P1, 86.21(7); C1-Fe-P2, 87.58(7); C1-Fe-I, 98.73(7); P1-Fe-P2, 168.06(2); P1-Fe-I, 85.56(2); P2-Fe-I, 85.32(2); Fe-C1-C2, 115.01(17); C1-C2-C3, 117.13(19); N1-C3-C2, 105.89(17); C3-N1-C4, 120.22(17); Fe-N1-C3, 119.54(14); Fe-N1-C4, 120.21(14); N1-C4-C5, 113.97(17); C4-C5-N2, 113.02(17); C5-N2-C9, 116.61(18); Fe-N2-C5, 112.33(13); Fe-N2-C9, 130.91(15).

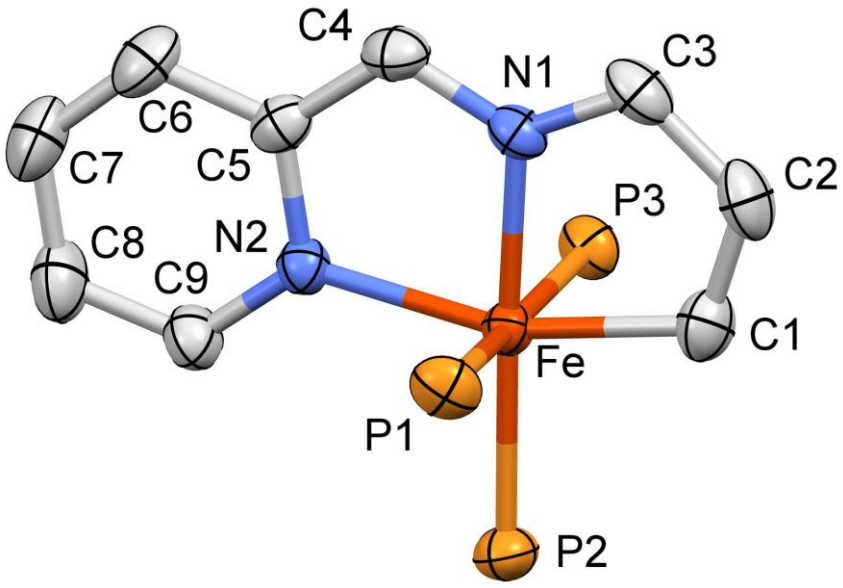

Figure 2.7. Molecular view of *mer*-{κ^3-N,N,C-2-py-CH=NCH$_2$-CH=CH}Fe(PMe$_3$)$_3$ (**17**) with methyl groups of PMe$_3$ removed for clarity. Selected interatomic distances (Å) and angles (^{o}): Fe-N1, 1.9534(14); Fe-N2, 2.0486(13); Fe-C1, 1.9602(17); Fe-P1, 2.2305(5); Fe-P2, 2.2207(5); Fe-P3, 2.2391(5); C1-C2, 1.349(3); C2-C3, 1.426(3); N1-C3, 1.315(2); N1-C4, 1.368(2); C4-C5, 1.384(2); N2-C5, 1.399(2); N2-C9, 1.346(2); C8-C9, 1.376(3); C7-C8, 1.391(3); C6-C7, 1.356(3); C5-C6, 1.418(2); N1-Fe-N2, 80.98(5); N1-Fe-C1, 80.44(7); N1-Fe-P1, 86.44(4); N1-Fe-P2, 177.71(4); N1-Fe-P3, 87.13(4); N2-Fe-C1, 161.42(7); N2-Fe-P1, 91.42(4); N2-Fe-P2, 101.31(4); N2-Fe-P3, 91.98(4); C1-Fe-P1, 87.35(6); C1-Fe-P2, 97.27(6); C1-Fe-P3, 87.18(5); P1-Fe-P2, 93.63(2); P1-Fe-P3, 172.17(2); P2-Fe-P3, 92.62(2); Fe-C1-C2, 114.34(14); Fe-N2-C9, 131.56(12); Fe-N2-C5, 111.17(10); Fe-N1-C3, 116.39(13); Fe-N1-C4, 115.74(11); C1-C2-C3, 114.78(14); N1-C3-C2, 114.03(16); C3-N1-C4, 127.86(16); N1-C4-C5, 115.88(15); N2-C5-C4, 116.22(15).

The molecular structure of *mer*-{κ^3-N,N,C-2-py-CH=NCH$_2$-CH=CH}Fe(PMe$_3$)$_3$ (**17**) is shown in Figure 2.7, with relevant metrics in the caption. The Fe-vinyl distance of 1.9602(17) Å is nearly identical to its precursor, and can be safely assigned as a single bond. While the C1–C2 distance of 1.349(3) Å is consistent with a double bond, C2–C3 shortens to 1.426(3) Å. In concert with this change is the

shortened N1–C3 distance of 1.315(2) Å, in agreement with a double bond. N1–C4 elongates to 1.368(2) Å, with the ligand featuring a $d(C–N)_{ave}$ of 1.35 Å, corresponding to an asymmetric 2-azaallyl unit.[40] The picolyl fragment features additional metric variances, with C4–C5 shortening to 1.384(2) Å, and pyridine N2–C5/C5–C6 distances of 1.399(2) and 1.418(2) Å that are slightly longer than normal.[32] Deprotonation of the ligand furnishes a 2-azaallyl unit that features a delocalized anion, with some anionic charge in the ring.

Table 2.3. Select crystallographic and refinement data for *mer*,*trans*-{κ^3-N,N,C-2-py-CH=NCH$_2$-CH=CH}Fe(PMe$_3$)$_2$I (**15**) and *mer*-{κ^3-N,N,C-2-py-CH=NCH$_2$-CH=CH}Fe(PMe$_3$)$_3$ (**17**).

	15	**17**
formula	$C_{15}H_{27}FeN_2P_2I$	$C_{18}H_{35}FeN_2P_3$
formula wt	480.07	428.24
space group	$P2_1/n$	P-1
Z	4	2
a, Å	8.5494(14)	8.8875(7)
b, Å	13.792(2)	9.4239(7)
c, Å	17.322(8)	14.2393(10)
α, deg	90	85.191(4)
β, deg	98.124(7)	81.684(4)
γ, deg	90	70.182(4)
V, Å^3	2022.0(6)	1109.41(15)
ρ_{calc}, g cm^{-3}	1.577	1.282
μ, mm^{-1}	2.427	0.899
temp, K	223(2)	223(2)
λ (Å)	0.71073	0.71073
R indices	R1 = 0.0328	R1 = 0.0410
[$I > 2\sigma(I)$][a,b]	wR2 = 0.0782	wR2 = 0.1026
R indices[b]	R1 = 0.0426	R1 = 0.0557
(all data)[a]	wR2 = 0.0830	wR2 = 0.1095
GOF[c]	1.078	1.060

[a]$R_1 = \Sigma|F_o| - |F_c||/\Sigma|F_o|$. [b]$wR_2 = [\Sigma w(|F_o| - |F_c|)^2/\Sigma wF_o^2]^{1/2}$. [c]*GOF* (all data) = $[\Sigma w(|F_o| - |F_c|)^2/(n - p)]^{1/2}$, n = number of independent reflections, p = number of parameters.

2.6 Calculations for the Electronic Structure of 17

X-ray crystallographic analysis of *mer*-{κ^3-N,N,C-2-py-CH=NCH$_2$-CH=CH}Fe(PMe$_3$)$_3$ (**17**) implicated an Fe(II)–C(sp^2) complex with a delocalized anion, and the electronic structure was explored via calculations. The truncated molecular orbital diagram of **17** in Figure 2.8 illustrates the results. The calculated metric parameters are within 0.03 Å of the distances from the structural analysis. The three lowest energy orbitals are the "t$_{2g}$" set for an octahedral species

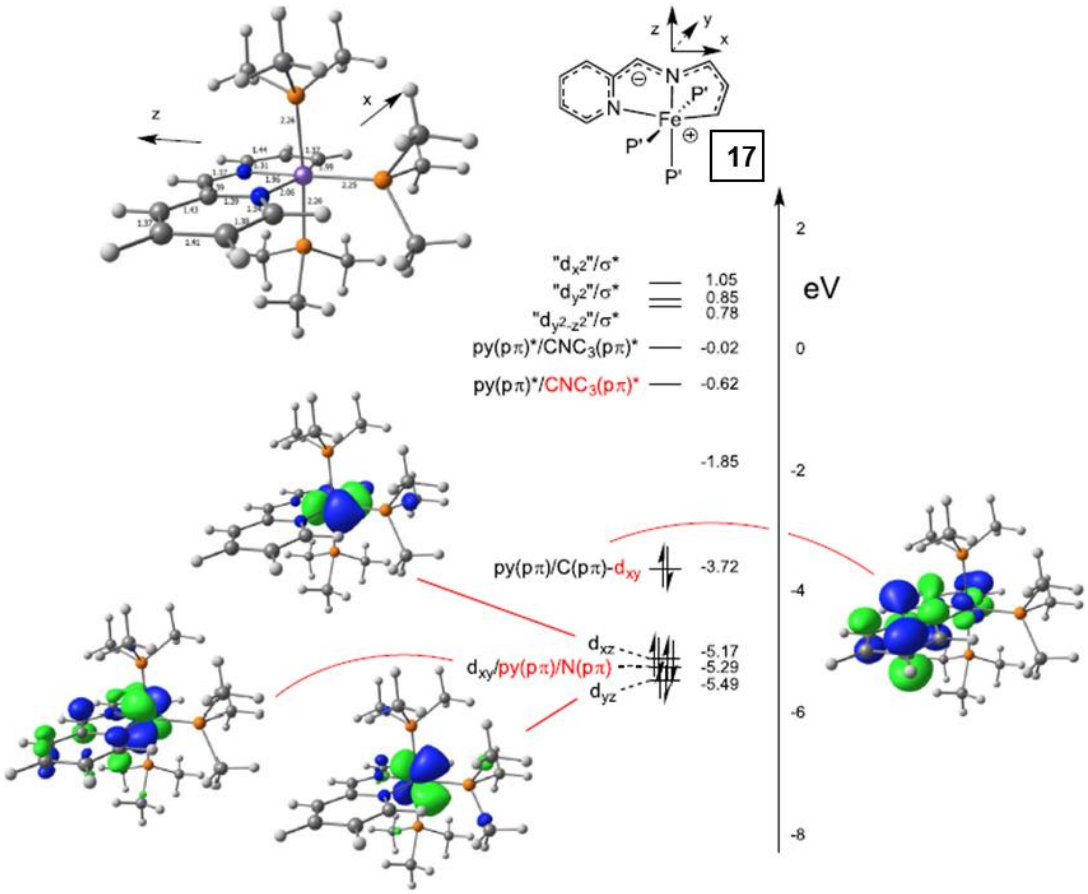

Figure 2.8. Truncated molecular orbital diagram of *mer*-{κ^3-N,N,C-2-py-CH=NCH$_2$-CH=CH}Fe(PMe$_3$)$_3$ (**17**) (P' = PMe$_3$), including illustrations of four occupied orbitals (principal components in black; minor in red). Optimized geometry (M06/6-31+G(d)) shown in upper left; bond lengths in Å.

(d_{yz}, d_{xy} and d_{xz}), with a minor amount of chelate π-orbitals admixed with d_{xy}. The HOMO is a chelate-based π^*-orbital with a minor amount of d_{xy}. The small amount of mixing between d_{xy} and the chelate π-orbitals suggest an Fe(II)-vinyl species with a delocalized chelate anion, and not an Fe(II)-alkylidene.

2.7 Synthesis and Metalation of *trans*-(2-py)CH=NCMe$_2$-CH=CHPh

Since Fe complexes incorporating 2-py-CH=NCH$_2$-CH=CH$_2$ resulted in decomposition upon protonation, potentially due to olefin isomerization, gem-dimethyl chelate variants were examined. Lindley previously prepared *trans*-PhCH=NC(Me$_2$)CH=CH$_2$, but found that attempts to metalate it with *cis*-Me$_2$Fe(PMe$_3$)$_4$ were unproductive, potentially due to steric influences. Efforts to prepare a pyridine analog were successful, with the synthetic route shown in Scheme 2.8. Palladium-catalyzed Heck coupling[41,42] of 1,1'-dimethylprop-2-en-1-ol with phenyl iodide yielded the coupled product **A** in 42% yield.[43] Silver-mediated azidation employing trimethylsilyl azide (TMSN$_3$) yielded the tertiary allylic azide **B**.[44]

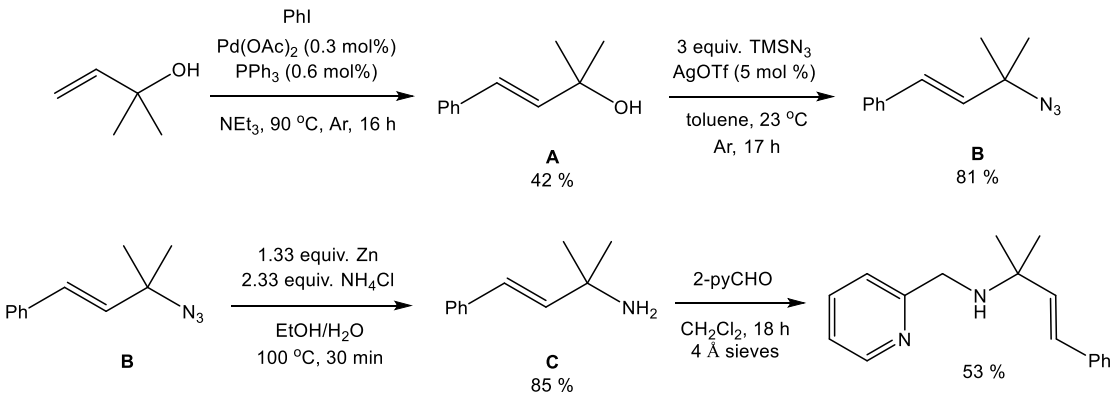

Scheme 2.8. Preparation of *trans*-(2-py)CH=NC(Me$_2$)CH=CHPh

Reduction of the azide with zinc powder and ammonium chloride led to formation of the desired allylic amine precursor **C**.[45] Lastly, condensation of the amine with 2-pyridinecarboxaldehyde yielded the ligand *trans*-(2-py)CH=NC(Me_2)CH=CHPh (53%) as a yellow oil.

Treatment of *trans*-(2-py)CH=NC(Me_2)CH=CHPh with *cis*-$Me_2Fe(PMe_3)_4$ led to an immediate dark violet color, and workup after only 2 h at 23 °C afforded *mer*,*trans*-{κ^3-N,N,C-(2-py)CH=NC(Me_2)CH=CPh}Fe(PMe_3)$_2CH_3$ (**18**) as violet crystals in 65% yield (Eq 2.4). The gem-dimethyl effect imposed by the ligand C(sp^3) atom led to facile C-H activation to yield complex **18** under ambient conditions. A $^{31}P\{^1H\}$ NMR spectrum confirmed the *trans* positioning of the two PMe_3 ligands (s, δ 0.56), and the pendant Fe-CH_3 exhibited a triplet pattern at δ 2.13 (J_{PH} = 13 Hz) by ^1H NMR spectroscopy.

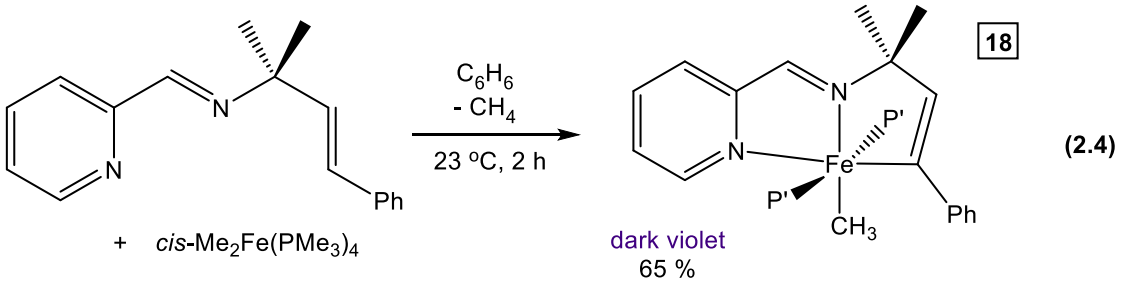

(2.4)

2.8 Protonation of 18

Studies of *mer*,*trans*-{κ^3-N,N,C-(2-py)CH=NC(Me_2)CH=CPh}Fe(PMe_3)$_2CH_3$ (**18**) focused solely on protonation, which is illustrated in Scheme 2.9. Protonation of **18** with H[BAr^F_4] *in vacuo* led to a violet solid, tentatively assigned as [{κ^3-N,N,C-(2-py)CH=NC(Me_2)CH=CPh}Fe(PMe_3)$_2$] [BAr^F_4] (**19**) with a yield of 70%. Dissolution

of the violet solid in THF under a dinitrogen atmosphere led to an immediate change in solution color to red. NMR and IR analysis of the red product confirmed its formulation as the N_2 adduct [{κ^3-N,N,C-(2-py)CH=NC(Me_2)CH=CPh}Fe(PMe_3)$_2N_2$] [BAr^F_4] (**20**), with the IR spectrum showing an absorption at 2116 cm^{-1} corresponding to the ν(NN) stretch.[38,46] A singlet at δ 9.10 in the $^{31}P\{^1H\}$ NMR spectrum confirmed the C_s symmetry.

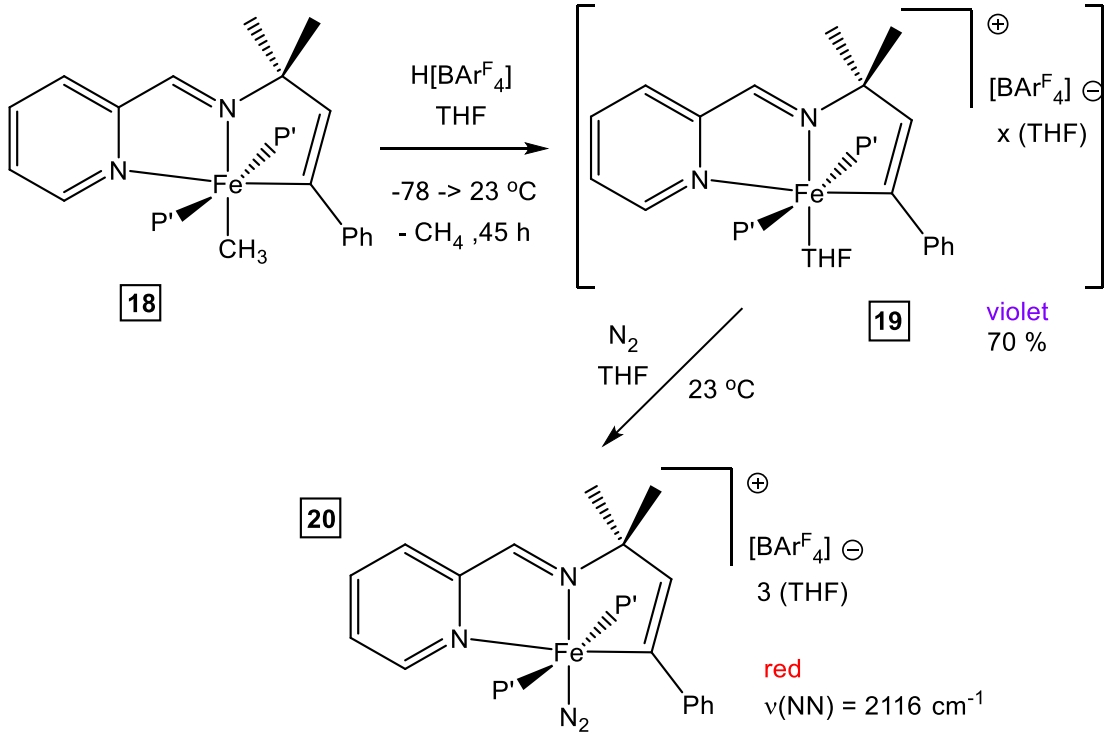

Scheme 2.9. Treatment of **18** with H[BAr^F_4]

2.9 Calculations for the Electronic Structure of 6

Since treatment of the cationic alkylidene complex [*mer*-{κ^3-C,N,C-(2-C_6H_4)CH=N(1,2-C_6H_4)C(^{i}Pr)=}Fe(PMe_3)$_3$] [BAr^F_4] (**6**)[38] with various alkenes yielded

no metathesis products, the electronic structure was explored via calculations, and the truncated molecular orbital diagram is illustrated in Figure 2.9. The diagram features

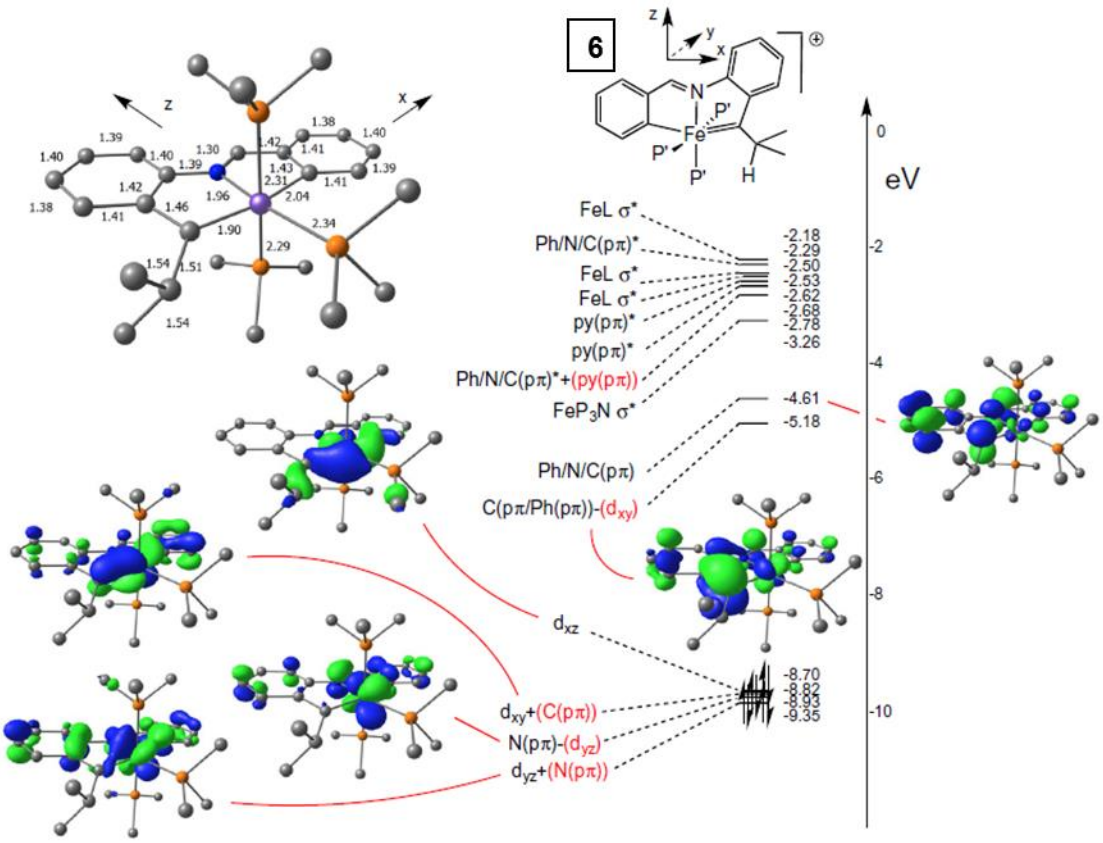

Figure 2.9. Truncated molecular orbital diagram of [*mer*-{κ^3-C,N,C-(2-C_6H_4)CH=N(1,2-C_6H_4)C(^{i}Pr)=}Fe(PMe_3)$_3$] [$BAr^F{}_4$] (**6**, P' = PMe_3), including illustrations of four occupied and the first two unoccupied orbitals (principal components black; minor in red). Optimized geometry (M06/6-31+G(d)) shown in upper left; bond lengths in Å.

highly admixed Fe/ligand orbitals, with two orbitals being essentially d_{yz} +/- N(pπ), where the d-orbital is spread within bonding and anti-bonding interactions of the imine and both conjugated phenyl groups. While two electrons are in d_{xz}, the orbital that is Fe=C π-bonding also has two electrons. The Fe=C π-bonding orbital is largely d_{xy} in

composition, and its π-antibonding orbital partner shows the cation localizes on the carbon of the alkylidene. Figure 2.10 illustrates the valence bond depiction of **6** based on the calculations, where the complex is Fe(II) d^6 chelated to an C(sp^2) cation. Mössbauer spectral parameters of **6** (δ = 0.07(1) mm s^{-1}; ΔE_Q = 1.97(1) mm s^{-1}) are similar to its Fe(II) vinyl precursor *trans*-(pipvd)Fe(PMe_3)$_2N_2$ (**3**) (δ = 0.07(1) mm s^{-1}; ΔE_Q = 2.20(1) mm s^{-1}),[38] indicating similar electron densities on Fe, which is in agreement with the molecular orbital diagram.

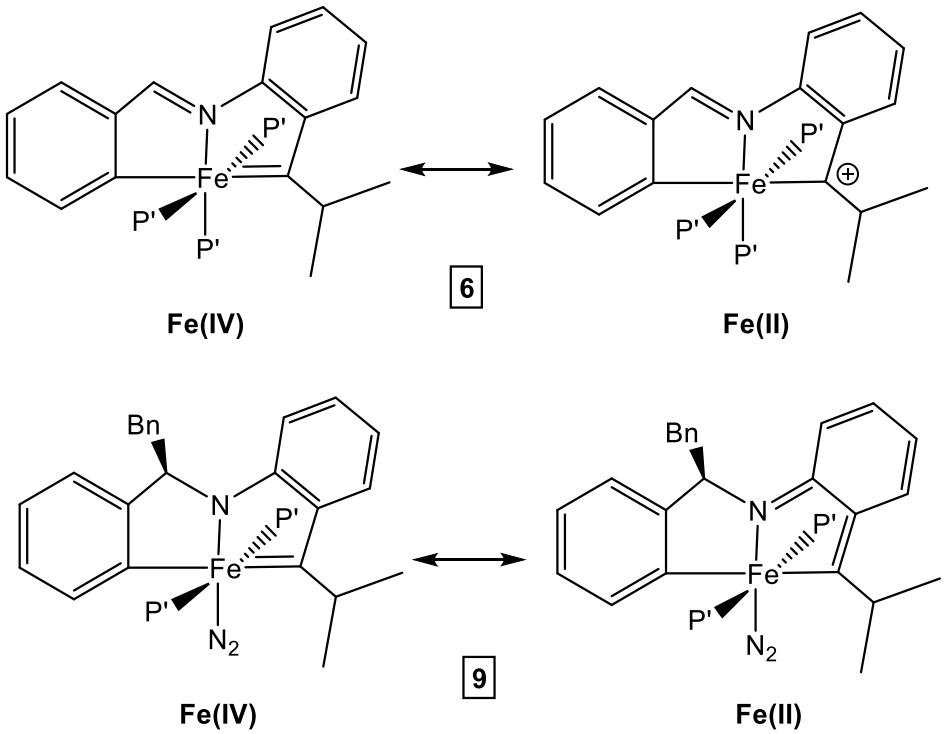

Figure 2.10. Valence bond representations of the cation [*mer*-{κ^3-C,N,C-(2-C_6H_4)CH=N(1,2-C_6H_4)C(^{i}Pr)=}Fe(PMe_3)$_3$] [BAr^F_4] (**6**) and neutral *mer*,*trans*-{κ^3-C,N,C-(2-C_6H_4)CH(Bn)N(1,2-C_6H_4)C(^{i}Pr)=}Fe(PMe_3)$_2N_2$ (**9**).

2.10 Calculations for the Electronic Structure of 9

The valence bond depiction of *mer,trans*-{κ^3-C,N,C-(2-C_6H_4)CH(Bn)N(1,2-C_6H_4)C(^{i}Pr)=}Fe(PMe_3)$_2N_2$ (**9**)[39] in Figure 2.10 indicates that a formal Fe(II) species necessitates disruption of the aromaticity of the aromatic ring attached to the "alkylidene." Crystal structure metrics for **9** reveal several shortened bond distances for C_{aryl}–N (1.326(2) Å) and C_{aryl}–C_{alk} (1.420(2) Å), along with a long "Fe=C" distance of 1.9535(16) Å. These metrics are consistent with the Fe(II) resonance form, and the truncated molecular orbital diagram in Figure 2.11 support the Fe(II)

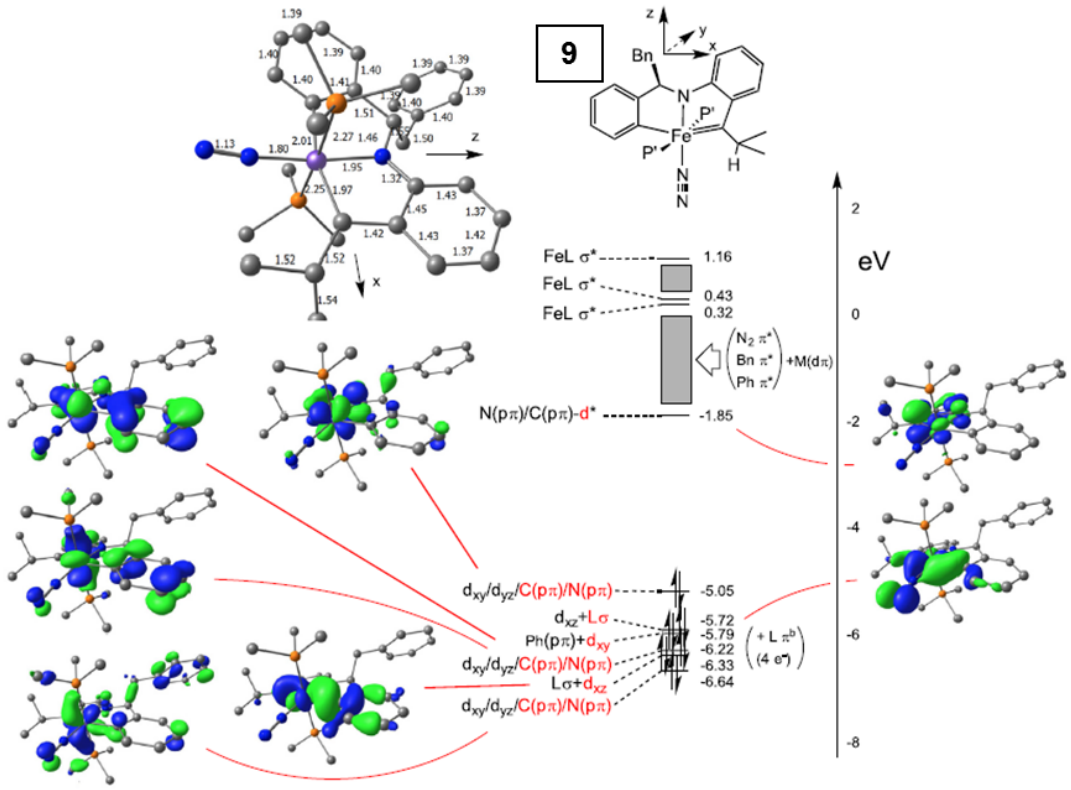

Figure 2.11. Truncated molecular orbital diagram of *mer,trans*-{κ^3-C,N,C-(2-C_6H_4)CH(Bn)N(1,2-C_6H_4)C(^{i}Pr)=}Fe(PMe_3)$_2N_2$ (**9**, P' = PMe_3), including several illustrations of six occupied and the first unoccupied orbitals (principal components in black; minor in red). The shaded boxes are regions of energy in which several orbitals of dominant ligand composition exist. Optimized geometry (M06/6-31+G(d)) shown in upper left; bond lengths in Å.

designation. The calculations indicate that three occupied and one unoccupied orbitals are linear combinations of d_{xy}, d_{yz}, C(pπ) and N(pπ) due to the 1,2-^{i}PrC,NR-C_6H_4 group interacting as a unit. In addition, the six occupied orbitals have significant Fe composition admixed with chelate orbitals, making it difficult to assess the d-count of Fe due to the covalency of the system. The unoccupied orbital at -1.85 eV has the correct phase to be interpreted as the "Fe=C" π-antibonding orbital, yet lacks significant interaction between the metal and the C(sp^2). Taken together, the molecular orbital diagram and crystal structure metrics of **9** suggest that the Fe(II) resonance form is an important component of the electronic ground state.

Conclusion

A series of octahedral Fe(II) vinyl chelates complexes *mer*,*trans*-{κ^3-N,N,C-2-py-CH=NCH$_2$-CH=CH}Fe(PMe$_3$)$_2$CH$_3$ (**12**), *mer*,*trans*-{κ^3-N,N,C-2-py-CH=NCH$_2$-CH=CH}Fe(PMe$_3$)$_2$I (**15**) and *mer*,*trans*-{κ^3-N,N,C-(2-py)CH=NC(Me$_2$)CH=CPh}Fe(PMe$_3$)$_2$CH$_3$ (**18**) were prepared as potential precursors for the synthesis of Fe(IV) alkylidenes. Protonation of all complexes with H[BAr$^F{}_4$] led to methane loss, which led to decomposition of **12** and **15**, but **18** formed an N$_2$ adduct when dissolved under an N$_2$ atmosphere. Dehydroiodination of **15** afforded the putative Fe(II) alkylidene *mer*-{κ^3-N,N,C-2-py-CH=NCH$_2$-CH=CH}Fe(PMe$_3$)$_3$ (**17**). X-ray structural analysis and computational studies showed **17** is best considered an Fe(II) vinyl complex with an anion delocalized in the chelate π-system. Calculations for the electronic structures of prior Fe(IV) alkylidenes [*mer*-{κ^3-C,N,C-(2-C$_6$H$_4$)CH=N(1,2-C$_6$H$_4$)C(^{i}Pr)=}Fe(PMe$_3$)$_3$] [BAr$^F{}_4$] (**6**) and *mer*,*trans*-{κ^3-C,N,C-(2-C$_6$H$_4$)CH(Bn)N(1,2-C$_6$H$_4$)C(^{i}Pr)=}Fe(PMe$_3$)$_2$N$_2$ (**9**) portray the "alkylidene" of **6** as carbenium-like and **9** as a vinyl carbon.

Experimental

General considerations. All manipulations were performed using either glovebox or high vacuum line techniques, unless stated otherwise. All glassware was oven dried at 180 ^{o}C. THF and ether were distilled under nitrogen from purple sodium benzophenone ketyl and vacuum transferred from the same prior to use. Hydrocarbon solvents were treated in the same manner with the addition of 1–2 mL/L tetraglyme. Benzene-d_6 was dried over sodium, vacuum transferred and stored over sodium. THF-d_8 was dried over sodium, and vacuum transferred from sodium benzophenone ketyl prior to use. Chloroform-d_1 (Cambridge Isotope Laboratories) was used as received. 2-py-CH=NCH_2CH=CH_2,[34] *E*-PhCH=CHCMe_2NH_2,[43-45] *cis*-Me(I)Fe(PMe_3)$_4$, *cis*-Me_2Fe(PMe_3)$_4$,[22] [(Et_2O)$_2$H] [(3,5-(CF_3)$_2$$C_6H_3$)$_4$B] (H[BArF 4]),[27] Fe($PMe_3$)$_4$[47] and $FeCl_2$(PMe_3)$_2$[35] were prepared according to literature procedures.

NMR spectra were obtained using Inova 400 MHz, 500 MHz and 600 MHz spectrometers. Chemical shifts are reported relative to benzene-d_6 (^{1}H δ 7.16; ^{13}C{^{1}H} δ 128.39), THF-d_8 (^{1}H δ 3.58; ^{13}C{^{1}H} δ 67.57) and chloroform-d_1 (^{1}H δ 7.26; ^{13}C{^{1}H} δ 77.16). Electronic structure calculations (M06/6-31+G(d) simulation) were performed by Dr. Thomas R. Cundari at the University of North Texas, Department of Chemistry, Center for Advanced Scientific Computing and Modeling (CASCaM). Accurate mass data were acquired on an Exactive Orbitrap mass spectrometer (Thermo Scientific) using a DART (IonSense Inc., Saugus, MA) ion source in positive ion mode and He for ionization, while software affiliated with the spectrometer was used to calculate the molecular weight. Solution magnetic measurements were

conducted via Evans' method in THF-d_8.[37] Elemental analyses were performed by Robertson Microlit Laboratories, Madison, New Jersey.

Procedures

1. *E*-2-py-CH=NCMe$_2$CH=CHPh. To a 25-mL flask containing 2-pyridinecarboxaldehyde (0.23 g, 2.1 mmol) and (*E*)-2-methyl-4-phenyl-3-buten-2-amine (0.34 g, 2.1 mmol) was added 10 mL CH_2Cl_2. Oven dried 4 Å sieves (2 g) were added to the solution, and the flask was covered with a rubber stopper and stirred for 20 h. The solution was filtered, and the volatiles removed, yielding the product as a yellow oil (0.28 g, 53%). ^{1}H NMR ($CDCl_3$): δ 1.52 (6H, s, CH_3), 6.34 (1H, d, 16 Hz, PhCH=CH), 6.53 (1H, d, 16 Hz, Ph-CH=CH), 7.22 (1H, t, 7 Hz, *p*-Ph C–H), 7.29–7.33 (3H, m, *m*-Ph C–H and pyridyl-5-CH), 7.40 (2H, d, 8 Hz, *o*-Ph C–H), 7.74 (1H, t, 8 Hz, pyridyl-4-CH), 8.07 (1H, d, 8 Hz, pyridyl-3-CH), 8.43 (1H, s, N=CH), 8.63 (1H, d, 5 Hz, pyridyl-6-CH). ^{13}C NMR ($CDCl_3$): δ 28.32, 61.76, 121.28, 124.70, 126.49, 127.46, 128.49, 128.60, 136.64, 136.79, 137.20, 149.44, 155.35, 158.64. HRMS (DART-MS) m/z: [M+H]+ calc. for 251.1504; Found 251.1536.

2. *mer,trans*-{κ^3-N,N,C-2-py-CH=NCH$_2$CH=CH}Fe(PMe$_3$)$_2$CH$_3$ (12). A 60 mL bomb reactor was charged with 2-py-CH=NCH$_2$CH=CH2 (300 mg, 2.05 mmol) and 5 mL benzene. A separate vial was charged with *cis*-$(PMe_3)_4Fe(CH_3)_2$ (801 mg, 2.05 mmol) and 5 mL benzene, and the solution was added to the bomb, resulting in an immediate color change from faint yellow to dark violet. The mixture was warmed to 30 °C and stirred for 2 d, with the solution gradually changing color to dark brown. The volatiles were removed *in vacuo*, and the solid residue was taken up in diethyl

ether and transferred to a separate 50-mL flask. The solvent was removed *in vacuo*, and the solid was washed with pentane (3x25 mL) and filtered. The pentane solution was concentrated, cooled to -78 °C for 30 min, and filtered to afford brown crystals of **12** (684 mg, 90%). ^{1}H NMR (C_6D_6): δ 0.57 (18H, t, 3 Hz, $P(CH_3)_3$), 1.37 (3H, t, 13 Hz, Me), 4.39 (2H, br s, CH_2), 6.45 (1H, dtt, 9, 7, 2 Hz, NCH_2CH), 6.90 (1H, br d, 8 Hz, py-3-CH), 7.01 (1H, td, 7, 2 Hz,, py-4-CH), 7.04 (1H, ddt, 9, 6, 2 Hz, Fe–CH=CH), 7.08 (1H, m, 9 Hz, py-5-CH), 8.55 (1H, d, 6 Hz, py-6-CH), 9.05 (1H, s, N=CH). ^{13}C NMR (C_6D_6): δ -6.17 (t, 34 Hz), 10.14 (t, 11 Hz), 69.63, 120.60, 121.07, 125.77, 126.18, 152.34, 152.65, 161.76, 174.29 (t, 37 Hz). ^{31}P NMR (C_6D_6): δ 9.04. Anal. for $C_{16}H_{30}FeN_2P_2$ (calc.) C 52.19; H 8.21; N 7.61; (found) C 51.92; H 8.04; N 7.55.

3. *mer,trans*-{κ^3-N,N,C-2-py-CH=NCH$_2$CH=CH}Fe(PMe$_3$)$_2$CH$_3$ (12) via *cis,trans*-(2-py-CH=NCH$_2$CH=CH$_2$)FeCl$_2$(PMe$_3$)$_2$ (13) *a.* To a 25 mL flask charged with 2-py-CH=NCH$_2$CH=CH$_2$ (121 mg, 0.828 mmol) and $FeCl_2(PMe_3)_2$ (231 mg, 0.828 mmol) was added 5 mL THF via vacuum transfer at -78 °C. The solution was allowed to warm to 23 °C, changed to a magenta color, and was stirred for an additional 3 h. The volatiles were removed *in vacuo*, and the magenta solid was washed with pentane (3x10 mL). The pentane solution was filtered, affording magenta crystals of **13** (204 mg, 58%). ^{1}H NMR (THF-d_8): δ 1.18 ($\nu_{1/2}$ = 14 Hz), 62.94 ($\nu_{1/2}$ = 588 Hz); low solubility hampered analysis by ^{1}H NMR spectroscopy. Crystalline **13** was used without further purification or analysis. *b.* To a 25 mL flask fitted with a stopcock and charged with **7** (75 mg, 0.18 mmol) was added 10 mL THF via vacuum transfer at -78

^{o}C. The magenta solution was warmed to 23 ^{o}C, and MeLi (1.6 M in Et_2O, 0.22 mL, 0.35 mmol) was added via syringe. The solution was stirred for 20 h, and became dark brown. The volatiles were removed and the residue was washed with pentane (3x10 mL), yielding an oily brown material. ^{1}H and ^{31}P NMR spectra (C_6D_6) were consistent with the production of **12**. ^{1}H NMR (THF-d_8): δ 62.94 ($\nu_{1/2}$ = 534 Hz).

4. [*mer,trans*-{κ^3-N,N,C-2-py-CH=NCH$_2$CH=CH}Fe(PMe$_3$)$_2$CH$_3$] [X$^-$] (14, X$^-$ = PF$_6^-$). To a 25-mL flask charged with **12** (100 mg, 0.272 mmol) and $[Cp_2Fe]PF_6$ (90 mg, 0.27 mmol) was added 10 mL THF via vacuum transfer at -78 ^{o}C. The dark brown solution was allowed to warm slowly over 20 h, and a color change to violet was observed at 23 ^{o}C. The volatiles were removed and the residue washed with pentane (3x10 mL). Violet microcrystals (113 mg, 81%) were collected via filtration of the pentane solution after washing with pentane. ^{1}H NMR (THF-d_8): δ -14.06 ($\nu_{1/2}$ = 775 Hz), 6.39 ($\nu_{1/2}$ = 105 Hz). μ_{eff} (Evans) = 1.9 μ_B.

5. *mer,trans*-{κ^3-N,N,C-(2-pyridyl)CHNCH$_2$CH=CH}Fe(PMe$_3$)$_2$I (15). To a 25-mL flask charged with **12** (300 mg, 0.815 mmol) and iodine (103 mg, 0.406 mmol) was added 12 mL THF at -78 C. The solution was stirred under N_2 for 3 d at 23 ^{o}C, and the color gradually changed from dark brown to dark green. The volatiles were removed and the residue was washed with pentane (3x10 mL). The solid was taken up in 10 mL C_6H_6 and filtered, followed by removal of the solvent and 3 mL of pentane was added to the residue. Brown microcrystals (106 mg, 26%) were isolated via filtration. Crystals suitable for X-ray diffraction were obtained via slow evaporation of a concentrated Et_2O solution. ^{1}H NMR (C_6D_6): δ 0.95 (18H, ‘‘t”, 4 Hz, PMe_3), 3.89

(2H, br s, CH_2), 6.06 (1H, q, 7 Hz, N-CH_2-CH), 6.87 (2H, t, 8 Hz, py-4/5-CH and Fe–CH=CH), 6.93 (1H, t, 7 Hz, py-5-CH), 7.93 (1H, dt, 8, 2 Hz, Fe–CH=CH), 8.40 (1H, s, N=CH), 9.68 (1H, d, 6 Hz, py-6-CH). $^{13}C\{^1H\}$ NMR (C_6D_6): δ 12.69 (t, 12 Hz), 67.71 (t, 3 Hz), 121.68, 121.99, 125.02 (t, 6 Hz), 129.45, 157.44, 157.77 (t, 2 Hz), 160.06, 172.47 (t, 33 Hz). ^{31}P NMR (C_6D_6): δ -1.16. Anal. for $C_{15}H_{27}FeN_2P_2I$ (calc.) C 37.53; H 5.67; N 5.84; (found) C 37.80; H 5.62; N 5.75.

6. *mer*-{κ^3-N,N,C-(2-pyridyl)CHNCHCH=CH}Fe(PMe_3)$_3$ (17). A 25-ml flask fitted to a 31-mL gas bulb was charged with **15** (40 mg, 0.081 mmol) and ^{t}BuOK (9 mg, 0.8 mmol). PMe_3 (4.9 cm Hg, 0.081 mmol) was transferred via vacuum transfer to the gas bulb, and subsequently frozen in the flask at 77 K. 5 mL THF was vacuum transferred to the flask, and the solution warmed to -78 C. The dark green solution was allowed to warm slowly to 23 ^{o}C over 15 h, and the color changed to orange-brown. The volatiles were removed and the residue was washed with pentane (3x5 mL). The residue was taken up in pentane and filtered, followed by removal of the solvent to afford a dark brown solid (39 mg,>95%). Crystals suitable for X-ray diffraction were obtained via slow evaporation of a concentrated pentane solution at -30 C. ^1H NMR (C_6D_6): δ 1.03 (9H, d, 5 Hz, PMe_3), 1.30 (18H, ‘‘t”, PMe_3), 5.24 (1H, m, 6 and 2 Hz, py-4-CH), 5.63 (1H, br dt, 9, 1 Hz, py-3-CH), 5.66 (1H, q, 2 Hz, N-CH-py), 6.33 (1H, m, 7, 1 Hz, py-5-CH), 6.52 (1H, tq, 4, 2 Hz, FeCH=CH-CH), 6.56 (1H, dtt, 8, 4, 1 Hz, Fe–CH=CH), 6.70 (1H, d, 6 Hz, py-6-Hz), 6.93 (1H, dtt, 7, 3, 2 Hz, Fe–CH). $^{13}C\{^1H\}$ NMR (C_6D_6): δ 15.95 (dd, 10 and 2 Hz), 16.05 (dd, 10 and 2 Hz), 21.37 (dt, 17 and 3 Hz), 102.88 (t, 2 Hz), 103.85, 108.28 (t, 2 Hz), 133.03 (t, 2 Hz), 136.81 (d, 8 Hz), 138.84 (t, 2 Hz),

153.93 (d, 3 Hz), 161.81 (d, 3 Hz), 189.39 (td, 25 and 12 Hz). ^{31}P NMR (C_6D_6): δ 19.36 (ABB', ''d", J_{PP} = 54 Hz), 23.47 (ABB', ''t", J_{PP} = 51 Hz). Anal. for $C_{18}H_{36}FeN_2P_3$ (calc.) C 50.48; H 8.24; N 6.54; (found) C 50.29; H 7.92; N 6.45.

7. *mer,trans*-{κ^3-N,N,C-(2-py)CH=NC(Me)$_2$CH=CPh}Fe(PMe$_3$)$_2$CH$_3$ (18). To a 50-mL flask charged with *E*-2-py-CH=NCMe$_2$CH=CHPh (0.25 g, 1.00 mmol) was added 5 mL C_6H_6 at 23 °C. To a separate vial charged with *cis*-Me$_2$Fe(PMe$_3$)$_4$ (390 mg, 0.999 mmol) was added 5 mL C_6H_6, and this solution was added to the original, which became dark violet. The mixture was stirred at 23 °C for 2 h. The volatiles were removed and the residue taken up in 10 mL pentane. The pentane mixture was filtered, concentrated and cooled to -78 C for 30 min, affording violet microcrystals that were collected by filtration (309 mg, 65%). ^{1}H NMR (C_6D_6): δ 0.41 (18H, t, 3 Hz, PMe$_3$), 1.97 (6H, s, N-C(CH$_3$)$_2$), 2.13 (3H, t, 13 Hz, Fe–CH$_3$), 6.03 (1H, t, 6 Hz, Fe–C=CH), 6.93 (1H, m, py-3-CH), 7.04 (2H, m, py-4/5-CH), 7.14 (1H, t, 7 Hz, *p*-Ph CH), 7.19 (2H, d, 8 Hz, *o*-Ph CH), 7.31 (1H, t, 8 Hz, *m*-Ph CH), 8.41 (1H, br s, py-6-CH), 9.53 (1H, s, N=CH). ^{13}C NMR (C_6D_6): δ -2.36 (t, 35 Hz), 12.63 (t, 9 Hz), 29.78, 75.97 (t, 2 Hz), 120.50 (t, 2 Hz), 121.77, 123.54, 126.82, 127.28, 128.34, 128.57, 137.02 (t, 4 Hz), 152.14, 152.58, 154.86, 164.29, 170.71 (t, 32 Hz). ^{31}P NMR (C_6D_6): δ 0.56. Anal. for $C_{24}H_{38}FeN_2P_2$ (calc.) C 61.02; H 8.11; N 5.93; (found) C 60.73; H 8.01; N 5.99.

8. [*mer,trans*-{κ^3-N,N,C-(2-py)CH=NC(Me)$_2$CH=CPh}Fe(PMe$_3$)$_2$N$_2$][BAr$^F_4$] (20). To a 50-mL flask charged with **18** (75 mg, 0.16 mmol) and H[BAr$^F_4$] (161 mg, 0.159 mmol) was transferred 10 mL THF at -78 °C. The resulting blue solution was allowed to slowly warm to 23 °C over 45 h. The volatiles were removed, and the violet solid

was washed with pentane (3x10 mL). The pentane solution was filtered, and violet microcrystals, which crystallized with 3 equiv THF, were collected (170 mg, 70%). Dissolution of the crystals in THF-d_8 under N_2 produced a color change from blue to red-brown as **20** formed completely. ^{1}H NMR (THF-d_8): δ 0.97 (18H, t, 4 Hz, PMe_3), 1.62 (6H, s, N-C(CH_3)$_2$), 1.77 (12H, m, THF), 3.62 (12H, m, THF), 5.71 (1H, t, 6 Hz, Fe–C=CH), 7.05 (1H, br s, py-3-CH), 7.15 (1H, t, 7 Hz, *p*-Ph CH), 7.20 (2H, d, 8 Hz, *o*-Ph CH), 7.28 (2H, t, 7 Hz, *m*-Ph CH), 7.55 (4H, br s, BAr^F_4 *p*-Ph CH), 7.76 (9H, br s, BAr^F_4 *o*-Ph CH), 8.11 (2H, d, 4 Hz, py-(4,5)-CH), 8.94 (1H, d, 6 Hz, py-6-CH), 9.06 (1H, t, 5 Hz, N=CH). ^{13}C NMR (THF-d_8): δ 11.63 (t, 12 Hz), 29.74, 75.35 (t, 2 Hz), 118.29, 122.36, 124.53, 126.29, 126.70, 128.08, 128.63, 128.65, 128.86, 129.98 (q, 32 Hz), 135.70, 136.75 (t, 5 Hz), 137.60, 152.08, 160.60, 162.32 (d, 50 Hz), 163.11 (d, 50 Hz), 170.41 (24 Hz). ^{31}P NMR (THF-d_8): δ 9.10. IR (Nujol mull): ν(N_2) = 2116 cm^{-1}.

9. Attempt to Synthesize 15 on NMR Tube Scale from $(Me_3P)_4FeI(CH_3)$: Evidence for *trans*-{κ^2-N,N-2-py-CH=NCH$_2$CH=CH$_2$}Fe(PMe$_3$)$_2$(CH$_3$)I (16). To an NMR tube charged with 2-py-CH=NCH$_2$CH=CH$_2$ (7 mg, 0.05 mmol) and $MeFe(I)(PMe_3)_4$ (24 mg, 0.048 mmol) was added 573 mg C_6D_6, resulting in a dark green solution. The tube was flame sealed with a torch, and NMR spectra were taken over the course of 80 h at 23, 30, 55, 75, 90, and 130 °C. No color change from the initial green was observed despite temperature and reaction time. The major product was characterized by ^{1}H and ^{31}P NMR. ^{1}H NMR (C_6D_6): δ 0.95 (18H, br s, PMe_3), 1.32 (3H, br t, 3 Hz,CH_3), 3.87 (2H, s, N-CH_2), 5.86 (1H, m, N-CH_2-CH=CH_2), 6.06

(1H, br d, 6 Hz, N-CH_2-CH=CH_2), 6.82 (1H, m, N-CH_2-CH), 6.87 (2H, m, py-(3,4)-CH), 7.93 (1H, m, Fe–CH=CH), 8.35 (1H, s, N=CH), 9.68 (1H, s, py-6-CH). ^{31}P NMR (C_6D_6): δ 1.13. **15** was produced in 54% conversion as determined by ^{1}H NMR, based on product-to-free ligand methylene ratios (1.86:1.59).

Single crystal X-ray diffraction studies. Upon isolation, the crystals were covered in polyisobutenes and placed under a cold N_2 stream on the goniometer head of a Siemens P4 SMART CCD area detector (graphite-monochromated MoKα radiation, λ = 0.71073 Å). The structures were solved by direct methods (SHELXS). All non-hydrogen atoms were refined anisotropically unless stated, and hydrogen atoms were treated as idealized contributions (Riding model).

References

(1) Lutz, E. F. *J. Chem. Ed.* **1986**, *63*, 202.

(2) Reuben, B.; Wittcoff, H. *J. Chem. Ed.* **1988**, *65*, 605.

(3) Schwab, P.; France, M. B.; Ziller, J. W.; Grubbs, R. H. *Angew. Chem. Int. Ed.* **1995**, *34*, 2039.

(4) Scholl, M.; Ding, S.; Lee, C. W.; Grubbs, R. H. *Org. Lett.* **1999**, *1*, 953.

(5) Schrock, R. R.; Hoveyda, A. H. *Angew. Chem. Int. Ed.* **2003**, *42* (38), 4592–4633.

(6) Schrock, R. R. *Angew. Chem. Int. Ed.* **2006**, *45*, 3748.

(7) Grubbs, R. H. *Angew. Chem. Int. Ed.* **2006**, *45*, 3760.

(8) Chauvin, Y. *Angew. Chem. Int. Ed.* **2006**, *45*, 3740.

(9) Eisenstein, O.; Hoffmann, R.; Rossi, A. R. *J. Am. Chem. Soc.* **1981**, *103*, 5582.

(10) Li, Y.; Huang, J.-S.; Zhou, Z.-Y.; Che, C.-M.; You, X.-Z. *J. Am. Chem. Soc.* **2002**, *124*, 13185.

(11) Klose, A.; Solari, E.; Florinai, C.; Re N.; Chiesi-Villa, A.; Rizzoli, C. *Chem. Commun.* **1997**, 2297.

(12) Russell, S. K.; Hoyt, J. M.; Bart, S. C.; Milsmann, C.; Stieber, S. C. E.; Semproni, S. P.; DeBeer, S.; Chirik, P. J. *Chem. Sci.* **2014**, *5*, 1168.

(13) Esposito, V.; Solari, E.; Floriani, C.; Re, N.; Rizzoli, C.; Chiesi-Villa, A. *Inorg. Chem.* **2000**, *39*, 2604.

(14) Brookhart, M.; Tucker, J. R. *J. Am. Chem. Soc.* **1981**, *103*, 979.

(15) Brookhart, M.; Studabaker, W. B.; Husk, G. R. *Organometallics* **1985**, *4*, 943.

(16) Kuo, G.-H.; Helquist, P.; Kerber, R. C. *Organometallics* **1984**, *3*, 806.

(17) Kremer, K. A. M.; Kuo, G.-H.; O'Connor, E. J.; Helquist, P.; Kerber, R. C. *J. Am. Chem. Soc.* **1982**, *104*, 6119.

(18) Bodnar, T.; Cutler, A. R. *J. Organomet. Chem* **1981**, *213*, C31-C36.

(19) Davison, A.; Selegue, J. P. *J. Am. Chem. Soc.* **1978**, *100*, 7763.

(20) Bruce, M. I.; Swincer, A. G. *Aust. J. Chem.* **1980**, *33*, 1471.

(21) Casey, C. P.; Miles, W. H.; Tukada, H.; O'Connor, J. M. *J. Am. Chem. Soc.* **1982**, *104*, 3761.

(22) Karsch, H. H. *Chem. Ber.* **1977**, *110*, 2699.

(23) Xu, G.; Sun, H.; Li, X. *Organometallics* **2009**, *28*, 6090.

(24) Camadanli, S.; Beck, R.; Flörke, U.; Klein, H.-F. *Organometallics* **2009**, *28*, 2300.

(25) Volpe, E. C.; Wolczanski, P. T.; Lobkovsky, E. B. *Organometallics* **2010**, *29*, 364.

(26) Bartholomew, E. R.; Volpe, E. C.; Wolczanski, P. T.; Lobkovsky, E. B.; Cundari, T. R. *J. Am. Chem. Soc.* **2013**, *135*, 3511.

(27) Brookhart, M.; Grant, B.; Volpe, Jr., A. F. *Organometallics* **1992**, *11*, 3920.

(28) Vergnaud, J.; Ayed, T.; Hussein, K.; Vendier, L.; Grellier, M.; Bouhadir, G.; Barthelat, J.-C.; Sabo-Etienne, S.; Bourissou, D. *Dalton Trans.* **2007**, 2370.

(29) Summerscales, O. T.; Batista, E. R.; Scott, B. L.; Wilkerson, M. P.; Sutton, A. D. *Eur. J. Inorg. Chem.* **2016**, 4551.

(30) Meinholz, M. M.; Pandey, S. K.; Deuerlein, S. M.; Stalke, D. *Dalton Trans.* **2011**, *40*, 1662.

(31) Schore, N. E.; LaBelle, B. E. *J. Org. Chem.* **1981**, *46*, 2306.

(32) Allen, F.H.; Kennard, O.; Watson, D. G.; Brammer, L.; Orpen, A. G.; Taylor, R. *J. Chem. Soc., Perkin Trans. II* **1987**, S1-S19.

(33) Kingsbury, J. S.; Harrity, J. P. A.; Bonitatebus, P. J.; Hoveyda, A. H. *J. Am. Chem. Soc.* **1999**, *121*, 791.

(34) Larock, R. C.; Rogness, D. C.; Markina, N. A.; Waldo, J. P. *J. Org. Chem.* **2012**, *77*, 2743.

(35) H. H. Karsch, *Chem. Ber.* **1977**, *110*, 2222.

(36) Gomberg, M. *J. Am. Chem. Soc.* **1900**, *22*, 757.

(37) (a) Evans, D. F. *J. Chem. Soc.* **1959**, 2003. (b) Schubert, E. M. *J. Chem. Ed.* **1992**, *69*, 62.

(38) Lindley, B. M.; Swidan, A.; Lobkovsky, E. B.; Wolczanski, P. T.; Adelhardt, M.; Sutter, J.; Meyer, K. *Chem. Sci.* **2015**, *6*, 4730.

(39) Lindley, B. M.; Jacobs, B. P.; MacMillan, S. N.; Wolczanski, P. T. *Chem. Commun.* **2016**, *52*, 3891.

(40) Frazier, B. A.; Bartholomew, E. R.; Wolczanski, P. T.; DeBeer, S.; Santiago-Berrios, M.; Abruña, H. D.; Lobkovsky, E. B.; Bart, S. C.; Mossin, S.; Meyer, K.; Cundari, T. R. *Inorg. Chem.* **2011**, *50*, 12414.

(41) Heck, R. F.; Nolley, Jr., J. P. *J. Org. Chem.* **1972**, *37*, 2320.

(42) Mizoroki, T.; Mori, K.; Ozaki, A. *Bull. Chem. Soc. Jap.* **1971**, *44*, 581.

(43) Alexanian, E. J.; Schmidt, V. A. *Angew. Chem. Int. Ed.* **2010**, *49*, 4491.

(44) Rueping, M.; Vila, C.; Uria, U. *Org. Lett.* **2012**, *14*, 768.

(45) Mi, A.; Lin, W.; Ziang, X.; He, Z.; Jin, Y.; Gong, L. *Synth. Commun.* **2002**, *32*, 3279.

(46) Bartholomew, E. R.; Volpe, E. C.; Wolczanski, P. T.; Lobkovsky, E. B.; Cundari, T. R. *J. Am. Chem. Soc.* **2013**, *135*, 3511.

(47) Guan, H.; Bhattacharya, P.; Krause, J. A. *Organometallics* **2011**, *30*, 4720.

(48) Kajiyama, K.; Yoshimune, M.; Nakamoto, M.; Matsokawa, S.; Koyima, S.; Akiba, K. *Org. Lett.* **2001**, *3*, 1873.

Chapter 3

Synthesis of Low Coordinate Fe(II) Chelates Bearing κ-C,N/P Type Ligands as Precursors to Fe(IV) Alkylidenes

Introduction

Efforts to generate octahedral Fe(IV) alkylidenes via protonation of Fe(II) vinyl precursors failed to elicit species that were productive for olefin metathesis.[1,2] Subsequent exposure of the cationic Fe(IV) complexes to nucleophiles led to production of neutral Fe(IV) alkylidenes, which exhibited similar reactivity towards alkenes.[3] Approaches to the preparation of Fe alkylidenes focused on developing suitable low-coordinate Fe(II) complexes that employ labile chelate donor ligands, similar to the Grubbs-Hoveyda Ru catalysts.[4-6]

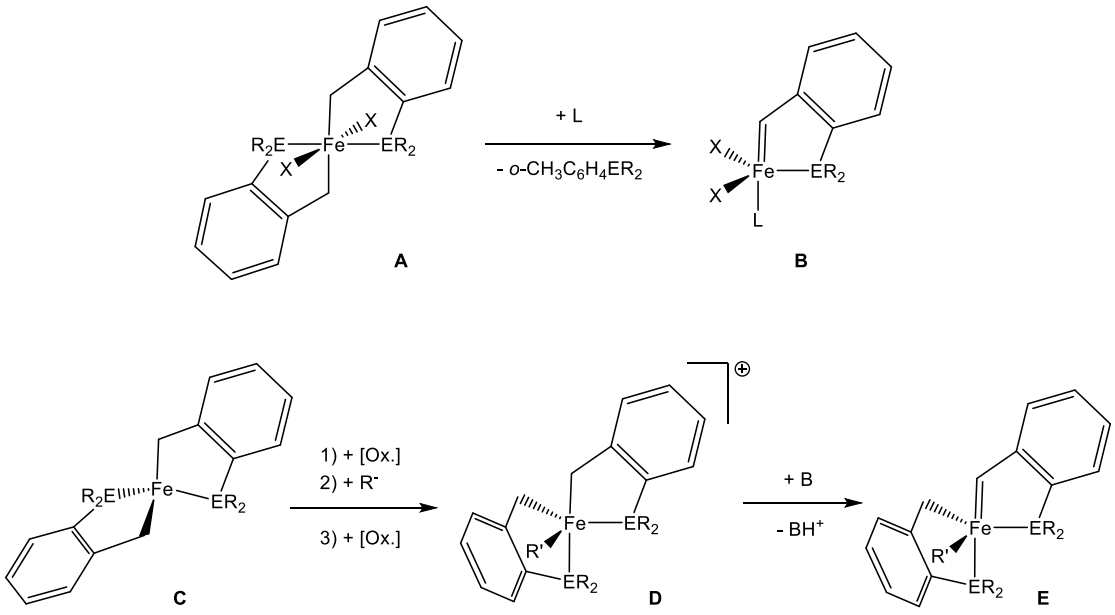

Scheme 3.1. New approaches towards synthesis of Fe alkylidenes

Several synthetic approaches to generating Fe(IV) alkylidenes from Fe(II)-CH_2R species are illustrated in Scheme 3.1. One method involves inducing α-H abstraction from the Fe(IV) benzyl complex **A**, while another pathway features sequential oxidation/alkylation of the Fe(II) complex **C** to make the cationic Fe(IV) species **D**. Deprotonation of **D** with exogenous base could produce the Fe(IV) alkylidene **E**. The former method has ample precedent for d^0 Ta(V)-$CH_2X(CH_3)_3$ (X = C, Si) systems,[7-10] and it was envisaged that either method may afford low-coordinate Fe alkylidenes that possess a pendant donor ligand.

Results and Discussion

3.1 Synthesis of *o*-Phenyl Derived C,N and C,P Ligands

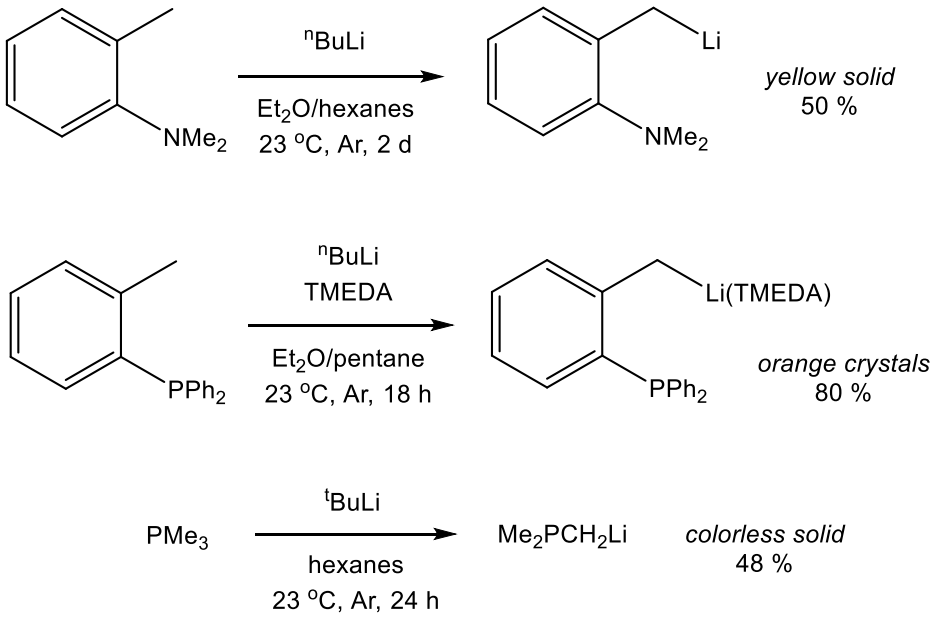

Scheme 3.2. Preparation of alkyllithium chelate precursors

Initial ligand designs for the preparation of Fe(II)-CH_2R that incorporate labile nitrogen or phosphorus donors in the ligand framework focused on isolation of

alkyllithium chelate precursors suitable for salt metathesis. Deprotonation of *o*-$CH_3C_6H_4NMe_2$, *o*-$C_6H_4PPh_2$ and PMe_3 afforded the products in high yield,[11-14] as shown in Scheme 3.2. Since potential steric issues could inhibit chelation of the PPh_2-based ligand, the alternative PMe_2 variant was pursued. Eq 3.1 details the modified approach towards the preparation of *o*-$CH_3C_6H_4PMe_2$ in good yield.[15] Treatment of *o*-$CH_3C_6H_4PMe_2$ with ^{n}BuLi led to an intractable mixture, in contrast to the chelate precursors prepared in Scheme 3.2. It was envisaged that *cis*-$Me_2Fe(PMe_3)_4$[16] may activate the $ArCH_3$ C-H bond, and the alkyllithium was not pursued any further.

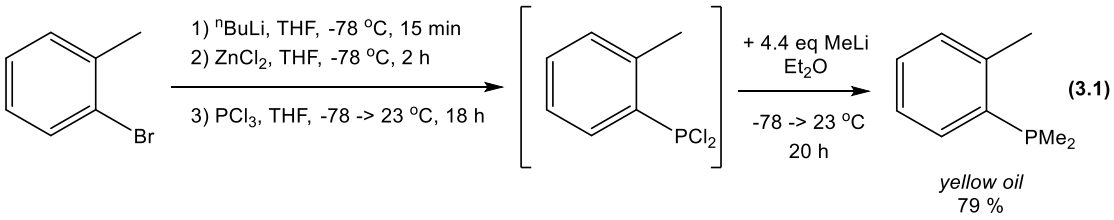

(3.1)

3.2 Metalation Reactions of Li(*o*-$CH_2C_6H_4NMe_2$) with $FeCl_x$

Efforts to prepare Fe(II)-CH_2R complexes first focused on chelation of the synthesized *o*-benzylamine ligand. Treatment of $FeCl_2$ with 2 equiv. Li(*o*-$CH_2C_6H_4NMe_2$) yielded orange-brown [Fe(*o*-$CH_2C_6H_4NMe_2$)]$_2$(κ-μ-CH_2,N-*o*-$CH_2C_6H_4NMe_2$)$_2$ (**1**) in 66% yield (Scheme 3.3). Evans' method measurements[17] of **1** yielded a μ_{eff} = 8.5 μ_B. The origin of the high magnetic moment has two possibilities: 1) two ferromagnetically coupled high spin Fe(II) d^6 centers (maximum: S_T = 4; μ_{SO} = 8.9 μ_B), or 2) two non-interacting Fe centers (μ_{SO} = 6.9 μ_B) with significant spin-orbit coupling. As shown in Scheme 3.3, efforts towards preparing an Fe(III) derivative afforded **1** and a new diamagnetic species. ^{1}H NMR spectroscopy and mass

spectrometry confirmed the organic product to be *o*-NMe_2-$C_6H_4CH_2CH_2C_6H_4$-*o*-NMe_2. Given the prior oxidatively-triggered CC coupling of the Fe(II) ene-amide

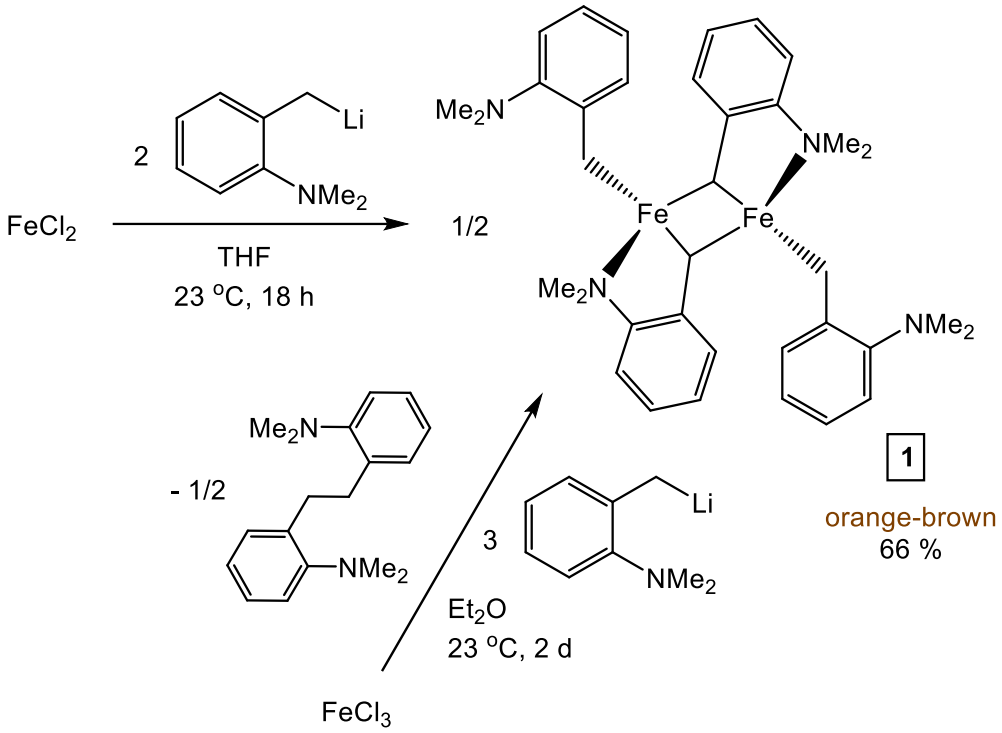

Scheme 3.3. Preparation of dimer **1** using $FeCl_x$ sources

complex {(2,6-$^{i}Pr_2C_6H_3$)(1-^{c}Hexenyl)N}$_2$Fe(PMe_3),[18] a similar coupling mechanism may be operative, hence the absence of any Fe(III) containing products. Formation of "FeR_2Cl" may trigger CC coupling, generating the organic byproduct and "FeCl", and the latter species could redistribute with starting $FeCl_3$ to produce $FeCl_2$, which can then proceed to make **1** as the sole Fe-containing product.

3.3 X-Ray Crystal Structure of Dimer 1

The abnormally high magnetic moment and low solubility of [Fe(*o*-$CH_2C_6H_4NMe_2$)]$_2$(κ-μ-CH_2,N-*o*-$CH_2C_6H_4NMe_2$)$_2$ (**1**), originally formulated as a

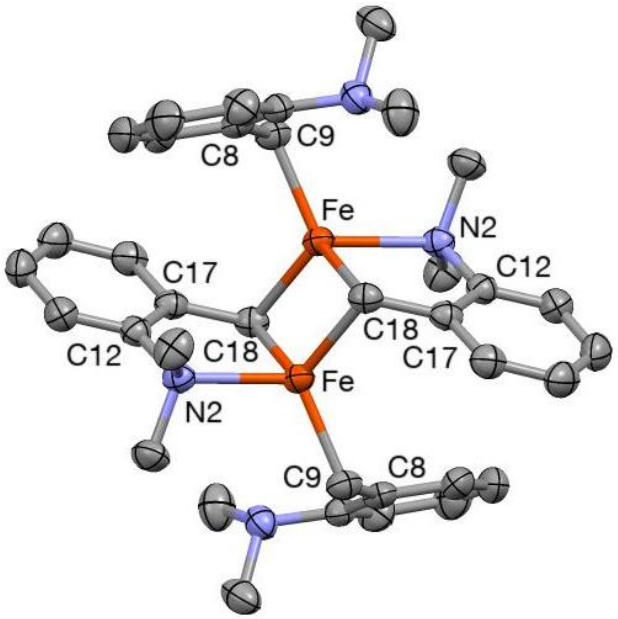

Figure 3.1. Molecular view of dimer [Fe(*o*-$CH_2C_6H_4NMe_2$)]$_2$(κ-μ-CH_2,N-*o*-$CH_2C_6H_4NMe_2$)$_2$ (**1**). Selected interatomic distances (Å) and angles (°): Fe-Fe, 2.5930(5); Fe-C9, 2.0650(19); Fe-μ-C18, 2.136(2), 2.221(2); Fe-N2, 2.2028(16); C18-C18, 2.593(3); C9-Fe-μ-C18, 113.46(8), 124.60(8); C9-Fe-N2, 112.89(7); N2-Fe-μ-C18, 79.70(6), 112.25(7); μ-C18-Fe-μ-C18, 106.98(6); Fe-μ-C18-Fe, 73.01(6); Fe-C9-C8, 106.62(13); Fe-μ-C18-C17, 108.74(12), 109.23(13); Fe-N2-C12, 111.68(11).

monomer from the ^{1}H NMR spectrum (one set of ligand resonances), prompted an X-ray structural analysis of the compound. A view of centrosymmetric dimer **1** is shown in Figure 3.1, with relevant metrics provided in the caption. Both Fe centers feature a terminal benzyl, an amine and two bridging benzyl ligands. The bridging κ-μ-CH_2,N-*o*-$CH_2C_6H_4NMe_2$ chelate links to both Fe centers above and below the diamond core,

with angles of (μ-C18)–Fe–(μ-C18) = 106.98(6)° and Fe–(μ-C18)–Fe = 73.01(6)°. Manzer reported the analogous Mn-dimer [Mn(*o*-$CH_2C_6H_4NMe_2$)](κ-μ-CH_2,N-*o*-$CH_2C_6H_4NMe_2$)$_2$[Mn(κ^2-*o*-$CH_2C_6H_4NMe_2$)], which features a similar Mn_2(μ-CH_2Ar)$_2$ geometry.[19,20] Notable bond metrics include terminal Fe–C and Fe–N distances of 2.0650(19) and 2.2028(16) Å, respectively. The diamond core bridges feature asymmetric distances, with d(Fe–μ-C18) = 2.136(2) and 2.221(2) Å, where the longer distance is affiliated with its chelating amine. The benzyl CH bonds range from 2.00(2)-3.02(2) Å, which may imply agostic interactions with the high spin Fe(II) centers. However, these distances are likely shortened due to the benzyl geometry (Fe–(μ-C18)–C17 = 108.74(12), 109.23(13)) rather than any significant interactions with Fe.

3.4 Metalation of Li(TMEDA)(*o*-$CH_2C_6H_4PPh_2$) with $FeCl_2$ and Resulting Crystal Structure

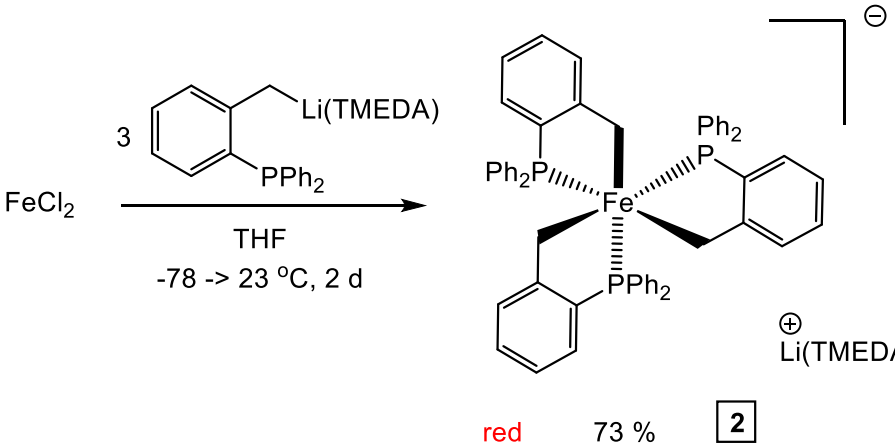

(3.2)

The paramagnetism of [Fe(*o*-$CH_2C_6H_4NMe_2$)]$_2$(κ-μ-CH_2,N-*o*-$CH_2C_6H_4NMe_2$)$_2$ (**1**) prompted the preparation of a phosphorus analog. While treatment of $FeCl_2$ with 2

equiv of Li(TMEDA)(*o*-$CH_2C_6H_4PPh_2$) led to an intractable mixture, 3 equiv of the alklyllithium afforded [*fac*-Fe(κ-C,P-*o*-$CH_2C_6H_4PPh_2)_3$][$Li(TMEDA)_2$] (**2**) in 73% yield as a red microcrystals (Eq 3.2). Broad resonances in the ^1H NMR spectrum at positions indicative of a diamagnetic compound confirmed the stronger field imparted by switching to a phosphine chelate. NMR studies were undertaken to assess the geometry of **2**. Two resonances were present in the $^{31}P\{^1H\}$ NMR spectrum in a 1:2 ratio (δ -13.37, -15.71), which indicated two unique phosphorous environments. In agreement with this asymmetry, a $^{13}C\{^1H\}$ spectrum revealed two CH_2 moieties (δ 45.10, 56.26) in a 2:1 ratio. Taken together, the NMR spectra point toward a *mer*-geometry of **2** in solution.

Intriguingly, [*fac*-Fe(κ-C,P-*o*-$CH_2C_6H_4PPh_2)_3$][$Li(TMEDA)_2$] (**2**) was confirmed to possess *fac*-geometry in the solid state by X-ray structural analysis, with a view presented in Figure 3.2. Long Fe–C bonds of 2.106(10) Å (ave) signify the anionic charge on the Fe(II) center. Acute chelate bite angles of 81.2(14)° (ave) are smaller than the interchelate C–Fe–P angles that average 89.5(22)°. Steric interactions of the phosphines are evident from the P–Fe–P angle of 103.6(27)° (ave), which leads to a small C–Fe–C angle that averages to 83.8(12)°. In addition, *trans*-C–Fe–P angles of 164.2(6)° (ave) show a moderate deviation from pseudo-octahedral symmetry. Combined NMR studies of **2** did not indicate a mixture of the *mer*/*fac* complexes, as only two resonances were present in the $^{31}P\{^1H\}$ spectrum (three resonances would be expected for a mixture). Further evidence for the *mer*-geometry in solution comes from the $^{13}C\{^1H\}$ NMR spectra, where only two CH_2 resonances were recorded. This

seems to imply that if the *mer*-structure isomerizes to the *fac*-isomer, the latter structure may crystallize exclusively over the *mer*-isomer.

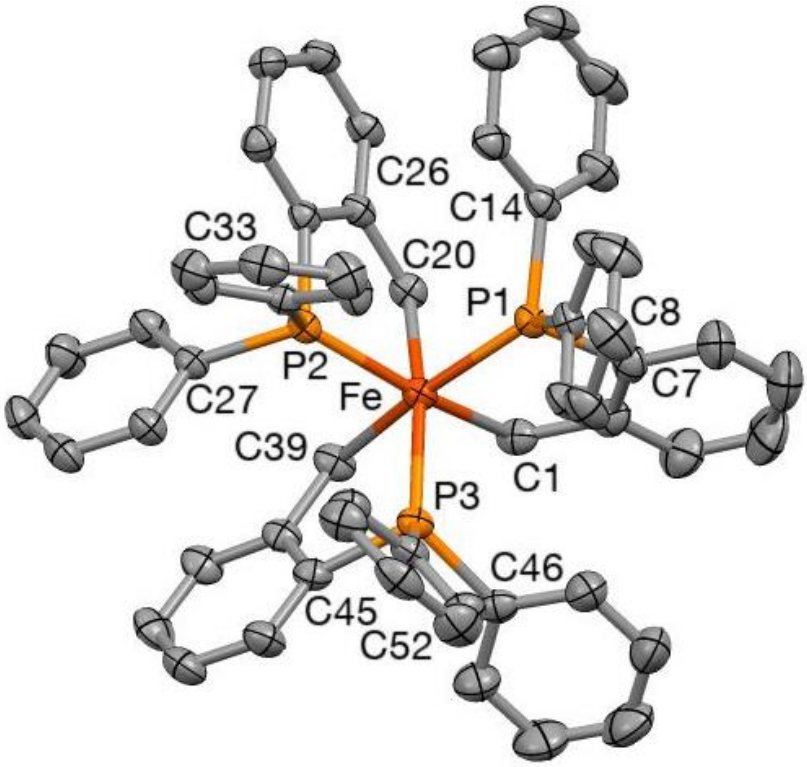

Figure 3.2. Molecular view of the anion of [*fac*-Fe(κ-C,P-*o*-$CH_2C_6H_4PPh_2)_3$][Li(TMEDA)$_2$] (**2**). Selected interatomic distances (Å) and angles (°): Fe-C1, 2.1028(18); Fe-C20, 2.0976(18); Fe-C39, 2.1160(18); Fe-P1, 2.2170(5); Fe-P2, 2.2278(5); Fe-P3, 2.2198(5); PC_{ipso}(ave), 1.854(16); C1-Fe-C20, 82.84(7); C1-Fe-C39, 83.65(8); C20-Fe-C39, 85.13(7); P1-Fe-P2, 102.391(19); P1-Fe-P3, 106.74(2); P2-Fe-P3, 101.81(2); C1-Fe-P1, 82.34(5); C1-Fe-P2, 163.59(6); C1-Fe-P3, 91.64(6); C20-Fe-P1, 87.22(5); C20-Fe-P2, 81.72(5); C20-Fe-P3, 164.24(5); C39-Fe-P1, 164.77(6); C39-Fe-P2, 89.53(6); C39-Fe-P3, 79.58(5).

3.5 Oxidation Studies of 1 and 2

Following the successful preparation of both [Fe(*o*-$CH_2C_6H_4NMe_2$)]$_2$(κ-μ-CH_2,N-*o*-$CH_2C_6H_4NMe_2)_2$ (**1**) and [*fac*-Fe(κ-C,P-*o*-$CH_2C_6H_4PPh_2)_3$][Li(TMEDA)$_2$] (**2**), reactivity studies were undertaken to assess their viability as Fe alkylidene

precursors. Initial probes focused on treatment of **1** with various oxidants, with the results presented in Scheme 3.4. Oxidation of **1** with stoichiometric I_2 or S_8 resulted in clean formation of *o*-NMe_2-$C_6H_4CH_2CH_2C_6H_4$-*o*-NMe_2, with no evidence of any Fe(III) products by ^{1}H NMR spectroscopy. This result is in accordance with the CC coupled product observed when attempting to prepare an Fe(III) trialkyl complex in Scheme 3.3. Oxidation of **1** with AdN_3 led to CC coupling of the ligands along with trace amine- and imine-products derived from adamantyl nitrene insertion into the Fe-benzyl bonds. The metal products were not determined for these reactions. A

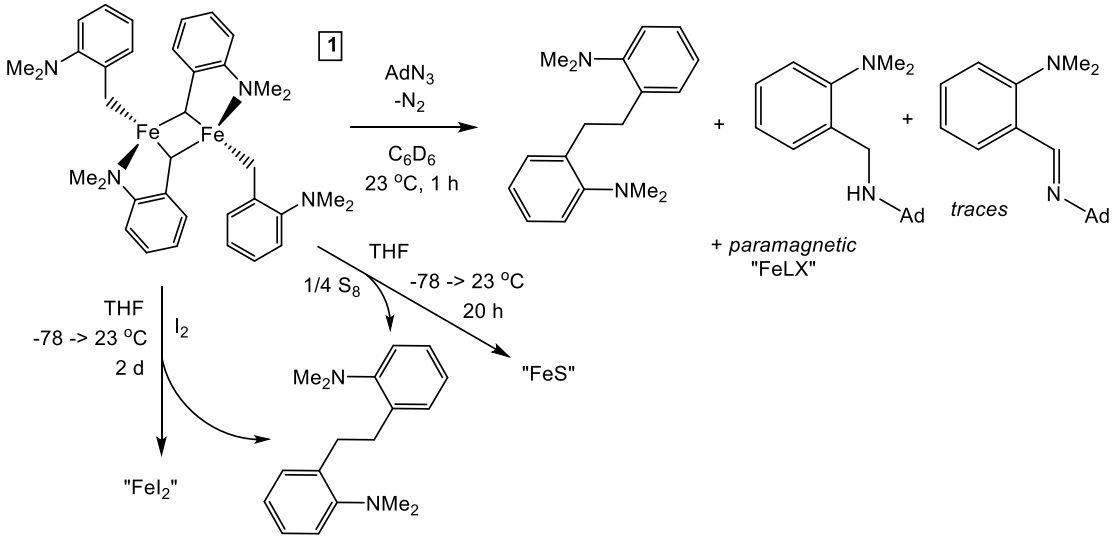

Scheme 3.4. Oxidative degradations of **1** revealing nitrene insertion and CC coupling products

similar oxidation of [*fac*-Fe(κ-C,P-*o*-$CH_2C_6H_4PPh_2)_3$][Li(TMEDA)$_2$] (**2**) with [Cp_2Fe]PF_6 afforded the related coupled product *o*-PPh_2-$C_6H_4CH_2CH_2C_6H_4$-*o*-PPh_2 (Eq 3.3). The prior chelates were abandoned as Fe alkylidene precursors in favor of mixed ligand complexes.

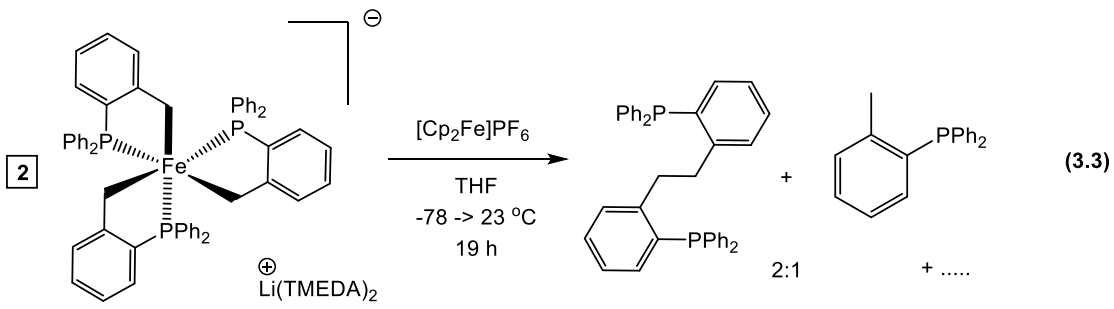

(3.3)

3.6 Synthesis of Fe(II) Chelates Bearing Ancillary Ligands

Since oxidation of the aforementioned chelates triggered ligand coupling rather than generating isolable Fe(III) species, new chelate complexes incorporating ancillary ligands were developed. Treatment of the N-heterocyclic carbene precursor $[(Me_2IPr)FeCl(\mu\text{-}Cl)]_2$[21,22] with 4 equiv Li(*o*-$CH_2C_6H_4NMe_2$) provided yellow microcrystalline $(Me_2IPr)Fe(CH_2C_6H_4NMe_2)_2$ (**3**-C,N) in 57% yield, as Eq 3.4 indicates. Evans' method measurements[17] yielded a μ_{eff} = 5.2 μ_B, consistent with a high spin Fe(II) center. Coordination of the amine could lead to 4- or 5-coordinate species, although there is ample precedent for the 3-coordinate complex due to weak donor strength of the amine.[23-30]

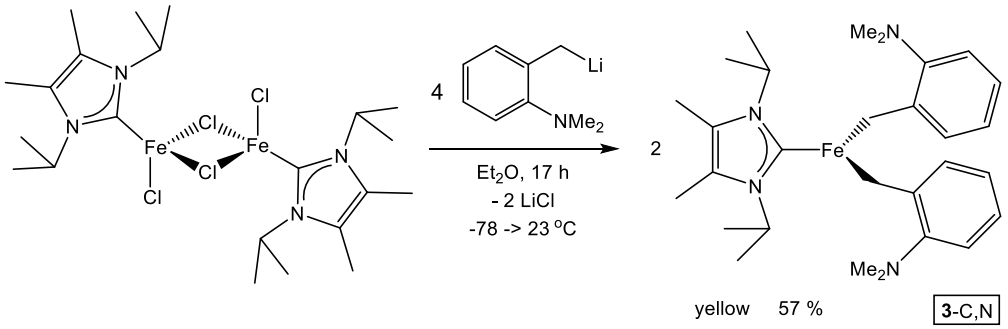

(3.4)

Treatment of $FeCl_2$ with $LiCH_2PMe_2$ led to an intractable mixture, yet changing the Fe starting material to $[(Me_2IPr)FeCl(\mu\text{-}Cl)]_2$ produced an orange,

microcrystalline product. Magnetic moments determined for the anticipated product $(Me_2IPr)Fe(\kappa^2\text{-}C,P\text{-}CH_2PMe_2)_2$ (**3**-C,P) were lower than expected, prompting an X-ray structural analysis. The structural analysis confirmed formation of the binuclear $[(Me_2IPr)_2Fe](\mu\text{-}\kappa\text{-}C,P\text{-}CH_2PMe_2)_2[Fe(\kappa\text{-}C,P\text{-}CH_2PMe_2)_2]$ (**4**), generated through ligand redistribution of **3**-C,N (Scheme 3.5). The μ_{eff} of 5.0(3) μ_B[17] is consistent with a single high spin Fe(II) center.

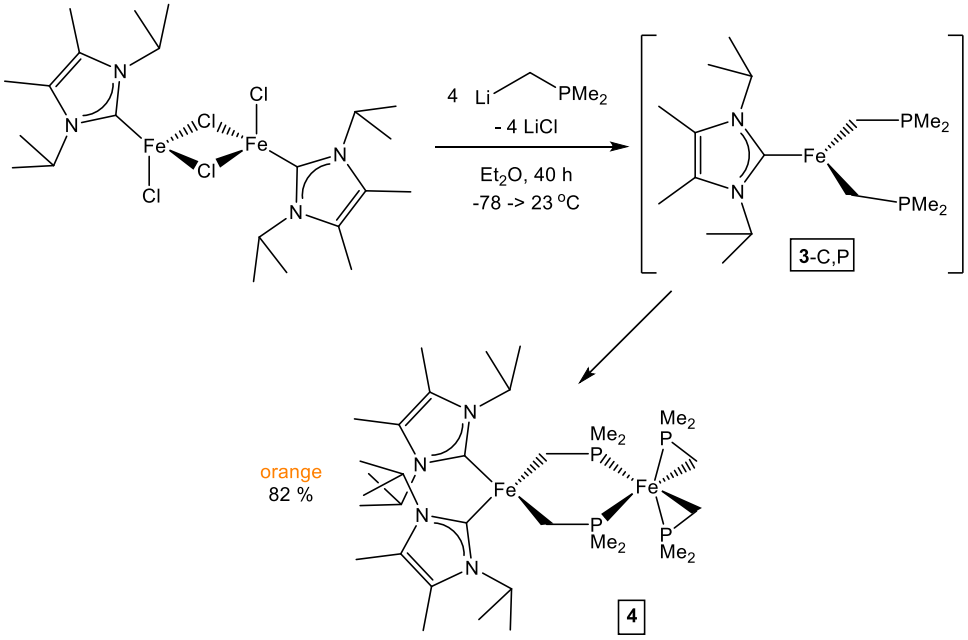

Scheme 3.5. Preparation of complex **4** through ligand redistribution of **3**-C,P

Phosphines as ancillary ligands were also pursued, and treatment of $FeCl_2(PMe_3)_2$[31] with 2 equiv $LiCH_2PMe_2$ led to the isolation of $(PMe_3)_2Fe(\kappa\text{-}C,P\text{-}CH_2PMe_2)_2$ (**5**) as a sticky brown diamagnetic product in 24% yield, as Eq 3.5 indicates. Crystallization of **5** was unsuccessful due to its high solubility, and the geometry was determined through NMR spectroscopy. The ^1H NMR spectrum was

consistent with the structure containing a mirror plane, as the $^{31}P\{^{1}H\}$ NMR spectrum revealed two resonances consistent with bound PMe_3. Complex **5** has essentially the same coordination environment as the pseudo-octahedral site in binuclear $[(Me_2IPr)_2Fe](\mu\text{-}\kappa\text{-}C,P\text{-}CH_2PMe_2)_2[Fe(\kappa\text{-}C,P\text{-}CH_2PMe_2)_2]$ (**4**), which indicates that the μ_{eff} of **4** likely contains high spin tetrahedral and low spin (S = 0) octahedral Fe(II) centers.

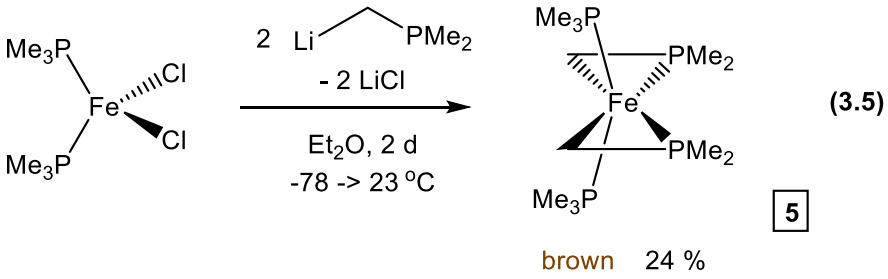

(3.5)

Since deprotonation of *o*-$CH_3C_6H_4PMe_2$ with ^{n}BuLi gave an intractable mixture, a C-H bond activation methodology was employed using Karsch's *cis*-$Me_2Fe(PMe_3)_4$ complex.[16,32,33] Addition of 2 equiv *o*-$CH_3C_6H_4PMe_2$ to *cis*-$Me_2Fe(PMe_3)_4$ for 1 day at 23 °C, followed by heating the mixture to 55 °C for 3 h produced *trans*,*cis*-$(PMe_3)_2Fe(\kappa\text{-}C,P\text{-}CH_2C_6H_4\text{-}o\text{-}PMe_2)_2$ (**6**) as yellow crystals in 55% yield, as shown in Eq 3.6. The diamagnetic product features two resonances in the $^{31}P\{^{1}H\}$ spectrum as triplets at δ 18.79 and 53.50 (J_{PP} = 33 Hz), which establishes the *trans*,*cis*-orientation of the phosphine ligands.

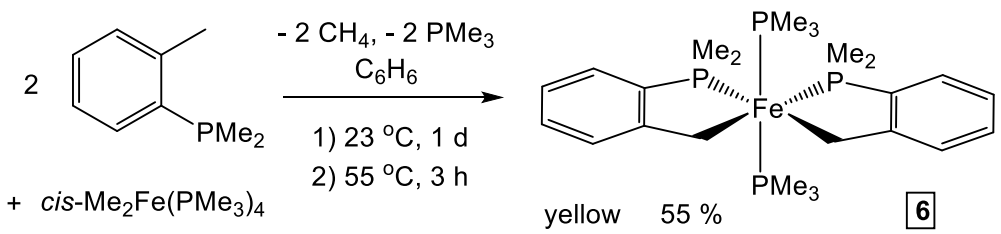

(3.6)

3.7 X-Ray Crystal Structure of Binuclear Complex 4

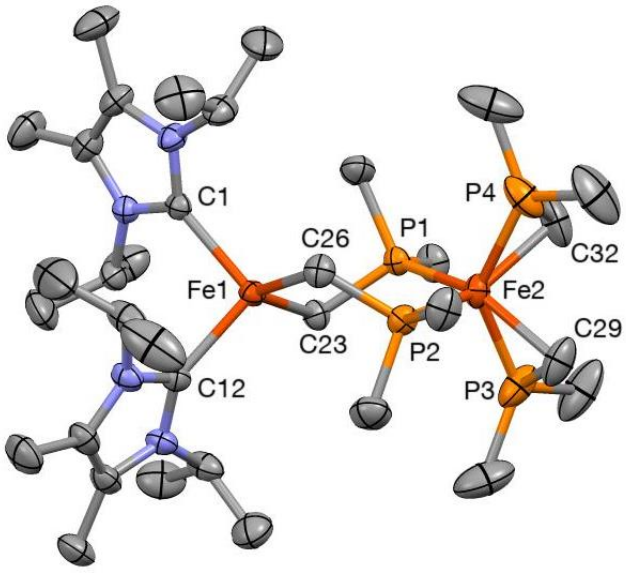

Figure 3.3. Molecular view of $[(Me_2IPr)_2Fe](\mu\text{-}\kappa\text{-}C,P\text{-}CH_2PMe_2)_2[Fe(\kappa\text{-}C,P\text{-}CH_2PMe_2)_2]$ (**4**). Selected interatomic distances (Å) and angles (°): Fe1-C1, 2.173(2); Fe1-C12, 2.165(2); Fe1-C23, 2.114(2); Fe1-C26, 2.111(2); Fe2-P1, 2.1842(6); Fe2-P2, 2.1917(6); Fe2-P3, 2.1055(7); Fe2-P4, 2.1090(7); Fe2-C29, 2.111(2); Fe2-C32, 2.117(2); C29-P3, 1.739(3); C32-P4, 1.738(3); C23-P1, 1.804(2); C26-P2, 1.805(2); C1-Fe1-C12, 99.67(7); C1-Fe1-C23, 109.33(8); C1-Fe1-C26, 113.24(8); C12-Fe1-C23, 112.67(8); C12-Fe1-C26, 113.24(8); C23-Fe1-C26, 109.24(8); P1-Fe2-P2, 97.59(2); P1-Fe2-P3, 100.92(3); P1-Fe2-P4, 108.75(3); P2-Fe2-P3, 108.39(3); P2-Fe2-P4, 101.32(3); P3-Fe2-P4, 134.32(3); C29-Fe2-P3, 48.72(8); C29-Fe2-P1, 149.62(8); C29-Fe2-P2, 94.46(8); C29-Fe2-P4, 95.97(9); C32-Fe2-P4, 48.56(8); C32-Fe2-P1, 93.35(8); C32-Fe2-P2, 149.88(8); C32-Fe2-P3, 96.86(9); Fe2-C29-P3, 65.48(8); Fe2-P3-C29, 65.80(9); Fe2-C32-P4, 65.48(8); Fe2-P4-C32, 65.97(9).

A molecular view of $[(Me_2IPr)_2Fe](\mu\text{-}\kappa\text{-}C,P\text{-}CH_2PMe_2)_2[Fe(\kappa\text{-}C,P\text{-}CH_2PMe_2)_2]$ (**4**) is given in Figure 3.3, with metrics provided in the caption, while Table 3.1 lists additional crystallographic information. The C–Fe1–C angles average 109.6(52)°, consistent with a regular tetrahedron, where the bond distances (d(FeC(P)) = 2.113(2) Å (ave), d(FeC(NN)) = 2.169(6) Å (ave)) are attributable to a high spin

Fe(II) center. The six-coordinate Fe center is highly distorted, where the CH_2 groups are 149.67(8)^o and 148.88(8)^o from the phosphorus atoms in the bridging ligand. The phosphines nearly comprise a tetrahedron, with five P–Fe–P angles averaging 103.4(49)^o (P3–Fe2–P4 = 134.32(3)^o). The μ_{eff} of **4** is consistent with a high spin Fe(II) center (S = 2), and it naturally follows that the pseudo-octahedral center is diamagnetic. Despite the different magnetic spin states of both Fe(II) centers, both have essentially identical Fe carbon distances (d(Fe2–C) = 2.114(4) Å).

Table 3.1. Select crystallographic and refinement data for [Fe(*o*-$CH_2C_6H_4NMe_2$)]$_2$(κ-μ-CH_2,N-*o*-$CH_2C_6H_4NMe_2$)$_2$ (**1**), [*fac*-Fe(κ-C,P-*o*-$CH_2C_6H_4PPh_2$)$_3$][Li(TMEDA)$_2$] (**2**) and [(Me_2IPr)$_2$Fe](μ-κ-C,P-CH_2PMe_2)$_2$[Fe(κ-C,P-CH_2PMe_2)$_2$] (**4**).

	1	**2**	**4**
formula	$C_{36}H_{48}Fe_2N_4$	$C_{84}H_{95}FeN_4P_3Li$	$C_{34}H_{72}FeN_4P_4$
formula wt	648.48	1316.33	772.53
space group	$P2_1/c$	$P\bar{1}$	$P2_1/n$
Z	2	2	4
a, Å	9.8560(7)	13.2061(6)	13.1748(6)
b, Å	14.5425(11)	14.0219(6)	24.7344(12)
c, Å	12.4977(9)	20.7264(10)	13.3583(7)
α, deg	90	98.823(2)	90
β, deg	111.796(4)	101.703(2)	91.399(2)
γ, deg	90	93.670(2)	90
V, Å^3	1663.2(2)	3695.8(3)	4351.8(4)
ρ_{calc}, g cm^{-3}	1.295	1.183	1.179
μ, mm^{-1}	0.902	0.315	0.840
temp, K	223(2)	223(2)	223.15
λ (Å)	0.71073	0.71073	0.71073
R indices	R1 = 0.0374	R1 = 0.0407	R1 = 0.0327
[$I > 2\sigma(I)$]^{a,b}	wR2 = 0.0931	wR2 = 0.0885	wR2 = 0.0750
R indices^b	R1 = 0.0480	R1 = 0.0623	R1 = 0.0463
(all data)^a	wR2 = 0.0994	wR2 = 0.0988	wR2 = 0.0821
GOF^c	1.013	1.025	1.036

$^aR_1 = \Sigma F_o| - |F_c|| / \Sigma|F_o|$. $^bwR_2 = [\Sigma w(|F_o| - |F_c|)^2 / \Sigma wF_o^2]^{1/2}$. ^cGOF (all data) = $[\Sigma w(|F_o| - |F_c|)^2/(n - p)]^{1/2}$, n = number of independent reflections, p = number of parameters.

3.8 Reactivity Studies of Complexes 3-C,N, 5 and 6

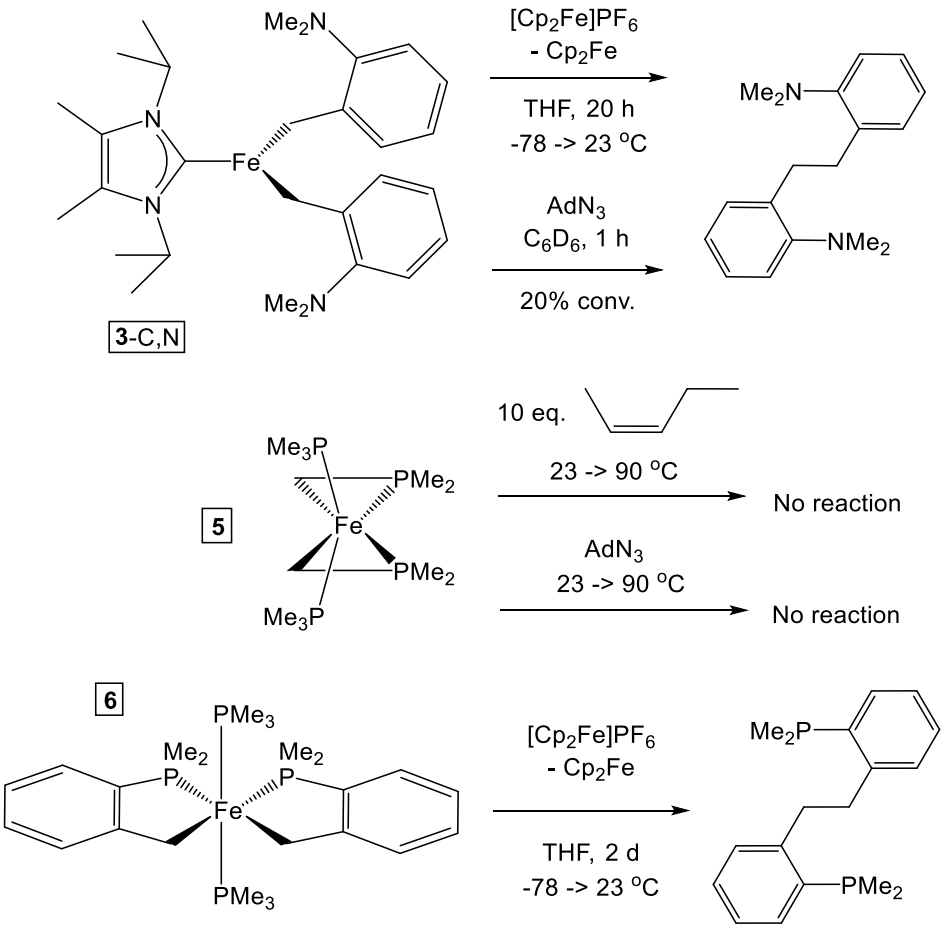

Scheme 3.6. Reactivity studies of complexes **3**-C,N, **5** and **6**

With the mixed chelate complexes $(Me_2IPr)Fe(CH_2C_6H_4NMe_2)_2$ (**3**-C,N), $(PMe_3)_2Fe(\kappa\text{-}C,P\text{-}CH_2PMe_2)_2$ (**5**) and *trans,cis*-$(PMe_3)_2Fe(\kappa\text{-}C,P\text{-}CH_2C_6H_4\text{-}o\text{-}PMe_2)_2$ (**6**) isolated, oxidation studies were conducted for each species, as shown in Scheme 3.6. Treatment of **3**-C,N with either $[Cp_2Fe]PF_6$ or adamantyl azide generated the coupled degradation product *o*-NMe_2-$C_6H_4CH_2CH_2C_6H_4$-*o*-NMe_2. While **3**-C,N could not facilitate formation of a stable Fe(III) species, complex **5** was considerably more

stable, as treatment of **5** with adamantyl azide led to no reaction. Thermolysis of the mixture at 90 ^{o}C only led to azide degradation, with no reactivity of **5**. Exposure of **5** to excess *cis*-2-pentene at elevated temperatures also led to no reaction, despite the potential for forming an alkylidene through α-PMe_2 migration. Given the stability of **5**, it was envisaged that oxidation of **6** may afford a stable Fe(III) product. Treatment of **6** with $[Cp_2Fe]PF_6$ only led to the degradation product *o*-PMe_2-$C_6H_4CH_2CH_2C_6H_4$-*o*-PMe_2. For all reactivity studies, the identity of the metal containing products were not identified, and further experiments were abandoned due to the instability of the Fe chelates upon oxidation.

The instability of the Fe(II) chelates with respect to oxidation may be due to the electron withdrawing nitrogen or phosphorus ligands within the chelate. Oxidation to Fe(III) makes for a less electron-rich metal center, which in turn destabilizes the chelate complex. An alternative approach to assessing distribution of electron density within metal complexes has been recently conceptualized in these laboratories as Charge Distribution Via Reporters (CDVR).[34] For this methodology, the charge on Fe is $\mathbf{c}_{Fe}$ = +2.0, with each CH_2 charge likely to be $\mathbf{c}_R \leq$ -0.65. Using complexes $(PMe_3)_2Fe(\kappa\text{-}C,P\text{-}CH_2PMe_2)_2$ (**5**) and *trans,cis*-$(PMe_3)_2Fe(\kappa\text{-}C,P\text{-}CH_2C_6H_4\text{-}o\text{-}PMe_2)_2$ (**6**) as examples, the phosphine groups compensate the charge on Fe with ~ -0.7 for the Fe(II) species. Oxidation to Fe(III) must be accompanied with the ligand charge units summing to -1.0, and while trialkylphosphines can accommodate ~ +0.10, the aryl-phosphines employed in this study are more electron-withdrawing. Any putative Fe(III) species would likely be unstable, and CC ligand coupling seems to be the natural consequence of oxidation.

Conclusion

A series of Fe chelate complexes $[Fe(o\text{-}CH_2C_6H_4NMe_2)]_2(\kappa\text{-}\mu\text{-}CH_2,N\text{-}o\text{-}CH_2C_6H_4NMe_2)_2$ (**1**), [*fac*-$Fe(\kappa\text{-}C,P\text{-}o\text{-}CH_2C_6H_4PPh_2)_3][Li(TMEDA)_2]$ (**2**), $(Me_2IPr)Fe(CH_2C_6H_4NMe_2)_2$ (**3**-C,N), $(PMe_3)_2Fe(\kappa\text{-}C,P\text{-}CH_2PMe_2)_2$ (**5**) and *trans,cis*-$(PMe_3)_2Fe(\kappa\text{-}C,P\text{-}CH_2C_6H_4\text{-}o\text{-}PMe_2)_2$ (**6**) were prepared through either salt metathesis or C-H bond activation. The viability of these chelates as Fe alkylidene precursors were probed via treatment with oxidants. Putative Fe(III) species were unstable, with oxidative degradation products in the form of CC coupled ligands observed for each chelate oxidized.

Further development of Fe chelates was abandoned in favor of pursuing low-coordinate Fe alkyl species as alkylidene precursors.

Experimental

General Considerations. All manipulations were performed using either glovebox or high vacuum line techniques under inert atmosphere (Ar), unless stated otherwise. All glassware was oven dried at 180 ºC. THF and ether were distilled under nitrogen from purple sodium benzophenone ketyl and vacuum transferred from the same prior to use. Hydrocarbon solvents were treated in the same manner with the addition of 1-2 mL/L tetraglyme. Tetramethylethylenediamine (TMEDA) was stirred over sodium/benzophenone, then vacuum transferred to a fresh flask containing charged with sodium and benzophenone. Benzene-d_6 was dried over sodium, vacuum transferred and stored over sodium. THF-d_8 was dried over sodium, and vacuum transferred from sodium benzophenone ketyl prior to use. Chloroform-d_1 (Cambridge Isotope Laboratories) was used as received. $LiCH_2C_6H_4$-*o*-NMe_2,[12,13] $LiCH_2PMe_2$,[14] 1,3-diisopropyl-4,5-dimethyl-1*H*-imidazol-3-ium-2-ide (Me_2IPr),[21] $CH_3C_6H_4$-*o*-PPh_2,[11] $FeCl_2(PMe_3)_2$,[31] and *cis*-$Me_2Fe(PMe_3)_4$[16] were prepared according to literature procedures. $[(Me_2IPr)FeCl(\mu\text{-}Cl)]_2$[22] was prepared by stirring $FeCl_2$ with 1 equiv Me_2IPr in THF for 1 h (until solids dissolve completely) at 23 ºC, followed by evaporation of the solvent under vacuum. Organic products were determined by NMR spectral analysis and mass spectrometry (DART). All other chemicals were commercially available and used as received.

NMR spectra were obtained using Inova 400 MHz, 500 MHz and 600 MHz spectrometers. Chemical shifts are reported relative to benzene-d_6 (^{1}H δ 7.16; ^{13}C{^{1}H} δ 128.39), THF-d_8 (^{1}H δ 3.58; ^{13}C{^{1}H} δ 67.57) and chloroform-d_1 (^{1}H δ 7.26;

$^{13}C\{^{1}H\}$ δ 77.16). Accurate mass data were acquired on an Exactive Orbitrap mass spectrometer (Thermo Scientific) using a DART (IonSense Inc., Saugus, MA) ion source in positive ion mode using helium for DART ionization, while software affiliated with the spectrometer was used to calculate the molecular weight. Solution magnetic measurements were conducted via Evans' method in C_6D_6 or THF-d_8.[17] Analytical data were obtained from the CENTC Elemental Analysis Facility at the University of Rochester, funded by NSF CHE-0650456.

Procedures

1. Li(TMEDA)$CH_2C_6H_4$-*o*-PPh_2. This procedure is in accordance with César *et. al.*[11] Addition of ^{n}BuLi in hexanes (10.4 mmol, 1.60 M) to a 100-mL flask charged with $CH_3C_6H_4$-*o*-PPh_2 (2.40 g, 8.69 mmol), 30 mL ether, 3 mL pentane and 1.60 mL TMEDA resulted in precipitation of orange microcrystals, and the mixture was stirred at 23 °C for 18 h. Filtration of the precipitate yielded the title compound as orange crystals (2.757 g, 80%). ^{1}H NMR (C_6D_6): δ 1.66 (4H, s), 1.83 (12H, s), 6.23 (1H, t, 7 Hz), 6.77 (1H, t, 7 Hz), 7.03 (1H, m), 7.11 (3H, m), 7.18 (4H, m), 7.60 (4H, t, 7 Hz). ^{13}C NMR (C_6D_6): δ 45.10, 56.26, 107.84, 120.28, 128.51, 128.55, 128.63, 129.36, 133.34, 134.66, 134.86, 137.25, 168.69. ^{31}P NMR (C_6D_6): δ -15.52 (s).

2. $CH_3C_6H_4$-*o*-PMe_2. This procedure is a modification of the Wright *et. al.* procedure.[15] A 3-neck 100-mL flask was fit with a glass stopper, a solid addition glass finger charged with $ZnCl_2$ (1.912 g, 14.03 mmol), and a 180 ° Schlenk adapter. The glassware was degassed, and 16 mL THF was added via vacuum transfer to the flask. *o*-Bromotoluene (2.000 g, 11.69 mmol) was added to the flask, which was then cooled

to -78 °C. Addition of ^{n}BuLi in hexanes (12.8 mmol, 1.60 M) resulted in a cloudy suspension, which was stirred for 15 min at -78 °C. An additional 16 mL THF was added via vacuum transfer, the $ZnCl_2$ solid was added to the suspension at -78 °C, and the mixture was stirred for 2 h. PCl_3 (1.2 mL, 14 mmol) was added via vacuum transfer, and the mixture was allowed to warm slowly to 23 °C with stirring over 18 h. The solution was cooled to 0 °C and the volatiles removed *in vacuo*, yielding a colorless oil. 30 mL ether was transferred under vacuum to the flask. With the flask cooled to -78 °C, 32.2 mL of MeLi in ether (51.5 mmol, 1.60 M) was added, and the mixture became translucent yellow with a colorless precipitate. The mixture was allowed to warm slowly over 20 h. The flask was cooled with to 0° C, and 30 mL ice cold water was slowly added to the flask, generating small amounts of gas evolution until no effervescence was observed. The flask was removed from the adapter, the mixture added to a 250-mL Erlenmeyer flask and diluted with 50 mL ether. The mixture was filtered, and the organic layer was separated from the aqueous layer. The aqueous layer was extracted with 2x25 mL portions of ether, the combined organic extracts dried over $MgSO_4$ and filtered. Removal of the solvent *in vacuo* at 0 °C yielded a yellow oil (1.421 g, 79%), which was stored under a nitrogen in a glovebox. Its purity was estimated at ~93% based on its ^{31}P NMR spectrum. ^{1}H NMR (C_6D_6): δ 1.03 (6H, d, 4 Hz), 2.48 (3H, s), 7.01 (1H, m), 7.09 (2H, m), 7.24 (1H, m). ^{13}C NMR (C_6D_6): δ 13.57 (d, 14 Hz), 20.04 (d, 23 Hz), 126.38, 128.36, 128.60 (d, 1 Hz), 130.26 (d, 4 Hz), 168.68. ^{31}P NMR (C_6D_6): δ -58.05.

3. [Fe(*o*-$CH_2C_6H_4NMe_2$)]$_2$(κ-μ-CH_2,N-*o*-$CH_2C_6H_4NMe_2$)$_2$ (1). *a.* To a 50-mL flask charged with $FeCl_2$ (225 mg, 1.78 mmol) and $LiCH_2C_6H_4$-*o*-NMe_2 (500 mg, 3.54 mmol) was added 25 mL THF via vacuum transfer at -78 ^oC, resulting in a dark-orange solution. The solution was allowed to warm slowly with stirring for 18 h. The volatiles were removed, and the residue was taken up in 15 mL THF and filtered through dried Celite. Removal of the solvent *in vacuo* followed by washing the residue with hexanes (3 x 15 mL) resulted in brown-orange microcrystals (380 mg, 66%), with a purity of ~94% based on NMR spectroscopy. *b.* To a 25-mL flask charged with $FeCl_3$ (115 mg, 0.709 mmol) and $LiCH_2C_6H_4$-*o*-NMe_2 (300 mg, 2.13 mmol) was added 10 mL ether via vacuum transfer at -78 ^oC. The light orange suspension was allowed to warm slowly with stirring for 2 d, resulting in a dark red-orange solution at 21 ^oC. Evaporation of the volatiles, and washing the residue with pentane (3x10 mL) resulted in brown microcrystals of **1**. Crystals suitable for X-ray diffraction were obtained via slow evaporation of a concentrated ether solution. ^1H NMR (C_6D_6): δ -18.41 (4H), 2.61 (4H), 17.53 (4H), 18.44 (4H), 89.07 (12H). μ_{eff} (Evans) = 8.5 μ_B.

4. [fac-Fe(κ^2-C,P-*o*-$CH_2C_6H_4PPh_2$)$_3$][Li(TMEDA)] (2). To a 25-mL flask charged with $FeCl_2$ (43 mg, 0.34 mmol) and Li(TMEDA)$CH_2C_6H_4$-*o*-PPh_2 (400 mg, 1.00 mmol) was added 15 mL THF via vacuum transfer at -78 ^oC. The yellow suspension was allowed to warm slowly to 23°C and stirred for 2 d, during which time the solution turned a dark-red. The volatiles were removed, and the residue taken up in 10 mL THF and filtered through dried Celite. The THF was removed, and the residue was washed with hexanes (3 x 10 mL), and the red suspension filtered in hexanes to afford

a red powder (275 mg, 73%). Crystals suitable for X-ray diffraction were obtained via letting a concentrated C_6D_6 solution stand for 12 h at 23°C. ^{1}H NMR (C_6D_6): δ 1.41 (4H, br s), 1.64-1.70 (24H, br "s"), 2.42 (1H, s), 3.44 (1H, s), 3.55 (4H, br s), 6.76 (2H, br s), 6.79-6.94 (14H, m), 7.00 (4H, m), 7.03-7.05 (10H, m), 7.06 (1H, t, 7 Hz), 7.10 (1H, dd, 4 7 and 4 Hz), 7.14 (1H, br s), 7.23-7.29 (3H, m), 7.37 (5H, m), 7.94 (4H, m). ^{31}P NMR (C_6D_6): δ -13.37 (1P), -15.71 (2P).

5. (Me_2IPr)Fe($CH_2C_6H_4$-*o*-NMe_2)$_2$ (3-C,N). To a 25-mL flask charged with (Me_2IPr)$FeCl_2$ (218 mg, 0.710 mmol) and $LiCH_2C_6H_4$-*o*-NMe_2 (200 mg, 1.42 mmol) was added 10 mL ether via vacuum transfer at -78 °C. The yellow suspension did not change color, and was allowed to slowly warm with stirring for 17 h. At 23 °C, the solution turned brown-orange with colorless precipitate, and was filtered. The ether solution was concentrated and cooled to -78 °C for 15 min. The solution was filtered, and concentrated to afford yellow microcrystals (202 mg, 57%), whose purity was assessed at ~97% based on NMR spectroscopy. ^{1}H NMR (C_6D_6): δ -27.95 (2H), -13.69 (2H), -9.21 (6H), 16.14 (12H), 25.57 (2H), 38.88 (2H), 40.45 (12H). μ_{eff} (Evans) = 5.2 μ_B. Anal. for $C_{29}H_{44}FeN_4$ (calc.) C 69.04, H 8.79, N 11.10; (found) C 68.98, H 8.81, N 11.01.

6. [(Me_2IPr)$_2$Fe](κ-μ-C,P-CH_2PMe_2)$_2$[Fe(κ^2-C,P-CH_2PMe_2)$_2$] (4). To a 25 mL flask charged with (Me_2IPr)$FeCl_2$ (277 mg, 0.902 mmol) and $LiCH_2PMe_2$ (148 mg, 1.80 mmol) was added via vacuum transfer 15 mL ether at -78 °C, resulting in an orange solution. The solution was allowed to warm slowly with stirring for 40 h. The volatiles were removed, and the orange residue taken up in 10 mL THF and filtered through

dried Celite. Removal of the solvent, followed with washing the residue with hexanes (3 x 10 mL), resulted in an orange powder (285 mg, 82%). Crystals suitable for X-ray diffraction were obtained via layering a concentrated THF solution of **4** with pentane (1:3) and letting the solution stand at 23 °C for 12 h. ^{1}H NMR (C_6D_6): δ 0.78 (2H), 2.31 (6H), 2.65 (6H), 5.42 (12H), 17.24 (6H), 27.15 (4H). μ_{eff} (Evans) = 5.0(3) μ_B.

7. $(PMe_3)_2Fe(\kappa^2\text{-}C,P\text{-}CH_2PMe_2)_2$ (5). To a 25-mL flask charged with $FeCl_2(PMe_3)_2$ (340 mg, 1.22 mmol) and $LiCH_2PMe_2$ (200 mg, 2.44 mmol) was added 15 mL ether via vacuum transfer at -78 ºC, resulting in a dark-brown solution. The solution was allowed to slowly warm to 23 °C for 2 d. The brown solution was filtered and the volatiles removed, producing a dark-brown residue. Attempts at trying to crystallize the compound from hexanes failed, as no solid precipitate was observed, regardless of concentration or temperature. The volatiles were evaporated, and the sticky brown solid was harvested (107 mg, 24%). ^{1}H NMR (C_6D_6): δ -1.81 (2H, s), -0.48 (2H, s), 1.17 (18H, "t", 3 Hz), 1.30 (6H, br s), 1.36 (6H, br s). ^{13}C NMR (C_6D_6): δ -6.98, 14.51, 16.66, 26.54. ^{31}P NMR (C_6D_6, ^{31}P coupling constants determined through spin simulation program MesReNova): δ -19.58, 30.06 (AA' = 27 Hz; XX' = 24 Hz, AX = A'X' = 61 Hz). Anal. for $C_{12}H_{34}FeP_4$ (calc.) C 40.24, H 9.57; (found) C 40.45, H 9.06.

8. *cis,trans*-$(PMe_3)_2Fe(\kappa^2\text{-}C,P\text{-}CH_2C_6H_4\text{-}o\text{-}PMe_2)_2$ (6). A 60-mL bomb reactor was charged with $CH_3C_6H_4$-*o*-PMe_2 (250 mg, 1.63 mmol) and 15 mL benzene. A separate vial was charged with *cis*-$Me_2Fe(PMe_3)_4$ (319 mg, 0.817 mmol) and 3 mL benzene, and the it was added to the bomb, resulting in an orange solution. The solution was stirred for 1 d at 23 °C, followed by heating to 55 ºC for 3 h. The volatiles were

removed, and the solid residue was taken up in pentane/benzene and transferred to a separate 25 mL flask. The solvent was removed, and 10 mL pentane was added via vacuum transfer. The pentane mixture was cooled to -78 ^{o}C for 15 min, and filtered to afford a yellow powder (230 mg, 55%). ^{1}H NMR (C_6D_6): δ 0.87 (18H, d, 5 Hz), 1.40 (6H, t, 3 hz), 1.43 (6H, t, 2 Hz), 2.00 (2H, m), 2.39 (2H, dq, 15, 7 Hz), 7.03 (2H, t, 7 Hz), 7.10 (2H, t, 7 Hz), 7.23 (2H, dt, 7, 3 Hz), 7.43 (2H, d, 7 Hz). ^{13}C NMR (C_6D_6): δ 17.30 (t, 10 Hz), 20.10, 23.84 (“t”, 8 Hz), 34.78 (t, 16 Hz), 123.18, 125.38, 128.59, 128.96 (t, 6 Hz), 145.40, 163.57 (t, 24 Hz). ^{31}P NMR (C_6D_6): δ 18.79 (t, 33 Hz), 53.50 (t, 33 Hz). Anal. for $C_{24}H_{42}FeP_4$ (calc.) C 56.48, H 8.30; (found) C 56.46, H 8.32.

9. Treatment of 1 with I_2. To a 25-mL flask charged with **1** (99 mg, 0.15 mmol) and I_2 (39 mg, 0.15 mmol) was added 10 mL THF via vacuum transfer at -78 ^{o}C, resulting in a dark brown solution. The solution was allowed to warm slowly with stirring for 2 d. Removal of the volatiles followed by washing the residue with pentane (3 x 10 mL) left a dark brown residue. Poor solubility of the residue in C_6D_6 prompted using THF-d_8 for ^{1}H NMR analysis, which showed one product consistent with NMe_2-C_6H_4-*o*-CH_2CH_2-C_6H_4-*o*-NMe_2, further observed by DART-MS. ^{1}H NMR (THF-d_8): δ 2.62 (12H, br s), 2.94 (4H, br s), 6.89-7.23 (8H, m). HRMS (DART-MS) m/z: $[M + H]^+$ Calcd for 269.1973; Found 269.20119.

10. Treatment of 1 with S_8. To a 25-mL flask charged with **1** (100 mg, 0.15 mmol) and S_8 (10 mg, 0.039 mmol) was added 10 mL THF via vacuum transfer at -78 ^{o}C, resulting in a brown solution. The solution was allowed to warm slowly with stirring for 20 h, resulting in a brown solution. Removal of the volatiles followed by washing

the residue with hexanes (3 x 10 mL) left a dark brown residue. Analysis of the residue by ^{1}H NMR in C_6D_6 showed formation of NMe_2-C_6H_4-*o*-CH_2CH_2-C_6H_4-*o*-NMe_2.

11. Treatment of 1 with AdN_3. To a vial charged with **1** (11 mg, 0.017 mmol) and 0.5 mL C_6D_6 was added AdN_3 (6 mg, 0.034 mmol), resulting in a brown-orange solution. Analysis of the mixture after 1 h at 21 ^{o}C by ^{1}H NMR showed consumption of the starting materials and production of NMe_2-C_6H_4-*o*-CH_2CH_2-C_6H_4-*o*-NMe_2 as the major product. ^{1}H NMR (C_6D_6): δ 2.48 (12H, s), 3.19 (4H, s), 7.02 (4H, m), 7.13 (2H, t, 7 Hz), 7.31 (2H, d, 7 Hz). HRMS (DART-MS) m/z: $[M + H]^+$ Calcd for 269.1973; Found 269.20130. Trace amounts of the nitrene insertion products AdN=C(H)-C_6H_4-*o*-NMe_2 and AdN(H)$CH_2C_6H_4$-*o*-NMe_2 were observed by DART-MS. HRMS (DART-MS) m/z: $[M + H]^+$ Calcd for 283.2130 and 285.2286; Found 283.21670 and 285.23224.

12. Oxidation of 3-C,N with $FcPF_6$. To a 25-mL flask charged with **3-C,N** (100 mg, 0.198 mmol) and $FcPF_6$ (65 mg, 0.20 mmol) was added 10 mL THF via vacuum transfer at -78 ^{o}C, resulting in a dark orange solution. Allowing the solution to warm slowly with stirring for 20 h resulted in a brown-orange solution at 21 ^{o}C. Removal of the volatiles, followed by washing the residue with pentane (3 x 10 mL), resulted in brown-orange powder. ^{1}H NMR of the powder in C_6D_6 was consistent with the production of NMe_2-C_6H_4-*o*-CH_2CH_2-C_6H_4-*o*-NMe_2 and Fc (4.01 ppm).

13. Treatment of 3-C,N with AdN_3. To a vial charged with **3-C,N** (11 mg, 0.022 mmol) and 0.5 mL C_6D_6 was added AdN_3 (4 mg, 0.023 mmol), resulting in a yellow

solution. After 30 min at 21 °C, the solution turns orange-yellow, with no further color changes occurring regardless of reaction time. Analysis of the solution by ^{1}H NMR after 1 h shows decomposition of the azide, production of NMe_2-C_6H_4-*o*-CH_2CH_2-C_6H_4-*o*-NMe_2 (20% conversion) and (Me_2IPr)Fe($CH_2C_6H_4$-*o*-NMe_2)$_2$. Nitrene insertion products were not observed by DART-MS.

14. Treatment of 4 with AdN_3. To a vial charged with **4** (11 mg, 0.014 mmol) and 0.5 mL THF-d_8 was added AdN_3 (5 mg, 0.028 mmol), resulting in a brown-orange solution, with no observable effervescence. Analysis of the solution after 30 min at 21 °C by ^{1}H NMR indicated little consumption of the dimer and decomposition of the azide, with only trace amounts of the nitrene insertion product Ad$N(H)CH_2PMe_2$ observed by DART-MS. HRMS (DART-MS) m/z: $[M + H]^+$ Calcd for 226.1680; Found 226.17235.

15. Treatment of 5 with excess *cis*-2-pentene. To a vial charged with **5** (11 mg, 0.031 mmol) was added 0.5 mL C_6D_6. The solution was added to a J. Young tube, the solution frozen at 77 K, and the tube was degassed. *cis*-2-pentene (22.8 cm Hg, 0.307 mmol) was transferred to a 23.29-mL gas bulb, and then subsequently frozen at 77 K in the J. Young tube. The mixture was warmed to 21 °C, and ^{1}H analysis revealed no observable reactivity. Heating the solution to 55 °C, followed by 90 °C, resulted in no reaction for either starting material.

16. Treatment of 5 with AdN_3. To a vial charged with **5** (12 mg, 0.034 mmol) and 0.5 mL C_6D_6 was added AdN_3 (6 mg, 0.034 mmol). No reactivity was observed at 21

^{o}C, while heating the solution to 55 ^{o}C resulted in decomposition of the azide starting material.

17. Oxidation of 6 with $FcPF_6$. To a 25-mL flask charged with **6** (102 mg, 0.199 mmol) and $FcPF_6$ (66 mg, 0.20 mmol) was added 10 mL THF via vacuum transfer at -78 ^{o}C, resulting in a dark yellow solution. Allowing the solution to warm slowly with stirring for 2 d resulted in a yellow solution with grey solid. Removal of the volatiles followed by washing the residue with pentane (3 x 10 mL) resulted in a light yellow-grey powder. Analysis of the powder by ^{1}H NMR in C_6D_6 showed the production of Fc (4.01 ppm) and $Me_2PC_6H_4$-*o*-$CH_2CH_2C_6H_4$-*o*-PMe_2. ^{1}H NMR (C_6D_6): δ 0.84 (18H, s), 3.58 (3H, s), 7.02 (2H, t, 7 Hz), 7.09 (2H, t, 7 Hz), 7.21 (2H, d, 7 Hz), 7.44 (2H, d, 7 Hz). ^{31}P NMR (C_6D_6): δ -37.31.

Single crystal X-ray diffraction studies. Upon isolation, the crystals were covered in polyisobutenes and placed under a cold N_2 stream on the goniometer head of a Siemens P4 SMART CCD area detector (graphite-monochromated MoKα radiation, λ = 0.71073 Å). The structures were solved by direct methods (SHELXS). All non-hydrogen atoms were refined anisotropically unless stated, and hydrogen atoms were treated as idealized contributions (Riding model).

References

(1) Lindley, B. M.; Swidan, A.; Lobkovsky, E. B.; Wolczanski, P. T.; Adelhart, M.; Sutter, J.; Meyer, K. *Chem. Sci.* **2015**, *6*, 4730.

(2) Jacobs, B. P.; Agarwal, R. G.; Wolczanski, P. T.; Cundari, T. R.; MacMillan, S. N. *Polyhedron* **2016**, *116*, 47.

(3) Lindley, B. M.; Jacobs, B. P.; MacMillan, S. N.; Wolczanski, P. T. *Chem. Comm.* **2016**, *52*, 3891.

(4) Kingsbury, J. S.; Harrity, J. P. A.; Bonitatebus, P. J.; Hoveyda, A. H. *J. Am. Chem. Soc.* **1999**, *121*, 791.

(5) Gessler, S.; Randl, S.; Blechert, S. *Tetrahedron Letters* **2000**, *41*, 9973.

(6) Garber, S. B.; Kingsbury, J. S.; Gray, B. L.; Hoveyda, A. H. *J. Am. Chem. Soc.* **2000**, *122*, 8168.

(7) Wood, C. D.; McLain, S. J.; Schrock, R. R. *J. Am. Chem. Soc.* **1979**, *101*, 3210.

(8) Schrock, R. R.; Fellmann J. D. *J. Am. Chem. Soc.* **1978**, *100*, 3360.

(9) Li, L.; Hung, M.; Xue, Z. *J. Am. Chem. Soc.* **1995**, *117*, 12746.

(10) Xue, Z.; Morton, L. A. *J. Organomet. Chem.* **2011**, *696*, 3924.

(11) Noël-Duchesneau, L.; Lugan, N.; Lavigne, G.; Labande, A.; César, V. *Eur. J. Inorg. Chem.* **2015**, 1752.

(12) Manzer, L. E. *J. Am. Chem. Soc.* **1978**, *100*, 8068.

(13) Jastrzebski, J. T. B. H.; van Koten, G. *Inorg. Syn.*, Vol. 26, Kaesz, H. D., Ed., *Inorganic Syntheses, Inc.*: New York, 1089.

(14) Meinholz, M. M.; Pandey, S. K.; Deuerlein, S. M.; Stalke, D. *Dalton Trans.* **2011**, *40*, 1662.

(15) Solomon, S. A.; Allen, L. K.; Dane, S. B. J.; Wright, D. S. *Eur. J. Inorg. Chem.* **2014**, 1615.

(16) Karsch, H. H. *Chem. Ber.* **1977**, *110*, 2699.

(17) (a) Evans, D. F. *J. Chem. Soc.* **1959**, 2003. (b) Schubert, E. M. *J. Chem. Ed.* **1992**, *69*, 62.

(18) Jacobs, B. P.; Wolczanski, P. T.; Lobkovsky, E. B. *Inorg. Chem.* **2016**, *55*, 4223.

(19) Manzer, L. E.; Guggenberger, L. J. *J. Organomet. Chem.* **1977**, *139*, C34.

(20) Latten, J. L.; Dickson, R. S.; Deacon, G. B.; West, B. O.; Tiekink, E. R. T. *J. Organomet. Chem.* **1992**, *435*, 101.

(21) Ryan, S. J.; Schimler, S. D.; Bland, D. C.; Sanford, M. S. *Org. Lett.* **2015**, *17*, 1866.

(22) Dunsford, J. J.; Cade, I. A.; Fillman, K. L.; Neidig, M. L.; Ingleson, M. J. *Organometallics* **2014**, *33*, 370.

(23) Zhang, H.; Ouyang, Z.; Liu, Y.; Zhang, Q.; Wang, L.; Deng, L. *Angew. Chem. Int. Ed.* **2014**, *53*, 8432.

(24) Wang, L.; Hu, L.; Zhang, H.; Chen, H.; Deng, L. *J. Am. Chem. Soc.* **2015**, *137*, 14196.

(25) Zhang, L.; Liu, Y.; Deng, L. *J. Am. Chem. Soc.* **2014**, *136*, 15525.

(26) Xiang, L.; Xiao, J.; Deng, L. *Organometallics* **2011**, *30*, 2018.

(27) Liu, Y.; Wang, L.; Deng, L. *Organometallics* **2015**, *34*, 4401.

(28) Liu, Y.; Xiao, J.; Wang, L.; Song, Y.; Deng, L. *Organometallics* **2015**, *34*, 599.

(29) Liu, Y.; Luo, L.; Xiao, J.; Wang, L.; Song, Y.; Qu, J.; Luo, Y.; Deng, L. *Inorg. Chem.* **2015**, *54*, 4752.

(30) Mo, Z.; Ouyang, Z.; Wang, L.; Fillman, K.; Neidig, M. L.; Deng, L. *Org. Chem. Front.* **2014**, *1*, 1040.

(31) Karsch, H. H. *Chem. Ber*. **1977**, *110*, 2222.

(32) Bartholomew, E. R.; Volpe, E. C.; Wolczanski, P. T.; Lobkovsky, E. B.; Cundari, T. R. *J. Am. Chem. Soc.* **2013**, *135*, 3511.

(33) Volpe, E. C.; Wolczanski, P. T.; Lobkovsky, E. B. *Organometallics* **2010**, *29*, 364.

(34) Wolczanski, P. T. *Organometallics* **2017**, *36*, 622.

Chapter 4

Preparation of Fe(IV)=NR via Oxidation of Fe(II) Alkyl Complexes with Azides Leads to Nitrene Insertion into the Fe-C Bond

Introduction

In the pursuit of Fe(II)-CH_2R complexes as suitable precursors to Fe(IV) alkylidenes, a series of Fe(II) chelates bearing κ-C,N/P type ligands were prepared.[1] Oxidation studies of the chelates resulted in CC ligand coupling as the major product, with no discernable Fe(III) species isolated. Given the disappointing results, Fe complex synthesis refocused on the preparation of Fe(II)-$CH_2C(CH_3)_3$. Scheme 4.1 illustrates synthetic methods for generating Fe(IV) neopentylidene species through

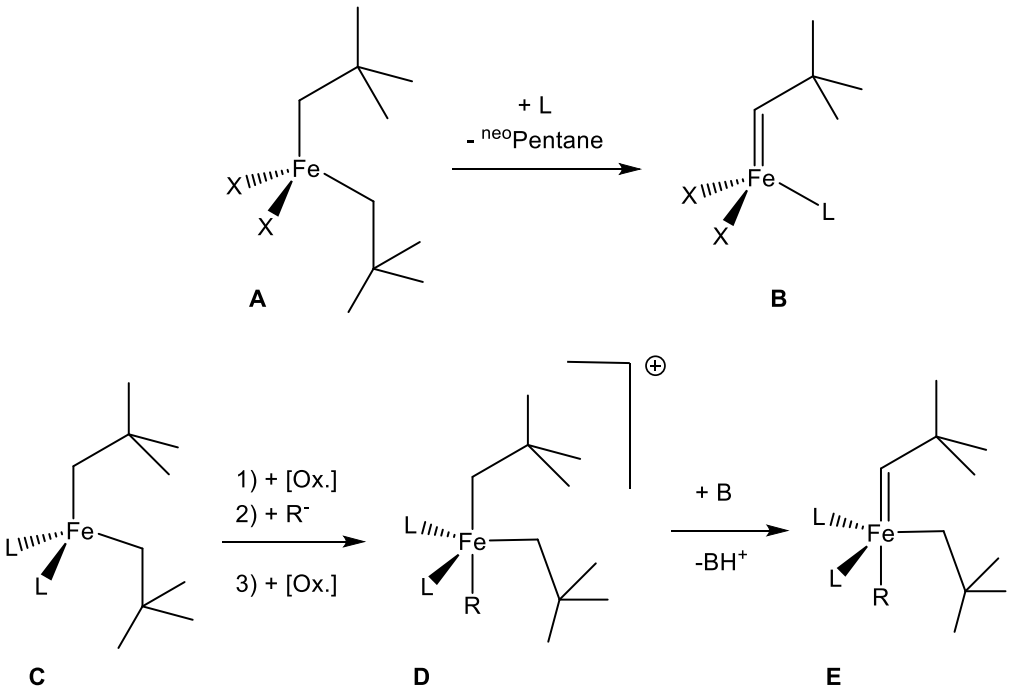

Scheme 4.1. Synthetic methods for the preparation of Fe(IV) neopentylidenes

either α-H abstraction of Fe(IV) precursor (**A**) induced through addition of a neutral ligand, or via sequential oxidations of Fe(II) precursors (**C**) followed by deprotonation. Ample precedent for alkylidene formation via α-H abstraction from d^0 early metal systems exists.[2-5]

Since Fe(II) chelate complexes were shown to undergo oxidative degradation to generate CC coupled products, a similar degradation route could occur for Fe(II) neopentyl complexes. It was envisaged that employing a bulky alkyl group featuring a quaternary Fe-carbon motif may inhibit ligand coupling and allow for formation of stable Fe(III) species. The norbornyl anion is an intriguing option, as the homoleptic M(IV) norbornyl species originally reported by Bower and Tennent were remarkably stable in light of the high oxidation states.[6,7] These compounds are low spin, despite the weak field intrinsic to tetrahedral metal complexes. X-ray structural analysis reported by Hayton *et al*. illustrated its nearly ideal tetrahedral geometry.[8] Traditional arguments as to the stability of these unusual metal-norbornyl species focus on the lack of β-H elimination due to the formation of an unstable "bridgehead olefin," yet recent computations reported by Power *et al.* for $Fe(1\text{-}Nor)_4$ implicate London dispersion forces as a viable stabilizing force due to the large number of C-H entities within the complex.[9] In accordance with this, Fürstner *et al*. reported the synthesis of $Fe(cyclohexyl)_4$,[10] an unusual complex given that α- or β-hydride elimination does not occur despite the Fe center being surrounded by 4/16 H-atoms at the correct positions.

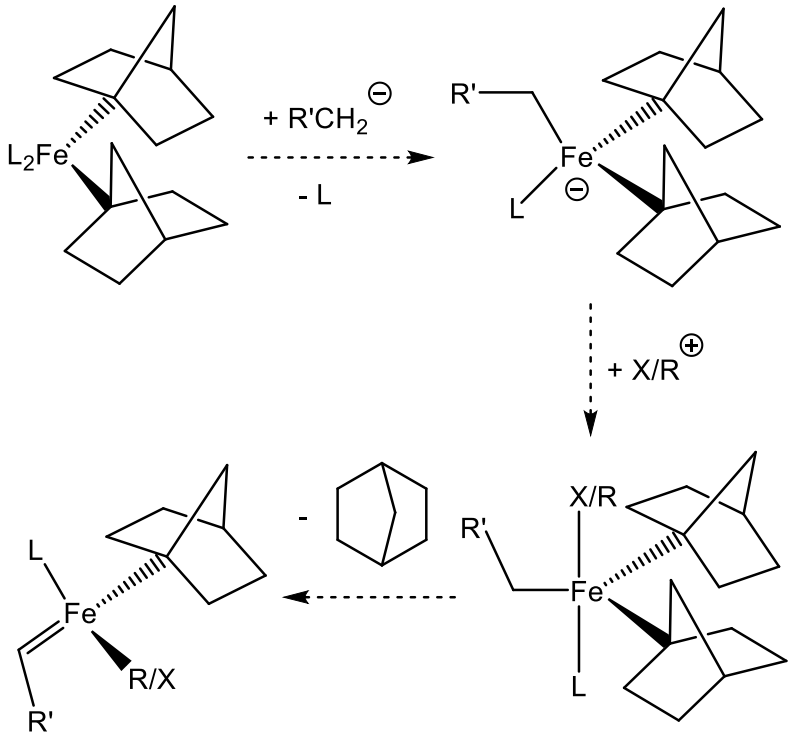

Scheme 4.2. Fe alkylidene preparation from a Fe(II) norbornyl precursor

Given the unusual stability metal-norbornyl groups possess, we sought to prepare Fe(II) norbornyl complexes that may be suitable for oxidation studies. Scheme 4.2 presents a synthetic pathway where alkylation followed by oxidative addition of X^+ (e.g. I_2, etc.) or R^+ (e.g. CH_3I, etc.) can generate an Fe(IV) species that may undergo α-H abstraction to generate the target Fe alkylidene.

An intriguing report by Deng *et al*. detailed the isolation of a low spin Fe(IV) bis(imido) complex that undergoes C-H activation of a remote isopropyl group on the imide phenyl at elevated temperatures,[11,12] as shown in Scheme 4.3. It was envisaged that treatment of a Fe(II) neopentyl complex (**A**) with an azide may furnish an Fe(IV) imide (**B**), and that the imide may promote C-H activation of the CH_2 unit to generate

the Fe(IV) alkylidene (**C**). As such, azide oxidation of Fe(II) alkyl complexes was pursued towards the isolation of Fe(IV) imides, with their utility towards alkylidene preparation investigated.

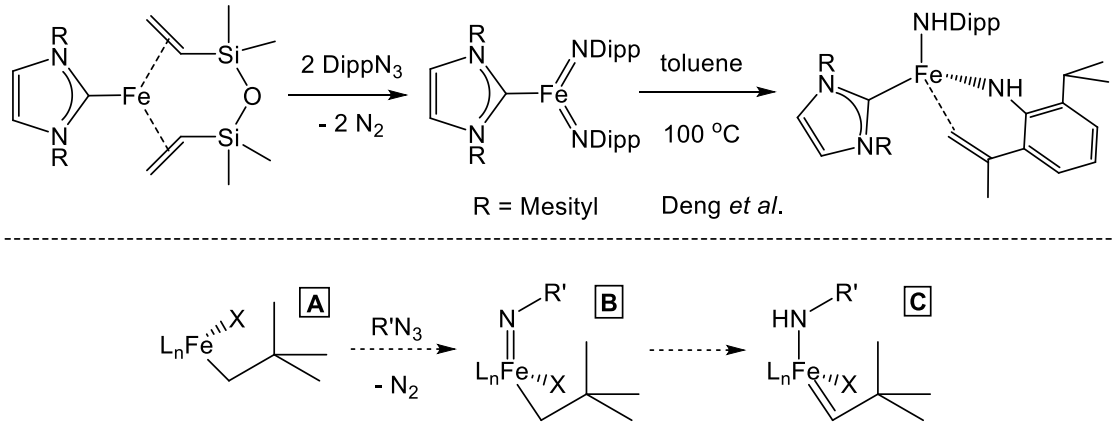

Scheme 4.3. Fe(IV) imide mediated C-H activation and potential application towards alkylidene preparation

Results and Discussion

4.1 Preparation of Fe(II) Neopentyl Complexes Bearing Ancillary Ligands

The stability of Fe(1-norbornyl)$_4$[6-9] prompted a survey into preparing the neopentyl variant. Treatment of $FeCl_2$ with 2 equiv. $LiCH_2C(CH_3)_3$[13] led to formation of Fe metal as the sole metal-containing product. Since the preparation of a homoleptic Fe(IV)-neopentyl species was unsuccessful, Fe(II) analogues bearing ancillary ligands were considered. Chirik *et al*. reported the synthesis of $(py)_2Fe\{CH_2C(CH_3)_3\}_2$ (**1**-py),[14] and replication of the method yielded the Fe(II) complex as red-purple crystals in 60% yield. Given the straightforward workup of the reaction and high yield of the Fe product, additional variants employing alternative

nitrogen donor ligands were prepared through simple salt metathesis, as shown in Scheme 4.4.[15,16] Dark blue (2,2'-bipy)Fe{$CH_2C(CH_3)_3$}$_2$ (**1**-bipy) was isolated in 56% yield, while colorless crystals of (TMEDA)Fe{$CH_2C(CH_3)_3$}$_2$ (**1**-TMEDA) were collected in 82%. Evans' method magnetic measurements[17] of **1**-bipy and **1**-TMEDA provided μ_{eff} values of 5.1 and 4.8 μ_B, respectively. Both values indicate high spin d^6 Fe(II) centers (S = 2).

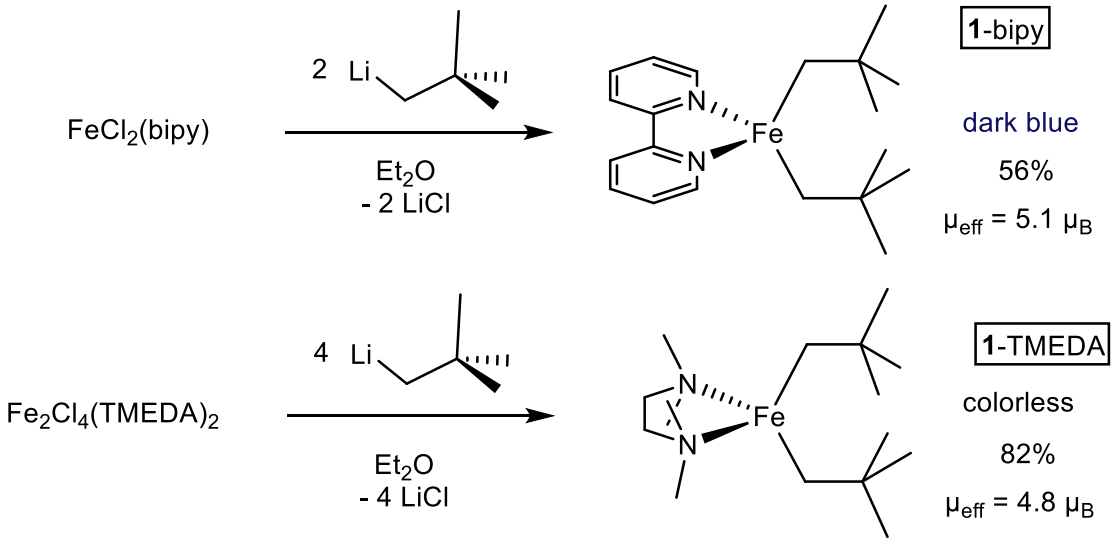

Scheme 4.4. Preparation of Fe(II)-neopentyl species bearing nitrogen donor ligands

The high spin nature of **1**-bipy and **1**-TMEDA prompted a switch to stronger field ancillary ligands such as phosphines or N-heterocyclic carbenes. Treatment of $FeCl_2(PMe_3)_2$[18] with 2 equiv. $LiCH_2C(CH_3)_3$ resulted in the isolation of $(Me_3P)_2$Fe{$CH_2C(CH_3)_3$}$_2$ (**1**-PMe_3) as a yellow-brown solid in only 15% yield (Scheme 4.5). Changing the Fe starting material to the N-heterocyclic carbene precursor [(Me_2IPr)FeCl(μ-Cl)]$_2$[19,20] led to formation of (Me_2IPr)Fe{$CH_2C(CH_3)_3$}$_2$ (**1**-Me_2IPr) as light yellow crystals in good yield (63%). Evans' method magnetic

measurements[17] of **1**-PMe_3 and **1**-Me_2IPr revealed μ_{eff} values of 5.5 and 5.0(3) μ_B, respectively. Both complexes are consistent with a high spin Fe(II) center.

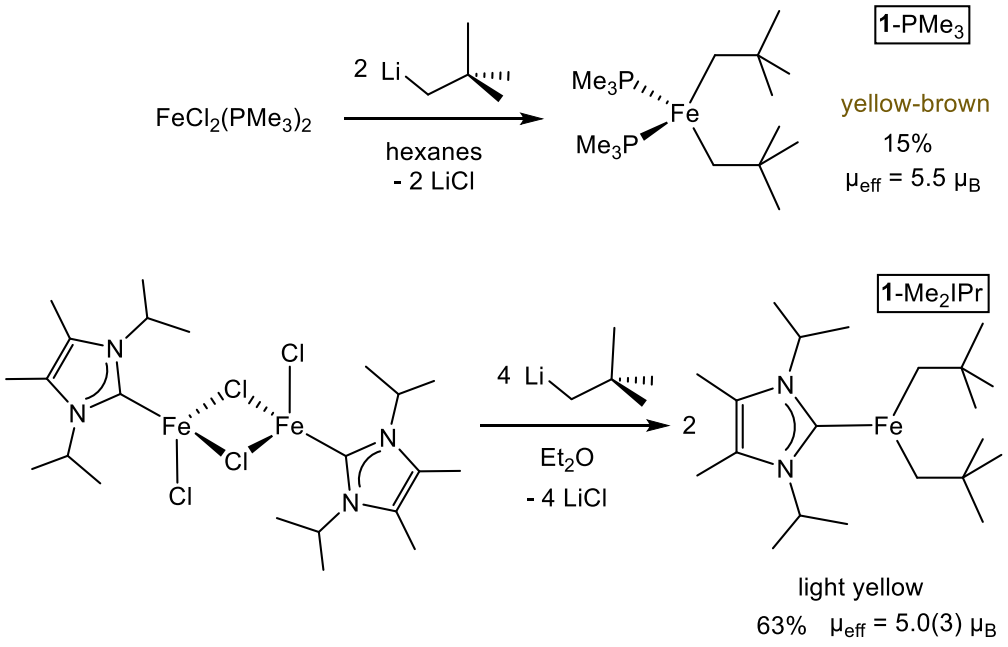

Scheme 4.5. Preparation of Fe(II)-neopentyl species bearing phosphine or NHC donor ligands

4.2 X-Ray Crystal Structures of 1-TMEDA

A molecular view of (TMEDA)Fe{$CH_2C(CH_3)_3$}$_2$ (**1**-TMEDA) is presented in Figure 4.1, with relevant metrics listed in the caption. The C_2-symmetric molecule is a considerably distorted tetrahedron, with an acute N-Fe-N angle of 79.12(6)°, and a wide C-Fe-C angle of 138.67(8)°. Russo *et al*. reported the crystal structure of the variant complex (TMEDA)Fe{$CH_2Si(CH_3)_3$}$_2$,[21] which has a smaller C-Fe-C angle of 128.83(14)°. Given the unusually wide Fe-C4-C5 angle of 125.39(9)°, the Fe-alkyl angle distortions of **1**-TMEDA seem to originate from minimizing the steric interaction of the two tert-butyl groups on the neopentyl ligands. The small N-Fe-N

angle is consistent with Russo's variant (N-Fe-N = 79.98°) and with the derivative complex (TMEDA)Fe(Mesityl)$_2$ reported by Noda and coworkers (N-Fe-N = 79.07°).[22] The Fe-N and Fe-C distances of 2.2959(11) and 2.0897(12) Å are typical for high spin Fe(II) complexes, with no significant deviances measured.

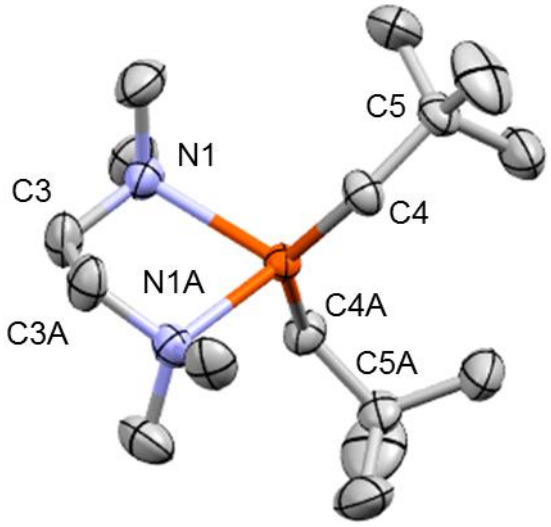

Figure 4.1. Molecular view of (TMEDA)Fe{$CH_2C(CH_3)_3$}$_2$ (**1**-TMEDA). Selected interatomic distances (Å) and angles (°): Fe-C4, 2.0897(12); Fe-N1, 2.2959(11); N1-C1, 1.4764(19); N1-C2, 1.4783(17); N1-C3, 1.4708(19); C4-C5, 1.5363(18); C5-C6, 1.522(2); C5-C7, 1.528(2); C5-C8, 1.528(2); C4-Fe-C4A, 138.67(8); N1-Fe-N1A, 79.12(6); C4-Fe-N1, 101.09(4); C4-Fe-N1A, 110.60(5), Fe-N1-C3, 105.67(8); Fe-C4-C5, 125.39(9).

X-ray crystal structure analysis of (Me_2IPr)Fe{$CH_2C(CH_3)_3$}$_2$ (**1**-Me_2IPr) determined the connectivity of the complex as a three-coordinate species, in agreement with ^{1}H NMR spectroscopic studies and magnetic measurements conducted via Evans' method.[17] The molecular structure of **1**-Me_2IPr is similar to the variant (IPr^i)Fe{$CH_2Si(CH_3)_3$}$_2$, whose structure was reported by Robert *et al*.[23]

4.3 Oxidation Studies of 1-L_n

Scheme 4.1 illustrates a synthetic pathway for preparing Fe(IV) alkylidenes (E) from Fe(II) neopentyl precursors (**C**). Oxidation of **C** should result in an Fe(III) neopentyl cation, as the first synthetic step. With the successful preparation of the Fe(II) neopentyl complexes **1**-L_n, oxidation studies were conducted for both (TMEDA)Fe{$CH_2C(CH_3)_3$}$_2$ (**1**-TMEDA) and (Me_2IPr)Fe{$CH_2C(CH_3)_3$}$_2$ (**1**-Me_2IPr), these species chosen due to their high preparatory yield and readily accessible precursors.

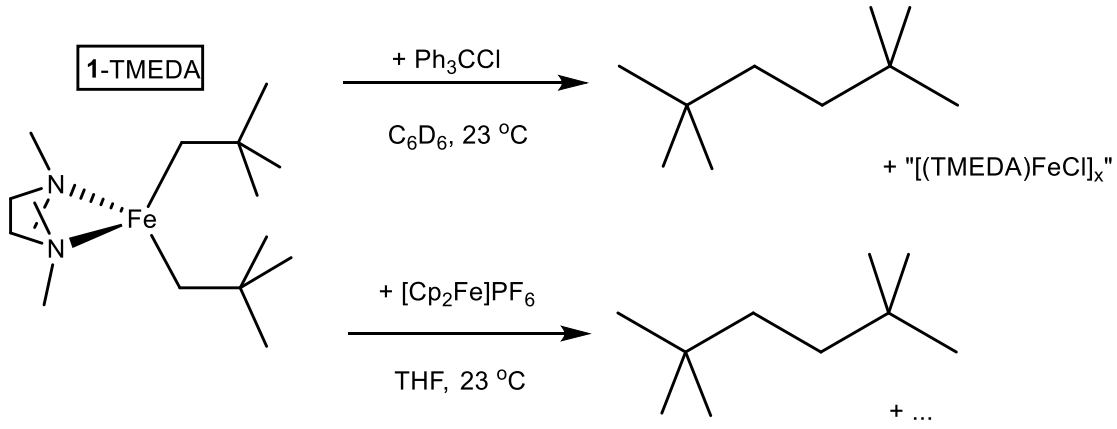

Scheme 4.6. One-electron oxidation attempts for **1**-TMEDA

One-electron oxidants were surveyed in their reactivity with **1**-TMEDA, and the results are summarized in Scheme 4.6. Treatment of **1**-TMEDA with trityl chloride (Ph_3CCl) produced the organic product bineopentyl, an oxidative degradation product resulting from CC coupling of the alkyl ligands. This oxidatively-triggered CC coupling process has been reported from these laboratories for oxidation of Fe(II) chelates and a Fe(II) ene-amide complex.[1,24] For the present case, oxidation of **1**-

TMEDA with Ph_3CCl generated one unidentified paramagnetic product alongside bineopentyl and Gomberg's dimer.[51] The Fe-containing byproduct was not identified due to the degradation of the putative Fe(III) product, although the lack of free TMEDA suggest a tentative formulation of the byproduct as "$[(TMEDA)FeCl]_x$". Oxidation of **1**-TMEDA with $[Cp_2Fe]PF_6$ led to a similar product distribution, with clean formation of bineopentyl, ferrocene and one new unidentified Fe-containing product. For both cases, isolation of an Fe(III) species was not realized.

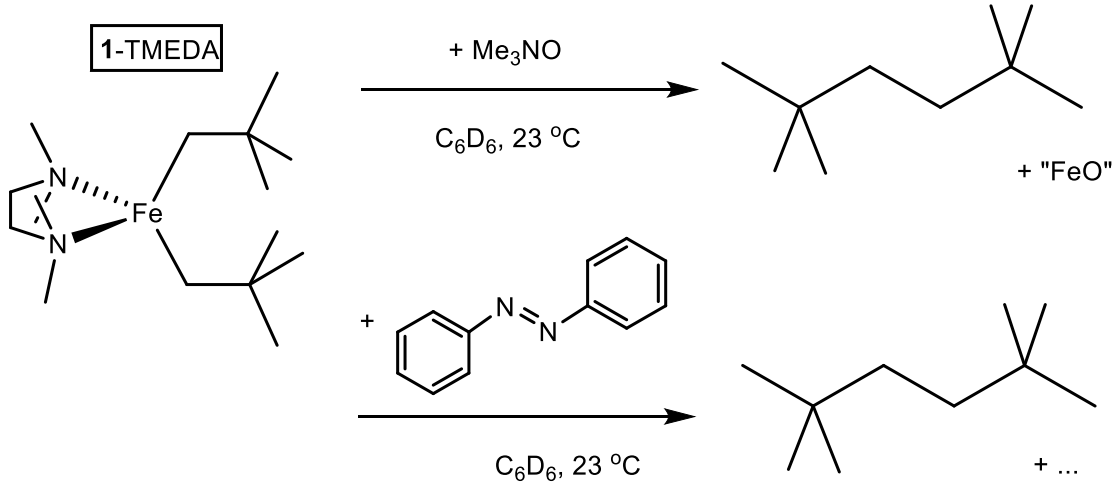

Scheme 4.7. Oxidation of **1**-TMEDA employing additional oxidants

Additional oxidation studies of **1**-TMEDA employing either trimethylamine N-oxide or azobenzene are presented in Scheme 4.7. Production of bineopentyl and liberation of TMEDA was noted for both reactions, and no discernable paramagnetic products were observed by ^1H NMR spectroscopy. Orange-brown "FeO" immediately precipitated upon addition of Me_3N-O to a solution of **1**-TMEDA. Attempts to

crystallize any Fe-containing product from the oxidation of **1**-TMEDA with azobenzene were unsuccessful.

Oxidative degradation of the putative Fe(III) neopentyl cations prompted switching the Fe(II) starting material to **1**-Me_2IPr. Addition of Me_3N-O to a benzene solution of **1**-Me_2IPr immediately produced a light orange precipitate (Eq 4.1). Analysis of the solution by ^{1}H NMR spectroscopy revealed bineopentyl and Me_3N to be the sole products, with neither Fe-containing product nor free NHC present in solution.

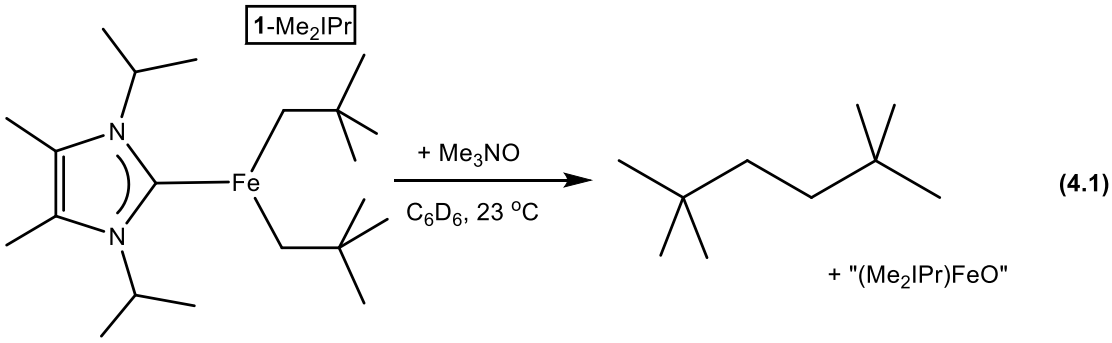

(4.1)

4.4 Attempts at Inducing α-H Abstraction, Alkylation or Carbene Transfer of 1-L_n

Failure to produce Fe(III) neopentyl complexes via oxidation prompted investigations into alternative methods of forming an Fe alkylidene from the Fe(II) neopentyl complexes **1**-L_n. Exposing complexes **1**-L_n to exogenous donor ligands may induce α-H abstraction to yield an Fe(II) alkylidene, which may exhibit greater stability upon oxidation. Scheme 4.8 summarizes several attempts at inducing α-H abstraction. Exposure of $(Me_3P)_2Fe\{CH_2C(CH_3)_3\}_2$ (**1**-PMe_3) to excess PMe_3 was

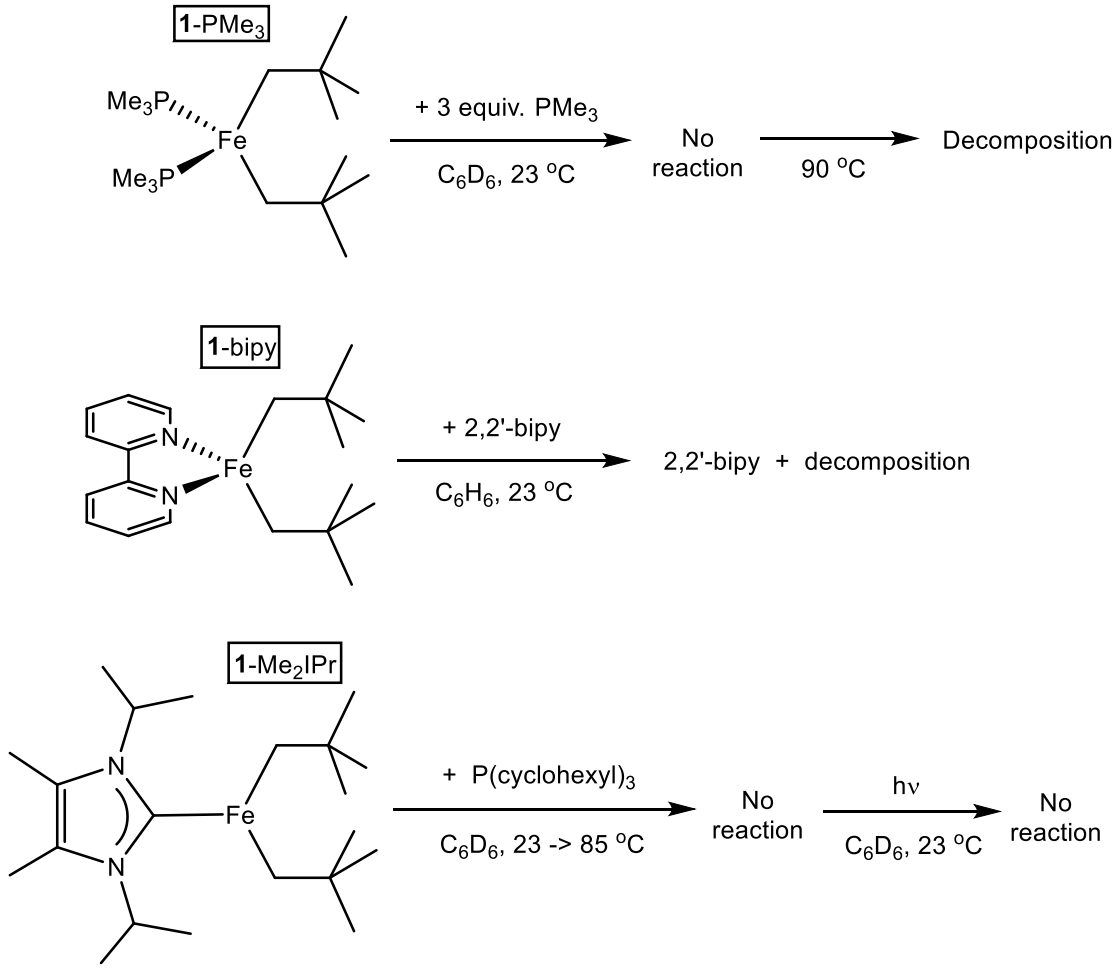

Scheme 4.8. Attempts to induce α-H abstraction for complexes **1**-L_n

unproductive, and heating the sample only led to decomposition of **1**-PMe_3. Treatment of blue (2,2'-bipy)Fe{$CH_2C(CH_3)_3$}$_2$ (**1**-bipy) with 1 equiv. 2,2'-bipy led to decomposition of **1**-bipy, with only free ligand observed by ^{1}H NMR spectroscopy. Conversely, addition of P(cyclohexyl)$_3$ to (Me_2IPr)Fe{$CH_2C(CH_3)_3$}$_2$ (**1**-Me_2IPr) was unproductive, and heating the sample or exposing it to UV-light failed to elicit any reaction.

The original methodology in oxidizing complexes **1**-L_n called for subsequently alkylating them to render a neutral Fe(III) trialkyl species (Scheme 4.1). Since initial oxidation was unsuccessful, efforts shifted towards alkylating **1**-L_n to make anionic Fe(II) species, after which oxidation studies would then be conducted with the anions. Treatment of $(py)_2Fe\{CH_2C(CH_3)_3\}_2$ (**1**-py) with 2 equiv. $LiCH_2C(CH_3)_3$ yielded a dark brown-violet powder (Eq 4.2). The ^1H NMR spectrum indicated formation of a new paramagnetic species, yet quenching the NMR sample revealed the presence of 2,2'-bipy, correlated to a known sample. The unknown paramagnetic product was not consistent with **1**-bipy, and its identity was not determined.

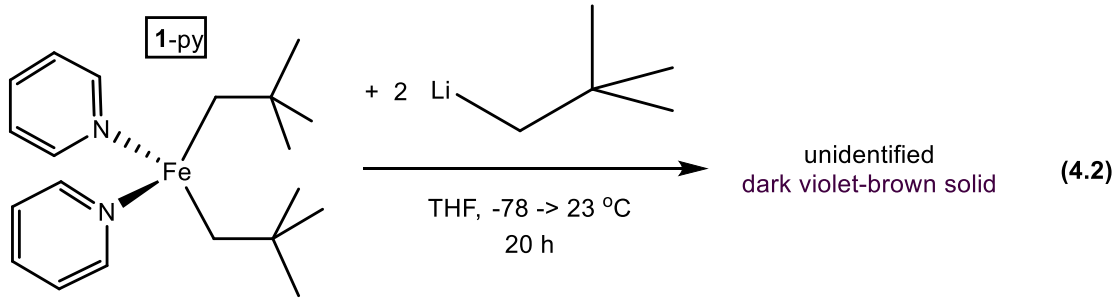

(4.2)

Alkylation of the three-coordinate complex **1**-Me_2IPr was considered as an approach towards generating a Fe(II) anion. Addition of $LiCH_2C(CH_3)_3$ to **1**-Me_2IPr did not produce any distinct color change, and ^1H NMR spectroscopy noted only the presence of both starting materials (Eq 4.3).

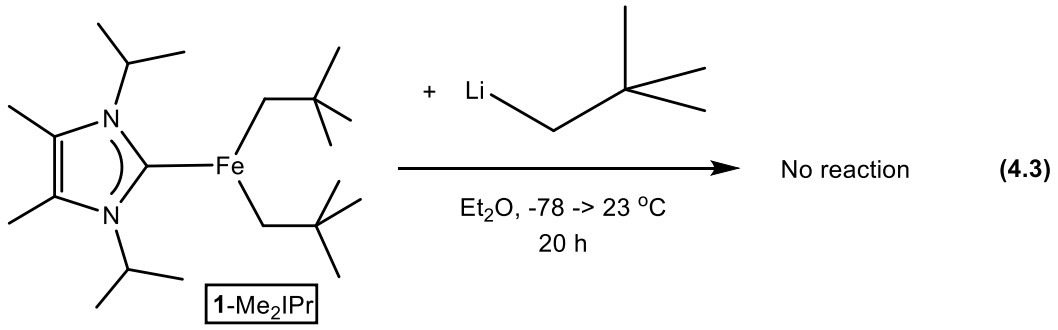

(4.3)

Diazoalkanes have been shown to act as carbene transfer reagents for the preparation of transition metal alkylidenes (e.g. Ru, Fe).[25-30] Phosphine ylides were also envisaged to potentially transfer the methylene fragment. Efforts towards carbene transfer to complex **1**-Me_2IPr are illustrated in Scheme 4.9. Addition of 2-diazo-1-phenylethanone[31] to a pentane solution of **1**-Me_2IPr produced an intractable mixture, with no distinct product formed. In accordance with this, treatment of **1**-Me_2IPr with a THF solution of the phosphine ylide $Me_3P{=}CH_2$[32] only produced free NHC and neopentane, consistent with degradation of the Fe starting material.

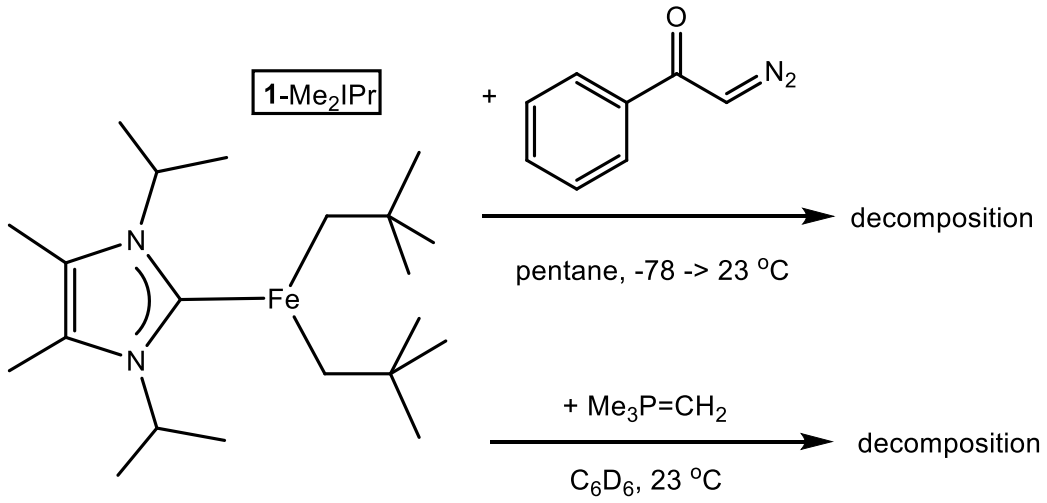

Scheme 4.9. Treatment of **1**-Me_2IPr with carbene transfer reagents

4.5 Treatment of 1-L_n with 1-Adamantyl Azide

Oxidation studies of complexes **1**-L_n resulted in CC ligand coupling with no evidence for the putative Fe(III) species, prompting a switch in oxidant. There is ample precedent for one- or two-electron oxidation of Fe complexes upon addition of organic azides,[12,33-37] forming Fe imides as the oxidized product. As shown in Scheme

4.3, Deng *et al*. reported the preparation of an Fe(IV) bis(imido) complex via azide oxidation of an Fe(0) precursor,[11] the former complex exhibiting remote intra-molecular C-H bond activation upon heating.[12] These results led us to employ azides as potential oxidants for complexes **1**-L_n.

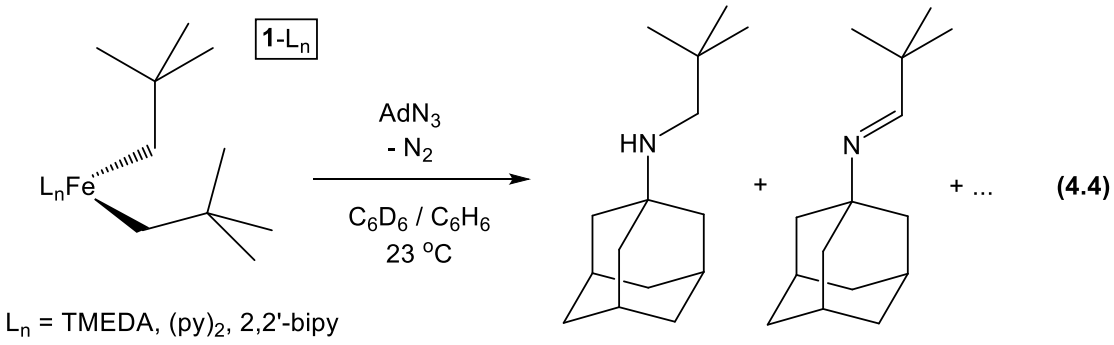

(4.4)

Initial treatment of $(py)_2Fe\{CH_2C(CH_3)_3\}_2$ (**1**-py) with 1-adamantyl azide immediately produced a brown solution with effervescence noted, consistent with N_2 extrusion (Eq 4.4). The ^1H NMR spectrum indicated consumption of **1**-py and the production of a mixture of diamagnetic products, with no paramagnetic species observed. Quenching the NMR sample with water revealed no difference in the resonance shifts, confirming the products as organic species. DART mass spectrometry revealed two major species with positive ion peak values of 220.2057 and 222.2212 m/z, which were consistent with the nitrene insertion products (1-Ad)N=CHC$(CH_3)_3$ and (1-Ad)NH$\{CH_2C(CH_3)_3\}$. Similar products were observed in treating a Fe(II) chelate with the same azide.[1] The same reactivity was noted in treating either (2,2'-bipy)$Fe\{CH_2C(CH_3)_3\}_2$ (**1**-bipy) or (TMEDA)$Fe\{CH_2C(CH_3)_3\}_2$ (**1**-TMEDA) with 1-adamantyl azide, as shown in Eq 4.4.

A possible pathway involves initial formation of the target Fe(IV) imide that undergoes Fe-C bond insertion to yield an Fe(II) amide. The Fe(II) neopentyl amide could undergo β-H elimination to generate (1-Ad)N=CHC(CH_3)$_3$. The Fe(II) amide could also form a dimer, which could then undergo β-H elimination to yield both organic products. Mechanistic studies were not pursued, given the degradation of the putative Fe species to organic products.

4.6 Treatment of 1-Me_2IPr with 1-Adamantyl Azide

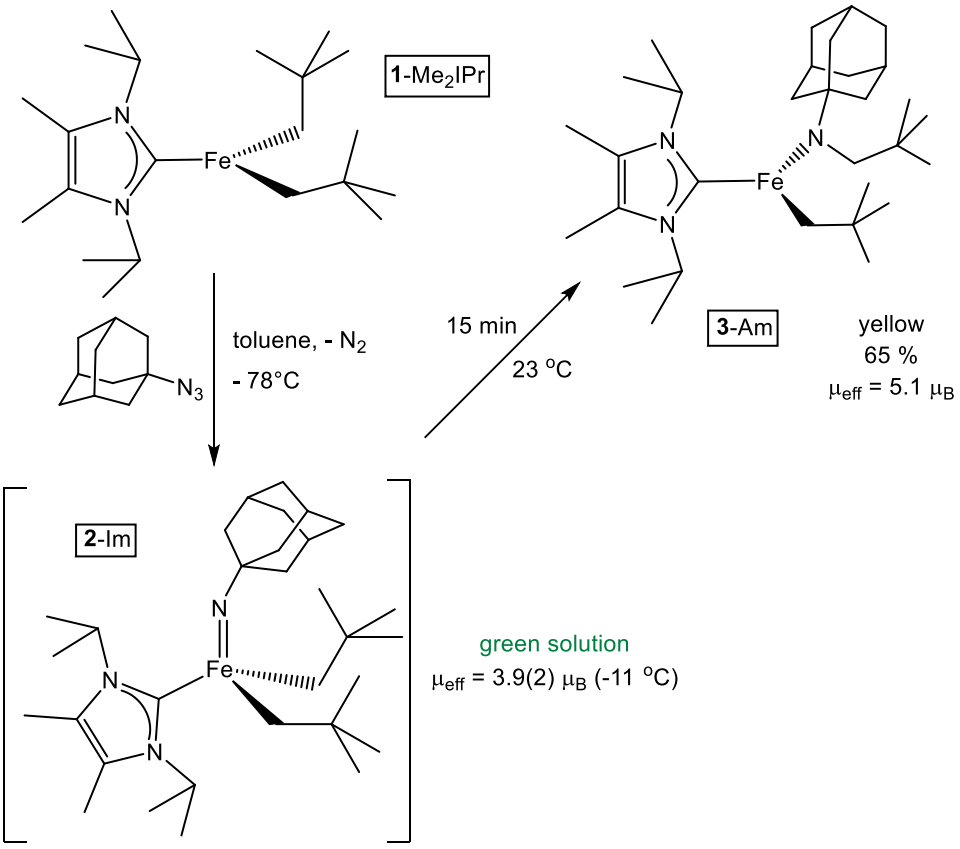

Scheme 4.10. Formation of a putative Fe(IV) imido and subsequent nitrene insertion

Oxidation of several **1**-L_n complexes with 1-adamantyl azide led to degradation to organic products (Eq 4.4), yet treatment of **1**-Me_2IPr with the same

azide produced a green solution with effervescence, as shown in Scheme 4.10. The solution color transitioned to light yellow after 15 minutes at 23 ^{o}C. The ^{1}H NMR spectrum of the yellow solution revealed one paramagnetic product, with the only organic species consistent with excess starting azide. Workup of the mixture led to the isolation of a yellow powder, and subsequent X-ray structural analysis revealed the yellow product to be (Me_2IPr)Fe{N(1-Ad)($CH_2C(CH_3)_3$)}($CH_2C(CH_3)_3$) (**3**-Am). The structure of **3**-Am is consistent with nitrene insertion into an Fe-C bond, yet is stable compared to the other cases studied. Evans' method magnetic measurements[17] produced a μ_{eff} of 5.1 μ_B, which indicates **3**-Am is a high spin Fe(II) center (S = 2).

The yellow Fe(II) amide **3**-Am presumably formed via nitrene insertion of the putative green Fe imide (Me_2IPr)Fe(=N(1-Ad))($CH_2C(CH_3)_3$)$_2$ (**2**-Im) (Scheme 4.10). Preparation of **2**-Im at -30 ^{o}C led to no observable color change even after several hours, allowing for the acquisition of a ^{1}H NMR spectrum of **2**-Im in d_8-toluene at -11 ^{o}C. The ^{1}H NMR spectrum revealed one paramagnetic product consistent with the presence of the NHC, an adamantyl group and two symmetric neopentyl ligands. Magnetic measurements in d_8-toluene at -11 ^{o}C revealed a μ_{eff} of 3.9(2) μ_B, a value consistent with an S = 3/2 spin center (μ_{SO} = 3.87 μ_B). An S = 3/2 spin center is an expected intermediate spin state for an Fe(III) center, but if **2**-Im is a genuine Fe(IV) species, then the expected spin states would be S = 0, 1 or 2 for low, intermediate and high spin, respectively. Experimental measurements of the magnetic moment for **2**-Im are exactly between the intermediate and high spin states. Attempts to crystallize **2**-Im for X-ray structural analysis were unsuccessful. IR spectroscopy of **2**-Im revealed a band at 1106 cm^{-1}, a feature not present for **3**-Am. Peters and Que reported resonance

Raman spectra of several five-coordinate Fe-imido complexes.[38] The band at 1106 cm^{-1} for **2**-Im does fall within a vibrational frequency range reported by Peters and Que for Fe-imido complexes (1084-1111 cm^{-1}).

4.7 X-Ray Crystal Structure of 3-Am

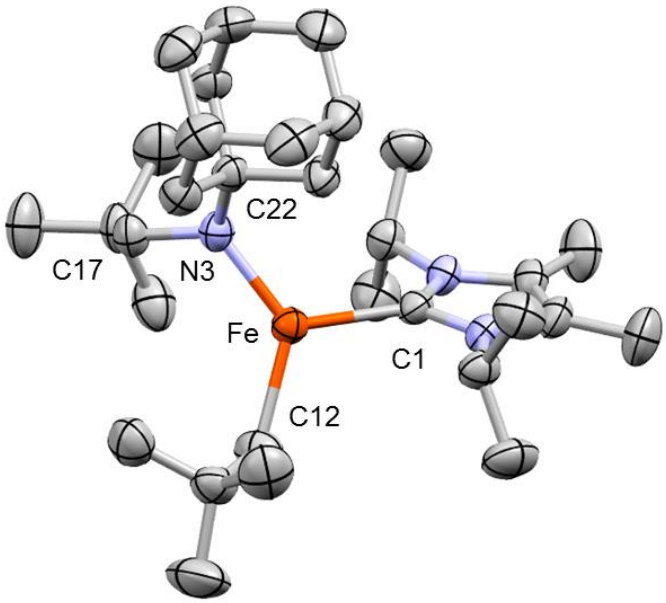

Figure 4.2. Molecular view of $(Me_2IPr)Fe\{N(1\text{-}Ad)(CH_2C(CH_3)_3)\}(CH_2C(CH_3)_3)$ (**3**-Am). Select interatomic distances (Å) and angles (°): Fe-N3, 1.9361(15); Fe-C1, 2.1409(19); Fe-C12, 2.068(2); N3-C17, 1.468(2); N3-C22, 1.461(3); C1-N1, 1.349(3); C1-N2, 1.361(2); N3-Fe-C1, 119.48(7); N3-Fe-C12, 127.41(8); C1-Fe-C12, 112.77(8); Fe-C12-C13, 122.56(4); Fe-N3-C17, 120.93(12); Fe-N3-C22, 118.74(12); C17-N3-C22, 114.61(15).

A molecular view of $(Me_2IPr)Fe\{N(1\text{-}Ad)(CH_2C(CH_3)_3)\}(CH_2C(CH_3)_3)$ (**3**-Am) is presented in Figure 4.2, with relevant metrics listed in the caption. Fe-N3-C angles of 118.74(12) and 120.93(12)° are consistent with formation of a Fe(II) amide, and the Fe-N3 distance of 1.9361(15) Å is comparable to the Fe(II) ene-amide

complex {(2,6-^{i}Pr$_2$-C$_6$H$_3$)(1-^{c}Hexenyl)N}$_2$FePMe$_3$ (d(Fe-N = 1.920(2) and 1.927(2) Å).[24] The Fe-C12 distance of 2.068(2) Å is slightly shorter than the analogous bonds for (TMEDA)Fe{CH$_2$C(CH$_3$)$_3$}$_2$ (**1**-TMEDA) and for Russo's reported (TMEDA)Fe{CH$_2$Si(CH$_3$)$_3$}$_2$ complex by ~0.02 and 0.01 Å, respectively.[21] The core angles feature a wide N3-Fe-C12 angle of 127.41(8)^{o} and an acute C1-Fe-C12 angle of 112.77(8)^{o}, and the Fe center is best described as slightly distorted from an ideal trigonal planar geometry. The newly formed N-C bond lengths of 1.468(2) and 1.461(3) Å are in agreement with expected values for C(sp^3)-N(sp^2) bonds.[39]

4.8 Preparation of Fe(II) Norbornyl Complexes Bearing Ancillary Ligands

Oxidation of the Fe(II) neopentyl complexes **1**-L$_n$ resulted in degradation to the CC coupled product bineopentyl, and alternative methods towards preparing Fe alkylidenes via α-H abstraction or carbene transfer failed. While azide oxidation of **1**-Me$_2$IPr resulted in formation of a putative Fe(IV) imide, subsequent nitrene insertion into the Fe-C bond precluded assessing the viability of the Fe imide as an alkylidene precursor (Scheme 4.3, conversion of Fe(IV) imido (**B**) to Fe(IV) alkylidene (**C**)).

The paucity of isolable oxidized Fe species prompted a switch to a different alkyl group. Given the stability of homoleptic metal-norbornyl complexes in high oxidation states,[6-9] it was envisaged that Fe(II) norbornyl complexes may be amenable to oxidation. Salt metathesis between suitable Fe(II) halide precursors and norbornyl lithium (1-norLi)[40,41] was envisaged to be a reasonable approach to preparing Fe(II)-norbornyl complexes, akin to the preparation of complexes **1**-L$_n$. Addition of 2 equiv. 1-norLi to FeCl$_2$(PMe$_3$)$_2$ led to isolation of orange-yellow crystals of (PMe$_3$)$_2$Fe(1-

nor)$_2$ (**4**-PMe$_3$) in 61% yield. Similar metathesis protocols employing [(TMEDA)FeCl(μ-Cl)]$_2$ and [(Me$_2$IPr)FeCl(μ-Cl)]$_2$ as the Fe precursors resulted in isolation of colorless (TMEDA)Fe(1-nor)$_2$ (**4**-TMEDA) and yellow (Me$_2$IPr)Fe(1-nor)$_2$ (**4**-Me$_2$IPr) in 53 and 54% yields, respectively.

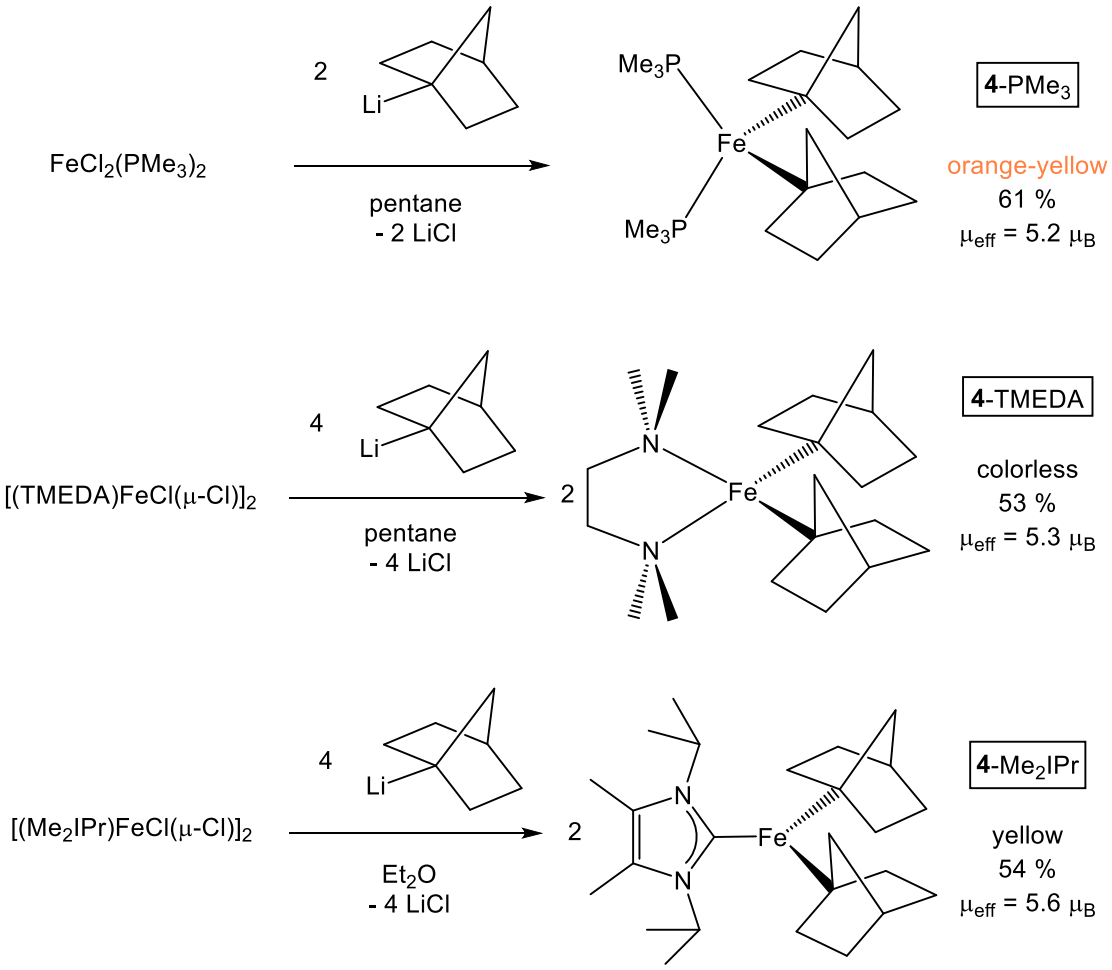

Scheme 4.11. Preparation of the Fe(II) norbornyl complexes **4**-L$_n$

Evans' method magnetic measurements[17] for **4**-PMe$_3$, **4**-TMEDA and **4**-Me$_2$IPr provided μ_{eff} values of 5.2, 5.3 and 5.6 μ_B, respectively. These values are

expected for high spin Fe(II) centers with considerable spin-orbit coupling, and are in agreement with the determined high spin Fe center for complexes **1**-L_n.

4.9 X-Ray Crystal Structures of 4-PMe_3 and 4-Me_2IPr

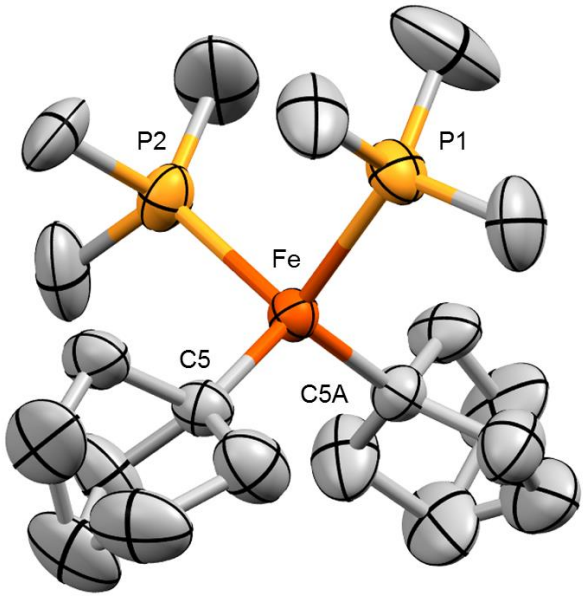

Figure 4.3. Molecular view of $(PMe_3)_2Fe(1\text{-nor})_2$ (**4**-PMe_3). Selected interatomic distances (Å) and angles (°): Fe-C5, 2.057(2); Fe-C5A, 2.057(2); Fe-P1, 2.4127(10); Fe-P2, 2.4076(9); C5-Fe-C5A, 120.32(12); P1-Fe-P2, 99.53(4); P1-Fe-C5, 109.00(6); P1-Fe-C5A, 109.00(6); P2-Fe-C5, 108.50(7); P2-Fe-C5A, 108.50(7).

A view of $(PMe_3)_2Fe(1\text{-nor})_2$ (**4**-PMe_3) is illustrated in Figure 4.3, with notable metrics listed in the caption. The C_{2v}-symmetric molecule exhibits considerable disorder for both norbornyl groups. The Fe-C distances of 2.057(2) Å are longer than those reported for $Fe(1\text{-nor})_4$,[8] which average to 1.993(9) Å, in agreement with the Fe(II) oxidation state for **4**-PMe_3.The C-Fe-P angles match expectations for a tetrahedral core, yet the C-Fe-C angle of 120.32(12)° indicates modest distortion from

ideal tetrahedral geometry. The latter angle renders an acute P-Fe-P angle of 99.53(4)°. Fe-phosphine distances of **4**-PMe_3 are fairly long in comparison to other Fe-PMe_3 complexes (d(Fe-P) = 2.4102(10) (ave)),[1] which may be due to the presence of the rather bulky norbornyl groups.

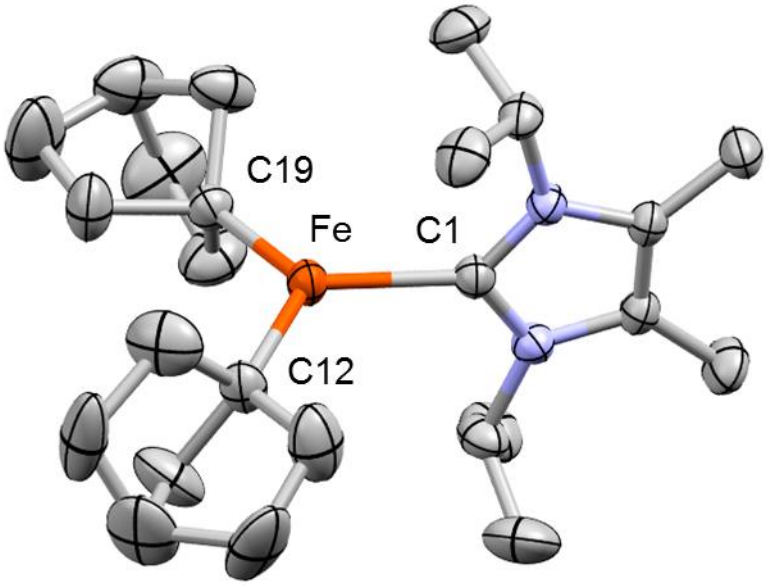

Figure 4.4. Molecular view of (Me_2IPr)Fe(1-nor)$_2$ (**4**-Me_2IPr). Selected interatomic distances (Å) and angles (°): Fe-C1, 2.1167(16); Fe-C12, 2.0489(18); Fe-C19, 2.0620(18); C1-Fe-C12, 119.59(7); C1-Fe-C19, 118.78(7); C12-Fe-C19, 120.32(7).

A view of (Me_2IPr)Fe(1-nor)$_2$ (**4**-Me_2IPr) is shown in Figure 4.4, and additional crystallographic information is provided in Table 4.1 for the Fe(II)-R_2 complexes. Complex **4**-Me_2IPr exhibits C_{2v} symmetry, with disorder present for both norbornyl groups. The structure is near idealized trigonal planar geometry, with the core angles ranging from 118.78(7) to 120.32(7)°. Fe-C_{alk} distances (2.0555(18) Å (ave)) are close to those seen for complex **4**-PMe_3 (d(Fe-C) = 2.057(2) Å).

Table 4.1. Select crystallographic and refinement data for (TMEDA)Fe{$CH_2C(CH_3)_3$}$_2$ (**1**-TMEDA), $(PMe_3)_2$Fe(1-nor)$_2$ (**4**-PMe_3) and (Me_2IPr)Fe(1-nor)$_2$ (**4**-Me_2IPr).

	1-TMEDA	**4**-PMe_3	**4**-Me_2IPr
formula	$C_{16}H_{38}FeN_2$	$C_{20}H_{40}FeP_2$	$C_{25}H_{42}FeN_2$
formula wt	314.33	398.31	426.45
space group	*C*2/c	*P*nma	$P2_1$/n
Z	4	4	4
a, Å	17.2426(10)	18.2193(12)	9.1358(5)
b, Å	9.4301(6)	14.0581(7)	17.7649(9)
c, Å	12.7070(7)	9.3097(6)	15.1504(7)
α, deg	90	90	90
β, deg	107.361(3)	90	98.759(2)
γ, deg	90	90	90
V, Å^3	1972.0(2)	2384.5(2)	2430.2(2)
ρ_{calc}, g cm^{-3}	1.059	1.110	1.166
μ, mm^{-1}	0.758	0.766	0.633
temp, K	223(2)	223(2)	223(2)
λ (Å)	0.71073	0.71073	0.71073
R indices	R1 = 0.0293	R1 = 0.0410	R1 = 0.0427
$[I > 2\sigma(I)]^{a,b}$	wR2 = 0.0754	wR2 = 0.1212	wR2 = 0.0984
R indices^b	R1 = 0.0327	R1 = 0.0467	R1 = 0.0697
(all data)^a	wR2 = 0.0773	wR2 = 0.1282	wR2 = 0.1114
GOF^c	1.076	1.082	1.028

$^aR_1 = \Sigma|F_o| - |F_c||/\Sigma|F_o|$. $^bwR_2 = [\Sigma w(|F_o| - |F_c|)^2/\Sigma wF_o^2]^{1/2}$. ^{c}*GOF* (all data) = $[\Sigma w(|F_o| - |F_c|)^2/(n - p)]^{1/2}$, n = number of independent reflections, p = number of parameters.

4.10 Oxidation Studies of 4-L$_n$

Probes into the stability of complexes **4**-L$_n$ upon oxidation were conducted for each Fe norbornyl species. Treatment of (Me_2IPr)Fe(1-nor)$_2$ (**4**-Me_2IPr) with either Ph_3CCl or I_2 resulted in clean formation of the CC coupled product 1,1'-binorbornyl, as shown in Eq 4.5. ^{1}H NMR spectroscopy revealed formation of a new paramagnetic species consistent with "(Me_2IPr)FeX." While the stoichiometry of the oxidant suggest an Fe(I) byproduct rather than an Fe(III), the product was not further characterized.

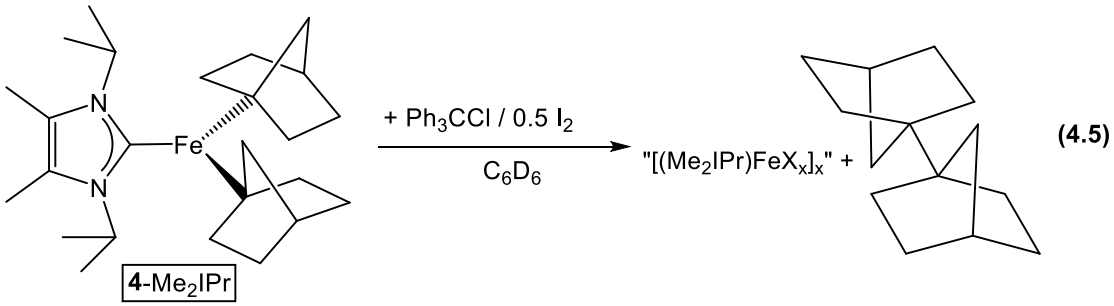

(4.5)

Contrary to the prior oxidations, treatment of **4**-Me_2IPr with CH_2I_2 led to an initial violet solution (Eq 4.6). The ^{1}H NMR spectrum indicated formation of a new paramagnetic product tentatively formulated as (Me_2IPr)Fe(1-nor)$_2$I (**5**), along with 1,1'-binorbornyl in a 1:1 ratio (23 ^{o}C, 30 min). Allowing the solution to stand at 23 ^{o}C for 17 h resulted in a yellow-brown solution, with ^{1}H NMR spectroscopy confirming the consumption of **5**, and the presence of 1,1'-binorbornyl and a paramagnetic product consistent with "(Me_2IPr)FeI_2". The Fe byproduct features different resonances in the NMR spectrum than that recorded for the oxidation with I_2 (Eq 4.5). For each oxidation, the Fe products were not isolated. The putative Fe(III) species **5** may have been on the cusp of stability, and facile oxidative degradation is a natural consequence.

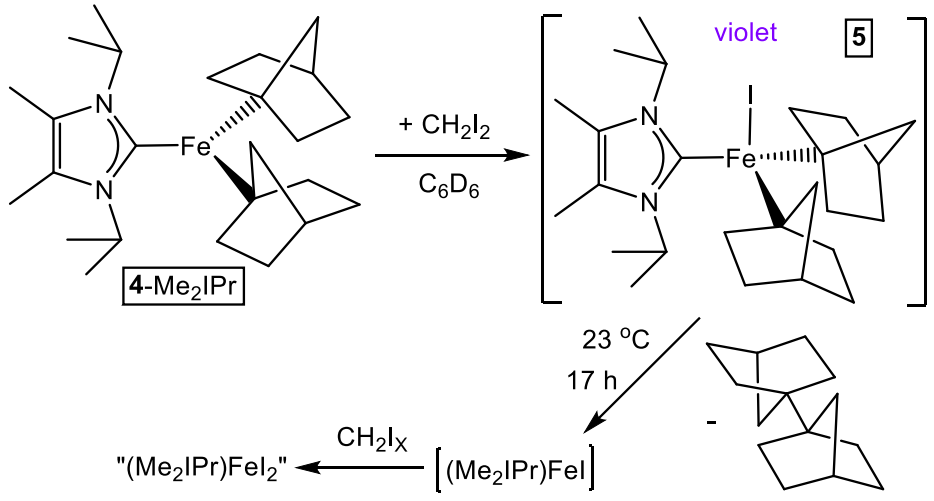

(4.6)

In assessing a variety of oxidants, complex **4**-Me_2IPr was also treated with Me_3NO and nitrous oxide, the latter of which has been reported to transfer an O-atom (Eq 4.7).[42-44] For both cases, precipitation of iron oxide was noted as orange-brown solid, and ^{1}H NMR spectroscopy confirmed the clean formation of 1,1'-binorbornyl as the sole major product.

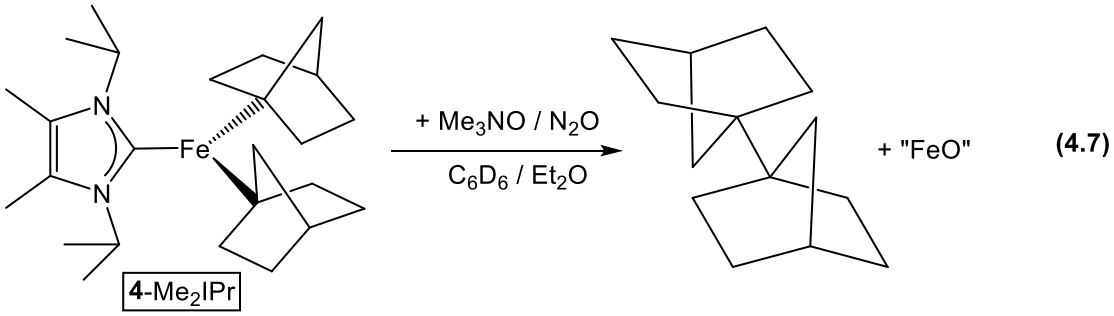

(4.7)

Treatment of either $(PMe_3)_2Fe(1\text{-nor})_2$ (**4**-PMe_3) or $(TMEDA)Fe(1\text{-nor})_2$ (**4**-TMEDA) with $[Cp_2Fe]PF_6$ led to oxidative decomposition to 1,1'-binorbornyl as the major product. Both reactions did not show any evidence, by ^{1}H NMR spectroscopy, for formation of stable Fe(III) species.

4.11 Alkylation and Carbene Transfer Studies of 4-L_n

The lack of stability upon oxidation of complexes **4**-L_n prompted investigation of alternative reactivity, similar to additional studies conducted for the neopentyl variants **1**-L_n. Attempts to alkylate either $(PMe_3)_2Fe(1\text{-nor})_2$ (**4**-PMe_3) or $(Me_2IPr)Fe(1\text{-nor})_2$ (**4**-Me_2IPr) with 1-norLi did not result in new products (Eq 4.8).

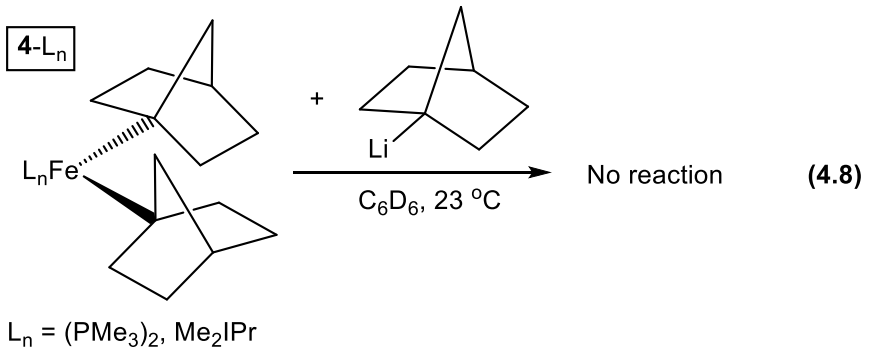

Efforts to affect carbene transfer from phosphine ylides or diazoalkyl substrates to **4**-Me_2IPr are presented in Scheme 4.12. Addition of $Me_3P{=}CH_2$ to a benzene solution of **4**-Me_2IPr led to decomposition products consistent with norbornane. In contrast, treatment of **4**-Me_2IPr with $Ph_3P{=}C(H)Ph$[45] was unproductive, with no degradation observed. Decomposition of **4**-Me_2IPr was noted upon addition of 2-diazo-1-phenylethanone, with no evidence of new Fe-containing products.

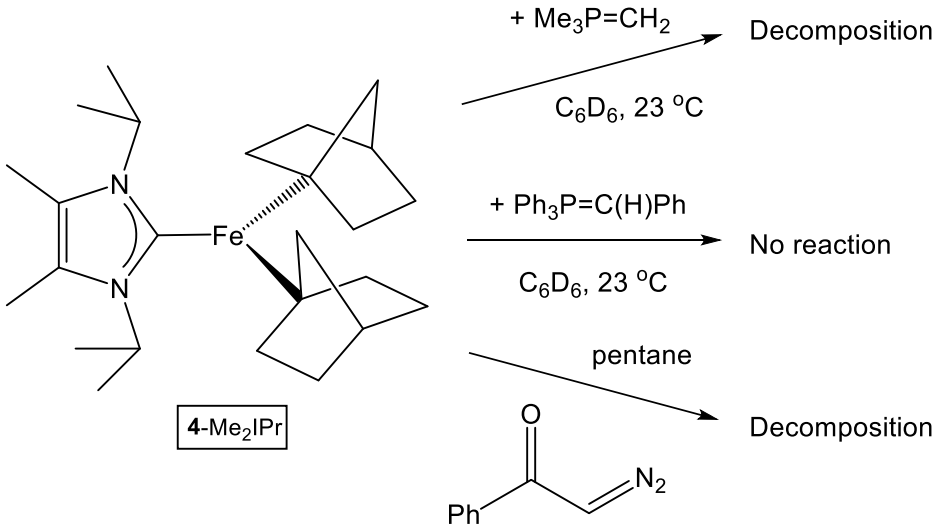

Scheme 4.12. Probes into transferring carbene to **4**-L_n

4.12 Treatment of 4-Me$_2$IPr with 1-Adamantyl Azide and Diphenyldiazomethane

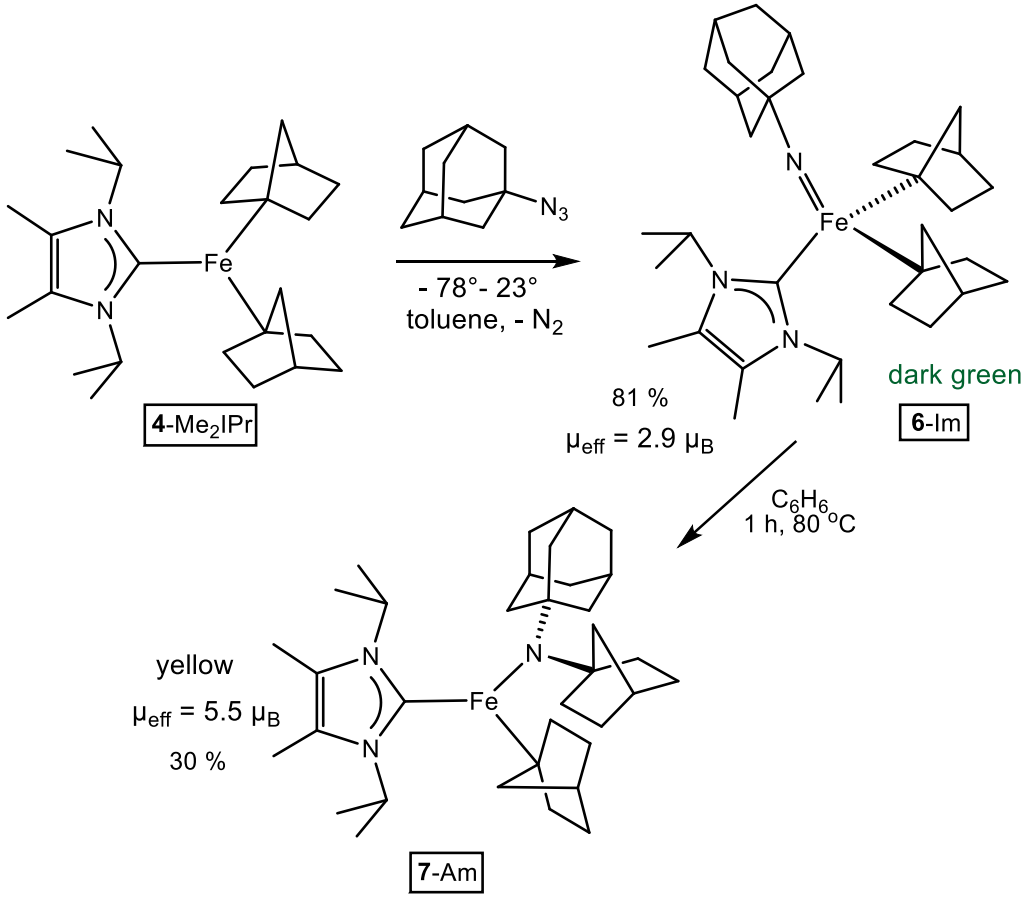

Scheme 4.13. Preparation of the Fe(IV) imide **6**-Im, and subsequent nitrene insertion

Successful oxidation of (Me$_2$IPr)Fe{CH$_2$C(CH$_3$)$_3$}$_2$ (**1**-Me$_2$IPr) with adamantyl azide prompted an identical investigation into the Fe(II) norbornyl complexes. Treatment of **4**-Me$_2$IPr with 1-adamantyl azide formed a dark green solution with effervescence (Scheme 4.13), similar to the physical changes that occurred for the aforementioned oxidation of the neopentyl variant. In contrast, the green color persisted for several days at 23 °C, allowing for workup of the reaction. Dark green

crystals of (Me_2IPr)Fe(=N(1-Ad))(1-nor)$_2$ (**6**-Im) were isolated in 81% yield. Heating a benzene solution of **6**-Im to reflux for 1 h generated a brown solution, and workup afforded (Me_2IPr)Fe{N(1-Ad)(1-nor)}(1-nor) (**7**-Am) as a yellow powder (30% yield).

Evans' method magnetic measurements[17] of the Fe(IV) imide **6**-Im produced a μ_{eff} value of 2.9(3) μ_B, consistent with an intermediate spin S = 1 Fe center. The magnetism of **6**-Im is copacetic with expectations for an Fe(IV) species. The magnetism of the putative variant (Me_2IPr)Fe(=N(1-Ad))($CH_2C(CH_3)_3$}$_2$ (**2**-Im, μ_{eff} = 3.9(2) μ_B) is unusually different, and the absence of any additional Fe-containing species in the ^{1}H NMR spectrum of **2**-Im at -11 ^{o}C only exacerbates the peculiar magnetic moment. Determination of the μ_{eff} of **7**-Am yielded a value of 5.5 μ_B, an expected value for a high spin Fe(II) center with moderate spin-orbit coupling.

IR spectroscopy of **6**-Im revealed a band at 1111 cm^{-1}, a feature not present in the IR spectra of **7**-Am. This vibrational frequency fits within one range recorded by Peters and Que for Fe-imides (1084-1111 cm^{-1}).[38] Unfortunately, no vibrational bands were seen when attempting to acquire a resonance Raman spectrum of **6**-Im to confirm this assignment.

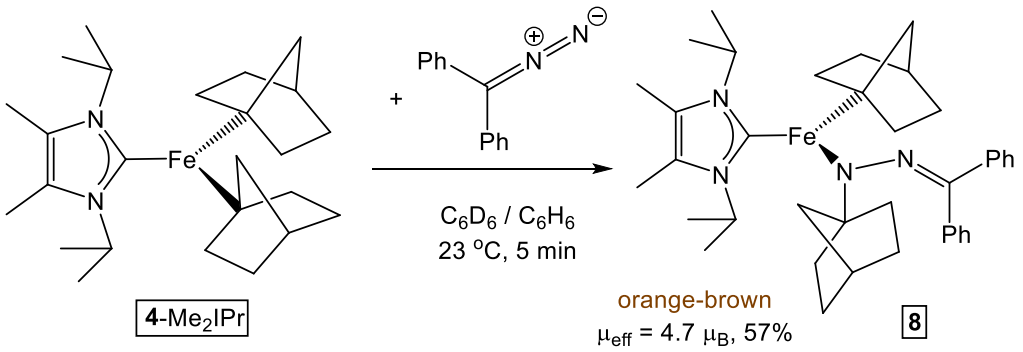

(4.9)

While testing the prospect of carbene transfer from diazoalkyl reagents to complex **4**-Me_2IPr (Scheme 4.12), it was found that addition of diphenyldiazomethane produced an orange-brown solid in 57% yield (Eq 4.9). X-ray structural analysis revealed the solid to be the nitrene insertion product (Me_2IPr)Fe{N(1-nor)(N=CPh_2)}(1-nor) (**8**). ^{1}H NMR spectroscopy of the crude reaction mixture after 5 minutes at 23 ^{o}C revealed quantitative formation of **8**, with no evidence of an Fe(IV) imide intermediate. There is ample precedent for the preparation of stable metal imide complexes via treatment with diphenyldiazomethane,[25-30] yet spectroscopic evidence for this species is absent in preparing complex **8**. Evans' method measurements produced a μ_{eff} of 4.7 μ_B, which is slightly lower than expected for a high spin Fe(II) center.

4.13 X-Ray Crystal Structures of 6-Im and 8

The molecular structure of (Me_2IPr)Fe(=N(1-Ad))(1-nor)$_2$ (**6**-Im) was determined through X-ray crystallography, and a view is presented in Figure 4.5. Fe-C_{alk} distances of 2.005(2) and 2.024(2) Å are shortened relative to (Me_2IPr)Fe(1-nor)$_2$ (**4**-Me_2IPr; d(Fe-C_{alk} = 2.0555(18) Å (ave))), and more closely match the Fe-C_{alkyl} distances for Fe(1-nor)$_4$ (1.993(9) Å (ave)).[8] Shortened Fe-C_{alk} bonds are expected due to the higher oxidation state Fe(IV) center of **6**-Im, and the short Fe-C_{NHC} distance of 2.074(2) Å corroborates this. The d(Fe-N3) length of 1.6723(18) Å is fairly long for three- or four-coordinate Fe(IV) imido complexes (1.612(2) - 1.670(2) Å),[12,33-37] and the Fe-N3-C26 angle of 168.04(15)^o is slightly bent in comparison to near-linear Fe=N-C moieties (176.2(3) - 178.23(18)^o). Core angles of **6**-Im implicate a

moderately distorted tetrahedron, nearly bordering on trigonal monopyramidal. C1-Fe-C12 is the smallest core angle at 96.98(8)°, and the two "basal" angles of C1-Fe-N3 and C1-Fe-C19 have widened to 120.62(8) and 119.23(9)°. The remaining core angles are slightly distorted from values expected for an ideal tetrahedron.

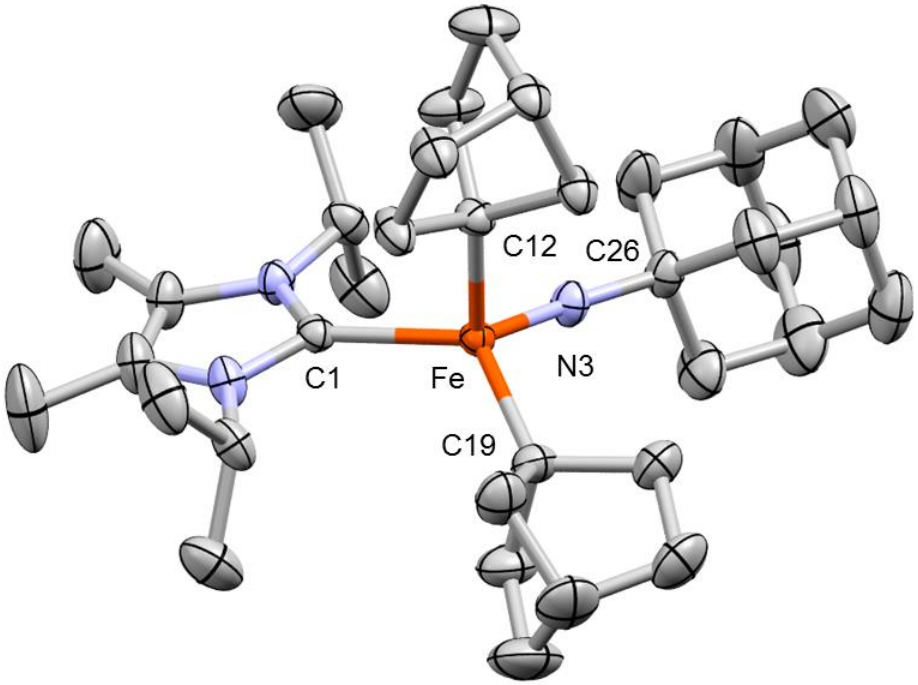

Figure 4.5. Molecular view of (Me_2IPr)Fe(=N(1-Ad))(1-nor)$_2$ (**6**-Im). Selected interatomic distances (Å) and angles (°): Fe-N3, 1.6723(18); Fe-C1, 2.074(2); Fe-C12, 2.005(2); Fe-C19, 2.024(2); N3-C26, 1.437(3); N3-Fe-C1, 120.62(8); N3-Fe-C12, 105.09(9); N3-Fe-C19, 107.90(9); C1-Fe-C12, 96.98(8); C1-Fe-C19, 119.23(9); C12-Fe-C19, 103.77(9); Fe-N3-C26, 168.04(15).

A view of the Fe(II) hydrazide complex (Me_2IPr)Fe{N(1-nor)(N=CPh_2)}(1-nor) (**8**) is shown in Figure 4.6, with metrics provided in the caption. Table 4.2 lists additional crystallographic information for the mixed donor complexes (Me_2IPr)Fe{N(1-Ad)($CH_2C(CH_3)_3$)}($CH_2C(CH_3)_3$) (**3**-Am), **6**-Im and **8**. Complex **8** is

C_s-symmetric, with Fe core angles suggestive of a slightly distorted trigonal planar molecule (113.41(6) - 123.96(6)°). The long Fe-C_{NHC} distance of 2.1450(16) Å is comparable to **3**-Am (2.1409(19) Å) and longer than **6**-Im (2.074(2) Å) due to the lower valent Fe(II) center. The short N4-C26 distance of 1.305(2) Å matches expected values for an imine bond,[39] and the remaining metrics and angles show no significant deviation from expectations.

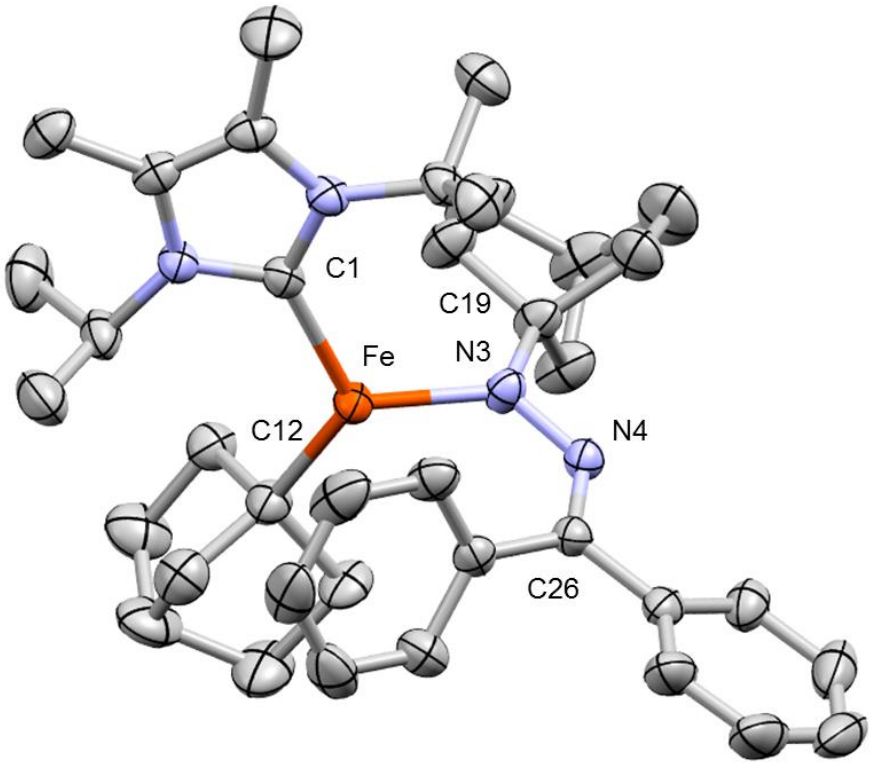

Figure 4.6. Molecular view of (Me_2IPr)Fe{N(1-nor)(N=CPh_2)}(1-nor) (**8**). Selected interatomic distances (Å) and angles (°): Fe-N3, 2.0023(14); Fe-C1, 2.1450(16); Fe-C12, 2.0780(17); N3-N4, 1.3521(18); N3-C19, 1.457(2); N4-C26, 1.305(2); N3-Fe-C1, 117.91(6); N3-Fe-C12, 113.41(6); C1-Fe-C12, 123.96(6); Fe-N3-C19, 119.90(10); Fe-N3-N4, 128.29(10); N4-N3-C19, 109.43(13); N3-N4-C26, 121.57(14).

Table 4.2. Select crystallographic and refinement data for (Me_2IPr)Fe{N{(1-Ad)($CH_2C(CH_3)_3$)}($CH_2C(CH_3)_3$) (**3**-Am), (Me_2IPr)Fe(=N(1-Ad))(1-nor)$_2$ (**6**-Im) and (Me_2IPr)Fe{N(1-nor)(N=CPh_2)}(1-nor) (**8**).

	3-Am	**6**-Im	**8**
formula	$C_{31}H_{57}FeN_3$	$C_{35}H_{57}FeN_3$	$C_{38}H_{52}FeN_4$
formula wt	527.64	575.68	620.68
space group	*P*bca	*P*ca2$_1$	*P*2$_1$/c
Z	8	4	4
a, Å	17.5509(14)	18.6271(8)	10.4328(4)
b, Å	17.9085(18)	9.9600(4)	20.1032(7)
c, Å	20.3687(16)	17.6223(7)	17.3563(6)
α, deg	90	90	90
β, deg	90	90	106.003(2)
γ, deg	90	90	90
V, Å^3	6402.1(10)	3269.4(2)	3499.1(2)
ρ_{calc}, g cm^{-3}	1.095	1.170	1.178
μ, mm^{-1}	0.492	0.488	0.462
temp, K	223(2)	223(2)	223(2)
λ (Å)	0.71073	0.71073	0.71073
R indices	R1 = 0.0457	R1 = 0.0326	R1 = 0.0371
[$I > 2\sigma(I)$][a,b]	wR2 = 0.1214	wR2 = 0.0716	wR2 = 0.0834
R indices[b]	R1 = 0.0750	R1 = 0.0441	R1 = 0.0589
(all data)[a]	wR2 = 0.1372	wR2 = 0.0764	wR2 = 0.0949
GOF[c]	1.068	1.030	1.012

[a]$R_1 = \Sigma F_o| - |F_c||/\Sigma|F_o|$. [b]$wR_2 = [\Sigma w(|F_o| - |F_c|)^2/\Sigma wF_o^2]^{1/2}$. [c]*GOF* (all data) = $[\Sigma w(|F_o| - |F_c|)^2/(n - p)]^{1/2}$, n = number of independent reflections, p = number of parameters.

4.14 Expanded Scope of Nitrene Insertion

To assess the generality of nitrene insertion into Fe-C bonds, Fe(II) alkyl complexes were treated with varying azides, and the results are summarized in Table 4.3. The products were characterized *in situ* via ^{1}H NMR spectroscopy, and their respective magnetic moments were calculated via Evans' method.[17] Curiously, for all reactions monitored *in situ*, no putative Fe(IV) imido intermediates were observed, with the product Fe(II) amide being the only new species recorded, regardless of

reaction time. Entries 1 and 2 indicate that (Me_2IPr)Fe(1-nor)$_2$ (**4**-Me_2IPr) undergoes clean nitrene insertion from both phenyl- and trimethylsilyl azide. The extended reaction time for entry 2 was due to ambiguity of the product identity as the Fe(IV) or Fe(II) species. Trimethysilyl azide readily undergoes insertion upon addition to (Me_2IPr)Fe{$CH_2C(CH_3)_3$}$_2$ (**1**-Me_2IPr) in only 5 h, as entry 3 shows. Fe-C_{aryl} species are also compatible, as entry 4 illustrates that treating (Me_2IPr)Fe$(Mes)_2$[46] with 1-adamatyl azide quantitatively yields the product Fe(II) amide after 19 h. All four Fe(II) amide products have μ_{eff} values that range from 4.5-5.0 μ_B, which are consistent with high spin Fe(II) centers.

Table 4.3. Scope of nitrene insertion into Fe-C bonds

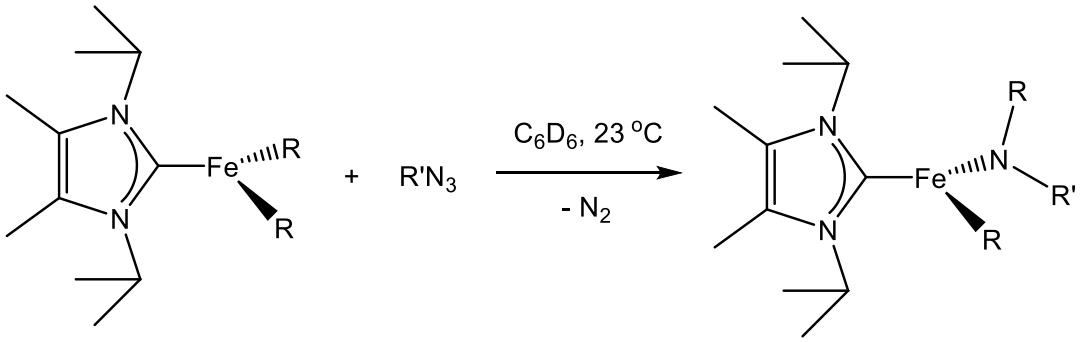

Entry	R	R'	Time (h)	Color	μ_{eff} (μ_B)
1	1-nor	Ph	0.5	yellow-orange	4.7
2	1-nor	Me_3Si	50	orange	5.0
3	$CH_2C(CH_3)_3$	Me_3Si	5	yellow	4.5
4	Mes	1-Ad	19	dark orange	4.9

Intriguingly, addition of tosyl azide to **4**-Me_2IPr led to clean formation of 2,2'-binorbornyl (Eq 4.10). Betley and coworkers reported catalytic C-H bond amination and olefin aziridination processes of organic azides mediated by a Fe(II) alkyl species.[33] Spectroscopic and computational studies implicate suggest an Fe(III) species bearing an imido-based radical. For the present case, if the tosyl imide is capable of reducing the putative Fe(IV)-imide to an Fe(III)-imidyl, then CC ligand coupling may be the likely consequence, given the coupling products observed for one-electron oxidations of **1**-L_n and **4**-L_n species.

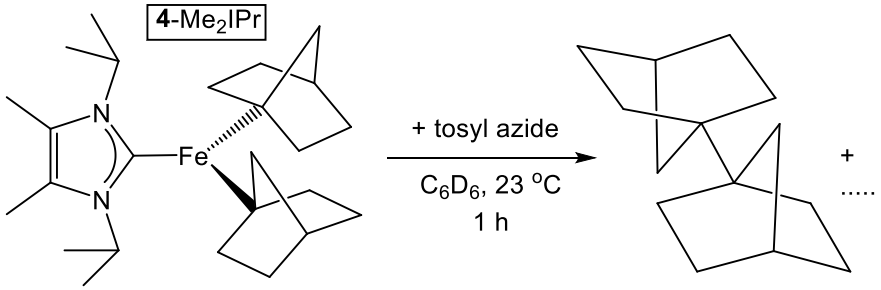

(4.10)

4.15 Kinetics of Nitrene Insertion for 2-Im and 6-Im

Studies into the rate of nitrene insertion into Fe-C bonds were relegated to the Fe(IV) imide complexes (Me_2IPr)Fe(=N(1-Ad))($CH_2C(CH_3)_3)_2$ (**2**-Im) and (Me_2IPr)Fe(=N(1-Ad))(1-nor)$_2$ (**6**-Im) since their transformation into their respective amide products could be monitored by ^{1}H NMR spectroscopy. Rapid nitrene insertion for **2**-Im at 23 °C (Scheme 4.10) prompted monitoring the consumption of **2**-Im by NMR at relatively low temperatures (-10 → 30 °C). A first-order dependence on [**2**-Im] was found, and an Eyring analysis of the first-order rate constants (Figure 4.7) yielded a $\Delta H^{\ddagger}$ of 22.3(8) kcal mol^{-1}, and a $\Delta S^{\ddagger}$ of 6.5(1) cal mol^{-1}. The calculated $\Delta G^{\ddagger}$

at 25 °C is 20.4(8) kcal mol^{-1}. The relatively low entropy value may be a consequence of moving from a 4- to 3-coordinate geometry upon nitrene insertion, which should free up conformational space.

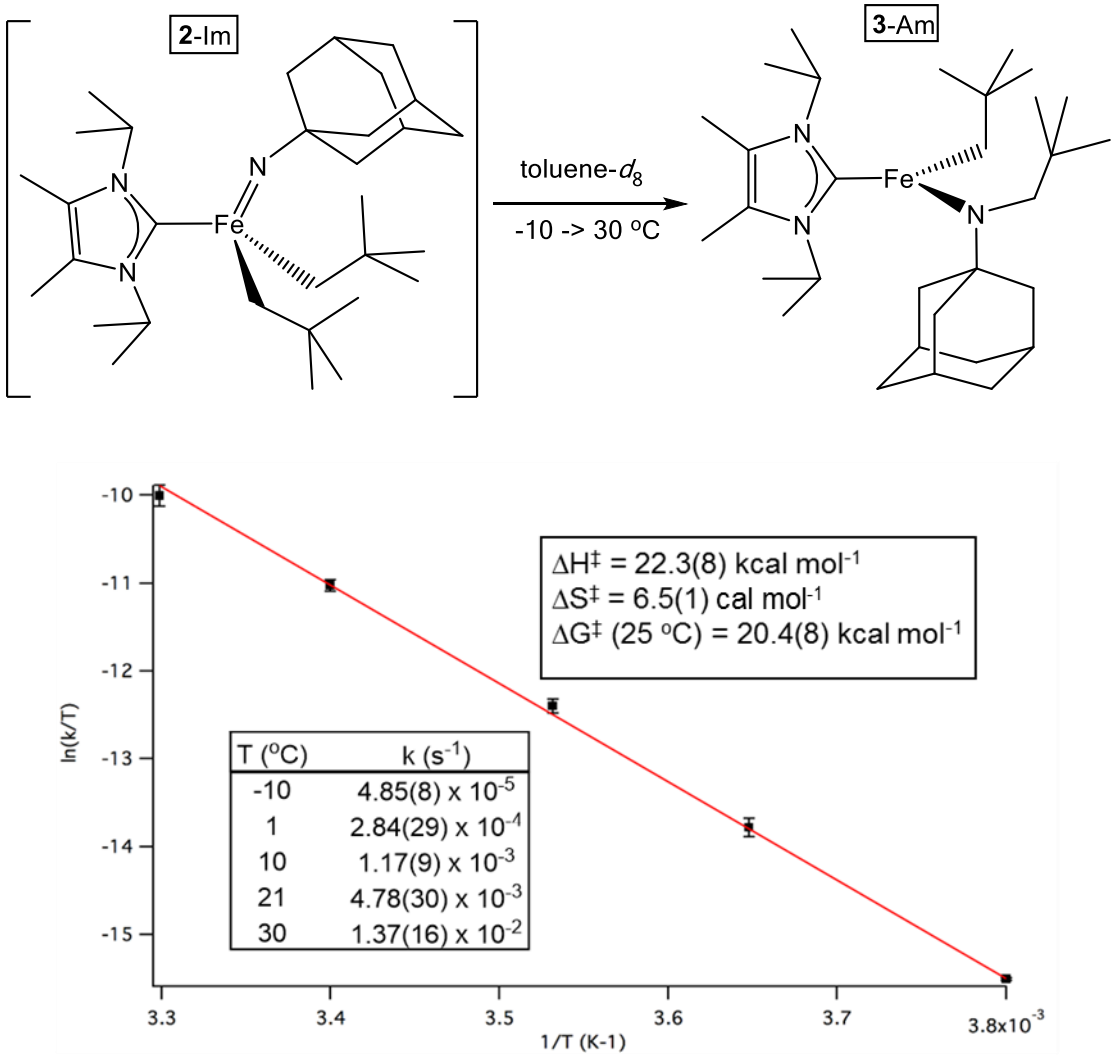

Figure 4.7. Rate constants and Eyring analysis for **2**-Im nitrene insertion

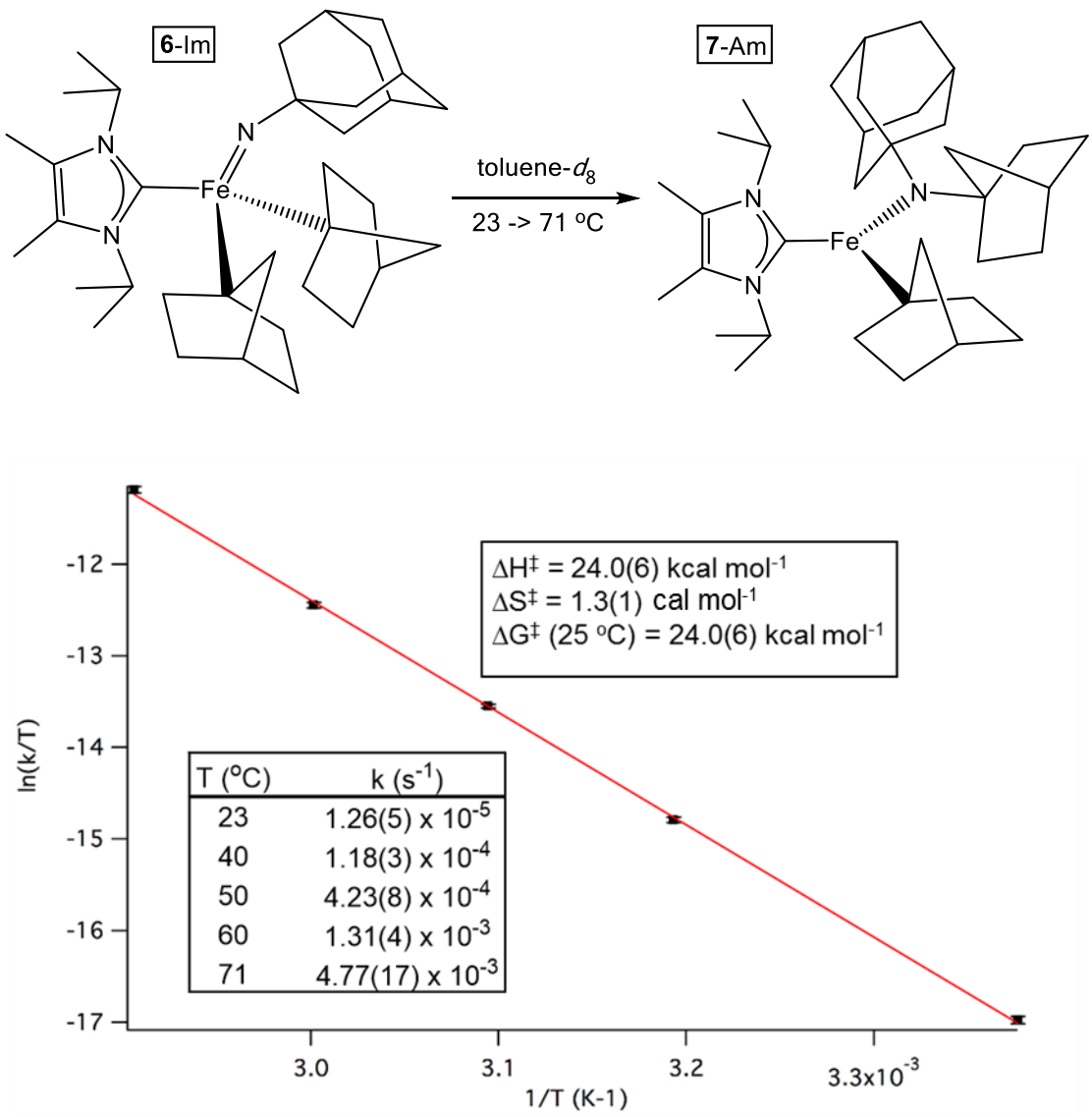

Figure 4.8. Rate constants and Eyring analysis for **6**-Im nitrene insertion

Kinetics studies for nitrene insertion of **6**-Im necessitated monitoring the process at higher temperatures (23 → 71 °C) due to the stability of the Fe(IV) species. Identical to **2**-Im, a first-order dependence on [**6**-Im] was found, and the Eyring analysis is presented in Figure 4.8, with rate constants provided in the inset. The

Eyring analysis provided a $\Delta H^{\ddagger}$ of 24.0(6) kcal mol^{-1}, and a $\Delta S^{\ddagger}$ of 1.3(1) cal mol^{-1}. The calculated $\Delta G^{\ddagger}$ at 25 ^{o}C is 24.0(6) kcal mol^{-1}. The nitrene insertion of **2**-Im to **3**-Am is more favorable than the conversion of **6**-Im to **7**-Am ($\Delta\Delta G^{\ddagger}$ (298 K) = 3.6 kcal mol^{-1}), which is in agreement with the lower rate constants of insertion for **6**-Im (e.g. k(**2**-Im, 21 ^{o}C) = 4.78(30) x 10^{-3} s^{-1}; k(**6**-Im, 23 ^{o}C) = 1.26(5) x 10^{-5} s^{-1})).

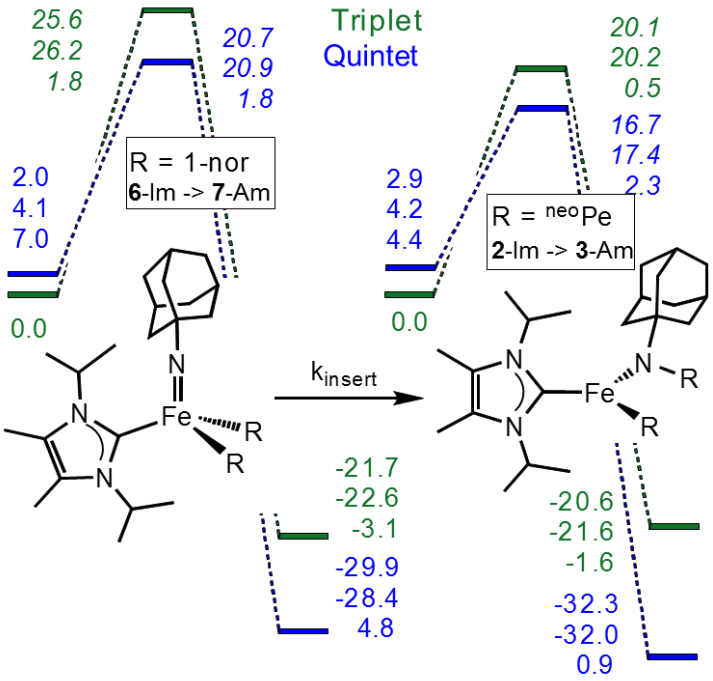

Figure 4.9. Triplet (green) and quintet (blue) surfaces for the **2**-Im → **3**-Am and **6**-Im → **7**-Am migratory insertions; energies are in kcal mol^{-1} for free energy and enthalpy, cal mol^{-1} for entropy, and the transition states are in *italics.* Values are in the order ΔG, ΔH, ΔS.

B3PW91-GD3/G-31+G(d)[9] simulations were applied to the nitrene insertions of **2**-Im and **6**-Im to gain further insight to the reaction coordinate, and the results are shown in Figure 4.9. Both reaction coordinates indicate the spin-flip from triplet imide

to quintet amide occurs prior to the transition state. The calculations reproduced the lower free energy barrier for neopentyl migration over norbornyl ($\Delta\Delta G^{\ddagger}$ (298 K) = 3.6 kcal mol^{-1}; $\Delta\Delta G^{\ddagger}$ (calc) = 4.2 kcal mol^{-1}). In addition, $\Delta\Delta G^{o}$ for **3**-Am formation relative to **7**-Am is 2.4 kcal mol^{-1}, indicating an earlier transition state in the reaction coordinate for **2**-Im. The $\Delta\Delta H^{\ddagger}$ of -3.5 kcal mol^{-1} favoring neopentyl migration is similar to the $\Delta\Delta H^{o}$ of -3.6 kcal mol^{-1}, indicating that the linear free energy relationship is principally enthalpic in origin.

4.16 Crossover Experiments

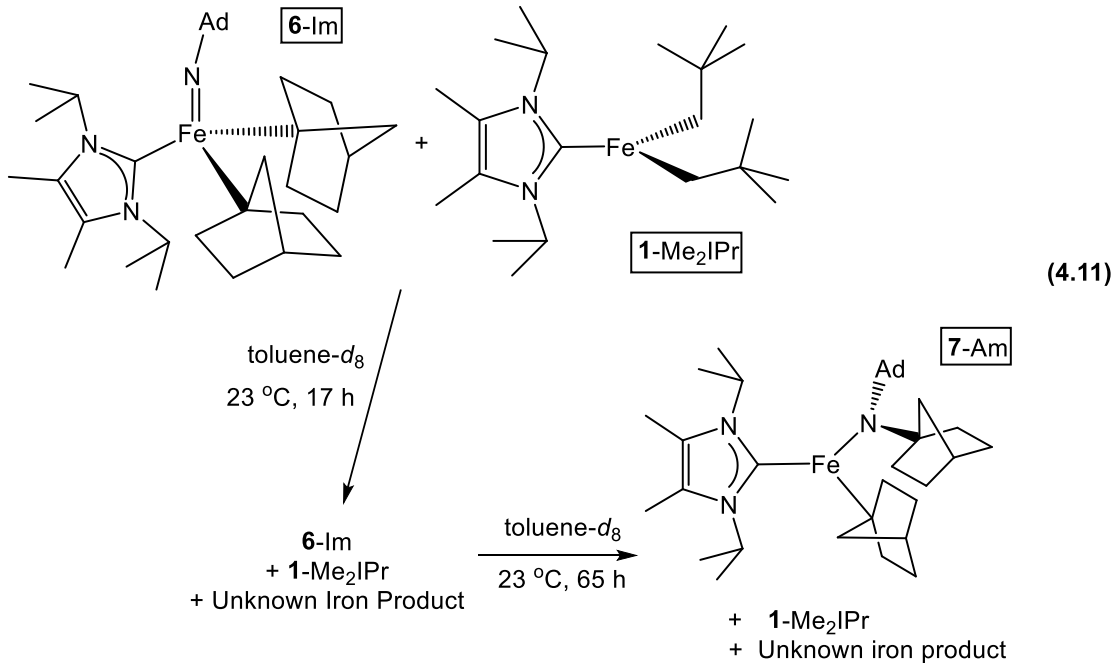

To assess whether nitrene insertion occurred through an intra- or intermolecular pathway, a series of crossover experiments were conducted. An equimolar toluene-d_8 solution of (Me_2IPr)Fe(=N(1-Ad))(1-nor)$_2$ (**6**-Im) and (Me_2IPr)Fe{$CH_2C(CH_3)_3$}$_2$ (**1**-Me_2IPr) was monitored via ^{1}H NMR spectroscopy for

65 h at 23 °C (Eq 4.11). Curiously, after 17 h, (Me_2IPr)Fe{N(1-Ad)(1-nor)}(1-nor) (**7**-Am) was not present in the NMR spectrum, and a new paramagnetic product was formed. Subsequent NMR spectra (up to 65 h) revealed the formation of **7**-Am, the consumption of **6**-Am, and the presence of both **1**-Me_2IPr and the unidentified product. NMR resonances consistent with (Me_2IPr)Fe{N(1-Ad)($CH_2C(CH_3)$)}{$CH_2C(CH_3)_3$) (**3**-Am) were not recorded, suggesting that intramolecular nitrene insertion was operative.

In an experiment identical to Eq 4.11, the rate constant for consumption of **6**-Im was calculated to be 1.09 x 10^{-5} s^{-1} (monitored for the first 17 h at 23 °C). This rate constant is nearly identical to that obtained from the kinetics presented in Figure 4.8 (k = 1.26(5) x 10^{-5} s^{-1} (ave)). Despite the absence of **7**-Am in the first 17 h of the reaction, the consumption of **6**-Im proceeded as expected based on earlier kinetics studies.

A second crossover experiment was conducted to probe if intermolecular nitrene transfer may occur from (Me_2IPr)Fe(=N(1-Ad))($CH_2C(CH_3)_3$)$_2$ (**2**-Im) to (Me_2IPr)Fe(1-nor)$_2$ (**4**-Me_2IPr) (Eq 4.12). Due to the rapid insertion that **2**-Im undergoes, several changes in methodology were implemented: 1) a sub-stoichiometric amount of 1-adamantyl azide was used to mitigate any remaining azide from reacting directly with **4**-Me_2IPr, 2) to ensure full consumption of the azide starting material, the reaction between (Me_2IPr)Fe{$CH_2C(CH_3)_3$}$_2$ (**1**-Me_2IPr) and adamantyl azide was allowed to stand for 2.5 minutes (~1 half-life), 3) after 2.5

minutes, **4**-Me_2IPr was added to the toluene-d_8 solution, and 4) the reaction was monitored after 15 minutes at 23 °C.

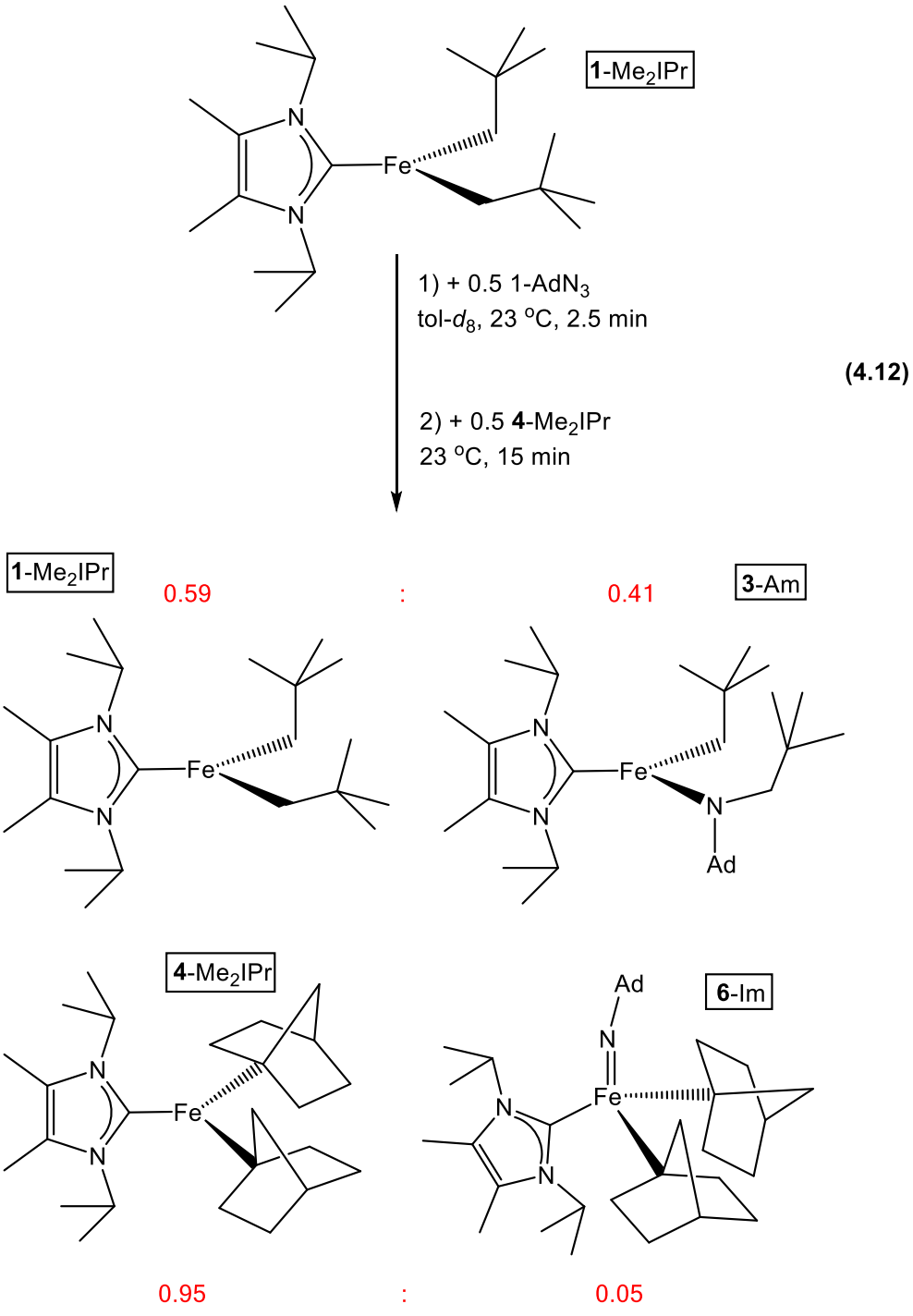

(4.12)

As Eq 4.12 indicates, the resultant mixture revealed the presence of **1**-Me_2IPr, **3**-Am, **4**-Me_2IPr and **6**-Im in the following ratios: 0.59, 0.41, 0.95 and 0.05, respectively. If intermolecular nitrene transfer was operative, the expected ratios should be 0.75, 0.25, 0.50 and 0.50, respectively. This is predicated on the assumption that after 1 half-life, there should be 0.50 eq **1**-Me_2IPr, 0.25 eq **3**-Am and 0.25 eq **2**-Im. Nitrene transfer from 0.25 eq **2**-Im to 0.50 eq **4**-Me_2IPr would generate 0.25 eq **1**-Me_2IPr and 0.25 eq **6**-Im, with 0.25 eq **4**-Me_2IPr remaining. For the actual product distributions shown in Eq 4.12, the near equimolar ratio of **1**-Me_2IPr and **3**-Am argue against the generation of free nitrene, and the trace amount of **6**-Im is likely due to unreacted adamantyl azide.

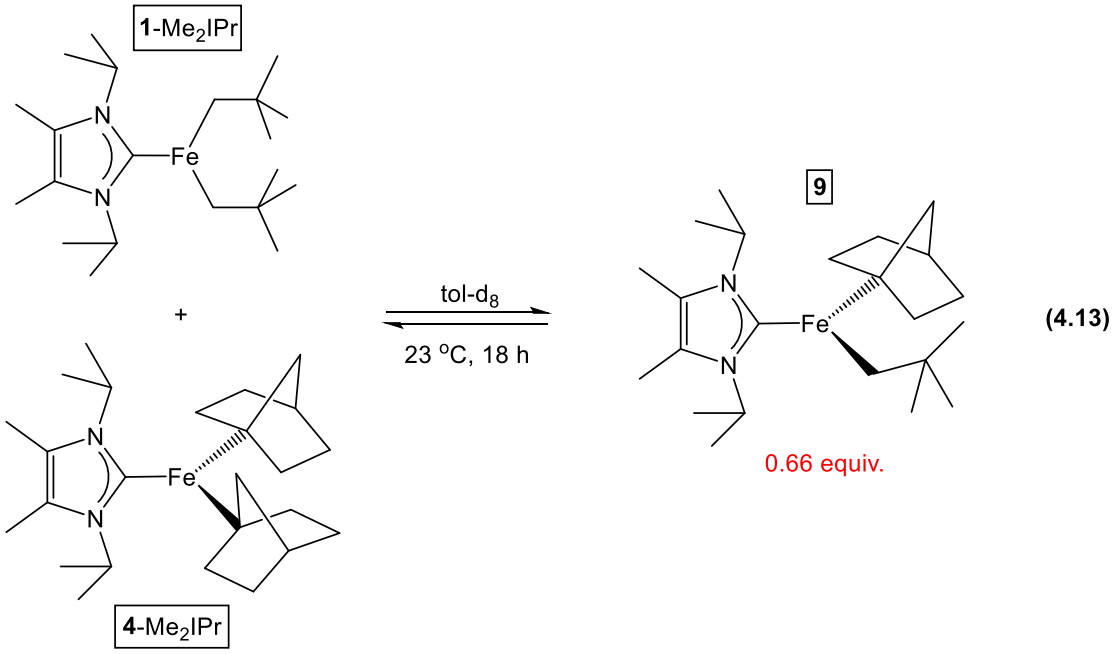

(4.13)

Initial probes into investigating the identity of the unknown product in Eq 4.11 focused on potential alkyl exchange between Fe neopentyl and Fe norbornyl species. Eq 4.13 shows that treatment of **1**-Me_2IPr with **4**-Me_2IPr yields the mixed alkyl

species (Me_2IPr)Fe{$CH_2C(CH_3)_3$}(1-nor) (**9**) in a statistical mixture with both starting materials. Further reaction time did not improve the conversion to product.

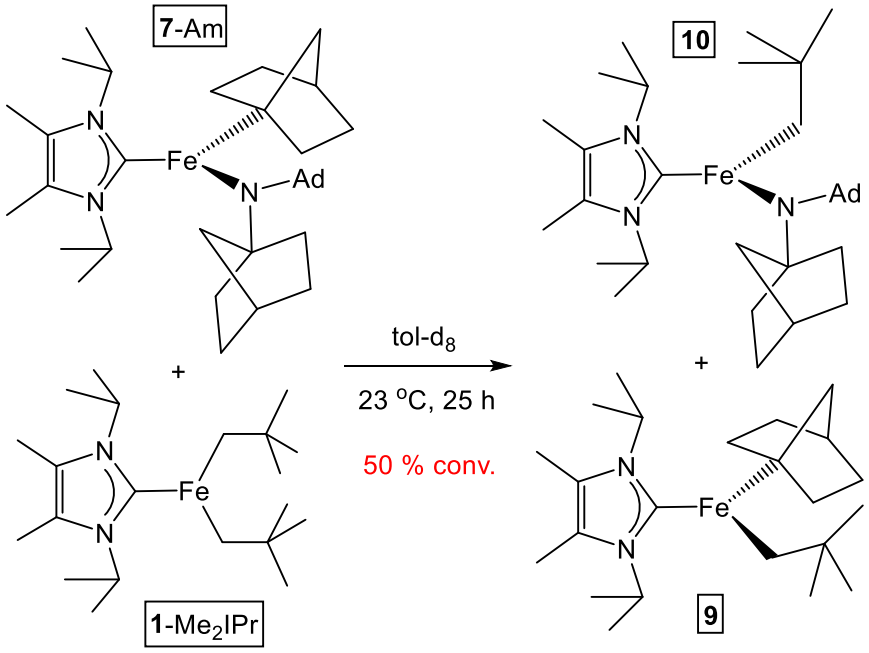

The identity of the new paramagnetic product shown in Eq 4.11 was tentatively assigned as a possible bimetallic species through bridging of the amide group from **7**-Am to **1**-Me_2IPr. To probe this possibility, pure samples of **7**-Am and **1**-Me_2IPr were mixed together, resulting in a yellow solution (Eq 4.14). ^{1}H NMR analysis of the mixture revealed two paramagnetic products, identified as **9** and (Me_2IPr)Fe{N(1-Ad)(1-nor)}($CH_2C(CH_3)_3$) (**10**), both produced in 50% conversion. Curiously, neither product was observed when treating **6**-Im with **1**-Me_2IPr. Due to this negative result, and competing alkyl exchange, characterization of the unidentified product in Eq 4.11 was abandoned.

4.17 Reactivity Studies of 6-Im

Further reactivity studies of (Me_2IPr)Fe(=N(1-Ad))(1-nor)$_2$ (**6**-Im) focused on exposing it to organic substrates capable of trapping free nitrene. Betley and coworkers reported catalytic C-H bond amination and aziridination of olefins from the reaction of organic azides with an Fe(II) dipyrromethene complex,[33] and current reactivity studies for **6**-Im attempted to mimic these chemical transformations.

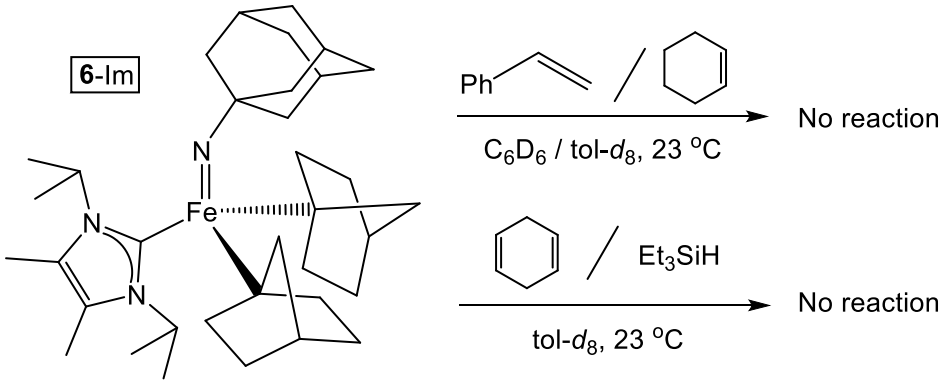

Scheme 4.14. Reactivity probes into olefin aziridination/R-H bond activation for **6**-Im

Scheme 4.14 highlights several approaches towards **6**-Im mediated olefin aziridination, and C-H and Si-H bond activations. Exposure of **6**-Im to an excess of either styrene or cyclohexene resulted in no aziridination products. Similar results were observed upon addition of either 1,4-cylohexadiene or triethylsilane to **6**-Im, with no reaction occurring for either case. For all cases studied, only conversion of **6**-Im to (Me_2IPr)Fe{N(1-Ad)(1-nor)}(1-nor) (**7**-Am) was noted. The lack of reactivity was discouraging towards developing useful organic transformations, but these results do buttress prior arguments on the conversion of **6**-Im to **7**-Am proceeding through an

intramolecular nitrene insertion, rather than an intermolecular pathway, given the lack of free nitrene-like behavior.

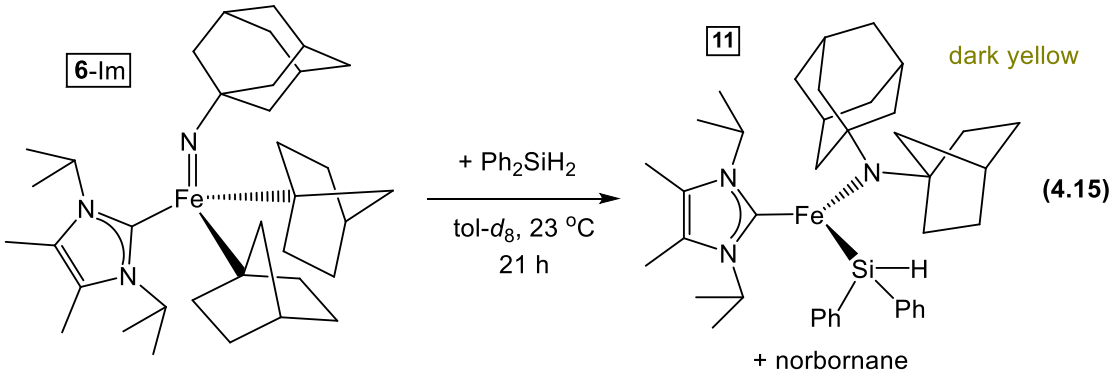

(4.15)

Treating **6**-Im with the less sterically bulky diphenylsilane resulted in formation of a dark yellow solution, as shown in Eq 4.15. ^{1}H NMR spectroscopy revealed the formation of 1.2 eq norbornane and one new paramagnetic species consistent with the formulation (Me_2IPr)Fe{N(1-Ad)(1-nor)}(Si(H)Ph_2) (**11**). DART mass spectrometry of the quenched NMR sample revealed a molecular ion peak of 246.2219 m/z, consistent with the calculated molecular weight for the secondary amine (1-Ad)NH(1-nor). The reaction proceeded to full conversion after only 21 h at 23 °C, significantly faster than the conversion of **6**-Im to **7**-Am. Two conceivable pathways could be operative: 1) protonolysis of an Fe-C bond to generate an Fe(IV) silyl species, that undergoes Fe-C nitrene insertion to generate **11**, or 2) nitrene insertion from **6**-Im to **7**-Am, followed by protonolysis of **7**-Am to yield **11**. Treatment of **7**-Am with diphenylsilane did not result in formation of **11**, disproving the latter reaction sequence. It should be noted that in Eq 4.15 complex **11** was formed in 67% yield after 5 h at 23 °C, implicating exchange of norbornyl for diphenylsilyl on a faster time-scale than nitrene insertion, hence the absence of **7**-Am in the NMR spectrum.

4.18 Efforts to Prepare Secondary Fe(II) Alkyl Species

Preparation of the Fe(II) neopentyl complexes **1**-L_n and norbornyl species **4**-L_n prompted investigations into the synthesis of secondary Fe alkyl complexes. Fürstner *et al*. recently reported the isolation of the secondary Fe alkyl complexes $Fe(cyclohexyl)_4$ and $Fe(2\text{-nor})_4$.[10] Similar salt metathesis strategies were employed towards the preparation of our own Fe(II) alkyl species, with the results shown in Eq 4.16. Treatment of $[(Me_2IPr)FeCl(\mu\text{-}Cl)]_2$ with isopropyl, cyclohexyl or 3-pentyl Grignard reagents generated intractable mixtures, in which paramagnetic species were not observed by ^1H NMR spectroscopy. Degradation of putative Fe(II)-$C(H)R_2$ complexes through β-H elimination appears to be the main decomposition pathway.

$$[(Me_2IPr)FeCl(\mu\text{-}Cl)]_2 \xrightarrow[Et_2O,\ -78 \rightarrow 23\ ^oC]{+\ 2\ ^{i}PrMgCl\ /\ ^{cy}HexMgCl\ /\ 3\text{-}pentylMgBr} \text{Decomposition} \qquad \textbf{(4.16)}$$

In contrast to the aforementioned alkylation attempts, addition of diphenylmethyl lithium[47] to $[(Me_2IPr)FeCl(\mu\text{-}Cl)]_2$ generated paramagnetic red-orange $(Me_2IPr)Fe\{C(H)Ph_2\}_2$ (**12**) quantitatively (Eq 4.17). Allowing the solution to stand at 23 °C for 18 h resulted in decomposition to 1,1,2,2-tetraphenylethane (87% conv.), and yellow crystals grown from a concentrated pentane solution of **12** at -30 °C were consistent with the CC coupled organic degradation product. Since structural characterization of **12** remained elusive due to its instability, the product was characterized via NMR spectroscopy. Although the methine C-H resonance was not present in the ^1H NMR spectrum, the remaining integrations were consistent with the

formulation. Evans' method magnetic measurements[17] of **12** *in situ* provided a μ_{eff} value of 5.3 μ_B, consistent with a high spin Fe(II) center.

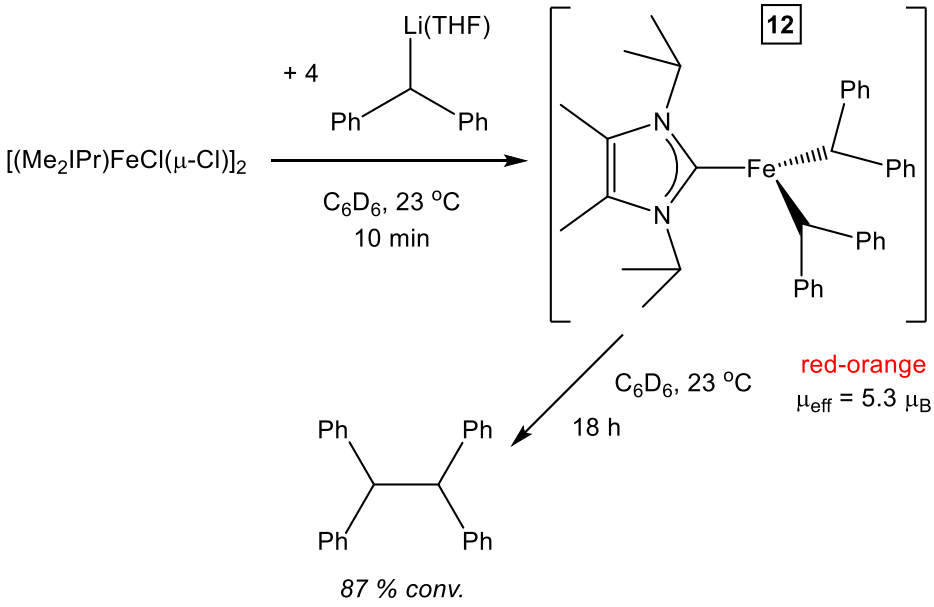

(4.17)

Due to the instability of complex **12**, and the dearth of successful alkylation attempts employing several secondary alkyl Grignards, attempts to prepare stable secondary Fe(II) alkyl species were abandoned.

Conclusion

A series of Fe(II) neopentyl complexes **1**-L_n were synthesized bearing the ancillary ligands TMEDA, PMe_3, 2,2'-bipy or the N-heterocyclic carbene Me_2IPr. Investigations into oxidation of complexes **1**-L_n generated the CC coupled byproduct bineopentyl, and further attempts to generate Fe(IV) alkylidenes through carbene transfer from diazoalkyl and phosphine ylides failed. Azide oxidation of **1**-L_n (L_n = TMEDA, 2,2'-bipy, py_2) generated organic amine/imine products consistent with nitrene insertion into the Fe-neopentyl bond. Treatment of $(Me_2IPr)Fe\{CH_2C(CH_3)_3\}_2$ (**1**-Me_2IPr) with adamantyl azide yielded the secondary Fe(II) amide product $(Me_2IPr)Fe\{N(1\text{-}Ad)(CH_2C(CH_3))\}(CH_2C(CH_3)_3)$ (**3**-Am) via nitrene insertion from the spectroscopically characterized Fe(IV) imide precursor $(Me_2IPr)Fe(=N(1\text{-}Ad))(CH_2C(CH_3)_3)_2$ (**2**-Im). The stability of $Fe(1\text{-}nor)_4$ prompted preparation of the Fe(II) norbornyl complexes **4**-L_n (L_n = TMEDA, PMe_3, Me_2IPr), and subsequent oxidation studies yielded the coupled degradation product 2,2'-binorbornyl exclusively. Azide oxidation of $(Me_2IPr)Fe(1\text{-}nor)_2$ (**4**-Me_2IPr) yielded $(Me_2IPr)Fe(=N(1\text{-}Ad))(1\text{-}nor)_2$ (**6**-Im), which was structurally characterized. The analogous nitrene insertion product $(Me_2IPr)Fe\{N(N=CPh_2)(1\text{-}nor)\}(1\text{-}nor)$ (**8**) was isolated upon addition of diphenyldiazomethane to **4**-Me_2IPr. Kinetics studies for the nitrene insertion process of **2**-Im and **6**-Im revealed a higher free energy of activation for **6**-Im of 24.0(6) kcal mol^{-1}, consistent with the longer reaction time necessary for nitrene insertion into the Fe-norbornyl bond. Crossover experiments indicated no free nitrene was generated, and treatment of **6**-Im with nitrene traps such as olefins or trialkylsilanes led to no organic products, arguing that nitrene insertion from Fe(IV)

imides proceed through an intramolecular pathway. Attempts to isolate secondary Fe(II) alkyl species were largely unsuccessful, with the only spectroscopically characterized product (Me_2IPr)Fe{C(H)Ph_2}$_2$ (**12**) decomposing at low temperatures to organic byproducts.

Experimental

General Considerations. All manipulations were performed using either glovebox or high vacuum line techniques, unless stated otherwise. All glassware was oven dried at 180 ^{o}C. THF and ether were distilled under nitrogen from purple sodium benzophenone ketyl and vacuum transferred from the same prior to use. Hydrocarbon solvents were treated in the same manner with the addition of 1-2 mL/L tetraglyme. Tetramethylethylenediamine (TMEDA) was stirred over sodium/benzophenone, then vacuum transferred to a fresh flask containing charged with sodium and benzophenone. Pyridine (py) was dried over 4 Å molecular sieves, followed by vacuum transfer to a flask containing fresh flame-dried sieves for storage. Benzene-d_6 was dried over sodium, vacuum transferred and stored over sodium. Toluene-d_8 was dried over sodium and stored over 4 Å molecular sieves under N_2 atmosphere. THF-d_8 was dried over sodium, and vacuum transferred from sodium benzophenone ketyl prior to use. Chloroform-d_1 (Cambridge Isotope Laboratories) was used as received. 1,3-diisopropyl-4,5-dimethyl-1H-imidazol-3-ium-2-ide (Me_2IPr),[19] $LiCH_2C(CH_3)_3$,[13] 1-chloronorbornane,[40] 1-norbornyllithium(1-norLi),[41] mesityllithium (MesLi),[48] $Ph_2C(H)Li(THF)_2$,[47] diphenyldiazomethane (Ph_2CN_2),[49] 2-diazo-1-phenylethanone,[31] $Ph_3P{=}C(H)Ph$,[45] $Me_3P{=}CH_2$,[32] $FeCl_2(PMe_3)_2$,[18] $[FeCl(\mu\text{-}Cl)(TMEDA)]_2$,[16] $FeCl_2$(2,2'-bipy),[15] $(py)_2Fe(CH_2C(CH_3)_3)_2$ (**1**-py)[14] and $(Me_2IPr)Fe(Mes)_2$[46] were prepared according to literature procedures. $[(Me_2IPr)FeCl(\mu\text{-}Cl)]_2$ was prepared by stirring $FeCl_2$ with 1 eq. Me_2IPr in THF for 1 h (until solids dissolve completely) at 23 ^{o}C, followed by evaporation of the solvent under vacuum.[20] All other chemicals were commercially available and used as received.

NMR spectra were obtained using Inova 300 MHz and 400 MHz spectrometers. Variable temperature NMR spectra for kinetics were done using an Inova 600 MHz spectrometer. Chemical shifts are reported relative to benzene-d_6 (^{1}H δ 7.16; ^{13}C{^{1}H} δ 128.39), THF-d_8 (^{1}H δ 3.58; ^{13}C{^{1}H} δ 67.57), toluene-d_8 (^{1}H δ 7.09; ^{13}C{^{1}H} δ 137.48), and chloroform-d_1 (^{1}H δ 7.26; ^{13}C{^{1}H} δ 77.16). Electronic structure calculations (B3PW91-GD3/6-31+G(d) simulation) and reaction coordinate calculations (B3PW91-GD3/G-31+G(d)[9] simulations) were performed by Dr. Thomas R. Cundari at the University of North Texas, Department of Chemistry, Center for Advanced Scientific Computing and Modeling (CASCaM). Accurate mass data were acquired on an Exactive Orbitrap mass spectrometer (Thermo Scientific) using a DART (IonSense Inc., Saugus, MA) ion source in positive ion mode using helium for DART ionization, while software affiliated with the spectrometer was used to calculate the molecular weight. Solution magnetic measurements were conducted via Evans' method in C_6D_6, THF-d_8 or tol-d_8.[17] Analytical data were obtained from the CENTC Elemental Analysis Facility at the University of Rochester, funded by NSF CHE-0650456.

Fitting of kinetic data was performed using Igor Pro 6. Heating of NMR tubes was done using a Hewlett-Packard 5890 Series II gas chromatograph oven or in a preheated Inova 600 MHz spectrometer. Cooling of NMR tubes was done using a precooled Inova 600 MHz spectrometer. Infrared spectra were recorded on a 20 Nicolet Avatar 370 DTGX spectrophotometer interfaced to an IBM PC (OMNIC software). UV-vis spectra were recorded on an Agilent Cary 60 UV-Vis spectrophotometer.

Procedures.

1. 3-pentylMgBr(Et_2O)$_4$. To a 50-mL flask charged with Mg turnings (0.322 g, 13.2 mmol) was added via vacuum transfer 25 mL ether at -78 ^oC. The mixture was warmed to 23 ^oC, and was then put under an argon atmosphere. 3-bromopentane (1.000 g, 6.621 mmol) was added via syringe to the mixture, followed by addition of 1,2-dibromoethane (0.1 mL, 1 mmol). The mixture was heated to reflux for 19 h. Filtration of the solution, followed by removal of the volatiles yielded a colorless residue. Washing the solid with pentane (3 x 10 mL) yielded a colorless solid (0.478 g, 15%) that was collected via filtration. The product was used without further purification. ^1H NMR (C_6D_6): δ 1.05 (24H, t, 7 Hz), 1.43 (6H, t, 7 Hz), 2.16 (4H, tt, 14 Hz and 6 Hz), 3.31 (16H, q, 7 Hz).

2. (PMe_3)$_2$Fe{$CH_2C(CH_3)_3$}$_2$ (1-PMe_3). To a 25-mL flask charged with $FeCl_2(PMe_3)_2$ (300 mg, 1.08 mmol) and $LiCH_2C(CH_3)_3$ (168 mg, 2.15 mmol) was added via vacuum transfer 10 mL hexanes at -78 ^oC. The solution was warmed to 23 ^oC and stirred for 17 h. The dark yellow-orange solution was filtered, concentrated and cooled to -78 ^oC, resulting in dark yellow crystals (58 mg, 15%) that were isolated by filtration. ^1H NMR (C_6D_6): δ 28.58 (18H), 75.24 (18H). μ_{eff} (Evans) = 5.5 μ_B. Anal. for $C_{16}H_{40}FeP_2$ (calc.) C 54.86, H 11.51; (found) C 54.732, H 11.340.

3. (2,2'-bipy)Fe{$CH_2C(CH_3)_3$}$_2$ (1-bipy). To a 25-mL flask charged with $FeCl_2$(2,2'-bipy) (301 mg, 1.06 mmol) and $LiCH_2C(CH_3)_3$ (166 mg, 2.13 mmol) was added via vacuum transfer 10 mL Et_2O at -78 ^oC. The solution was warmed to 23 ^oC, resulting in a dark blue solution, which was stirred for 20 h. Filtration of the solution followed by

concentrating the solution and cooling it to -78 ^{o}C yielded dark blue crystals (208 mg, 55%), which was isolated by filtration. ^{1}H NMR (C_6D_6): δ -74.35 (2H), 23.96 (18H), 27.62 (4H), 55.01 (2H), 83.44 (2H). μ_{eff} (Evans) = 5.1 μ_B. Anal. for $C_{20}H_{30}FeN_2$ (calc.) C 67.80, H 8.53, N 7.91; (found) C 65.364, H 8.076, N 7.944.

4. (TMEDA)Fe{$CH_2C(CH_3)_3$}$_2$ (1-TMEDA). To a 50-mL flask charged with [FeCl(μ-Cl)(TMEDA)]$_2$ (1.000 g, 2.058 mmol) and $LiCH_2C(CH_3)_3$ (0.643 g, 8.23 mmol) was added via vacuum transfer 25 mL Et_2O at -78 ^{o}C. The colorless suspension was allowed to warm slowly with stirring for 42 h, resulting in a light tan solution. Filtration of the solution followed by concentrating and cooling it to -78 ^{o}C yielded colorless crystals (1.065 g, 82%), which was isolated by filtration. Crystals suitable for X-ray diffraction were obtained via slow evaporation of a concentrated ether solution at -30 ^{o}C. ^{1}H NMR (C_6D_6): δ 24.57 (18H), 72.76 (12H). μ_{eff} (Evans) = 4.8 μ_B.

5. (Me_2IPr)Fe{$CH_2C(CH_3)_3$}$_2$ (1-Me_2IPr). To a 25-mL flask charged with $FeCl_2$ (140 mg, 1.10 mmol) and Me_2IPr (200 mg, 1.10 mmol) was added via vacuum transfer 10 mL THF at -78 ^{o}C. The solution was warmed to 23 ^{o}C and was stirred for 1 h. The volatiles were evaporated, and the faint tan residue washed with hexanes (3 x 10 mL). $LiCH_2C(CH_3)_3$ (173 mg, 2.20 mmol) was added to the flask, and 10 mL Et_2O was added via vacuum transfer at -78 ^{o}C. The solution was allowed to warm slowly for 20 h, resulting in a brownish-yellow solution. Filtration of the solution, followed by evaporating the volatiles resulted in a brown-yellow residue. The residue was taken up in pentane, cooled to -78 ^{o}C and filtered to yield light tan microcrystals (263 mg, 63%). Crystals suitable for X-ray diffraction were obtained via slow evaporation of a

concentrated pentane solution at -30 °C. ^{1}H NMR (THF-d_8): δ -25.43 (12H), 30.56 (6H), 41.20 (18H). μ_{eff} (Evans) = 5.0(3) μ_B. Anal. for $C_{21}H_{42}FeN_2$ (calc.) C 66.65, H 11.19, N 7.40; (found) C 67.229, H 10.903, N 9.516.

6. (Me$_2$IPr)Fe{N(1-Ad)(CH$_2$C(CH$_3$))}(CH$_2$C(CH$_3$)$_3$) (3-Am). To a 25-mL flask charged with **1**-Me$_2$IPr (200 mg, 0.529 mmol) and 1-adamantylazide (94 mg, 0.529 mmol) was added 7 mL toluene at -78 °C, resulting in a dark green solution with considerable effervescence. The solution was stirred for 0.5 h at -78 °C, with no observable color change. Warming the solution to 23 °C and stirring for 0.5 h results in a yellow solution. The volatiles were evaporated, and the yellow residue taken up in hexanes. Cooling the solution to -78 °C for 15 min, followed by filtration yields a yellow solid (180 mg, 65%). Crystals suitable for X-ray diffraction were obtained via slow evaporation of a concentrated ether solution at -30 °C. ^{1}H NMR (C_6D_6): δ -36.14 (9H), -3.31 (12H), 7.55 (2H), 9.00 (6H), 11.48 (3H), 12.58 (6H), 31.67 (3H). μ_{eff} (Evans) = 5.1 μ_B. IR (Nujol, cm^{-1}): 1632 (m), 1369 (s), 1305 (m), 1276 (w), 1265 (w), 1223 (s), 1205 (s), 1182 (w), 1167 (w), 1121 (s), 1097 (s), 1066 (s), 1019 (m), 985 (m) 975 (m), 948 (m), 927 (m), 906 (w), 896 (w), 885 (m), 814 (m), 778 (w), 749 (m), 713 (w), 634 (s), 587 (s).

7. (Me$_2$IPr)Fe(=N(1-Ad))(CH$_2$C(CH$_3$)$_3$)$_2$ (2-Im). To a vial charged with **1**-Me$_2$IPr (13 mg, 0.034 mmol) was added 555 mg tol-d_8. The yellow solution was filtered into a J Young NMR tube, and a separate glass capillary containing tol-d_8 was inserted into the NMR tube. 1-adamantylazide (9 mg, 0.051 mmol) was added to the headspace of the NMR tube and sealed, followed by laying it on its side upright to keep the azide

separate from the solution. The tube was cooled to -10 °C in a separate dry ice/acetone bath while keeping the azide and solution separate. After cooling the solution for 20 min, the solution was shaken throughout the tube to fully react with the azide, resulting in a dark green solution. The NMR tube was inserted into an Inova 600 MHz spectrometer, precooled to -11 °C. After letting the solution temperature equilibrate for 5 min, ^{1}H NMR spectra were recorded, showing the formation of the pure Fe imide. Allowing the solution to warm for 15 min results in a dark yellow solution, consistent with formation of **3**-Am. This method was repeated a second time to obtain two magnetic moments for the Fe imide intermediate. ^{1}H NMR (tol-d_8, -11 °C): δ -10.07 (18H), 7.20 (3H), 8.87 (3H), 11.73 (12H), 12.35 (6H), 15.24 (3H), 29.67 (6H). μ_{eff} = 3.9(2) μ_B. UV-vis (Et_2O, 0 °C), λ_{max} (nm, ε, M^{-1} cm^{-1}) 362 (2559), 454 (604), 555 (277), 647 (238). IR (Nujol, cm^{-1}): 1635 (m), 1414 (w), 1319 (w), 1296 (s), 1283 (s), 1230 (s), 1213 (s), 1183 (s), 1166 (w), 1148 (w), 1131 (s), 1106 (m), 1097 (m), 1064 (w), 1051 (s), 1019 (w), 990 (m), 962 (w), 926 (m), 902 (m), 811 (m), 801 (m), 749 (m), 722 (m).

8. $(PMe_3)_2Fe(1\text{-nor})_2$ $(4\text{-}PMe_3)$. To a 25-mL flask charged with $FeCl_2(PMe_3)_2$ (273 mg, 0.979 mmol) and 1-norLi (200 mg, 1.959 mmol) was added via vacuum transfer 15 mL pentane at -78 °C. The solution was allowed to warm slowly with stirring for 20 h, resulting in a orange-yellow solution at 23 °C. Filtration of the solution, followed by concentration and cooling it to -78 °C yielded orange-yellow microcrystals (239 mg, 61%), which were collected by filtration. Crystals suitable for X-ray diffraction were obtained via slow evaporation of a concentrated pentane solution at -30 °C. ^{1}H

NMR (C_6D_6): δ -22.72 (4H), 10.44 (4H), 27.11 (4H), 50.70 (2H), 92.47 (18H). μ_{eff} (Evans) = 5.2 μ_B.

9. (TMEDA)Fe(1-nor)$_2$ (4-TMEDA). To a 25-mL flask charged with [FeCl(μ-Cl)(TMEDA)]$_2$ (119 mg, 0.245 mmol) and 1-norLi (100 mg, 0.979 mmol) was added via vacuum transfer 10 mL pentane at -78 ^{o}C. The colorless solution was allowed to warm slowly with stirring for 19 h, resulting in a translucent pink solution with colorless precipitate. The solution was filtered and concentrated, resulting in colorless crystals. Cooling the solution to -78 ^{o}C and filtering isolated **4**-TMEDA (93 mg, 53%). ^{1}H NMR (C_6D_6): δ -6.14 (4H), 12.13 (5H), 21.47 (5H), 31.41 (4H), 37.38 (3H), 86.52 (4H), 112.81 (12H), 138.76 (2H). μ_{eff} (Evans) = 5.3 μ_B. Anal. for $C_{20}H_{38}FeN_2$ (calc.) C 66.29, H 10.57, N 7.73; (found) C 66.873, H 10.635, N 7.607.

10. (Me$_2$IPr)Fe(1-nor)$_2$ (4-Me$_2$IPr). To a 25-mL flask charged with [(Me$_2$IPr)FeCl(μ-Cl)]$_2$ (300 mg, 0.489 mmol) and 1-norLi (200 mg, 1.96 mmol) was added via vacuum transfer 15 mL Et_2O at -78 ^{o}C. The colorless suspension was allowed to warm slowly with stirring for 20 h, resulting in a dark orange-brown solution at 23 ^{o}C. The solution was filtered, and the volatiles evaporated. The residue was taken up in pentane, and the solution cooled to -78 ^{o}C. Filtration of the solution yielded light yellow microcrystals (226 mg, 54%). Crystals suitable for X-ray diffraction were obtained via slow evaporation of a concentrated ether solution at -30 ^{o}C. ^{1}H NMR (C_6D_6): δ -37.80 (12H), 30.93 (6H), 40.53 (4H), 56.06 (4H), 57.29 (2H), 73.42 (2H). μ_{eff} (Evans) = 5.6 μ_B.

11. (Me_2IPr)Fe(=N(1-Ad))(1-nor)$_2$ (6-Im). To a 25-mL flask charged with **4**-Me_2IPr (200 mg, 0.469 mmol) and 10 mL C_6H_6 was added 1-adamantylazide (83 mg, 0.468 mmol), resulting in an immediate color change to dark green with considerable effervescence. The solution was stirred at 23 ^oC for 0.5 h. The volatiles were evaporated, and the dark residue taken up in pentane. The solution was cooled to -78 ^oC. Dark green microcrystals (220 mg, 81%) were collected via filtration. Crystals suitable for X-ray diffraction were obtained via cooling a concentrated ether/pentane solution (4:1 v/v) to -30 ^oC. ^1H NMR (C_6D_6): δ -22.34-21.67 (10H), -20.43 (4H), -12.74 (2H), -7.83 (4H), -5.25 (4H), 3.77 (6H), 5.27 (6H), 9.16 (4H), 14.39 (4H), 15.81 (12H), 17.19 (6H), 17.57 (4H). μ_{eff} (Evans) = 2.9(3) μ_B. UV-vis (Et_2O), λ_{max} (nm, ε, M^{-1} cm^{-1}) 362 (4639), 452 (1515), 581 (966), 656 (804). IR (Nujol,cm^{-1}): 1643 (m), 1422 (w), 1367 (s), 1351 (s), 1319 (w), 1297 (s), 1284 (s), 1237 (m), 1210 (w), 1197 (m), 1178 (s), 1136 (w), 1135 (w), 1125 (w), 1111 (w), 1096 (m), 1083 (w), 1064 (w), 1019 (w), 979 (w), 962 (m), 932 (m), 905 (w), 895 (w), 884 (m), 882 (m), 829 (m), 809 (m), 798 (m), 743 (s), 679 (w).

12. (Me_2IPr)Fe{N(1-Ad)(1-nor)}(1-nor) (7-Am). To a 25-mL flask charged with **4**-Me_2IPr (100 mg, 0.234 mmol) and 10 mL C_6H_6 was added 1-adamantylazide (42 mg, 0.24 mmol). The flask was fit with a reflux condenser, and the mixture was heated to reflux for 1 h. The dark green solution gradually changed to a brown color. The volatiles were evaporated and the residue washed with pentane (3 x 10 mL), yielding a yellow powder. Cooling the pentane solution of the residue to -78 ^oC, followed by filtering the mixture isolated the yellow powder (40 mg, 30%). ^1H NMR (C_6D_6): δ

-9.54 (12H), 2.52 (3H), 3.08 (6H), 5.06 (3H), 7.43 (4H), 27.44 (4H), 32.25 (2H), 53.46 (2H), 72.07 (2H), 88.59 (1H). μ_{eff} (Evans) = 5.3 μ_B. Anal. for $C_{35}H_{57}FeN_2$ (calc.) C 73.02, H 9.98, N 7.30; (found) C 73.348, H 10.130, N 7.229. IR (Nujol, cm^{-1}): 1631 (w), 1369 (s), 1299 (m), 1259 (m), 1221 (s), 1166 (m), 1147 (w), 1134 (w), 1117 (m), 1096 (m), 1074 (m), 1023 (w), 978 (w), 948 (w), 929 (m), 905 (w), 886 (w), 835 (w), 812 (w), 781 (w), 743 (w), 725 (w), 624 (w).

13. (Me_2IPr)Fe{N(N=CPh_2)(1-nor)}(1-nor) (8). To a 25-mL flask charged with **4**-Me_2IPr (61 mg, 0.14 mmol) and Ph_2CN_2 (28 mg, 0.14 mmol) was added via vacuum transfer 10 mL C_6H_6 at -78 °C. Warming the solution to 23 °C resulted in an immediate color change to brown-orange, with no observed effervescence. After stirring the solution for 1 h, the volatiles were evaporated, and the brown residue washed with hexanes (3 x 10 mL), and the brown-orange solid was collected (51 mg, 57%). Crystals suitable for X-ray diffraction were obtained via cooling a concentrated ether solution to -30 °C. ^{1}H NMR (C_6D_6): δ -35.81 (2H), -34.26 (2H), -25.86 (4H), -9.79 (12H), -6.68 (4H), 10.26 (5H), 27.77 (4H), 32.42 (6H), 40.71 (2H), 42.58 (1H), 49.00 (2H), 58.24 (1H), 74.49 (2H). μ_{eff} (Evans) = 4.7 μ_B.

14. (Me_2IPr)Fe{C(H)Ph_2}$_2$ (12). To a vial charged with [(Me_2IPr)FeCl(μ-Cl)]$_2$ (7 mg, 0.01 mmol) and Ph_2C(H)Li(THF)$_2$ (15 mg, 0.05 mmol) was added 0.6 mL C_6D_6, resulting in an immediate color change to red-orange. The solution was filtered and added to a J Young tube. A C_6D_6 capillary was added to the tube and sealed. The product was characterized through ^{1}H NMR spectroscopy. After 18 h at 23 °C, the

product decomposed to 1,1,2,2-tetraphenylethane (87% conv.). ^{1}H NMR (C_6D_6): δ -76.89 (4H), -38.57 (6H), -16.10 (12H), 26.28 (8H), 33.28 (8H). μ_{eff} (Evans) = 5.3 μ_B.

15. (Me_2IPr)Fe{N(1-Ad)(Mes)}(Mes). To a vial charged with (Me_2IPr)Fe(Mes)$_2$ (10 mg, 0.021 mmol) and 1-adamantylazide (4 mg, 0.02 mmol) was added 0.6 mL C_6D_6. Letting the reaction sit for 19 h at 23 °C resulted in a dark orange solution. The solution was filtered and added to a J Young NMR tube along with a C_6D_6 capillary. The product was characterized by ^{1}H NMR spectroscopy. ^{1}H NMR (C_6D_6): δ -2.70 (6H), -1.18 (6H), 4.96 (6H), 15.63 (3H), 16.38 (2H), 16.59 (6H), 18.76 (12H), 109.13 (6H). μ_{eff} (Evans) = 4.9 μ_B.

16. (Me_2IPr)Fe{N(Ph)(1-nor)}(1-nor). To a vial charged with **4**-Me_2IPr (11 mg, 0.026 mmol) and phenylazide (4 mg, 0.03 mmol) was added 0.6 mL C_6D_6. Letting the reaction sit for 30 min at 23 °C resulted in a dark yellow-orange solution. The solution was filtered and added to a J Young NMR tube along with a C_6D_6 capillary. The product was characterized by ^{1}H NMR spectroscopy, and the titled product was shown to be 71% pure. ^{1}H NMR (C_6D_6): δ -74.06 (1H), -50.42 (2H), -10.67 (12H), -5.05 (4H), 7.56 (2H), 11.26 (2H), 12.01 (6H), 20.65 (4H), 30.18 (2H), 32.96 (2H), 47.40 (4H), 60.31 (2H), 77.59 (2H). μ_{eff} (Evans) = 4.7 μ_B.

17. (Me_2IPr)Fe{N($SiMe_3$)(1-nor)}(1-nor). To a vial charged with **4**-Me_2IPr (12 mg, 0.028 mmol) and trimethylsilylazide (4 mg, 0.03 mmol) was added 0.6 mL C_6D_6. Letting the reaction sit for 19 h at 23 °C resulted in an orange solution. The solution was filtered and added to a J Young NMR tube along with a C_6D_6 capillary. The product was characterized by ^{1}H NMR spectroscopy. ^{1}H NMR (C_6D_6): δ -15.61 (8H),

-4.07 (12H), 11.01 (6H), 14.76 (2H), 26.54 (2H), 43.51 (1H), 49.94 (2H), 68.09 (2H), 85.06 (1H). μ_{eff} (Evans) = 5.0 μ_B.

18. (Me_2IPr)Fe{N($SiMe_3$)($CH_2C(CH_3)_3$)}($CH_2C(CH_3)_3$). To a vial charged with **1**-Me_2IPr (11 mg, 0.033 mmol) and trimethylsilylazide (4 mg, 0.03 mmol) was added 0.6 mL C_6D_6. After 5 h at 23 ºC, a yellow solution formed. The solution was filtered and added to a J Young NMR tube along with a C_6D_6 capillary. The product was characterized by ^{1}H NMR spectroscopy. ^{1}H NMR (C_6D_6): δ -17.94 (9H), -6.81 (12H), 9.29 (3H), 11.46 (2H), 15.66 (6H), 29.40 (9H). μ_{eff} (Evans) = 4.5 μ_B.

19. (Me_2IPr)Fe{$CH_2C(CH_3)_3$}(1-nor) (9). To a vial charged with **1**-Me_2IPr (10 mg, 0.026 mmol) and **4**-Me_2IPr (11 mg, 0.026 mmol) was added 0.6 mL tol-d_8, resulting in a yellow solution. Monitoring the ^{1}H NMR spectra of the mixture over 18 h showed both starting materials along with a new product in a 1:1:2 ratio, respectively. The product was not isolated, only characterized in situ. ^{1}H NMR (tol-d_8): δ -33.03 (12H), 10.66 (1H), 12.47 (1H), 28.71 (6H), 37.36 (9H), 44.45 (2H), 60.74 (2H), 81.64 (1H).

20. (Me_2IPr)Fe{N(1-Ad)(1-nor)}($CH_2C(CH_3)_3$) (10). To a vial charged with **7**-Am (9 mg, 0.02 mmol) and **1**-Me_2IPr (6 mg, 0.02 mmol) was added 0.6 mL tol-d_8. The yellow solution was monitored via ^{1}H NMR spectroscopy over 25 h at 23 ºC. Both starting materials were observed, along with **9** and a new paramagnetic product **10**, which was identified as the title compound. The starting material/product ratios were as follows: **7**-Am, 0.8; **1**-Me_2IPr, 1.3; **9**, 1; **10**, 1.2. ^{1}H NMR (tol-d_8): δ -8.52 (16H), 4.75 (3H), 5.16 (9H), 14.00 (12H), 27.31 (3H), 30.05 (6H), 30.67 (2H), 34.07 (3H), 55.93 (1H).

21. (Me_2IPr)Fe{N(1-Ad)($CH_2C(CH_3)_3$)}(1-nor). To a vial charged with **3**-Am (10 mg, 0.019 mmol) and **4**-Me_2IPr (8 mg, 0.02 mmol) was added 0.6 mL tol-d_8. The yellow solution was monitored via ^{1}H NMR spectroscopy over 18 h at 23 ^{o}C. Both starting materials were observed, along with **9** and a new paramagnetic product **A**, which was identified as the title compound. The starting material/product ratios were as follows: **3**-Am, 1.3; **4**-Me_2IPr, 1.4; **9**, 1.1; **A** 1. ^{1}H NMR (tol-d_8): δ -43.07 (6H), -25.64 (2H), -3.87 (14H), 4.30 (9H), 4.52 (4H), 9.29 (4H), 28.18 (3H), 29.36 (6H), 41.57 (3H), 45.67 (2H), 62.90 (3H), 76.49 (1H).

22. Oxidation of 1-py with AdN_3. To a 25-mL flask charged with **1**-py (139 mg, 0.390 mmol) and 5 mL toluene was added 1-adamantylazide, resulting in a color change from dark violet to brown, with effervescence observed. The solution was stirred for 43 h at 23 ^{o}C. The volatiles were removed, and the residue washed with hexanes (3 x 10 mL). Analysis of the residue by ^{1}H NMR showed no paramagnetic species. One series of broad, diamagnetically shifted resonances were observed. DART analysis of the crude residue showed molecular ion peaks consistent with the formation of (1-Ad)NH{$CH_2C(CH_3)_3$} and (1-Ad)N=C(H)C(CH_3)$_3$. HRMS (DART-MS) m/z: $[M + H]^+$ Calcd for 220.2021, 222.2177; Found 220.2057, 222.2212.

23. Oxidation of 1-bipy with AdN_3. To a vial charged with **1**-bipy (10 mg, 0.028 mmol) and 0.6 mL C_6D_6 was added 1-adamantylazide (5 mg, 0.03 mmol), resulting in a dark brown solution. The mixture was allowed to stand for 3 h at 23 ^{o}C, after which it was monitored by ^{1}H NMR. No paramagnetic species were observed, with the major products being (1-Ad)NH{$CH_2C(CH_3)_3$} and (1-Ad)N=C(H)C(CH_3)$_3$.

24. Oxidation of 1-TMEDA with AdN_3. To a 25-mL flask charged with **1**-TMEDA (200 mg, 0.636 mmol) and 10 mL C_6H_6 was added 1-adamantylazide (113 mg, 0.638 mmol), resulting in a brown solution with minimal effervescence. The solution was stirred for 19 h at 23 °C. The volatiles were removed, and the brown residue washed with hexanes (3 x 10 mL). Analysis of the brown residue by ^{1}H NMR showed (1-Ad)N=C(H)C$(CH_3)_3$ and (TMEDA)Fe$\{CH_2C(CH_3)_3\}_2$ (**1**-TMEDA) in a 1:1 ratio (imine resonances were severely broadened, appearing as singlets). No new paramagnetic products were observed. ^{1}H NMR (imine, C_6D_6): δ 1.11 (9H), 1.57 (3H), 1.61 (6H), 1.74 (6H), 2.02 (3H), 7.46 (1H).

25. Oxidation of 1-TMEDA with azobenzene. To a vial charged with **1**-TMEDA (12 mg, 0.038 mmol) and azobenzene (7 mg, 0.04 mmol) was added 0.6 mL C_6D_6, resulting in an orange solution. Monitoring the reaction over 21 h at 23 °C via ^{1}H NMR showed the formation of bineopentyl (60% conv.) and liberated TMEDA in a 1:1 ratio. No new paramagnetic species were observed. ^{1}H NMR (bineopentyl, C_6D_6): δ 0.90 (18H, s), 1.18 (4H, s).

26. Oxidation of 1-TMEDA with $FcPF_6$. To a vial charged with **1**-TMEDA (10 mg, 0.032 mmol) and $FcPF_6$ (11 mg, 0.033 mmol) was added 0.6 mL C_6D_6 and one drop of THF. The dark yellow solution was allowed to stand at 23 °C for 17 h, resulting in a dark orange solution. Analysis of the sample by ^{1}H NMR showed the formation of bineopentyl (85% conv.), the Fe starting material and ferrocene. Three new paramagnetically shifted resonances were also observed in a 5:5:9 integration ratio.

Given that there was no observed free TMEDA and that bineopentyl forms readily, the new Fe-containing product was not pursued.

27. Oxidation of 1-TMEDA with Me_3NO. To a vial charged with **1**-TMEDA (16 mg, 0.051 mmol) and Me_3NO (4 mg, 0.05 mmol) was added 0.6 mL THF-d_8. The solution immediately changed from faint yellow to an orange-brown solution, with light orange precipitate. After letting the mixture stand at 23 °C for 45 min, the solution was filtered. ^{1}H NMR analysis of the solution showed clean formation of bineopentyl (50% conv.) and Me_3N, with no paramagnetic products observed.

28. Oxidation of 1-TMEDA with Ph_3CCl. To a vial charged with **1**-TMEDA (8 mg, 0.03 mmol) and Ph_3CCl (7 mg, 0.03 mmol) was added 0.6 mL C_6D_6, producing a yellow solution. Monitoring the solution via ^{1}H NMR after 20 min at 23 °C showed the formation of bineopentyl and Gomberg's dimer ($Ph_2C{=}C(CH{=}CH)_2C(H)\text{-}CPh_3$),[51] along with very little consumption of Ph_3CCl. Free TMEDA was not observed. The Fe starting material was fully consumed, with the formation of a new paramagnetic product that was not isolated nor characterized, since oxidative coupling of the neopentyl ligands was determined to be the main decomposition pathway.

29. Oxidation of 1-Me_2IPr with Me_3NO. To a vial charged with **1**-Me_2IPr (15 mg, 0.040 mmol) and Me_3NO (3 mg, 0.04 mmol) was added 0.6 mL C_6D_6 at 23 °C. The solution immediately turned dark orange in color, with light orange precipitate formation observed. Analysis of the solution by ^{1}H NMR showed the clean formation of bineopentyl and Me_3N, with no paramagnetic species observed.

30. Oxidation of 4-PMe_3 with $FcPF_6$. To a 25-mL flask charged with **4**-PMe_3 (100 mg, 0.251 mmol) and $FcPF_6$ (83 mg, 0.25 mmol) was added via vacuum transfer 10 mL THF at -78 ^oC, resulting in a dark red solution. The solution was allowed to warm slowly with stirring for 20 h, resulting in a brown solution. The volatiles were removed, and the residue washed with pentane (3 x 10 mL), yielding a brown-yellow powder. Analysis of the powder by ^1H NMR in THF-d_8 showed one broad resonance for a new paramagnetic species, and several broad resonances corresponding to ferrocene and an unidentified organic byproduct. Further elaboration of the new materials was not pursued.

31. Oxidation of 4-TMEDA with $FcPF_6$. To a 25-mL flask charged with **4**-TMEDA (100 mg, 0.276 mmol) and $FcPF_6$ (91 mg, 0.28 mmol) was added via vacuum transfer 10 mL THF at -78 ^oC, resulting in a dark red-orange solution. The solution was allowed to warm slowly with stirring for 20 h, resulting in a dark yellow solution. The volatiles were removed, and the residue washed with pentane (3 x 10 mL), yielding a grey-yellow powder. Analysis of the powder by ^1H NMR in THF-d_8 showed no paramagnetic species were present, with the only observable broad resonances corresponding to ferrocene and 1,1'-binorbornyl.

32. Oxidation of 4-TMEDA with AdN_3. To a vial charged with **4**-TMEDA (12 mg, 0.033 mmol) and 0.6 mL C_6D_6 was added 1-adamantylazide (6 mg, 0.03 mmol). No effervescence was observed, and the solution gradually turned brown-orange in color over the course of 30 min at 23 ^oC. Analysis of the solution by ^1H NMR showed the presence of the starting Fe complex, free TMEDA and series of broad, diamagnetic

resonances, with the approximate ratios of 1:1:1, respectively (50% conv.). DART-MS analysis of the quenched NMR sample showed the presence of (1-Ad)NH(1-nor). The imine (1-Ad)N=C(H)C(CH_3)$_3$ was not observed by DART-MS ^{1}H NMR (C_6D_6): δ 1.18 (3H), 1.30 (3H), 1.49 (6H), 1.59 (2H), 1.78 (1H), 1.87 (5H), 1.97 (2H), 2.05 (4H). HRMS (DART-MS) m/z: $[M + H]^+$ Calcd for 246.2177; Found 246.2215.

33. Oxidation of 4-Me_2IPr with Ph_3CCl. To a vial charged with **4**-Me_2IPr (12 mg, 0.028 mmol) and Ph_3CCl (8 mg, 0.03 mmol) was added 0.6 mL C_6D_6, resulting in a color change from light yellow to brown-yellow. Analysis of the solution by ^{1}H NMR after 30 min at 23 ^{o}C showed one major paramagnetic product, one trace paramagnetic product, and 1,1'-binorbornyl (quant.). The Fe-containing product was not isolated, and the ^{1}H NMR spectrum only indicated the presence of ligated Me_2IPr. A possible formulation could be $[(Me_2IPr)FeCl_x]_x$, yet the NMR features are not consistent with $[(Me_2IPr)FeCl(\mu\text{-}Cl)]_2$. ^{1}H NMR ($[(Me_2IPr)FeCl_x]_x$, C_6D_6): δ -16.19 (12H), 12.65 (6H), 17.02 (2H); (1,1'-binorbornyl, C_6D_6): δ 1.25 (8H, m), 1.36 (4H, t, 9 Hz), 1.61 (4H, m), 2.23 (2H, s).

34. Oxidation of 4-Me_2IPr with Me_3NO. To a vial charged with **4**-Me_2IPr (11 mg, 0.026 mmol) and Me_3NO (2 mg, 0.03 mmol) was added 0.6 mL C_6D_6, resulting in an immediate color change to brown. Analysis of the solution by ^{1}H NMR after 30 min at 23 ^{o}C showed 1,1'-binorbornyl formation with trace amounts of paramagnetic products.

35. Oxidation of 4-Me_2IPr with TosN_3. To a vial charged with **4**-Me_2IPr (11 mg, 0.026 mmol) and 0.6 mL C_6D_6 was added TosN_3 (5 mg, 0.03 mmol), resulting in a

brown-yellow solution. Analysis of the solution by ^{1}H NMR after 1 h at 23 ^{o}C showed 1,1'-binorbornyl formation (quant) and $TosN_3$ starting material, with no observable paramagnetic products.

36. Oxidation of 4-Me_2IPr with N_2O. To a 25-mL flask charged with **4**-Me_2IPr (100 mg, 0.234 mmol) was added via vacuum transfer 10 mL ether at -78 ^{o}C. The solution was frozen using a liquid nitrogen bath (77 K). A separate 23.3-mL gas bulb was charged with N_2O (22.4 cm Hg, 0.28 mmol). The N_2O was transferred and frozen in the 25-mL flask, the flask was warmed to -78 ^{o}C using a dry ice-acetone bath, and the reaction glassware was degassed. The solution was allowed to warm slowly with stirring 2 d, resulting in a brown-orange solution with a tan suspension. Deflection of a pressure gauge confirmed the production of gas. The volatiles were removed, and the residue washed with pentane (3 x 10 mL), resulting in a tan solid with a brown film. Analysis of the tan solid by ^{1}H NMR showed the formation of 1,1'-binorbornyl and free Me_2IPr, with no observable paramagnetic products.

37. Oxidation of 4-Me_2IPr with CH_2I_2. To a vial charged with **4**-Me_2IPr (11 mg, 0.026 mmol) and 0.6 mL C_6D_6 was added CH_2I_2 (7 mg, 0.03 mmol). The yellow solution immediately changed to a violet color. Allowing the solution stand for 17 h at 23 ^{o}C resulted in a yellow solution with dark precipitate. ^{1}H NMR spectra acquired after 30 min at 23 ^{o}C revealed a new paramagnetic product produced consistent with the formulation of "(Me_2IPr)Fe(I)(1-nor)$_2$" (**5**), along with formation of 1,1'-binorbornyl (1:1 ratio). Analysis of the solution after 17 h by ^{1}H NMR showed the formation of binorbornyl and a new paramagnetic product consistent with the

formulation "(Me_2IPr)FeI_2", the products in a 1:0.5 ratio. The prior paramagnetic species responsible for the violet color was not observed after 17 h. ^{1}H NMR (30 min, C_6D_6): δ -15.31 (4H), -12.10 (4H), 9.70 (6H), 11.07 (12H), 16.10 (4H), 20.29 (2H), 22.85 (4H), 25.69 (4H), 31.72 (2H), 38.93 (4H). ^{1}H NMR (17 h, C_6D_6): δ 10.11 (12H), 20.36 (2H), 40.07 (6H).

38. Oxidation of 4-Me_2IPr with I_2. To a vial charged with **4**-Me_2IPr (13 mg, 0.030 mmol) and I_2 (4 mg, 0.015 mmol) was added 0.6 mL C_6D_6. The initial yellow solution gradually turned a dark orange color with dark, magnetic precipitate. The mixture was allowed to stand at 23 °C for 21 h, and was then filtered through Celite. ^{1}H NMR analysis of the solution showed the formation of 1,1'-binorbornyl and a new paramagnetic product. The paramagnetic product NMR resonances were not consistent with those observed for the product obtained from CH_2I_2. Formation of magnetic Fe^0 and no observable free Me_2IPr may suggest the formulation of the paramagnetic product as "(Me_2IPr)$_2$$FeI_2$", presumably formed through disproportionation of "(Me_2IPr)FeI". ^{1}H NMR (C_6D_6): δ 6.37 (12H), 17.87 (2H), 31.84 (6H).

39. Treatment of 1-PMe_3 with PMe_3. To a vial charged with **1**-PMe_3 (15 mg, 0.043 mmol) was added 0.6 mL C_6D_6. The solution was added to a J Young tube, and the solution frozen with liquid nitrogen. A separate 109-mL gas bulb was charged with PMe_3 (2.2 cm Hg, 0.13 mmol). The PMe_3 was transferred under vacuum to the NMR tube, which was then sealed and warmed to 23 °C. Analysis of the yellow solution by ^{1}H NMR at 23 °C over 2 d showed no reaction. Warming the solution to 90 °C for 20 h

resulted in the formation of a dark yellow solution with dark precipitate. Only free PMe_3 was observed by ^1H NMR.

40. Treatment of 1-bipy with 2,2'-bipy. To a 25-mL flask charged with **1**-bipy (100 mg, 0.282 mmol) and 2,2'-bipy (44 mg, 0.28 mmol) was added 10 mL C_6H_6, resulting in a dark blue solution. The mixture was allowed to stir at 23 ^oC for 21 h, resulting in a dark violet solution. The volatiles were removed, and the dark residue washed with hexanes (3 x 10 mL), resulting in a dark grey solid. ^1H NMR analysis of the solid showed no paramagnetic species were present, only several aromatic resonances and several unidentified diamagnetic resonances. Quenching the NMR sample and analyzing it by NMR showed no difference in the aromatic resonances. The NMR was correlated to a pure sample of 2,2'-bipy.

41. Treatment of 1-Me_2IPr with tricyclohexylphosphine ($^cHex_3P$). To a vial charged with **1**-Me_2IPr (12 mg, 0.032 mmol) and $^cHex_3P$ (9 mg, 0.03 mmol) was added 0.6 mL C_6D_6. The yellow solution was monitored by ^1H NMR at 23 ^oC for 2 h, which showed no observed reaction between the starting materials. Warming the solution to 55 ^oC for 4 h resulted in no reaction, and further warming to 85 ^oC for 2 h caused no change. Exposing the solution to UV light for 2 h also yielded no reaction.

42. Treatment of 1-py with $LiCH_2C(CH_3)_3$. To a 25-mL flask charged with **1**-py (70 mg, 0.20 mmol) and $LiCH_2C(CH_3)_3$ (31 mg, 0.39 mmol) was added via vacuum transfer 10 mL THF at -78 ^oC. The solution was allowed to warm slowly with stirring for 20 h, resulting in a dark brown-violet solution. The volatiles were evaporated, and the residue washed with hexanes (3 x 10 mL), resulting in a dark powder. ^1H NMR

analysis of the powder showed one new paramagnetic species, along with diamagnetic byproducts. Quenching the NMR sample showed clean formation of 2,2'-bipy, with no free pyridine. The new paramagnetic species resonances were not consistent with **1**-bipy. The new product in question was not pursued.

43. Treatment of 1-bipy with $LiCH_2C(CH_3)_3$. To a 25-mL flask charged with **1**-bipy (100 mg, 0.282 mmol) and $LiCH_2C(CH_3)_3$ (44 mg, 0.56 mmol) was added via vacuum transfer 10 mL TMEDA at -78 ^oC. The solution was warmed to 23 ^oC, and allowed to stir for 69 h. The volatiles were removed, and the residue washed with hexanes (3 x 10 mL), resulting in a dark red-brown solid. ^1H NMR of the solid in C_6D_6 showed no new paramagnetic species, and the quench of the sample showed no evidence of free TMEDA. Due to low solubility of the product in C_6H_6 and THF, the product was not pursued any further.

44. Treatment of 1-Me_2IPr with $LiCH_2C(CH_3)_3$. To a 25-mL flask charged with **1**-Me_2IPr (100 mg, 0.264 mmol) and $LiCH_2C(CH_3)_3$ (21 mg, 0.26 mmol) was added via vacuum transfer 10 mL ether at -78 ^oC. The light tan suspension was allowed to warm slowly with stirring for 20 h, resulting in a brown solution. The volatiles were removed, and the residue was washed with pentane (3 x 10 mL), resulting in brown and colorless solid. Analysis of the solids by ^1H NMR showed only starting materials.

45. Treatment of 1-TMEDA with trans-R,R-1,2-diaminocyclohexane. To a vial charged with **1**-TMEDA (14 mg, 0.045 mmol) and trans-R,R-1,2-diaminocyclohexane (5 mg, 0.04 mmol) was added 0.6 mL C_6D_6. The faint tan solution was allowed to stand at 23 ^oC, resulting in a dark orange solution with brown precipitate. Analysis of

the mixture by ^{1}H NMR showed no paramagnetic species, only TMEDA and neopentane (0.91 ppm in C_6D_6).

46. Treatment of 4-PMe$_3$ with 1-norLi. To a vial charged with **4**-PMe$_3$ (12 mg, 0.030 mmol) and 1-norLi (3 mg, 0.03 mmol) was added 0.6 mL C_6D_6. The yellow solution was allowed to stand at 23 ^{o}C for 30 min. ^{1}H NMR analysis showed no reaction of the starting materials, so the solution was warmed to 55 ^{o}C for 45 h. ^{1}H NMR spectra of the brown solution showed no reaction of the Fe starting material, while the 1-norLi decomposed at that temperature.

47. Treatment of [(Me$_2$IPr)FeCl(μ-Cl)]$_2$ with ^{c}HexMgCl. To a 25-mL flask charged with [(Me$_2$IPr)FeCl(μ-Cl)]$_2$ (200 mg, 0.651 mmol) was added via vacuum transfer 10 mL ether at -78 ^{o}C. After the suspension was put under an argon atmosphere, an ether solution (5 mL) of ^{c}HexMgCl (0.65 mL, 1.3 mmol) was added dropwise, resulting in no observable color change. The solution was warmed slowly to 23 ^{o}C with stirring for 19 h, resulting in a dark brown solution with colorless solid. The volatiles were removed, and the residue washed with pentane (3 x 10 mL), resulting in a light brown solid. ^{1}H NMR analysis of the crude solid showed no paramagnetic species.

48. Treatment of [(Me$_2$IPr)FeCl(μ-Cl)]$_2$ with 3-pentylMgBr(Et$_2$O)$_4$. To a 25-mL flask charged with [(Me$_2$IPr)FeCl(μ-Cl)]$_2$ (65 mg, 0.21 mmol) and 3-pentylMgBr(Et$_2$O)$_4$ (200 mg, 0.424 mmol) was added via vacuum transfer 10 mL ether at -78 ^{o}C, resulting in a light yellow suspension. The solution was warmed slowly to 23 ^{o}C with stirring for 15 h, resulting in a colorless solution with gray solid. The volatiles were removed, and the residue washed with pentane (3 x 10 mL),

resulting in a faintly colored solid. ^{1}H NMR analysis of the crude solid showed free Me_2IPr and three paramagnetically shifted resonances that have integrations inconsistent with Me_2IPr or a 3-pentyl ligand.

49. Treatment of 1-Me_2IPr with $Me_3P=CH_2$. To a vial charged with **1**-Me_2IPr (16 mg, 0.042 mmol) and 0.6 mL C_6D_6 was added a 0.4 M THF solution of $Me_3P=CH_2$ (0.11 mL, 0.042 mmol). The yellow solution was allowed to stand at 23 ^{o}C for 4 h, resulting in a dark yellow solution. The volatiles were evaporated, and the dark residue was dissolved in 0.6 mL C_6D_6. ^{1}H NMR analysis of the solution showed no paramagnetic species were present. Only free Me_2IPr, $Me_3P=CH_2$ and neopentane were observed.

50. Treatment of 4-Me_2IPr with $Me_3P=CH_2$. To a vial charged with **4**-Me_2IPr (18 mg, 0.042 mmol) and 0.6 mL C_6D_6 was added a 0.4 M THF solution of $Me_3P=CH_2$ (0.11 mL, 0.042 mmol). The orange-yellow solution was allowed to stand at 23 ^{o}C for 4 h, after which the volatiles were evaporated. The residue was taken up in 0.6 mL C_6D_6. ^{1}H NMR analysis of the solution showed one new paramagnetic species and norbornane in a 1:1 ratio. Attempts at scaling the reaction (239 mg (Me_2IPr)Fe(1-nor)$_2$) yielded a colorless solid that possessd several of the paramagnetic resonances observed in the small scale reaction, but several peaks were missing. Attempts to grow crystals of the solid failed, and was not pursued any further due to observed production of norbornane as an undesirable byproduct.

51. Treatment of 4-Me_2IPr with $Ph_3P=C(H)Ph$. To a vial charged with **4**-Me_2IPr (11 mg, 0.026 mmol) and $Ph_3P=C(H)Ph$ (9 mg, 0.03 mmol) was added 0.6 mL C_6D_6,

resulting in an orange solution. ^{1}H NMR analysis of the reaction after 15 min at 23 ^{o}C showed no reaction between the starting materials. Heating the reaction to 55 ^{o}C for 2 h and to 90 ^{o}C for 17 h gave the same result. Heating the reaction to 125 ^{o}C for 4 h resulted in an orange solution with a dark precipitate. ^{1}H NMR analysis confirmed the presence of both starting materials, but also showed norbornane as well, confirming slow decomposition of the Fe starting material.

52. Treatment of 4-Me$_2$IPr with Me$_3$SiC(H)=N$_2$. To a vial charged with **4**-Me$_2$IPr (12 mg, 0.028 mmol) and 0.6 mL C_6D_6 was added a 2.0 M ether solution of Me$_3$SiC(H)=N$_2$ (14 μL, 0.028 mmol), resulting in an immediate color change to a dark brown solution. The solution was allowed to stand at 23 ^{o}C for 45 min. ^{1}H NMR analysis of the solution showed no observable paramagnetic species or free Me$_2$IPr. The only species observed was ether, trace amounts of norbornane and various silicon-containing species.

53. Treatment of 1-Me$_2$IPr with 2-diazo-1-phenylethanone. To a 25-mL flask charged with **1**-Me$_2$IPr (26 mg, 0.069 mmol) and 2-diazo-1-phenylethanone (10 mg, 0.069 mmol) was added via vacuum transfer 5 mL pentane at -78 ^{o}C. The solution was allowed to warm slowly with stirring for 16 h, resulting in a brown solution. The volatiles were evaporated, leaving a dark brown residue. ^{1}H NMR analysis of the residue showed neither starting material, and only one paramagnetically shifted resonance.

54. Treatment of 4-Me$_2$IPr with 2-diazo-1-phenylethanone. To a 25-mL flask charged with **4**-Me$_2$IPr (99 mg, 0.23 mmol) and 2-diazo-1-phenylethanone (34 mg,

0.23 mmol) was added via vacuum transfer 10 mL pentane at -78 ^{o}C. The solution was allowed to warm slowly with stirring for 17 h, resulting in a dark brown solution. The volatiles were evaporated, resulting in a dark brown residue. ^{1}H NMR analysis of the residue showed only the presence of norbornane, 1,1'-binorbornyl and pentane, with the resonances obfuscated by other broad, unidentified resonances. No starting materials or paramagnetic products were observed.

55. Treatment of 4-PMe$_3$ with 2-diazo-1-phenylethanone. To a 25-mL flask charged with **4**-PMe$_3$ (24 mg, 0.060 mmol) and 2-diazo-1-phenylethanone (9 mg, 0.06 mmol) was added via vacuum transfer 5 mL pentane at -78 ^{o}C. The solution was allowed to warm slowly with stirring for 16 h, resulting in a dark brown solution. The volatiles were evaporated, resulting in a dark brown residue. ^{1}H NMR analysis of the residue showed the major species present was 1,1'-binorbornyl with a series of paramagnetically shifted resonances in trace amounts. The new paramagnetic complex was not pursued, given its trace yield (<10%).

56. Treatment of 6-Im with styrene. To a vial charged with **6**-Im (14 mg, 0.024 mmol) and 0.6 mL C_6D_6 was added styrene (3 mg, 0.03 mmol). The dark green solution was allowed to stand at 23 ^{o}C for 2 h. Analysis by ^{1}H NMR showed no reaction. Heating the sample to 55 ^{o}C for 2 h resulted in a dark yellow solution. ^{1}H NMR spectra showed a paramagnetic product consistent with **7**-Am, with no consumption of the styrene.

57. Treatment of 6-Im with cyclohexene. To a vial charged with **6**-Im (10 mg, 0.017 mmol) and 0.6 mL tol-d_8 was added cyclohexene (2 mg, 0.02 mmol). The dark green

solution was allowed to stand at 23 °C for 68 h, with ^{1}H NMR spectra acquired over the duration. No reaction between the starting materials was observed over 68 h, with the imide only converting to **7**-Am.

58. Treatment of 6-Im with 1,4-cyclohexadiene. To a vial charged with **6**-Im (10 mg, 0.017 mmol) and 0.6 mL tol-d_8 was added cyclohexadiene (2 mg, 0.03 mmol). The dark green solution was allowed to stand at 23 °C for 42 h, with ^{1}H NMR spectra acquired over the duration. No reaction between the starting materials was observed over 42 h, with the imide only converting to **7**-Am. A trace amount of C_6H_6 (0.018 : 1 cyclohexene) was observed at the start of the reaction through 42 h, with no observable increase.

59. Treatment of 6-Im with triethylsilane. To a vial charged with **6**-Im (10 mg, 0.017 mmol) and 0.6 mL tol-d_8 was added triethylsilane (4 mg, 0.03 mmol). The dark green solution was allowed to stand at 23 °C for 47 h, with ^{1}H NMR spectra acquired over the duration. No reaction between the starting materials was observed over 47 h, with the imide only converting to **7**-Am.

60. Treatment of 6-Im with diphenylsilane. To a vial charged with **6**-Im (10 mg, 0.017 mmol) and 0.6 mL tol-d_8 was added diphenylsilane (4 mg, 0.02 mmol). The dark green solution was allowed to stand for 21 h at 23 °C, resulting in a dark yellow solution. ^{1}H NMR analysis of the solution showed 1.2 eq norbornane was produced along with a new paramagnetic product in quantitative yields. The integrations of the new complex were consistent with the formulation (Me_2IPr)Fe{N(1-Ad)(1-nor)}(Si(H)Ph_2) (**11**), which is also in agreement with the yellow solution color and

the norbornane produced. In addition, DART-MS of the reaction quench confirmed the presence of (1-Ad)NH(1-nor). ^{1}H NMR (Fe product,tol-d_8): δ -23.05 (12H), -9.40 (6H), -0.25 (4H), 2.68 (4H), 4.76 (3H), 5.48 (4H), 7.48 (3H), 14.90 (6H), 18.66 (3H), 54.90 (2H), 70.19 (2H), 94.44 (1H); (norbornane, tol-d_8): δ 1.16 (6H, br "s"), 1.44 (4H, br s), 2.16 (2H, s). HRMS (DART-MS) m/z: $[M + H]^+$ Calcd for 246.2177; Found 246.2219.

61. Crossover experiment of 6-Im with 4-Me$_2$IPr. To a vial charged with **1**-Me$_2$IPr (9 mg, 0.02 mmol) and 0.6 mL tol-d_8 was added 1-adamantylazide (2 mg, 0.01 mmol), resulting in a dark green solution. The solution was allowed to stand at 23 ^{o}C for 2.5 min, after which **4**-Me$_2$IPr (5 mg, 0.01 mmol) was added to the solution. The mixture was allowed to stand at 23 ^{o}C for 15 min, which resulted in a dark yellow solution. ^{1}H NMR analysis of the mixture showed a mix of **1**-Me$_2$IPr, **3**-Am, **4**-Me$_2$IPr and **6**-Im in the following ratio: 0.59, 0.41, 0.95 and 0.05. Trace amounts of **6**-Im and a near statistical mixture of **1**-Me$_2$IPr and **3**-Am imply that intramolecular nitrene transfer was not operative.

62. Crossover experiment of 6-Im with 1-Me$_2$IPr. To a vial charged with **6**-Im (9 mg, 0.02 mmol) and **1**-Me$_2$IPr (6 mg, 0.02 mmol) was added 0.6 mL tol-d_8. ^{1}H NMR spectra of the dark green solution were acquired over 65 h at 23 ^{o}C. After 17 h, a new paramagnetic product not consistent with **9**, (Me$_2$IPr)Fe{N(1-Ad)(CH$_2$C(CH$_3$)$_3$)}(1-nor) (**A**) or **10** was observed. After 65 h, while the new paramagnetic species was still present, **7**-Am was observed as the only amide containing species. No trace of **3**-Am was observed. In a separate, identical experiment with the addition of ferrocene (4 mg,

0.02 mmol) as an internal standard, the rate constant of imide insertion over 17 h at 23 ^{o}C was calculated to be 1.09 x 10^{-5} s^{-1}. This value was deemed to be consistent with the average rate constant (1.26 x 10^{-5} s^{-1}) obtained from kinetics measurements of the identical chemical process. These results imply that no intramolecular nitrene transfer occurred during the crossover experiment, and that the insertion process was not inhibited during the course of the study. The new paramagnetic species was not pursued nor characterized any further.

63. General procedure for 2-Im imide insertion kinetics measurements. To a vial charged with **1**-Me_2IPr (13 mg, 0.034 mmol) and ferrocene (3 mg, 0.02 mmol) was added ~0.6 mL tol-d_8. The solution was filtered into a J Young NMR tube. 1-adamantylazide (9 mg, 0.05 mmol) was added to the headspace bulb of the NMR tube, after which the tube was sealed and laid on its side upright to prevent azide addition to the solution. For the 21 ^{o}C reaction, the NMR tube was shaken to mix the reagents, followed by immediate insertion into an Inova 400 MHz spectrometer. For temperatures <23 ^{o}C, the NMR tube (with both reagents separate) was cooled down in a dry-ice/acetone bath set to the desired temperature, with the tube still laying on its side upright. For the 30 ^{o}C reaction, the NMR tube was warmed in a 30 ^{o}C water bath. After letting the temperature of the solution equilibrate for 15 min, the tube was shaken to mix the reagents, followed by insertion into an Inova 600 MHz spectrometer precooled to the same temperature. The progress of the reaction was then monitored by ^{1}H NMR spectroscopy over regular time intervals at a fixed temperature (-10, 1, 10, 21 and 30 ^{o}C), all performed in the absence of light. Each reaction was done in triplicate for each temperature.

64. General procedure for 6-Im imide insertion kinetics measurements. To a vial charged with **4**-Me_2IPr (12 mg, 0.028 mmol), ferrocene (3 mg, 0.02 mmol) and ~0.6 mL tol-d_8 was added 1-adamantylazide (5 mg, 0.03 mmol), resulting in an immediate color change to a dark green solution with light effervescence. The solution was filtered into a J Young NMR tube, which was then sealed. The 23 ^oC experiments were warmed in a Hewlett Packard 5890 Series II gas chromatograph oven, while temperatures >23 ^oC were warmed in an Inova 600 MHz spectrometer preheated to the desired temperature, with the tube allowed to equilibrate for 5 min prior to NMR acquisition. The progress of the reaction was then monitored by ^1H NMR spectroscopy over regular time intervals at a fixed temperature (23, 40, 50, 60 and 71 ^oC), all performed in the absence of light. Each reaction was done in triplicate for each temperature.

65. 6-Im imide insertion concentration dependence. To a vial charged with **4**-Me_2IPr (36 mg, 0.084 mmol), ferrocene (9 mg, 0.06 mmol) and ~0.6 mL tol-d_8 was added 1-adamantylazide (15 mg, 0.09 mmol), resulting in an immediate color change to a dark green solution (0.14 M **6**-Im) with light effervescence. The solution was filtered into a J Young NMR tube, which was then sealed. The NMR tube was inserted into a 600 MHz spectrometer preheated to 71 ^oC, after which the temperature was allowed to equilibrate for 5 min. ^1H NMR spectra were acquired over a 12 min period at a constant temperature. The experiment was done in triplicate. Time dependent concentration plots using ^1H NMR spectroscopy were successfully linearized to a first-order plot. k_{obs} (s^{-1}) = 4.68 x 10^{-3} (ave).

Imide insertion rate analysis. Time dependent concentration plots obtained using ^{1}H NMR spectroscopy were linearized, then fitted in Microsoft Excel using linear regression. The Eyring plot was fitted in Igor Pro 6 using linear regression weighted by the standard deviation of each point. The standard deviation of each data point was determined using propagation of error calculations.[50]

Single crystal X-ray diffraction studies. Upon isolation, the crystals were covered in polyisobutenes and placed under a cold N_2 stream on the goniometer head of a Siemens P4 SMART CCD area detector (graphite-monochromated MoKα radiation, λ = 0.71073 Å). The structures were solved by direct methods (SHELXS). All non-hydrogen atoms were refined anisotropically unless stated, and hydrogen atoms were treated as idealized contributions (Riding model).

References

(1) Jacobs, B. P.; Wolczanski, P. T.; MacMillan, S. N. *J. Organomet. Chem.* **2017**, Ahead of Print.

(2) Wood, C. D.; McLain, S. J.; Schrock, R. R. *J. Am. Chem. Soc.* **1979**, *101*, 3210.

(3) Schrock, R. R.; Fellmann J. D. *J. Am. Chem. Soc.* **1978**, *100*, 3360.

(4) Li, L.; Hung, M.; Xue, Z. *J. Am. Chem. Soc.* **1995**, *117*, 12746.

(5) Xue, Z.; Morton, L. A. *J. Organomet. Chem.* **2011**, *696*, 3924.

(6) Bower, B. K.; Tennent, H. G. *J. Am. Chem. Soc.* **1972**, *132*, 12814.

(7) Thiele, K.-H.; Dimitrov, V.; Schenke, D.; Krüger, A.; Rusina, A. *Wiss. Z. Tech. Hochsch. "Carl Schorlemmer" Leuna-Merseburg* **1986**, *28*, 197.

(8) Lewis, R. A.; Smiles, D. E.; Darmon, J. M.; Stieber, C. E.; Wu, G.; Hayton, T. W. *Inorg. Chem.* **2013**, *52*, 8218.

(9) Liptrot, D. J.; Guo, J.-D.; Nagase, S.; Power, P. P. *Angew. Chem. Int. Ed.* **2016**, *55*, 14766; *Angew. Chem.* **2016**, *128*, 14986.

(10) Casitas, A.; Rees, J. A.; Goddard, R.; Bill, E.; DeBeer, S.; Fürstner, A. *Angew. Chem. Int. Ed.* **2017**, Ahead of Print.

(11) Zhang, H.; Ouyang, Z.; Liu, Y.; Zhang, Q.; Wang, L.; Deng, L. *Angew. Chem. Int. Ed.* **2014**, *53*, 8432.

(12) Wang, L.; Hu, L.; Zhang, H.; Chen, H.; Deng, L. *J. Am. Chem. Soc.* **2015**, *137*, 14196.

(13) Fellmann, J. D.; Schrock, R. R. S. *J. Am. Chem. Soc.* **1978**, *100*, 3359.

(14) Fernández, I.; Trovitch, R. J.; Lobkovsky, E.; Chirik, P. J. *Organometallics* **2008**, *27*, 109-118.

(15) Charron, Jr., F. F.; Reiff, W. M. *Inorg. Chem.* **1986**, *25*, 2786-2790.

(16) Bedford, R. B.; Brenner, P. B.; Elorriaga, D.; Harvey, J. N.; Nunn, J. *Dalton Trans.* **2016**, *45*, 15811-15817.

(17) (a) Evans, D. F. *J. Chem. Soc.* **1959**, 2003. (b) Schubert, E. M. *J. Chem. Ed.* **1992**, *69*, 62.

(18) H. H. Karsch, *Chem. Ber*. **1977**, *110*, 2222-2235.

(19) Ryan, S. J.; Schimler, S. D.; Bland, D. C.; Sanford, M. S. *Org. Lett.* **2015**, *17*, 1866-1869.

(20) Dunsford, J. J.; Cade, I. A.; Fillman, K. L.; Neidig, M. L.; Ingleson, M. J. *Organometallics* **2014**, *33*, 370-377.

(21) Alborés, P.; Carrella, L. M.; Clegg, W.; García-Álvarez, P.; Kennedy, A. R.; Klett, J.; Mulvey, R. E.; Rentschler, E.; Russo, L. *Angew. Chem. Int. Ed.* **2009**, *48*, 3317.

(22) Noda, D.; Sunada, Y.; Hatakeyama, T.; Nakamura, M.; Nagashima, H. *J. Am. Chem. Soc.* **2009**, *131*, 6078.

(23) Danopoulos, A. A.; Braunstein, P.; Wesolek, M.; Monakhov, K. Y.; Rabu, P.; Robert, V. *Organometallics* **2012**, *31*, 4102.

(24) Jacobs, B. P.; Wolczanski, P. T.; Lobkovsky, E. B. *Inorg. Chem.* **2016**, *55*, 4223.

(25) Schwab, P.; France, M. B.; Ziller, J. W.; Grubbs, R. H. *Angew. Chem. Int. Ed.* **1995**, *34*, 2039.

(26) Schwab, P.; Grubbs, R. H.; Ziller, J. W. *J. Am. Chem. Soc.* **1996**, *118*, 100.

(27) Li, Y.; Huang, J.-S.; Zhou, Z.-Y.; Che, C.-M.; You, X.-Z. *J. Am. Chem. Soc.* **2002**, *124*, 13185.

(28) Klose, A.; Solari, E.; Floriani, C.; Re, N.; Chiesi-Villa, A.; Rizzoli, C. *Chem. Commun.* **1997**, 2297.

(29) Russell, S. K.; Hoyt, J. M.; Bart, S. C.; Milsmann, C.; Stieber, S. C. E.; Semproni, S. P.; DeBeer, S.; Chirik, P. J. *Chem. Sci.* **2014**, *5*, 1168.

(30) Esposito, V.; Solari, E.; Floriani, C.; Re, N.; Rizzoli, C.; Chiesi-Villa, A. *Inorg. Chem.* **2000**, *39*, 2604.

(31) Toma, T.; Shimokawa, J.; Fukuyama, T. *Org. Lett.* **2007**, *9*, 3195-3197.

(32) Stein, J.; Fackler, Jr., J. P.; Paparizos, C.; Chen, H. W. *J. Am. Chem. Soc.* **1981**, *103*, 2192-2198.

(33) King, E. R.; Hennessy, E. T.; Betley, T. A. *J. Am. Chem. Soc.* **2011**, *133*, 4917.

(34) Searles, K.; Fortier, S.; Khusniyarov, M. M.; Carroll, P. J.; Sutter, J.; Meyer, K.; Mindiola, D. J.; Caulton, K. G. *Angew. Chem. Int. Ed.* **2014**, *53*, 14139.

(35) Thomas, C. M.; Mankad, N. P.; Peters, J. C. *J. Am. Chem. Soc.* **2006**, *128*, 4956.

(36) Nieto, I.; Ding, F.; Bontchev, R. P.; Wang, H.; Smith, J. M. *J. Am. Chem. Soc.* **2008**, *130*, 2716.

(37) Kuppuswamy, S.; Powers, T. M.; Johnson, B. M.; Bezpalko, M. W.; Brozek, C. K.; Foxman, B. M.; Berben, L. A.; Thomas, C. M. *Inorg. Chem.* **2013**, *52*, 4802.

(38) Mehn, M. P.; Brown, S. D.; Jenkins, D. M.; Peters, J. C.; Que, Jr., L. *Inorg. Chem.* **2006**, *45*, 7417.

(39) Allen, F. H.; Kennard, O.; Watson, D. G.; Brammer, L.; Orpen, A. G.; Taylor, R. J. *J. Chem. Soc., Perkin Trans. II* **1987**, S1-S19.

(40) Bales, S. E.; Hudnall, P. M.; Burns, T. P.; Poindexter, G. S.; Rieke, R. D. *Org. Syn., Coll. Vol. 6* **1988**, 845; *Vol. 59* **1979**, 85.

(41) Byrne, E. K.; Theopold, K. H. *J. Am. Chem. Soc.* **1989**, *111*, 3887-3896.

(42) Heins, S. P.; Wolczanski, P. T.; Cundari, T. R.; MacMillan, S. N. *Chem. Sci.* **2017**, *8*, 3410.

(43) Tolman, W. B. *Angew. Chem. Int. Ed.* **2010**, *49*, 1018.

(44) Laplaza, C. E.; Odom, A. L.; Davis, W. M.; Cummins, C. C.; Protasiewicz, J. D. *J. Am. Chem. Soc.* **1995**, *117*, 4999.

(45) Manoni, F.; Connon, S. J. *Angew. Chem. Int. Ed.* **2014**, *53*, 2628.

(46) Xiang, L.; Xiao, J.; Deng, L. *Organometallics* **2011**, *30*, 2018.

(47) Eisch, J. J.; Yu, K.; Rheingold, A. L. *Eur. J. Org. Chem.* **2012**, 3165.

(48) Kajiyama, K.; Yoshimune, M.; Nakamoto, M.; Matsukawa, S.; Kojima, S.; Akiba, K. *Org. Lett.* **2001**, *3*, 1873-1875.

(49) Javed, M. I.; Brewer, M. *Org. Synth.* **2008**, *85*, 189.

(50) Taylor, J. R. *An Introduction to Error Analysis: The Study of Uncertainties in Physical Measurements*; *2nd Ed.*; University Science Books: Sausalito, **1997**.

(51) Gomberg, M. *J. Am. Chem. Soc.* **1900**, *22*, 757.

Appendix 1

Synthesis of Bis(2-(4-^{t}Butyl)pyridylcarbonyl)amine Towards C-H Bond Activation

Introduction

Free radical transformations of hydrocarbons, such as halogenation or autoxidation, functionalize the alkane precursor into valuable commodity chemicals such as alkyl halides or alcohols (Scheme A.1). Both chemical processes invoke radical character to activate C-H bonds, and typically exhibit poor chemoselectivity. For example, conversion of gaseous methane to methanol would allow transport of a viable energy source.[1] The high C-H bond strength of methane (105 kcal mol^{-1}) necessitates harsh reaction conditions, conducive to the over-oxidation of methane to form CO_2 as an undesired product.[1]

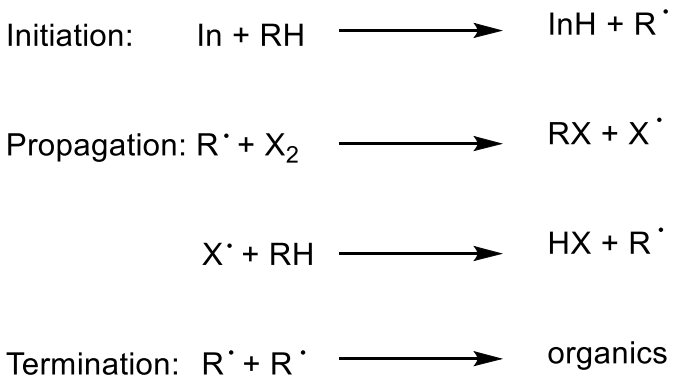

Scheme A.1. Autoxidation of an alkane via an initiator (In)

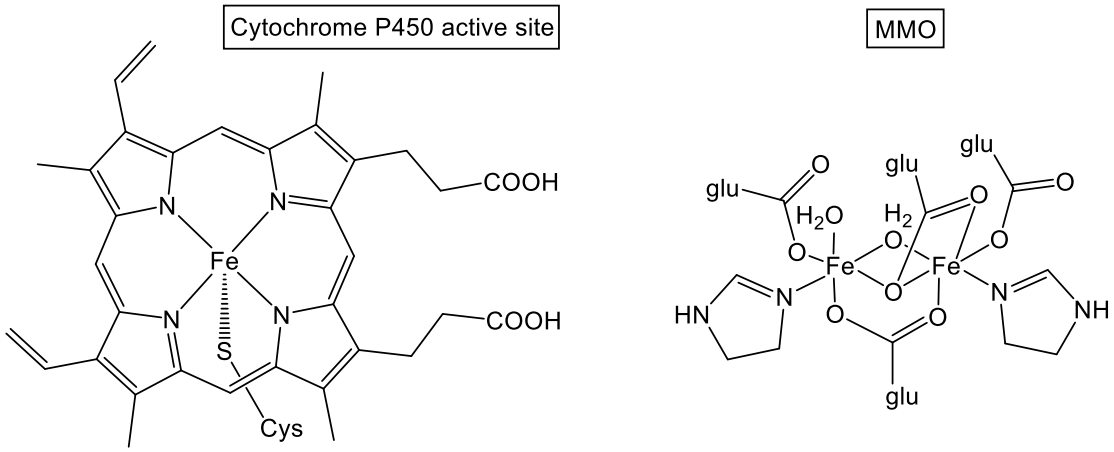

Figure A.1. Biological systems that moderate C-H bond activation

Biological systems such as cytochrome P450[2] and methane monooxygenase (MMO) moderate remote C-H bond activations, with the latter shown to effect methane oxidation to methanol (Figure A.1).[3-6] These systems activate C-H bonds through a process known as the rebound mechanism (Scheme A.2),[7,8] in which initial C-H activation by transition metal oxo species generates R·. Attack of R· on the metal-hydroxo moiety produces the target alcohol product, and the aqueous media regenerates metal catalyst.

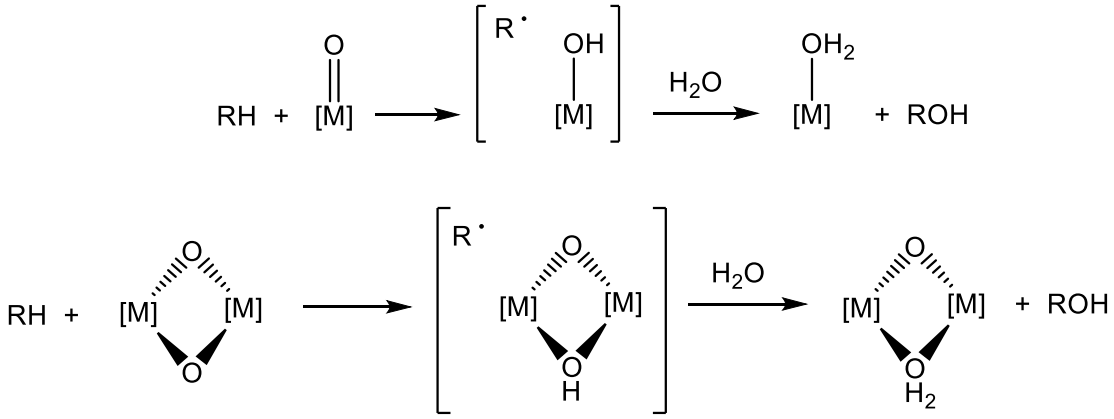

Scheme A.2. Rebound mechanism for biological hydrocarbon oxidation

Selectivity challenges of free radical oxidation of hydrocarbons in comparison to the ease of which biological systems affect similar transformations warrant investigations into synthetic molecules whose reactivity mimics biological transformations. Development of transition metal complexes that can activate C-H bonds with good selectivity represents a valuable synthetic methodology that could incorporate inert hydrocarbon feedstock as useful precursors.

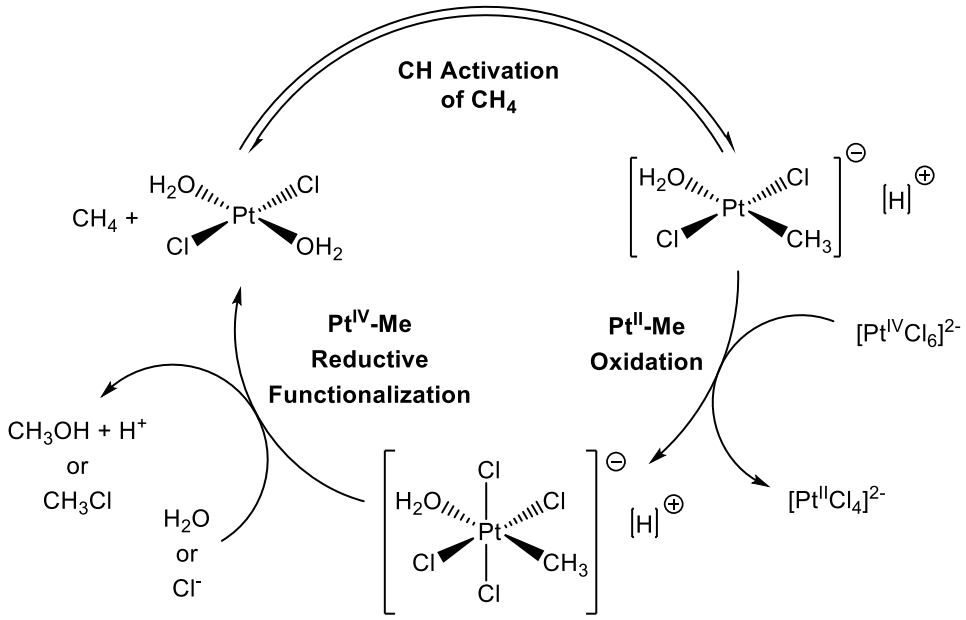

Scheme A.3. Proposed mechanism for Shilov's platinum-mediated oxidation of methane (scheme adapted from reference 10, scheme 11)

Considerable work has been conducted in the development of transition metal complexes that affect alkane oxidation. Shilov and coworkers demonstrated Pt(II)-mediated oxidation of methane employing stoichiometric amounts of K_2PtCl_6 in the early 1970s (Scheme A.3).[9,10] The high cost of the stoichiometric platinum oxidant presents a considerable disadvantage towards further development of the Shilov

system.[10] Periana *et al*. have reported efficient catalytic methane and ethane oxidation to alkyl bisulfates ($ROSO_3H$) in acidic media, employing the platinum-based catalyst (2,2'-bipyrimidine)$PtCl_2$ (Eq A.1).[10-12] Subsequent hydrolysis of the alkyl bisulfate products yields the target alcohol. While harsh reaction conditions (98% H_2SO_4, elevated temperatures up to 220 ^oC) are minor concerns for industrial interests, production of water as a byproduct mandates distillation to isolate methanol from the aqueous media, a prohibitively expensive process.[10]

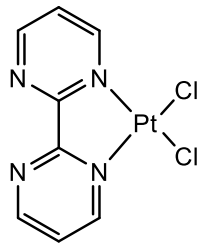

$$CH_4 + 2\ H_2SO_4 \xrightarrow[H_2SO_4,\ 220\ ^oC]{} CH_3OSO_3H + 2\ H_2O + SO_2 \qquad \textbf{(A.1)}$$

Bio-inspired transition metal complexes have been investigated by Borovik *et al*.,[13,14] such as the tripodal Mn complex $[Mn^{III}H_3buea(O)]^{2-}$ illustrated in Eq A.2.[14] The Mn^{III}-oxo species abstracts the H-atom from organic reagents such as 9,10-dihydroanthracene and 1,4-cyclohexadiene, yielding the Mn^{II}-hydroxo product along with the respective oxidized cyclic products, anthracene and benzene.

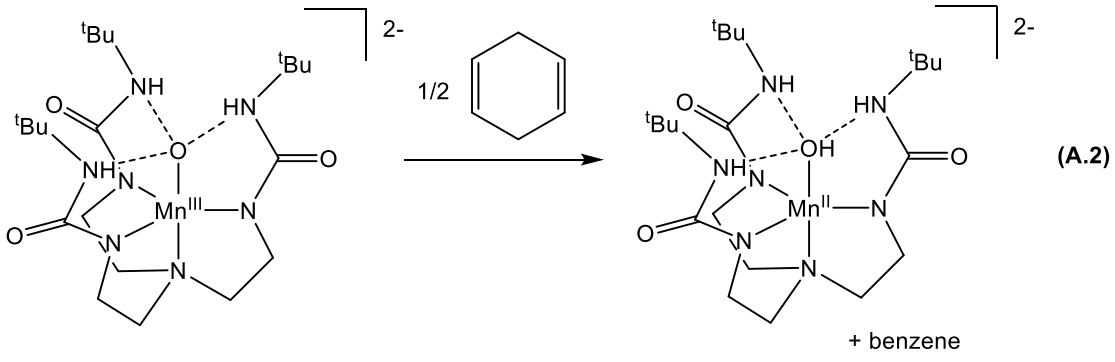

(A.2)

Our interest in pursuing C-H activation of hydrocarbon substrates, while maintaining control over radical behavior, led us to investigate ligand scaffolds similar to Borovik's tripodal tris-urea system, in which potential H-bonding interactions may encourage initial H-atom abstraction. Former colleague Erika Bartholomew prepared the three-coordinate ligand bis(2-pyridylcarbonyl) amine, Hbpca. It was envisaged that the presence of both carbonyl moieties may encourage initial H-atom abstraction through subsequent H-bonding interactions between the oxygen atoms. Scheme A.4 illustrates a potential catalytic cycle towards oxidation of an alkane (RH) to generate an alkyl halide (RX). (bpca)M^{n+} (**A**) oxidatively adds X_2 to generate (bpca)$M^{(n+2)+}X_2$ (**B**), which could then abstract H· from RH to produce (bpca)$M^{(n+2)+}HX_2$ (**C**) and R·. Radical rebound could then generate RX as the target product along with complex **D**, and subsequent HX loss would regenerate the initial catalyst.

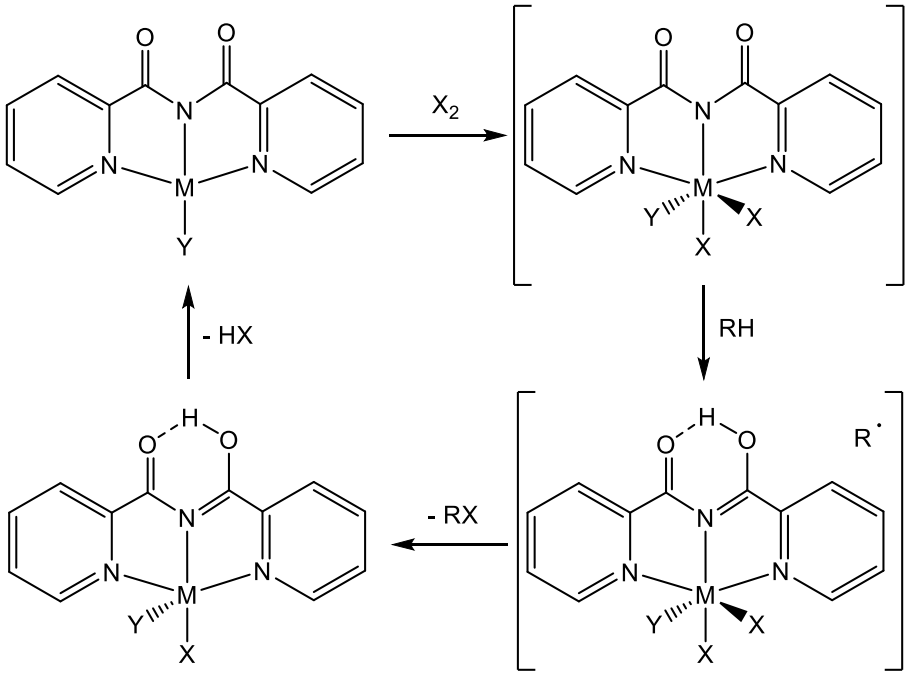

Scheme A.4. Proposed catalytic oxidation of RH by (bpca)M systems

Multiple first-row transition metal complexes incorporating bpca have been prepared (e.g. Mn,[15] Fe,[16] Co,[17,18] Ni,[19] Cu,[20] Zn[20]) as octahedral $(bpca)_2M(II)$ complexes, with all preparations done in aqueous media. Scheme A.4 illustrates that the desired metal complex incorporates one bpca ligand, a species not reported in prior literature. The four-coordinate complex **A** would likely undergo alternate undesired reactivity in aqueous media. As such, efforts focused on producing complex **A** in organic solvents. Eq A.3 indicates that treatment of Hbpca with $Fe\{N(TMS)_2\}_2(THF)$ was unproductive in various organic solvents. The absence of complex formation pointed to the insolubility of Hbpca, and prior metal-bpca complex preparation in aqueous media supports this conclusion.

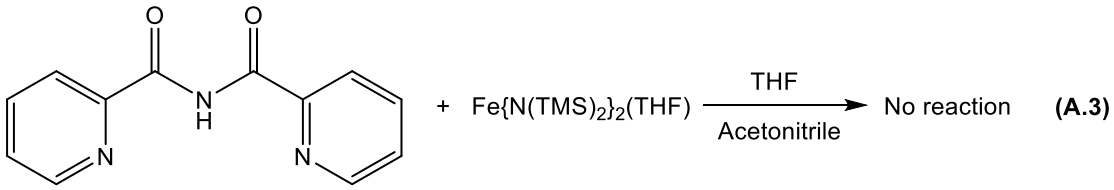

Insolubility of Hbpca in organic solvents prompted a ligand redesign, with efforts focused towards incorporation of tert-butyl groups on the pyridyl rings. Preparation of **^{t}Bu$_2$-Hbpca** was investigated, with the results presented herein.

A1.1 Ligand Synthesis from Prior Art

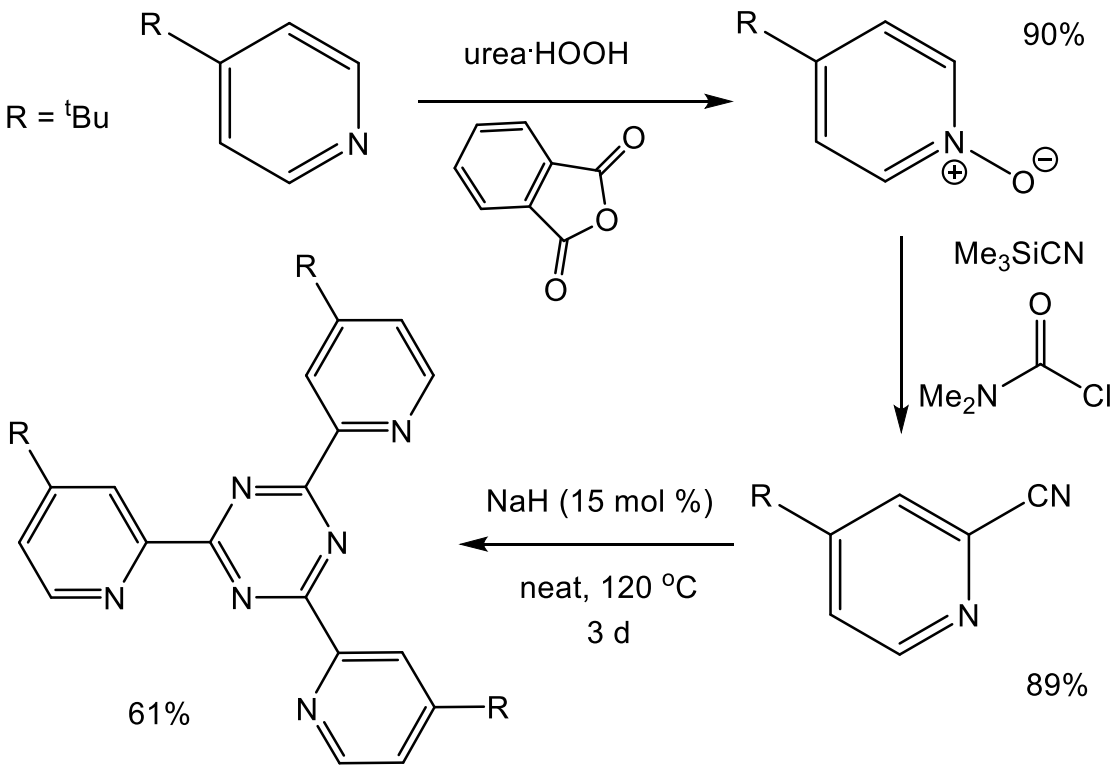

Scheme A.5. Preparation of **^{t}Bu$_2$-Hbpca** triazine precursor

Preparation of bis(4-*tert*-butyl-2-pyridylcarbonyl) amine (**^{t}Bu$_2$-Hbpca**) required the *tert*-butyltriazine precursor, as the bpca parent ligand was prepared through an identical manner.[21,22] Scheme A.5 illustrates the synthetic method towards preparing **^{t}Bu$_2$-Hbpca**. Treatment of 4-*tert*-butylpyridine with urea/hydrogen peroxide (UHP)[23] and phthalic anhydride formed the corresponding N-oxide as a white solid in 90% yield.[24] Addition of trimethylsilylcyanide and N,N-dimethylcarbamyl chloride to a dichloromethane solution of the N-oxide furnished 4-*tert*-butyl-2-cyanopyridine as a colorless oil in good yield.[25] Kajiwara *et al*. reported the cyclization of 4-*tert*-butyl-2-

cyanopyridine could be induced by addition of catalytic NaH,[22] and replication of the procedure on a small scale generated the target *tert*-butyltriazine product in reasonable yield after recrystallization from pentane.

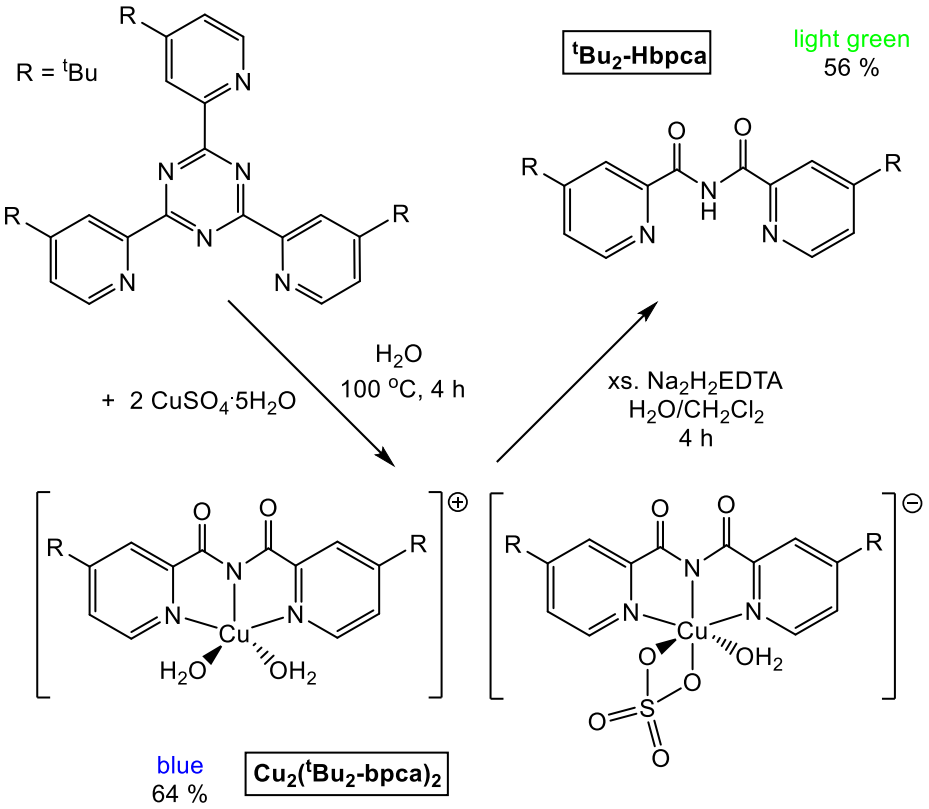

Scheme A.6. Hydrolysis of triazine and isolation of **^{t}Bu$_2$-Hbpca**

An aqueous suspension of *tert*-butyl-triazine and two equivalents of copper sulfate pentahydrate were heated to reflux, resulting in precipitation of **Cu$_2$(^{t}Bu$_2$-bpca)$_2$** as blue microcrystals in 64% yield (Scheme A.6).[22] Treatment of the dicopper species with excess Na_2H_2EDTA in a water/dichloromethane solution, followed by vigorous stirring for 4 h, yielded the target ligand **^{t}Bu$_2$-Hbpca** as a faint green powder in 56% yield (Scheme A.6).[22] The overall yield of ligand was 18% after 5 synthetic steps.

While small scale preparations of **^{t}Bu$_2$-Hbpca** were successful, working on 20 g scales of 4-*tert*-butylpyridine resulted in complex mixture formation upon synthesis of *tert*-butyltriazine. Efforts to recrystallize the product only produced trace amounts of product, and attempts to purify the mixture via filtration through silica plugs were unsuccessful. As such, the synthetic method was abandoned, and new methods of preparing **^{t}Bu$_2$-Hbpca** were sought.

A1.2 Alternative Approaches to bpca via Oxidation of 2-pyridylmethyl-2-picolinamide

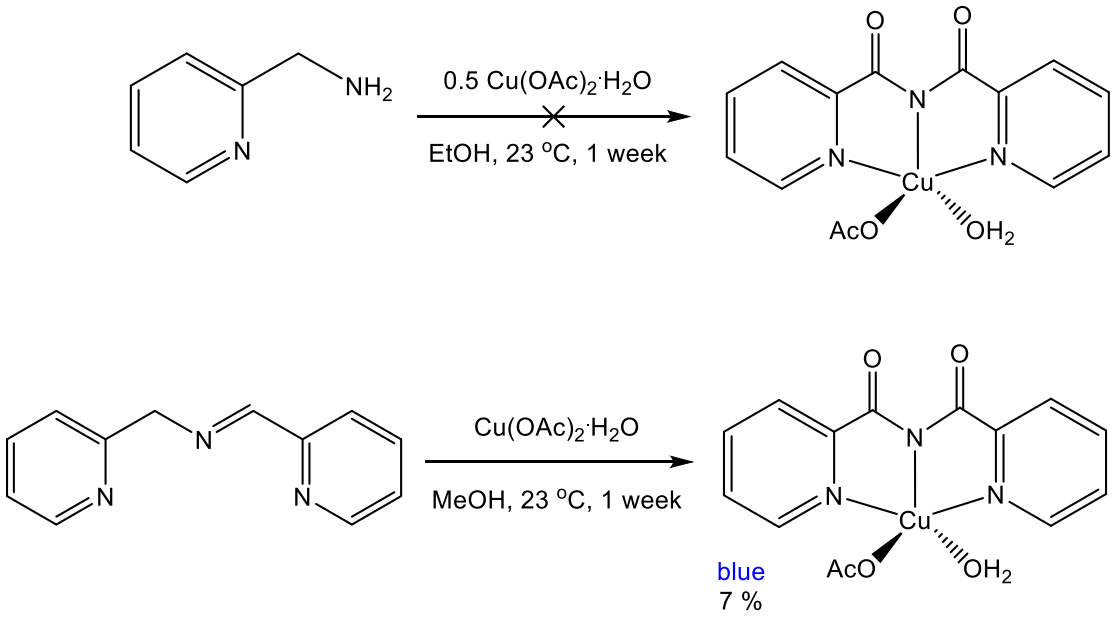

Scheme A.7. Attempts to produce **Cu(bpca)** via copper-mediated oxidation

Issues encountered upon scaling up the preparation of bis(4-*tert*-butyl-2-pyridylcarbonyl) amine (**^{t}Bu$_2$-Hbpca**) prompted investigations into alternative protocols. Manivannan *et al*. reported copper-mediated oxidative coupling of 2-aminomethylpyridine to generate **Cu(bpca)**,[26] and an additional report details copper-

mediated oxidation of 1,3-di-(2-pyridyl)-2-azapropene[27] to produce **Cu(bpca)**.[28] Scheme A.7 summarizes attempts to replicate both methodologies reported by Manivannan. Despite allowing the ethanol solution of copper and 2-aminomethylpyridine to stir for 1 week, blue microcrystals of the expected product were not formed, and reducing the volume did not induce precipitation of blue solid. Conversely, oxidation of 1,3-di-(2-pyridyl)-2-azapropene by copper acetate did yield trace amounts of blue crystals (7% yield) after 1 week. Disappointing results prompted a different synthetic approach.

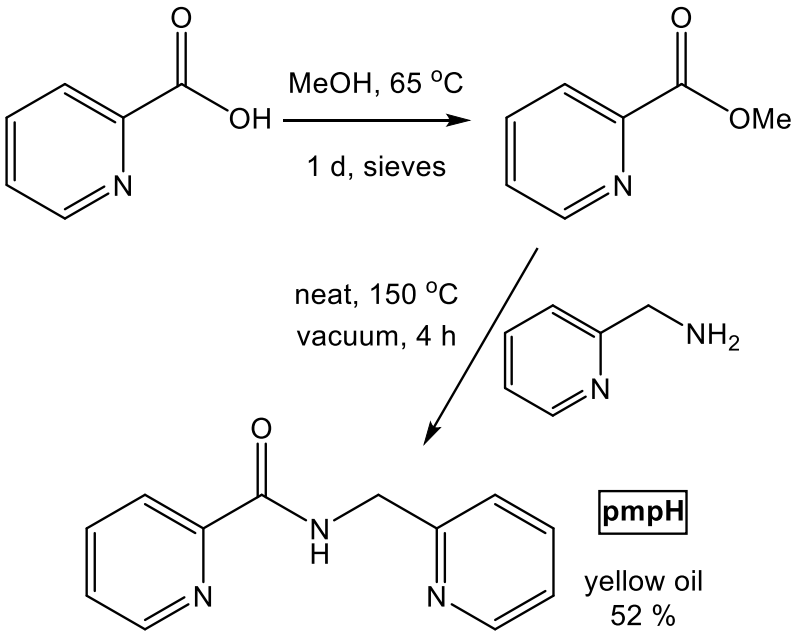

Scheme A.8. Synthesis of pmpH

Olmstead and Mascharak reported an unusual metal-mediated methylene oxidation of the "half-bpca" complex N-(2-picolyl)picolinamide (pmpH) that resulted in isolation of $M(bpca)_2$ complexes.[29] Intrigued by this process, efforts towards replicating this transformation, and subsequent ligand isolation, were undertaken.

Alcoholysis of 2-pyridine carboxylic acid yielded the corresponding methyl ester,[30] and subsequent treatment with 2-aminomethylpyridine at 150 °C produced pmpH,[31] isolated as a yellow oil, in 52% yield overall (Scheme A.8).

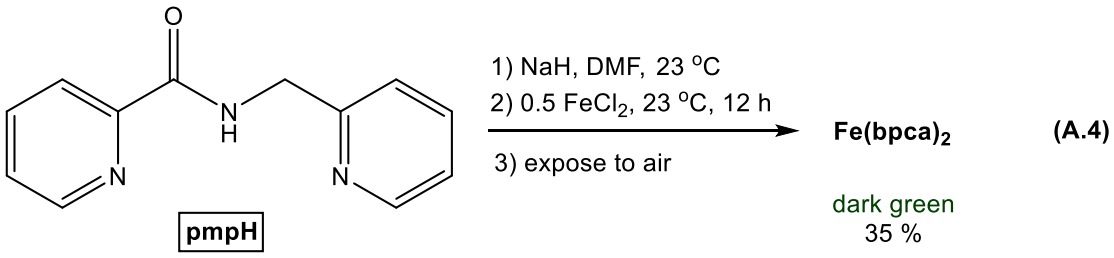

(A.4)

With pmpH isolated, efforts focused on affecting methylene oxidation, employing an Fe salt precursor.[29] Deprotonation of a DMF solution of pmpH by sodium hydride was followed with addition of 0.5 equivalents $FeCl_2$ (the original method employed $[Fe(DMF)_6](CLO_4)_3$). Exposure of the solution to air produced a dark green solution, and workup afforded **Fe(bpca)$_2$** as dark green crystals in 35% yield (Eq A.4). The IR spectrum of the dark green solid was consistent with the literature report.[29] Unfortunately, treatment of **Fe(bpca)$_2$** with Na_2H_2EDTA in water/dichloromethane did not liberate free ligand, as ^{1}H NMR did not reveal resonances consistent with free bpca (Eq A.5). Extrusion of copper from **Cu$_2$(bpca)$_2$** and the *tert*-butyl variant presumably occurs due to the lower coordination envrment and presence of weak water donors, neither of which **Fe(bpca)$_2$** possesses.

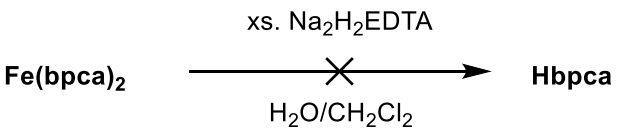

(A.5)

Further oxidations of pmpH with various organic oxidants (e.g. hydrogen peroxide, benzoyl peroxide, PCC) were unproductive. The paucity of successful

methods towards isolating bpca or any structural variants prompted abandoning the project.

Experimental

General considerations. All manipulations were performed using either glovebox or high vacuum line techniques, unless stated otherwise. All glassware was oven dried at 180 °C. THF and ether were distilled under nitrogen from purple sodium benzophenone ketyl and vacuum transferred from the same prior to use. Hydrocarbon solvents were treated in the same manner with the addition of 1-2 mL/L tetraglyme. Chloroform-d_1 (Cambridge Isotope Laboratories) was used as received. Urea-hydroperoxide,[23] 4-*tert*-butylpyridine *N*-oxide,[24] 4-*tert*-butyl-2-cyanopyridine,[25] 1,3,5-tris-(4-*tert*-butyl-2-pyridyl)triazine,[22] $Cu_2(^tBu_2\text{-bpca})_2$,[22] $^tBu_2$-Hbpca,[22] 1,3-di-(2-pyridyl)-2-azapropene,[27] methyl picolinate[30] and *N*-(2-picolyl)picolinamide (pmpH)[31] were prepared according to literature procedures. All other chemicals obtained commercially were used as received.

NMR spectra were obtained using Mercury 300 MHz and INOVA 400 MHz. Chemical shifts are reported relative to chloroform-d_1 (^{1}H δ 7.26; ^{13}C{1H} δ 77.16). Infrared spectra were recorded on a 20 Nicolet Avatar 370 DTGX spectrophotometer interfaced to an IBM PC (OMNIC software).

Procedures

1. Attempted oxidative coupling of 2-aminomethylpyridine with $Cu(OAc)_2{\cdot}2H_2O$. This preparation is in accordance with the procedure reported by Manivannan and coworkers.[26] To a 250-mL flask charged with $Cu(OAc)_2{\cdot}2H_2O$ (1.1 g, 5.5 mmol) and 60 mL ethanol was added 2-aminomethylpyridine (1.2 g, 11 mmol), resulting in a dark blue solution. The solution was allowed to stir for 1 d at 23 °C, and the solution

allowed to stand for 1 week. After 1 week, the solution turned green, and no solid had precipitated. The original preparation reported the crystallization of **Cu(bpca)(H_2O)(OAc)** as blue crystals from the ethanol solution in 61% yield, yet replication of this procedure was unsuccessful.

2. Attempted oxidation of 1,3-di-(2-pyridyl)-2-azapropene with $Cu(OAc)_2 \cdot 2H_2O$. This preparation is in accordance with the preparation reported by Manivannan and coworkers.[28] To a 250-mL flask charged with $Cu(OAc)_2 \cdot 2H_2O$ (672 mg, 3.37 mmol) and 50 mL methanol was added 1,3-di-(2-pyridyl)-2-azapropene (830 mg, 4.21 mmol), resulting in a dark violet solution. The solution was stirred for 1 d at 23 ^oC, and allowed to stand for 1 week. Blue crystals formed, and were collected via filtration (86 mg, 7%). IR spectroscopy of the crystals was consistent with the literature report for **Cu(bpca)(H_2O)(OAc)**.

3. Preparation of $Fe(bpca)_2$. This is a modification of the procedure reported by Mascharak and coworkers.[29] To a 2-neck 50-mL flask fit was charged with NaH (58 mg, 2.3 mmol) and fit with a solid addition finger charged with $FeCl_2$ (149 mg, 1.17 mmol). 5 mL DMF was added to the flask via syringe at 23 ^oC under an argon atmosphere. To a separate 25-mL flask charged with pmpH (500 mg, 2.34 mmol) was dissolved in 5 mL DMF, and the DMF solution was added to the NaH slurry. The mixture was stirred for 30 min at 23 ^oC. The $FeCl_2$ solid was added at 23 ^oC to the DMF solution, resulting in a red solution. The solution was allowed to stir for 12 h. The DMF solution was exposed to air with stirring for 2 h, resulting in a dark solution. The solution was filtered, and 10 mL THF was added, resulting in precipitation of

dark green crystals that were collected via filtration (221 mg, 35%). The IR spectrum of the green crystals was consistent with the literature report for **Fe(bpca)$_2$**.

4. Attempted hydrolysis of Fe(bpca)$_2$. To a 50-mL flask charged with **Fe(bpca)$_2$** (200 mg, 0.393 mmol) and $Na_2H_2EDTA{\cdot}2H_2O$ (586 mg, 1.57 mmol) was added 12 mL H_2O and 12 mL CH_2Cl_2. The solution was allowed to stir for 4 h at 23 ^oC. The dark green slurry was filtered, and the organic layer extracted with CH_2Cl_2 (3x10 mL). The colorless CH_2Cl_2 solution was dried, filtered and evaporated, resulting in no observed solid. ^1H NMR spectroscopy of the reaction mixture did not indicate the presence of free Hbpca.

References

(1) Crabtree, R.H. *J. Chem. Soc., Dalton Trans.* **2001**, 2437.

(2) Smith, D. A.; Ackland, M. J.; Jones, B. C. *Drug Discovery Today* **1997**, *2*, 406.

(3) Howard, J. B.; Rees, D. C. *Chem. Rev. (Washington, D. C.)* **1996**, *96*, 2965.

(4) Lipscomb, J. D. *Annu. Rev. Microbiol.* **1994**, *48*, 371.

(5) Ruettinger, W.; Dismukes, G. C. *Chem. Rev. (Washington, D. C.)* **1997**, *97*, 1.

(6) Siegbahn, P. E. M.; Blomberg, M. R. A. *Chem. Rev. (Washington, D. C.)* **2000**, *100*, 421.

(7) Groves, J. T. *J. Inorg. Biochem.* **2006**, *100*, 434.

(8) Hlavica, P. *Eur. J. Biochem.* **2004**, *271*, 4335.

(9) Shilov, A. E.; Shul'pin, G. B. *Chem. Rev.* **1997**, *97*, 2879.

(10) Gunsalus, N. J.; Koppaka, A.; Park, S. H.; Bischof, S. M.; Hashiguchi, B. G.; Periana, R. A. *Chem. Rev.* **2017**, Ahead of Print.

(11) Periana, R. A.; Taube, D. J.; Gamble, S.; Taube, H.; Satoh, T.; Fujii, H. *Science* **1998**, *280*, 560.

(12) Konnick, M. M.; Bischof, S. M.; Yousufuddin, M.; Hashiguchi, B. G.; Ess, D. H,; Periana, R. A. *J. Am. Chem. Soc.* **2014**, *136*, 10085.

(13) Lacy, D. C.; Gupta, R.; Stone, K. L.; Greaves, J.; Ziller, J. W.; Hendrich, M. P.; Borovik, A. S. *J. Am. Chem. Soc.* **2010**, *132*, 12188.

(14) Borovik, A. S. *Chem. Soc. Rev.* **2011**, *40*, 1870.

(15) Marcos, D.; Folgado, J. V.; Beltran-Porter, D.; Do, P.-G. M. T.; Pulcinelli, S. H.; De, A.-S. R. H. *Polyhedron* **1990**, *9*, 2699.

(16) Wocadlo, S.; Massa, W.; Folgado, J.-V. *Inorg. Chim. Acta* **1993**, *207*, 199.

(17) Davidson, R. B.; Sienerth, K. D. Abstracts of Papers, 245th ACS National Meeting & Exposition, New Orleans, LA, United States, April 7-11, 2013 (2013), INOR-1021.

(18) Kajiwara, T.; Sensui, R.; Noguchi, T.; Kamiyama, A.; Ito, T. *Inorg. Chim. Acta* **2002**, *337*, 299.

(19) Kamiyama, A.; Noguchi, T.; Kajiwara, T.; Ito, T. *Inorg. Chem.* **2002**, *41*, 507.

(20) Marcos, D.; Martinez-Manez, R.; Folgado, J. V.; Beltran-Porter, A.; Beltran-Porter, D.; Fuertes, A. *Inorg. Chim. Acta* **1989**, *159*, 11.

(21) Kamiyama, A.; Noguchi, T.; Kajiwara, T.; Ito, T. *Inorg. Chem.* **2002**, *41*, 507.

(22) Kajiwara, T.; Tanaka, H.; Nakano, M.; Takaishi, S.; Nakazawa, Y.; Yamashita, M. *Inorg. Chem.* **2010**, *49*, 8358.

(23) Lu, C.; Hughes, E. W.; Giguére, P. A. *J. Am. Chem. Soc.* **1941**, *63*, 1507.

(24) Kaczmarek, L.; Balicki, R.; Nantka-Namirski, P. *Chem. Ber.* **1992**, *125*, 1965.

(25) Shuman, R. T.; Ornstein, P. L.; Paschal, J. W.; Gesellchen P. D. *J. Org. Chem.* **1990**, *55*, 738.

(26) Sahu, R.; Padhi, S. K.; Jena, H. S.; Manivannan, V. *Inorg. Chim. Acta* **2010**, *363*, 1448.

(27) Frazier, B. A.; Bartholomew, E. R.; Wolczanski, P. T.; DeBeer, S.; Santiago-Berrios, M.; Abruña, H. D.; Lobkovsky, E. B.; Bart, S. C.; Mossin, S.; Meyer, K.; Cundari, T. R. *Inorg. Chem.* **2011**, *50*, 12414.

(28) Padhi, S. K.; Manivannan, V. *Inorg. Chem.* **2006**, *45*, 7994.

(29) Rowland, J. M.; Olmstead, M. M.; Mascharak, P. K. *Inorg. Chem.* **2002**, *41*, 2754.

(30) Louise-Leriche, L.; Păunescu, E.; Saint-André, G.; Baati, R.; Romieu, A.; Wagner, A.; Renard, P. *Chem. Eur. J.* **2010**, *16*, 3510.

(31) Arvapalli, V. S.; Chen, G.; Kosarev, S.; Tan, M. E.; Xie, D.; Yet, L. *Tetrahedron Letters* **2010**, *51*, 284.